UNCLASSIFIED

URITY CLASSIFICATION OF THIS PAGE

REPORT DOCUMENTATION PAGE

AD-A232 718

MAR 08 1991

	1b RESTRICTIVE MARKINGS
DECLASSIFICATION / DOWNGRADING SCHEDULE	3 DISTRIBUTION / AVAILABILITY OF REPORT Approved for public release, distribution unlimited
PERFORMING ORGANIZATION REPORT NUMBER(S) MIT-CE-R-90-24	5 MONITORING ORGANIZATION REPORT NUMBER(S) AFOSR-TR- 91 0133
NAME OF PERFORMING ORGANIZATION ssachusetts Institute of Tech. ot. of Civil Engineering	6b OFFICE SYMBOL (If applicable)
7a NAME OF MONITORING ORGANIZATION U.S. Air Force Office of Scientific Research	
ADDRESS (City, State, and ZIP Code) 7 Massachusetts Avenue ambridge, Massachusetts 02139	7b ADDRESS (City, State, and ZIP Code) Bolling Air Force Base BK1410 Washington D.C. 20332-6445
NAME OF FUNDING / SPONSORING ORGANIZATION AFOSR and AFESC	8b OFFICE SYMBOL (If applicable) NA BK1410
9 PROCUREMENT INSTRUMENT IDENTIFICATION NUMBER AFOSR-87-0260	
ADDRESS (City, State, and ZIP Code) OSR - Bolling AFB, Washington D.C.20332-6448 ESC - Tyndall AFB, Florida 32404-6061	10 SOURCE OF FUNDING NUMBERS

PROGRAM ELEMENT NO	PROJECT NO	TASK NO	WORK UNIT ACCESSION NO
61102F	2302	C2	

TITLE (Include Security Classification)

ochastic and Centrifuge Modelling of Jointed Rock Vol. II- Centrifuge Modelling of Jointed Rock

PERSONAL AUTHOR(S) Gerald Iglesia, Herbert H. Einstein, Robert V. Whitman

a. TYPE OF REPORT	13b. TIME COVERED	14. DATE OF REPORT (Year, Month, Day)	15. PAGE COUNT
Final	FROM 6/87 TO 5/90	1990, August, 31	281

SUPPLEMENTARY NOTATION

COSATI CODES			18. SUBJECT TERMS (Continue on reverse if necessary and identify by block number)
FIELD	GROUP	SUB-GROUP	Jointed (Fractured) Rock, Stochastic Modelling, Fracture Geometry

ABSTRACT (Continue on reverse if necessary and identify by block number)

The use of the centrifuge for geotechnical research has gained widespread acceptance in soil engineering, but to date, relatively few tests have been performed involving rock. One reason for the scarcity of rock mechanics experiments is the question as to whether a small-scale model subject to an elevated gravitational acceleration level reasonably simulates the prototype condition involving discontinuities. The objective of this research was to find out

(Continued on next page.)

DISTRIBUTION / AVAILABILITY OF ABSTRACT ☐ UNCLASSIFIED/UNLIMITED ☐ SAME AS RPT ☐ DTIC USERS	21 ABSTRACT SECURITY CLASSIFICATION
a. NAME OF RESPONSIBLE INDIVIDUAL JR S Wu	22b. TELEPHONE (Include Area Code) 202-767-6961 / 22c. OFFICE SYMBOL NA

D FORM 1473, 84 MAR 83 APR edition may be used until exhausted. All other editions are obsolete.

SECURITY CLASSIFICATION OF THIS PAGE

Block 19 - continued

if centrifuge modelling can be used for discontinua and to get further insight into arching mechanisms. To investigate this issue of scaling, a "modelling-of-models" approach was followed. This was done with a trapdoor model in the centrifuge. The model package was spun up gradually to a desired gravity level, at which the trapdoor was lowered and measurements of the force on the door with the corresponding displacement were taken. Different sizes of small-scale models and of trapdoors were used with various levels of acceleration. An initial series of experiments was conducted with granular materials, namely, New Jersey coarse sand and uniform sized glass beads. These experiments not only allowed us to make comparisons with preceding experiments on the arching mechanism under normal gravity; they also served as a benchmark for the experiments with jointed rock. The arching, a lowering of the load with increasing displacements was also observed at elevated gravity levels. However, the loads stayed at a low value over larger displacements under the high stress levels in the elevated gravity experiments compared to pre-existing experiments, with low stress loading at normal gravity. This result is very significant in the design of underground structures. The experiments showed that the scaling laws in granular materials are satisfied.

The experimental setup for jointed media involved a jointed rock mass model with the trapdoor underneath. The jointed medium was composed of aluminum rods, square in cross-section, which are juxtaposed side by side and on top of each other to simulate joint sets with uniform spacing. The results from this "modelling-of-models" exercise showed that geometrically similar setups at appropriately scaled g-levels exhibited similar load-displacement behavior. The force values, especially the minimum loads, conformed approximately with the usual centrifuge scaling laws. However, these forces occurred at the same absolute door displacement, in violation of these scaling rules. Similitude requirements in connection with the scaling of length dimensions were thus not met.

The results of the trapdoor tests and a review of existing arching theories allowed us to propose a new arching theory for small displacements. This approach assumes the development of an actual arch, as was done by others, but expresses the minimum load after mobilization of the arch independently of the lateral earth pressure coefficient K. This is advantageous since K is practically very difficult to determine.

MIT CE R-90-24

STOCHASTIC AND CENTRIFUGE MODELLING OF JOINTED ROCK

Part II - Centrifuge Modelling of Jointed Rock

Grant No. AFOSR-87-0260

Final Report 1990

Prepared by

Gerald Iglesia
Herbert H. Einstein
Robert V. Whitman

Sponsored by

U.S. Air Force
Air Force Office of Scientific Research
Bolling Air Force Base
Air Force Engineering Services Center
Tyndall Air Force Base

December 1990

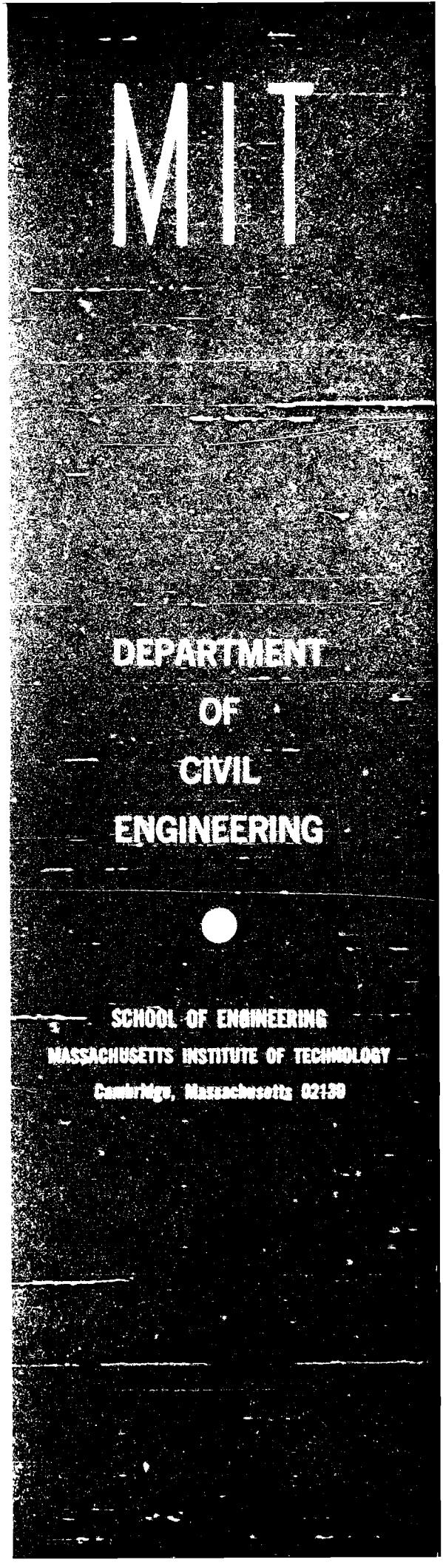

Acknowledgements

The research underlying this report was sponsored by the U.S. Air Force Office of Scientific Research and the U.S. Air Force Engineering and Services Center. The authors would like to acknowledge this support. In particular they would like to express their gratitude to Dr. S. Wu of AFOSR and Lt. S. Kuenen of AFESC for their encouragement and critical review of the work. This interaction went beyond the usual and was very beneficial to the project and to the authors. The authors would also like to thank Dr. P. Thompson formerly of AFESC for helping to initiate this research.

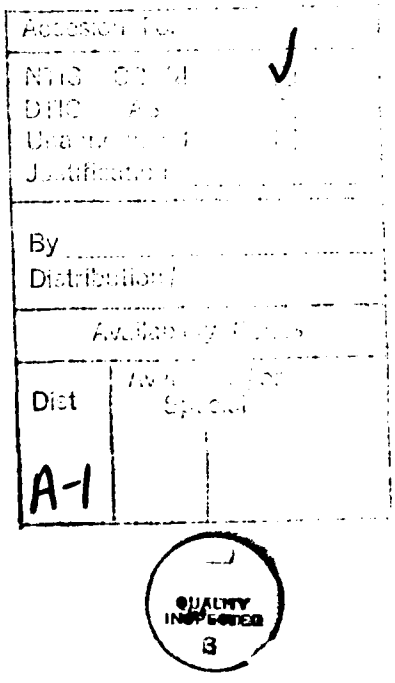

Contents

List of Figures

List of Tables

Chapter 1

Introduction

1.1 Background

Modelling, mathematical or physical, plays a significant role in the understanding of natural processes and system behavior. Mathematical models are based on assumptions and idealizations that render the situation under study suitable for analytical or numerical treatment. Physical models are built-up replicas, usually in a small and geometrically similar scale, of the prototype condition. With the rapid improvement of computer technology in recent years, mathematical models have become more attractive than physical models, and, thus, have proliferated in just about all branches of science and other areas of human knowledge.

The importance of physical models, however, has never been undermined by the popularity of mathematical models. Physical model testing provides results that are not always simulated by mathematical models, which are highly dependent on the input parameters and simplifying assumptions. Small-scale models remain relatively inexpensive, as compared with full-scale testing, especially when failure modes are being investigated. Consequently, they have been used extensively in various realms of engineering.

When a model is constructed smaller in size than and with the same material as the prototype, the former is proportionately lighter than the latter. This is usually not a

major problem in models where the dead weight of the system can either be ignored or simply included in the external loads, such as in many structural engineering applications. For geotechnical problems, however, the body forces can neither be neglected nor be readily replaced with equivalent external forces that will produce the same effects. It is well known that the behavior of geologic materials is grossly affected by stress levels. At low stress levels, for instance, most geomaterials tend to increase in volume, or dilate, when subjected to shearing loads. Hence, if a geotechnical system is to be modelled physically at a small scale, both the magnitude and the variation of the geostatic stresses have to be duplicated in the model. (For example, in a homogeneous ground mass, the vertical geostatic stress depends on the geomaterial's specific weight – which, in turn, is a function of the density and the gravitational acceleration – and varies linearly with depth.) The best way to do this is with a centrifuge, as in Figure 1-1, where the model revolves about an axis such that an artificial gravity field is induced by the centripetal acceleration brought about by the spinning action.

Through the years, physical modelling of geotechnical systems with the centrifuge has become quite popular. (See, e.g., Joseph et al., 1987.) Centrifuge modelling for geotechnical research has gained widespread acceptance in soil engineering, but to date relatively few tests have been performed involving rock. One reason for the scarcity of rock mechanics experiments is the lack of large-capacity centrifuges necessary to induce failure in rock models. Another is the question as to whether a small-scale model at an elevated gravitational acceleration level reasonably simulates the prototype situation, especially with the preponderance of discontinuities, or joints[1], in the rock mass. While the first reason cited here may well be addressed in due time with future technological advances, the second is more fundamental, for it challenges the validity of the centrifuge technique itself.

According to usual scaling laws, displacements – such as the amount of slip on a

[1] A *fracture* is a discontinuity in the rock mass which can be generated either by tensile or shear stresses. The engineering term for *rock fracture* is *joint*

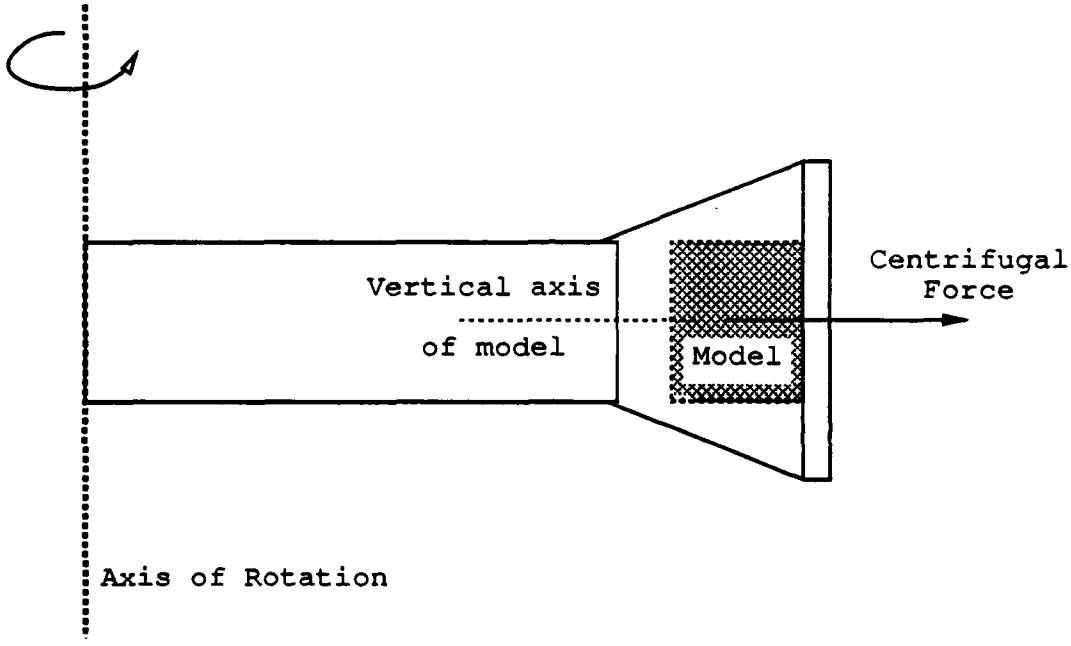

Figure 1-1: Physical modelling with a centrifuge

joint – are smaller in models than in full-scale situations. On the other hand, the force-displacement characteristics of rock joints are thought to be related to the absolute amount of displacement on the joint. Thus, there is concern whether the centrifuge modelling scheme applies to jointed rock masses.

To investigate this issue of scaling, a *modelling of models* approach (Figure 1-2) is followed. Based on centrifuge modelling principles, a $\frac{1}{N}$ scale model of a geotechnical system at N gravities should have a similar behavior as the prototype under normal gravity. This implies, then, that more than one model of the same prototype can be constructed using different scale factors N_1, N_2, etc., and, as long as the tests are performed at the appropriately scaled gravity level, the results should all be similar. That is, the behavior of a $\frac{1}{N_1}$ model at $N_1 g$ should be similar to that of a $\frac{1}{N_2}$ model at $N_2 g$, and so on.

The experimental setup adopted involves a jointed rock mass model with a trapdoor underneath. The model package is spun up gradually to a desired gravity level, at which the trapdoor is lowered, and measurements of the force on the door with the corresponding displacement are taken. Different sizes of small-scale models and of trapdoors are used with various levels of pseudo-gravitational acceleration in the centrifuge at which the door is moved down.

The trapdoor system, depicted in Figure 1-3, has been employed by several investigators [Engesser (1882), Terzaghi (1936), McNulty (1965), Ladanyi and Hoyaux (1969), Vardoulakis et al. (1981), Evans (1983), Stone (1988)] for examining the arching behavior of soils. Most of these tests, however, have been carried out under normal gravity, although McNulty (1965) has attempted to simulate realistic stress levels by applying air pressure as overburden. So far, only the experiments by Stone (1988) have been conducted in the centrifuge; the strains in the soil model were monitored, but the loads on the door were not measured at all. Aside from evaluating similitude in models of discontinua, therefore, this study involving trapdoor experiments on the centrifuge provides an excellent opportunity for further scrutiny of the arching effect in geomaterials.

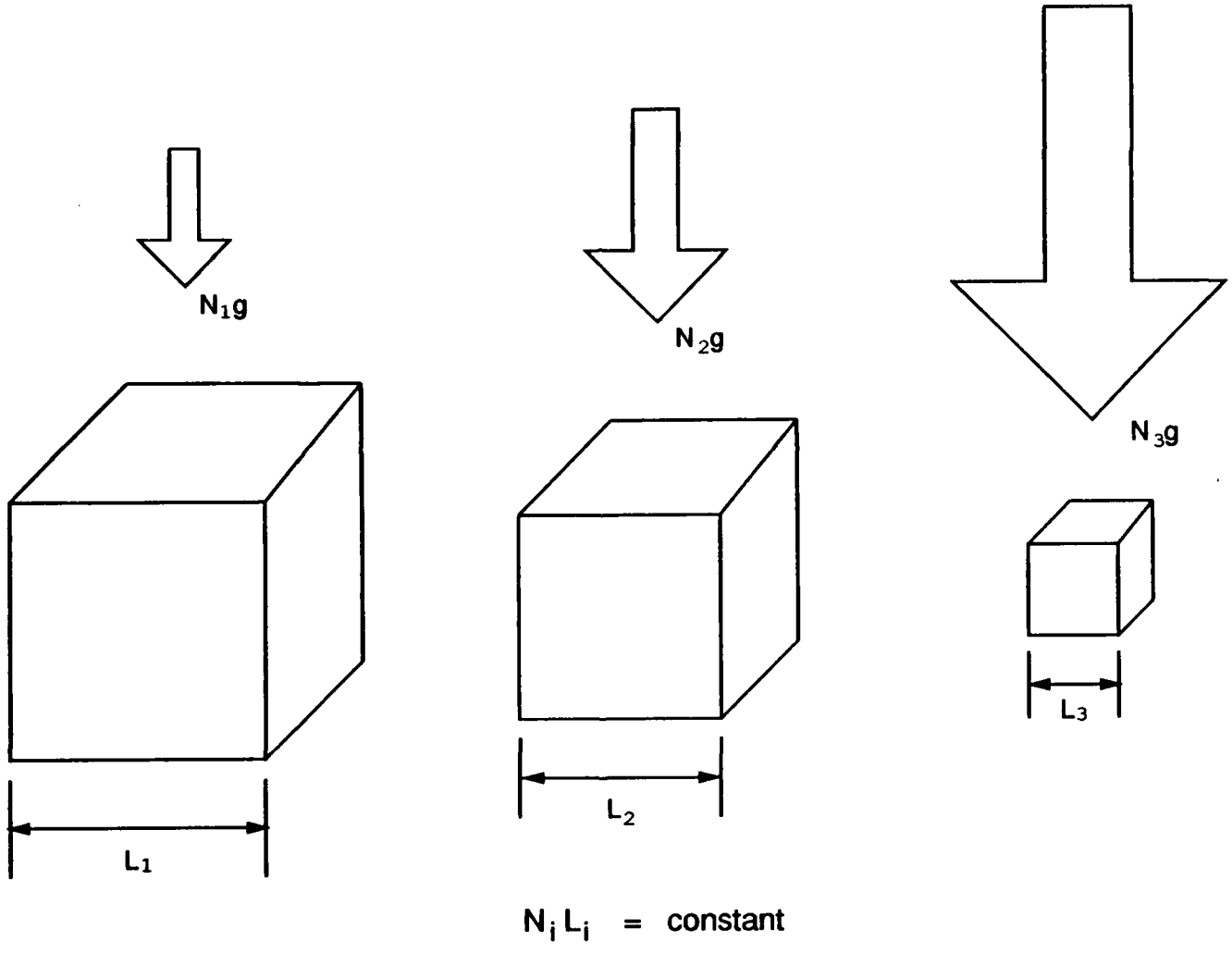

Figure 1-2: *Modelling of models* approach

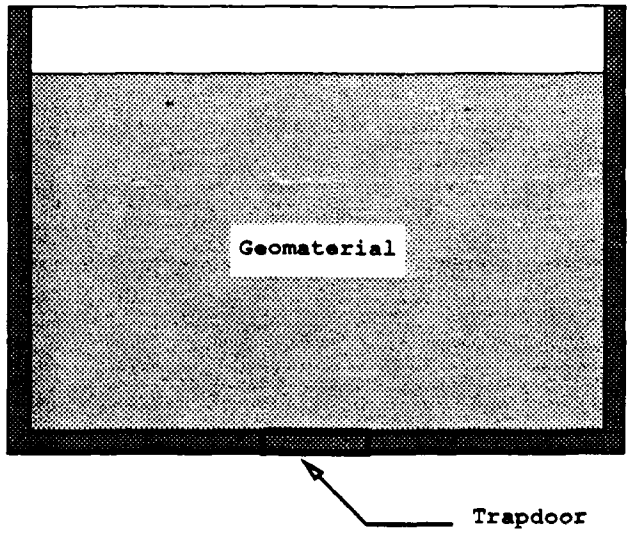

Figure 1-3: Trapdoor experiment to study geomaterial arching

1.2 The 'Arching' Concept

"Arching is one of most universal phenomena encountered in soils both in the field and in the laboratory." - Karl Terzaghi (1943)

When an inclusion, such as an underground structure, is present within a uniform ground mass, the local distribution of stresses and deformations is usually different from those in the free field. The nature of the stress redistribution influences the load that reaches the structure, whether it is due to the weight of the soil above the structure, to a surface loading, or to lateral earth pressures. The ground adjacent to the inclusion can cause the subterranean structure to have a much greater load-carrying ability than an otherwise unburied identical structure. Consequently, the design of tunnels, caverns, culverts, shafts, conduits, and the like is not carried out solely on the basis of geostatic stresses as loads.

The proportion of the superimposed load that reaches the subsurface structure is governed by the characteristics of the soil, the geometry and stiffness of the structure, the free field stresses, and whether the loading is static or dynamic (McNulty, 1965 and Bulson, 1985). In many practical cases, the stress redistribution leads to a decrease in loading over the deflecting or 'yielding' areas of the structure as well as an increase over adjoining less deformable portions. Thus, the transfer of pressure has become known as "arching." The arching phenomenon in geomaterials with the presence of inclusions is analogous to the axial loading of composite materials, where the equality of axial strains gives rise to different axial stresses in dissimilar components.

Depending upon relative stiffnesses in the ground mass, arching can either be active or passive. Active arching, also sometimes called positive arching[2], occurs when the structure is more compressible than the surrounding soil, as illustrated in Figure 1-4. When the system is subjected to loads, the resulting stress distribution across planes of

[2]Although this phenomenon brings about a net decrease in load on the underground structure, the word "positive" is adopted by convention, perhaps due to the favorable consequence of such a load reduction.

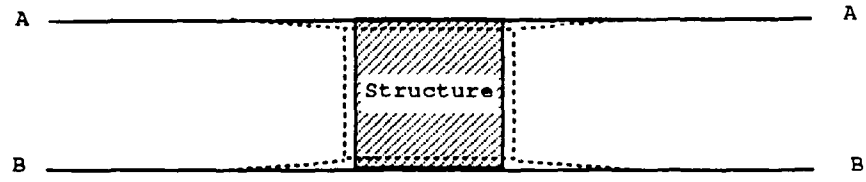

a. Deformations when structure is more compressible than surrounding soil

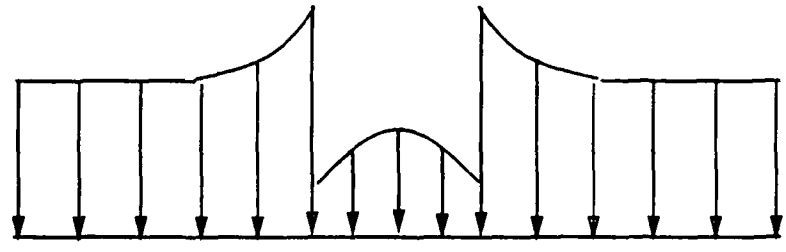

b. Stress distribution across plane AA or BB

Figure 1-4: Active arching

equal initial elevation (AA and BB) is similar to that shown in Figure 1-4b, where the stresses on the structure are less than those on the adjacent ground. If the inclusion deforms uniformly, the stresses on it tend to be lower toward the edges due to mobilized shear stresses in the soil.

Figure 1-5 shows the situation for passive, or negative, arching. Here the soil is more compressible than the structure, and therefore tends to undergo larger displacements, mobilizing shear stresses which increase the total pressure on the inclusion while decreasing the pressure in the adjacent ground. Assuming the structural deformations are uniform, the stresses are highest at the edges and lowest at the centerline.

If the geomaterial and the inclusion were to have identical constitutive (i.e, load vs. deformation) properties, under normal circumstances, the stresses along a horizontal layer would be fairly constant, and the distribution within the system would be linear and increasing with depth. No arching would be present in this case. The occurrence of such a situation is highly unlikely, simply because of the difference in mechanical characteristics between structural materials, like steel and concrete, and soils or rocks.

Most underground structures do not deform uniformly, and so the stress distributions are more complicated than those in Figures 1-4 and 1-5. A typical example is presented in Figure 1-6. The horizontal and vertical faces are more flexible towards the centers of the spans, resulting in the deformation patterns depicted. Thus, arching will be greater at the centers of the spans, leading to horizontal and vertical stress variations as shown. In this instance the faces of the structure are experiencing both active and passive arching simultaneously.

The word "arching" derives from the Latin *arcus*, for the shape of a bow, as in archery. Though many previous researchers have explained the observed non-hydrostatic pressure variations in soils as due to arching, they have seldom agreed on what the "arch" is quantitatively all about. Engesser (1882) postulates that the shape of the soil arch over an underground opening is a parabola with a slope at the sides equal to the friction angle of the granular medium. Terzaghi and Peck (1968) allude to a dome-shaped figure

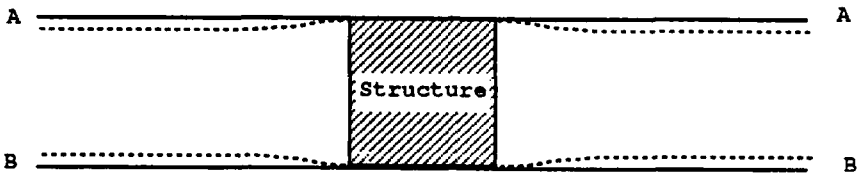

a. Deformations when structure is less compressible than surrounding soil

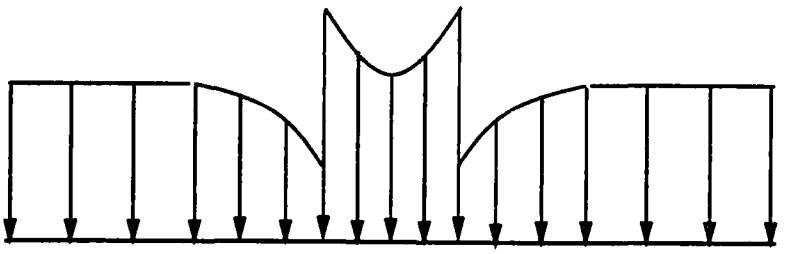

b. Stress distribution across plane AA or BB

Figure 1-5: Passive arching

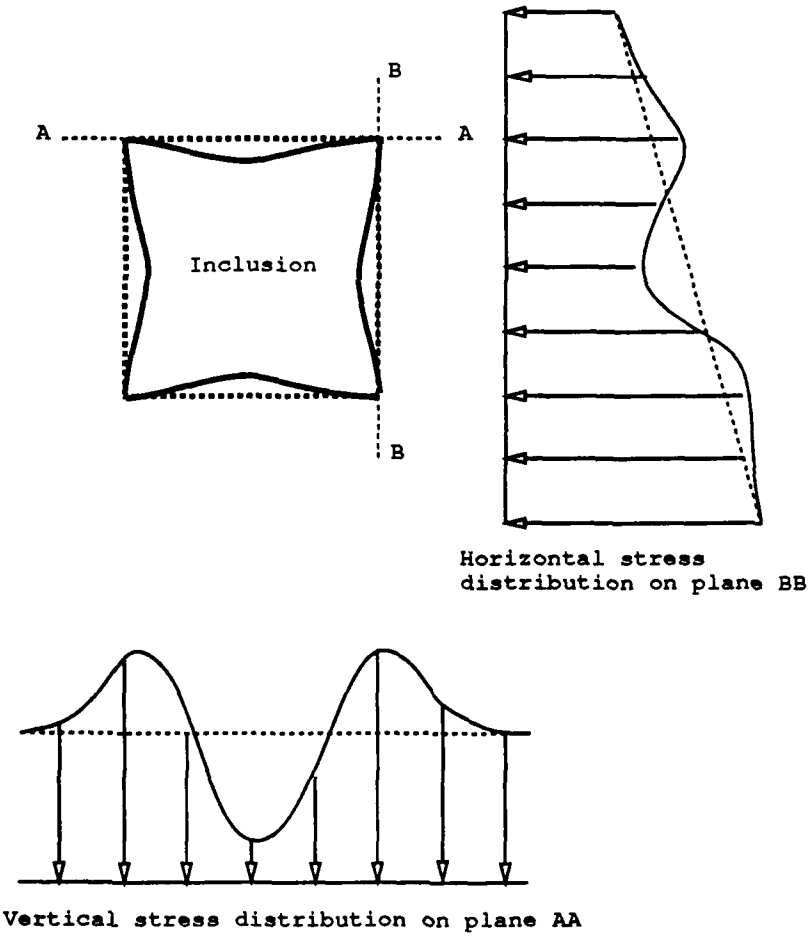

Figure 1-6: Typical deformation and stress patterns around a rectangular inclusion with flexible sides (from Evans, 1983)

in their classic book when they briefly discuss soil arching, although Terzaghi's (1943) theory assumes that the shearing resistance of the soil during arching (i.e., in his trapdoor experiments) is mobilized along vertical planes through the sides. Luscher and Höeg (1964) suggest arching as a "thrust ring action" in the soil surrounding an opening, and show the ring to be cylindrical. Handy (1985) notes that natural free-standing arches, such as Eskimo igloos, appear to follow a catenary, then presents an analysis – for arching behind retaining walls – which substitutes a catenary arch to describe the path of the minor principal stress. The current investigation will attempt to resolve these matters.

1.3 Scope of Work

There are two main aspects of this study: (1) scaling issues for geotechnical centrifuge models, and (2) arching in geomaterials. The bulk of the research task embodies a fair amount of experimentation with the trapdoor apparatus. Several tests with different model sizes of simulated jointed rock, as well as with granular soils, are performed. Square aluminum rods are laid out on top of the trapdoor to simulate the rock mass with uniformly-spaced joint sets; coarse sand and glass beads are the granular materials separately used to fill the model package. While most of the experiments are run at MIT, some of the tests with jointed media are done at the Ruhr-Universität Bochum (RUB) in Germany [Stone and Güttler (1989), Jessberger and Scherbeck (1990)] as part of a cooperative venture between the two schools.

Some theoretical calculations are carried out to help explain the results obtained from the various experiments. A reexamination of the theories put forward by previous investigators is a natural step in the process. Recommendations are then suggested on the applicability of the different theories.

The next chapter provides a review of preceding work on centrifuge modelling and other trapdoor experiments that have hitherto been conducted. Chapter 3 describes the details of the experimental setup, including the calibration procedures as well as dif-

ficulties encountered. The following two chapters give the results from the tests with granular media (Chapter 4) and with simulated jointed rock (Chapter 5). The theoretical aspects of the underlying mechanisms involved are discussed in Chapter 6. The conclusions drawn from this investigative effort are then presented in the final chapter. Appendix A is a summary listing of all the MIT centrifuge tests performed in connection with this research.

Chapter 2

Summary of Related Previous Work

2.1 Brief History of Centrifuge Model Testing

The beginnings of centrifuge modelling apparently date back to the 19th century when the French engineer Phillips (1869) suggested that a centrifuge be used to simulate self-weight stresses in structural beams. Since body force effects are relatively minor in beams and other similar structures, modelling with a centrifuge was not further pursued until an American, Bucky (1931), built one at Columbia University to study mining problems. At around the same time, two Soviet scientists, Pokrovsky (1933) and Davidenkov (1936), independently came up with very much the same idea.

The following couple of decades saw only a few centrifuge-related projects conducted in the United States, notably those by Panek and Clark in the fifties and sixties. Panek (1952) designed a centrifuge at College Park, Maryland for high-g testing [2-ft (0.61-m) radius, 90-lb (0.4-kN) payload at up to 2600g] and carried out experiments on bolted stratified mine roofs. Clark (1960-1963) supervised master's theses at the University of Missouri School of Mines involving centrifuge modelling, in a 3-ft (0.91-m) machine, of various geotechnical situations ranging from stability of rock slopes to behavior of mine openings.

In the Soviet Union, on the other hand, the centrifuge as a modelling tool has been

more frequently used, with more than 50 centrifuges built in a span of four decades for geotechnical model testing of dams, foundations, and earthfill embankments (Pokrovsky and Fyodorov, 1974). Many of these centrifuges were, however, dismantled after the completion of each project because the model tests were performed primarily to seek answers to specific design questions on particular projects. As a consequence, until recently, Soviet scientists have found it difficult to carry out the pure research necessary to verify the method of centrifuge modelling by experimental evidence.

Early centrifuge applications outside the U.S.A. and the U.S.S.R. were overseen by Hoek (1965) in South Africa to investigate the effect of gravitational force fields in mine models, and by Ramberg (1967) in Sweden to study gravity tectonics. In England, Schofield had a prototype machine in operation at Cambridge University by 1966 and, shortly after, ran soil mechanics experiments on a centrifuge, 2.7 m in radius, at the English Electric Company in Luton (Schofield, 1980). Schofield continued his work at the University of Manchester Institute of Science and Technology where he built a 1.5-m centrifuge in 1969 and initiated studies on excavations, bentonite-slurry-supported trenches, buried pipes and reinforced earth (e.g., Bolton et al., 1973). Rowe (1975) followed with a much larger capacity centrifuge in the mid-seventies at the Simon Engineering Laboratory of the University of Manchester to investigate foundation aspects of coastal and offshore structures.

Meanwhile, the United Kingdom Scientific Research Council approved in 1969 a proposal by Roscoe to build a machine with a 10-m rotor arm (4-m nominal radius) at Cambridge University. A few years after Roscoe's untimely death, this machine was completed in 1973 under the direction of Wroth and James. Management of geotechnical centrifuge operations at Cambridge was eventually turned over to Schofield upon his return from Manchester in 1974. Thereafter, centrifuge testing for soil mechanics problems flourished, with several professors from different countries visiting Cambridge to study the centrifuge technique. During this period, Canada, Denmark, France, Japan, and the Netherlands started setting up centrifuge modelling laboratories.

Subsequently, in the United States (Cheney and Fragaszy, 1984), there was a renewed interest in centrifuge model testing for geotechnical problems. Scott of the California Institute of Technology became actively engaged in centrifuge modelling in 1975 and advocated the construction of a very large centrifuge for geotechnical studies (Scott and Morgan, 1977), especially for dynamic problems. A small centrifuge was installed at the University of California at Davis in 1972 and replaced by a larger (1-m-radius arm) 44.5 $g \cdot kN$ centrifuge in 1976. Schmidt began cratering experiments on a 1-m-radius centrifuge at Boeing in 1976 and succeeded in verifying centrifuge scaling relations for cratering effects (Schmidt and Holsapple, 1980). Ko initiated centrifuge research at the University of Colorado in 1978 and has addressed issues related to underground tunnel construction, excavations in sand, and others (e.g., Ko et al., 1982).

Henceforth, many other US universities and research foundations, including MIT, have followed suit. A partial list of existing geotechnical centrifuge facilities in the United States is given in Table 2.1, which is based on a telephone survey conducted recently by Dobry and Elgamal (1989). Two centrifuges at the Sandia National Laboratories are not included in this list. One, called the Sandia 25 centrifuge, is among the largest in the Western world, with a 25-ft (7.6-m) radius, 8-ton (71.3-kN) payload, 240g maximum acceleration, and 800-g-ton (7127 g-kN) capacity. The other, a small-to-medium machine, the CA-2 centrifuge, has a radius of about 6 ft (1.83 m), maximum rated capabilities of 500 lb (2.23 kN) payload, 150g acceleration, and 15 $g \cdot ton$ (134 $g \cdot kN$) capacity. (These two centrifuges have been deliberately excluded from Table 2.1 because they are no longer considered active.) In addition, there are several other smaller installations being used, such as at the University of Kentucky, New Jersey Institute of Technology, and Ohio State University.

The status of geotechnical centrifuge research trends in the United States at present has been assessed by McWilliams (1989):

> "Currently there is considerable momentum towards geotechnical usage of centrifuges in this country. Cheney (1984) has printed an extensive bibliog-

Table 2.1: U.S. Geotechnical Centrifuges [from Dobry and Elgamal (1989)]

Size	Location	Centrifugal Acceleration (g)	Payload (lbs)	Capacity ($g \cdot ton$)	Representative Dimensions[a]		Comments
					Model (ft)	Prototype (ft)	
Large	U. California @ Davis	20	8,000	80	4	80	March 1989
		100	8,000	400	4	400	Summer 1989
	U. Colorado @ Boulder	200	4,400	440	3.3	660	Shaker Planned
Medium	RPI (N.Y.)	200	1,000	100	2	400	Shaker Planned
	Boeing (Washington)	600	400	120	1.5	900	Aerospace Appl.
Small	U. California @ Davis	100	200	10	1.2	120	With Shaker
	U. Colorado @ Boulder	100	300	15	1.3	130	With Shaker
	Caltech (California)	175	80	7.5	0.9	150	With Shaker
	Princeton U. (N. J.)	100	200	10	1.2	120	With Shaker
	U. Maryland	200	150	15	1.1	210	
	MIT (Massachusetts)	200	150	15	1.1	210	
	U. Florida	120	125	7.5	1	120	
	(2 centrifuges)	100	100	5	0.9	90	
	Tyndall AFB (Florida)	100	300	15	1.3	130	Military Appl.

[a] Representative Dimensions:

$$\text{Model} = (\text{Payload in } lbs/125)^{\frac{1}{3}}$$
$$\text{Prototype} = (\text{Model Dimension}) \cdot (\text{Centrifugal Acceleration})$$

raphy of centrifuge publications. There were 37 publications listed between 1931 to 1977, but in 1983 alone there were 32 publications. If the number of publications represents some measure of growth, then one can conclude that the amount of geotechnical centrifuge work is increasing at an almost exponential rate."

2.2 Centrifuge Modelling Principles

The scaling relationships involved in physical model testing with the centrifuge have been thoroughly discussed by several researchers: Bucky (1931), Pokrovsky and Fyodorov (1975), Scott and Morgan (1977), Schofield (1980), and Joseph et al. (1987), among others. The basic principles are reviewed in this section, starting with the classic remarks by Bucky (1931):

> "To produce at corresponding points in a small scale model the same unit stresses that exist in a full scale structure, the weight of the material of the model must be increased in the same ratio that the scale of the model is decreased with respect to the full scale structure. The effect of an increase in weight may be obtained by the use of centrifugal force, the model being placed in a suitable revolving apparatus."

The essential requirement, then, is that the stresses at geometrically similar points in the prototype and model should be the same. If the prototype and the centrifuge model are made of materials with identical mechanical properties, then, with identical stresses (σ), the strains (ϵ) in the prototype and in the model will also be identical. The strains can somehow be translated into deformations or displacements (δ) as follows:

$$\delta \approx \int_L \epsilon ds \tag{2.1}$$

in which the integration is performed over a characteristic length, L. Since the dimensions in the prototype are a scale factor N larger than those in the model, similarity of strains in model and prototype leads to

$$\delta_{prototype} = N \cdot \delta_{model}. \tag{2.2}$$

In other words, if a $\frac{1}{N}$ scale model of a prototype is spun at N gravities on the centrifuge, then the model's (scaled) mechanical behavior should resemble that of the prototype's.

2.2.1 Scaling Relations

There are other scaling relations that need to be fulfilled in centrifuge model testing to achieve similitude between model and prototype. These scaling relations can be determined in two ways: (1) by evaluation of the differential equations governing the behavior and (2) by dimensional analysis. In the first method, the governing equations are written for both the model and the prototype; then, with the model parameters expressed in terms of the prototype parameters, the two sets of equations are compared to obtain the scaling relations. The second method is based on Buckingham's (1914) Theorem [also called the Pi (Π) Theorem] and involves the identification of the dependent and independent variables of the phenomenon (without necessarily knowing the governing equations) and the formation of dimensionless products [or Pi (Π) groups] which should be the same for the model and the prototype. While the first method is suitable for cases where the governing principles and equations are well established, the second method is more general and can be used to explore situations in which the physics has not yet been fully understood. Joseph et al. (1987) present a comprehensive discussion of these methods and the derivation of scaling relations.

A summary of scaling relations for geotechnical centrifuge modelling is provided in Table 2.2. These scaling relations are generally valid only if the model is made of the same material as the prototype. One way of verifying the scaling relations is by creating models

Table 2.2: Centrifuge scaling relations (from Joseph et al., 1987)

Quantity	Symbol	$\frac{Model Dimension}{Prototype Dimension}$
1. For All Events		
Length	L	$1/N$
Displacement	u	$1/N$
Area	A	$1/N^2$
Volume	V	$1/N^3$
Mass	M	$1/N^3$
Density	ρ	1
Strain	ϵ	1
Force	F	$1/N^2$
Stress	σ	1
Energy	Π	$1/N^3$
Energy Density	π	1
2. For Dynamic Events		
Acceleration	a	N
Time	t	$1/N$
Velocity	v	1
Frequency	f	N
Strain Rate	$\dot{\epsilon}$	N
3. For Self-Weight		
Acceleration	a	N
4. For Diffusion Events		
Time	t	$1/N^2$
Velocity	v	N
Acceleration	a	N^3
Strain Rate	$\dot{\epsilon}$	N^2
5. For Laminar Flow through Porous Media		
Permeability	k	N
Head	L	$1/N$
Pressure	p	1
Hydraulic Gradient	i	1
Velocity	v	N
Flow Discharge	Q	$1/N$
Capillary Rise	D	$1/N$
Time	t	$1/N^2$
6. For Viscous Effects		
Force	F	$1/N^2$
Time	t	1
Velocity	v	$1/N$
Acceleration	a	$1/N$

at different scales and then performing the tests at the corresponding gravity levels. This scheme, as explained in the first chapter, is usually referred to as the *modelling of models* technique and is adopted in this study.

There are numerous instances where not all the similitude requirements are satisfied, in which case only the the most important parameters are usually considered. To achieve better model-prototype similarity in some situations, it may be necessary to alter the model material properties. A classic example is the liquefaction of soils during seismic shaking, where both dynamic – soil structure collapse and generation of pore pressures – and diffusion – eventual dissipation of pore pressures – components of the phenomenon are significant. From Table 2.2, there is an anomaly in the scaling of time between dynamic ($1/N$) and diffusion ($1/N^2$) events. According to Tan and Scott (1985), the correct approach to circumvent this difficulty is to utilize one time scale for modelling the whole process and a model fluid that is N times as viscous as the prototype fluid.

The use of the same material in the model as in the prototype implies that, for soils, the grain size is often kept the same in model and prototype. Strictly speaking, though, this disobeys the geometric scaling rule for length dimensions. Pokrovsky and Fyodorov (1975) contend that in most situations, the grain size is so small anyway, compared to the overall dimension of the model, that it seldom affects the macroscopic behavior significantly. A common question that crops up, then, is: how small can the model be before unscaled grain size begins to change the response of the model? Based on various tests of the *modelling-of-models* type, Fuglsang and Ovesen (1988) note that there seems to be no scale effect when the ratio of model width to grain size exceeds 25. This issue, however, has not yet really been fully resolved.

2.2.2 Errors Inherent in Centrifuge Testing

The ideal gravity field for modelling is an Ng field wherein the magnitude and direction does not change from point to point. In the centrifuge, the centripetal acceleration varies linearly with distance from the axis of rotation; consequently, the actual geostatic stress

variation is parabolic through the model depth, in contrast to the prototype where the distribution is linear. (Refer to Figure 2-1.) At the topmost surface, both model and prototype have zero total stress. Along the vertical axis of a typical cross-section, there is one other point at which the model stress equals exactly the prototype stress. Above this point, the model stress is less than the prototype stress; below this, the model stress is greater than the prototype stress. The difference in stresses is generally less than 2%, and, thus, it is neglected [Schofield (1980) and Joseph et al. (1987)].

The artificial gravity field generated in the centrifuge acts radially (Figure 2-2, and so the model geostatic stresses at two points at the same depth will generally not be the same, but the difference is usually negligible. Moreover, there exists a horizontal component (i.e., parallel to the platform of the model package) of acceleration that could be significant in some problems, e.g., slope stability, retaining structures, etc. In Figure 2-2, the g-field acceleration Ng at point A acts radially outward and can be resolved into components Ng_V and Ng_H. Along BD, normal to the shortest line from the axis of rotation O to the center of gravity C of the model package, the vertical component Ng_V remains constant while the horizontal component Ng_H is zero at C and varies linearly (Andersen, 1987). This horizontal component can attain values in the order of 10% of the nominal Ng, depending on the rotational speed and on the distance x of the point from OC. Consequently, for such tests, the effect of Ng_H should be taken into account.

Improper orientation of the platform as the centrifuge spins may also cause some errors. Most centrifuges are now constructed with a swinging bucket or platform for convenient placement of the model under initial gravity ($1g$) conditions. During rotation, the acceleration acting on the centrifuge platform, or on any mass resting on it, is the resultant of the (inertial) centripetal acceleration, $\omega^2 R$, and the earth's gravitational acceleration. Hence, the resultant acceleration vector makes an angle $\theta = \arctan(\frac{1g}{\omega^2 R})$ with the horizontal. A platform that is free to swing will rotate upwards until a line from the center of rotation to the center of mass of the platform and package is parallel to the resultant acceleration vector. Friction at the pivots may cause under-rotation

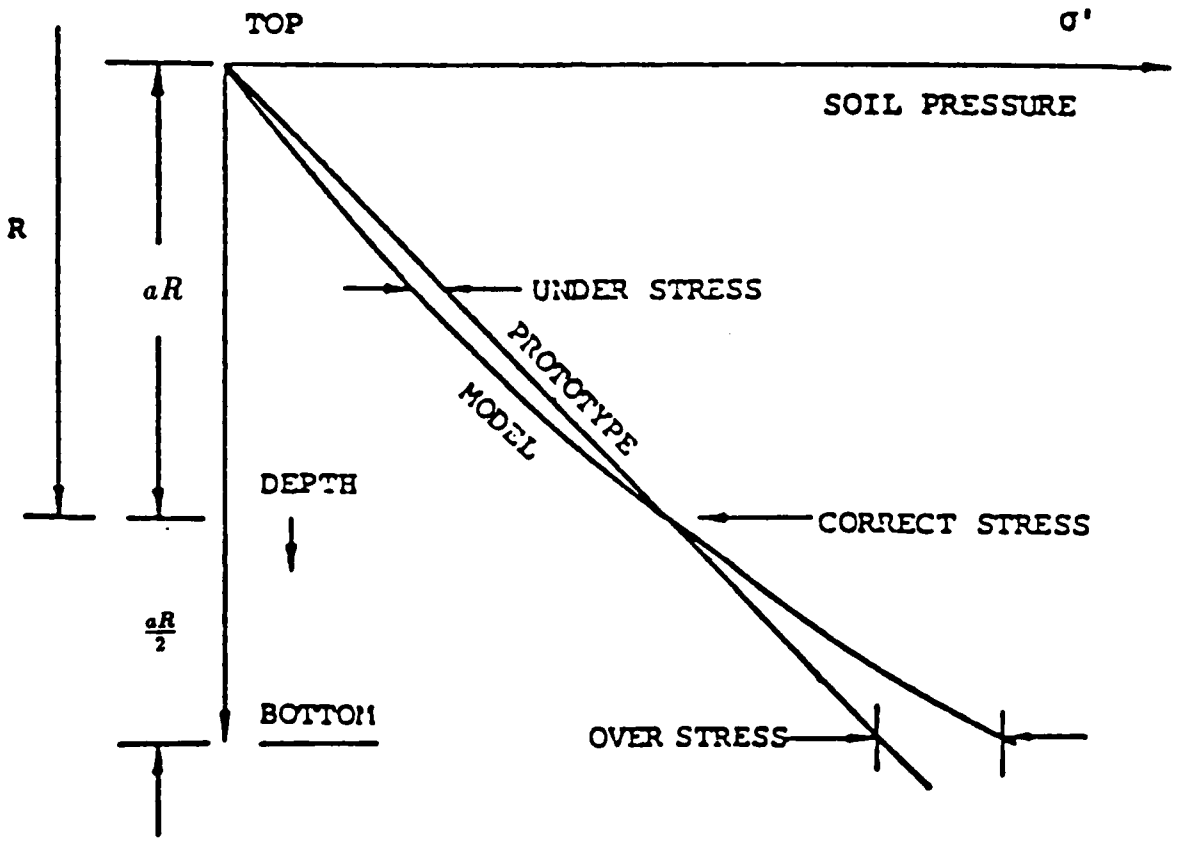

a: small fraction (e.g., $\frac{1}{15}$)

Figure 2-1: Model stress error with depth (from Schofield, 1980)

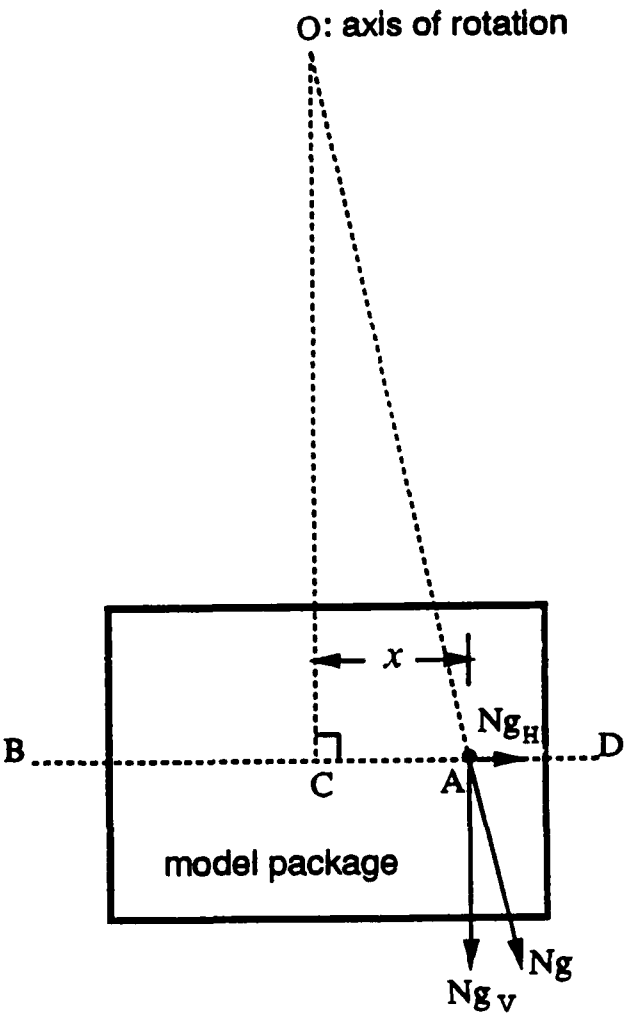

Figure 2-2: Components of the g-field

of the bucket, as in Figure 2-3. Also, if the center of gravity shifts its position during the test, then the platform orientation will change. Either of these situations will result in the acceleration vector not being perpendicular to the model ground surface. This error can be corrected (Bloomquist et al., 1984) by designing the bucket to over-rotate and then restraining it in the vertical direction by means of a bracket, or by using an accelerometer and a small motor to make slight changes in the platform orientation. (In the MIT centrifuge, no such correction scheme has been implemented, but the actual orientation of the bucket during an experiment is determined from two components of the acceleration vector measured by accelerometers installed at the platform base.)

Another potential source of error is the spin-up time or SUT – the time required to reach the desired acceleration when starting from rest. For geotechnical situations which do not depend on time, such as bearing capacity and slope stability for drained conditions, the results are not affected by the spin-up time. For some processes, however, such as sedimentation, large strain consolidation, and seepage, neglecting the SUT may lead to substantial errors. Bloomquist et al. (1984) present a simple correction procedure to account for the SUT in time-dependent cases. In essence, they suggest that the zero time in the model be adjusted such that the centrifuge scaling relations for time (Table 2.2) are fulfilled depending on the type of problem at hand.

A rather different type of error – due to Coriolis forces – occurs whenever there is model movement within the plane of rotation of the centrifuge arm. For a basic description of the Coriolis effect, consider a mass m moving radially at a constant rate v on a rotating carousel or turntable. Because of the rotation of the carousel, m does not move in a straight line, but in a curved path tangent to a diameter of the carousel at the center of rotation, as shown in Figure 2-4. In order for m to go along a curve, there must be a force to accelerate it in absolute space. This is the Coriolis force, which is always in the same direction, relative to the velocity, and of magnitude $2m\omega v$, where ω is the rotational speed. The apparent acceleration due to the Coriolis force is, then, $2\omega v$, and the error associated with Coriolis effects in a centrifuge environment can be

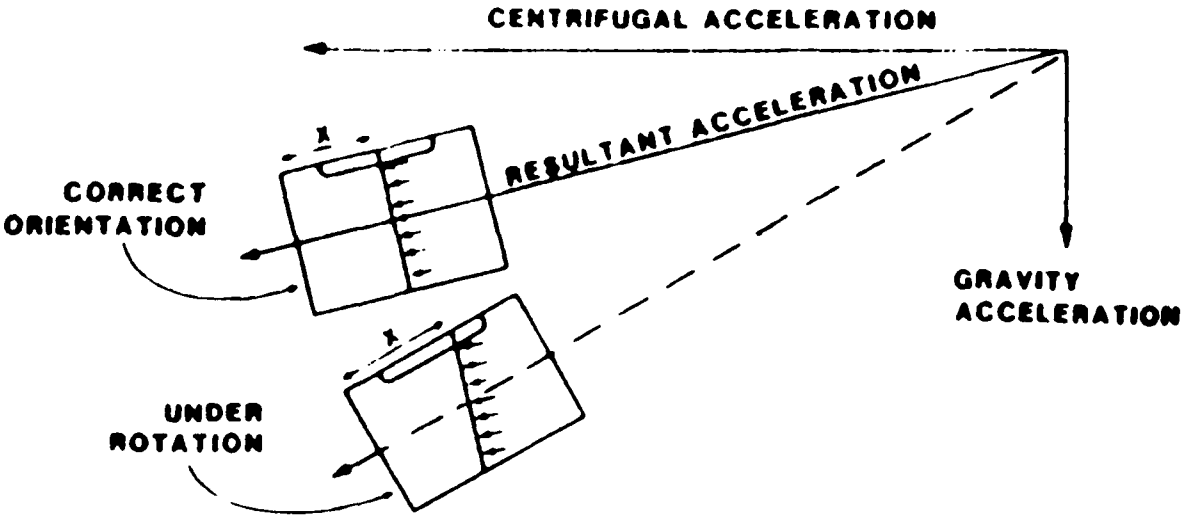

Figure 2-3: Bucket under-rotation due to pivot friction (from Bloomquist et al., 1984)

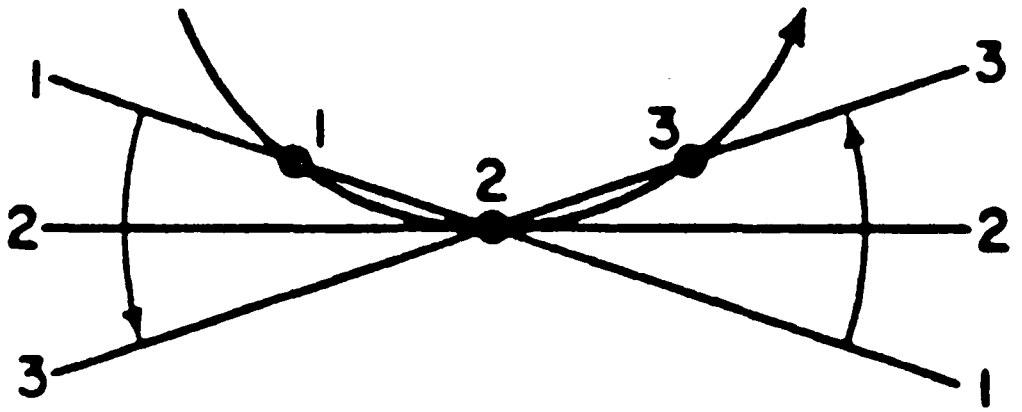

Figure 2-4: Three successive views of a point moving radially on a carousel (from Feynman et al., 1963)

estimated. This error may be significant in cases where the particle velocities in the model are extremely high, such as when explosions are involved. Under normal circumstances, however, the ratio of the Coriolis acceleration to the centrifuge acceleration is in the order of around 2% (Schofield, 1980).

There may be other errors, such as due to the swirling air in the centrifuge or to temperature and heat conduction effects, but these are considered to be negligible (Clark, 1981). Based on the foregoing, therefore, if the product of depth times the acceleration is the same in (centrifuge) model and prototype, the stresses at every corresponding point in a uniform model and prototype will, in general, differ by only a few per cent.

2.3 Previous Trapdoor Experiments

2.3.1 19th Century Tests

As mentioned in Chapter 1, several researchers have conducted experiments with a vertically translating trapdoor underneath a volume of soil to examine arching in geomaterials. The occurrence of arching in soils has long been recognized. Although it is present in many geotechnical scenarios, arching was first observed and investigated in a non-geotechnical context. During the early 1800's French military engineers were summoned to build magazine silos (Feld, 1948). They found that the base of the silo supported only a fraction of the total weight of material above it, and the side walls carried far more load than originally anticipated. Tests later showed that if a small section of the base were detached and lowered, the resulting load the section experienced was independent of the height of material in the silo. They concluded that an 'arch' had formed above this displaced section. In the latter part of the 19th century, this knowledge of the behavior within magazine silos was applied to the design of silos for grain and other particulate materials.

One of the earliest to perform trapdoor experiments with soil was Engesser (1882). His setup, displayed in Figure 2-5, consisted of a balance with the trapdoor on one end

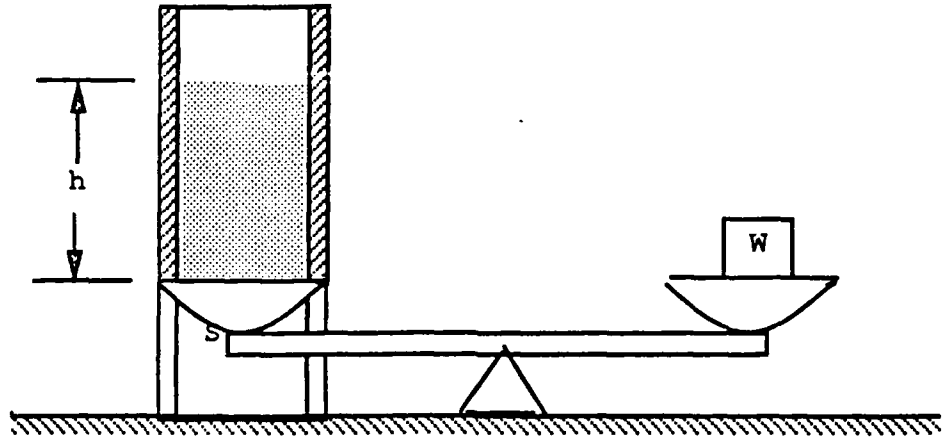

Plan View:

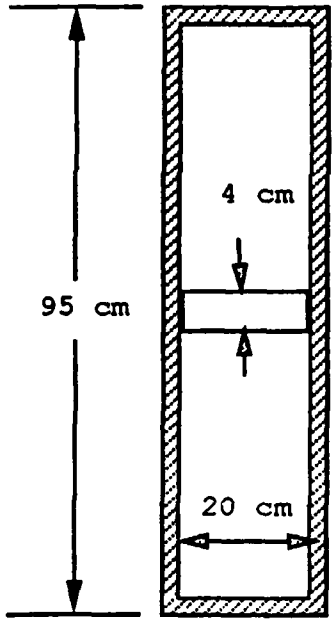

Results:

h (cm)	S (gm)
40	150
6	180
2.2	52

Figure 2-5: Engesser's (1882) trapdoor experiments

and a counterweight, W, on the other. The 95 $cm \times 20$ cm rectangular bin was filled to a desired depth, h, with sand (density $\rho = 1.5$ gm/cm^3, friction angle $\phi = 36.5°$), while ensuring through the counterweight that the 4-cm-wide trapdoor remained initially flush with the base of the container. Afterwards, the mass of the counterweight was reduced, causing the trapdoor to drop, and the chunk of soil (with mass S) that fell was collected and weighed. The tests were done for three depths of sand, and the results are tabulated in Figure 2-5. Engesser pointed out that the depth of overburden had to be greater than 1.5 times the width of the trapdoor for arching to occur.

2.3.2 Terzaghi's Investigations

The most widely known trapdoor experiments to examine the arching action in geomaterials were those reported by Terzaghi (1936) based on tests done by K. Kienzl in the former's laboratory in Vienna. Just as in Engesser's scheme, a trapdoor initially mounted flush with the base of a box containing sand (Figure 2-6) was moved downward to trigger arching in the soil. This time, however, the displacement of the door was monitored in addition to the total load on the door. The trapdoor measured 7.3 cm wide by 46.3 cm long, and the tests were conducted with both loose and dense ($\phi = 44°$) sand providing an overburden depth of about 31 cm. Horizontal and vertical stresses at various heights above the door were indirectly measured using the friction tape method. Figures 2-6a and 2-6b illustrate schematically the soil arching mechanism in the trapdoor setup, while Figures 2-6c through 2-6e show the principal results.

In Terzaghi's investigations, as can be seen in Figure 2-6c, the force on the trapdoor decreased rapidly as displacement commenced, with minimum values occuring at a displacement of only about 0.5% to 1% of the trapdoor width, depending upon the sand density. These minimum values were less than 10% of the overburden and tended to be lower for dense sand than for loose sand. After reaching the minimum value, the load increased slightly to about 13% of the overburden at a deflection of around 11% of the door width and remained fairly constant thereafter. Both tests with dense and loose sand

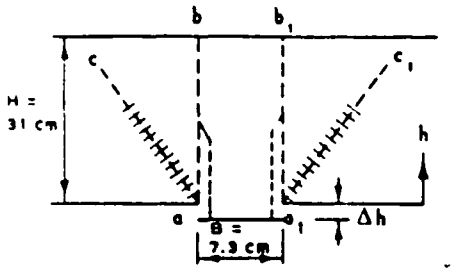

A. TEST SETUP AND SOIL BEHAVIOR ASSOCIATED WITH SMALL DEFLECTIONS

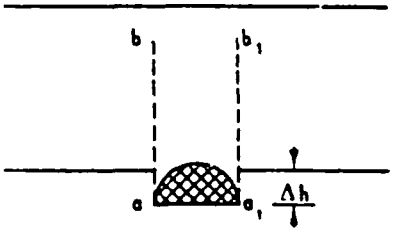

B. BEHAVIOR ASSOCIATED WITH LARGE DEFLECTIONS

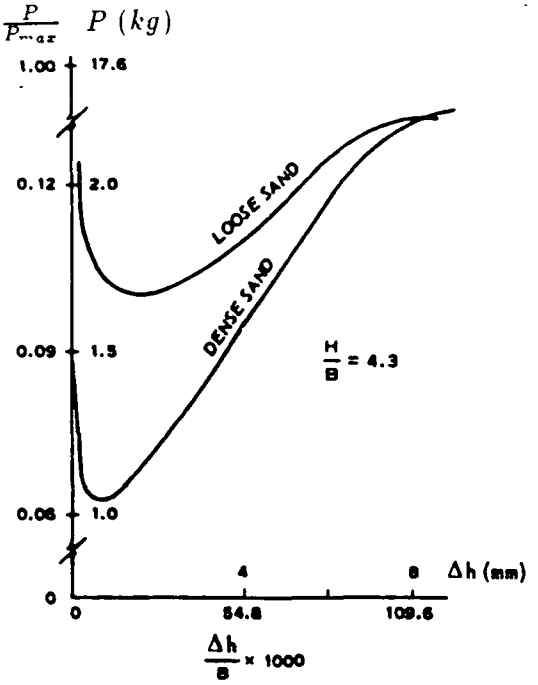

C. TRAPDOOR REACTION VS DEFLECTION

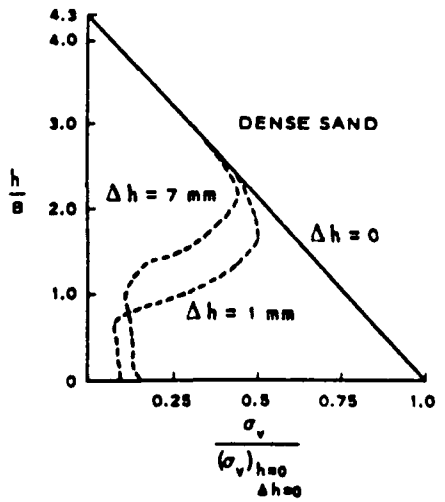

D. VARIATION OF VERTICAL SOIL STRESS ABOVE CENTER LINE OF TRAPDOOR

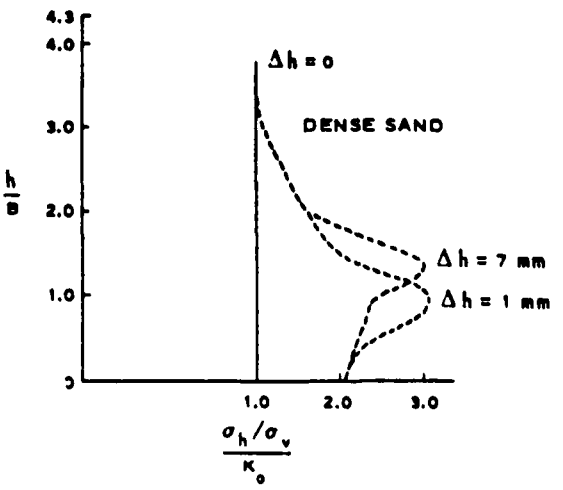

E. VARIATION OF EARTH PRESSURE COEFFICIENT ABOVE CENTER LINE OF TRAPDOOR

Figure 2-6: Terzaghi's (1936) trapdoor experiments (from McNulty, 1965)

registered the same magnitude of this ultimate trapdoor force.

The distribution of the vertical stress along the soil profile above the trapdoor at three values of door deflection is exhibited in Figure 2-6d; the corresponding variation of the coefficient of lateral stress (K), normalized with respect to the at-rest coefficient of earth pressure, K_0 ($\simeq 0.5$), is given in Figure 2-6. During deflection, the vertical stress above the trapdoor decreased greatly in the soil located less than three door widths above the trapdoor, while the ratio of horizontal to vertical earth pressure became as high as three times K_0 in the same region. When the door displacement got to about 1.4% of the door width, for instance, K was approximately 1.0 (or $2 \cdot K_0$) directly above the trapdoor and increased to 1.6 ($3 \cdot K_0$) at about one trapdoor width (B) above the door; at a distance of $3 \cdot B$ above the door, K was essentially equal to K_0. Terzaghi described K as an empirical constant and recommended that it be taken equal to 1.0 for analysis purposes.

The mechanism of the active arching recounted above has been explained as consisting of two stages, portrayed in Figures 2-6a and 2-6b. During the first, which corresponds to the reduction in the average trapdoor pressure from its geostatic value γH to its minimum value, the sand immediately above the trapdoor expands vertically and contracts horizontally, allowing the adjacent sand located in wedges b, a, c and b_1, a_1, c_1 in Figure 2-6a to expand horizontally and contract vertically. This subsidence causes a portion of the weight of the sand located between ac and a_1c_1 to be transferred by shear across the shaded areas to the motionless sand masses. The subsequent slight increase in trapdoor pressure to the ultimate value is associated with the disintegration of structure in the sand above the door due to excessive expansion and shifting of the planes of minimum resistance to positions ab and a_1b_1 in Figure 2-6b. Terzaghi and Peck (1968) have remarked that, with a trace of cohesion in the soil, the ultimate load on the trapdoor will not exceed the weight of a volume of soil represented by the shaded region in Figure 2-6b.

Terzaghi (1936) also presented some data from tests run by moving the trapdoor upward and downward in a cycle involving both passive and active arching. Hysteresis was very evident in both loose and dense sand tests. The initial portion of the passive

arching curve was linear, and had about the same slope as the initial portion of the active arching curve. Terzaghi also concluded that the state of soil stress associated with arching is not affected significantly by either seepage or "normal" vibrations.

2.3.3 McNulty's Experiments

To achieve stress levels commonly encountered in the field, McNulty (1965) applied air pressure at the surface of the sand in a Terzaghi-like trapdoor setup. He experimented with a circular trapdoor mounted flush with the bottom of a cylindrical soil chamber, allegedly in order to minimize the influence of sidewall friction. Both active and passive arching were dealt with separately as measurements were taken of the load acting on the trapdoor and the average upward or downnward displacement of the door. In addition, the effects of overburden depth, trapdoor diameter, surface pressure, and the constitutive properties of the soil were assessed.

Typical results from McNulty's series of axisymmetric tests are depicted in Figure 2-7. These data support previous observations that very small relative deflections can cause considerable changes in the load on the trapdoor. The load-displacement curves in the active arching cases indicate that the load reduction is greater as the depth of soil cover increases. In passive arching, the increase in load is greater as the burial depth increases, expecially at larger door displacements. McNulty has noted, however, that the influence of H/B on passive arching curves is minimal in the ranges of δ/B of interest in practical problems, i.e., if $H/B > 2$. He has also reported that the size of the trapdoor did not significantly affect the arching curves for the two trapdoor diameters considered [3" (76.2 mm) and 6" (152.4 mm)]. The surface pressure apparently has minor effect upon the shape of the arching curve for a particular soil, within the range of pressures applied [40-110 psi (28.2-77.5 kPa)].

In investigating the influence of soil properties, two sands were used. Sand 1 was Reid-Bedford Model sand - a clean, uniform, fine sand with $D_{10} = 0.16\ mm$ and average $\phi = 33°$; sand 2 was Cook's Bayou sand - a clean, uniform, medium sand with $D_{10} = 0.22$

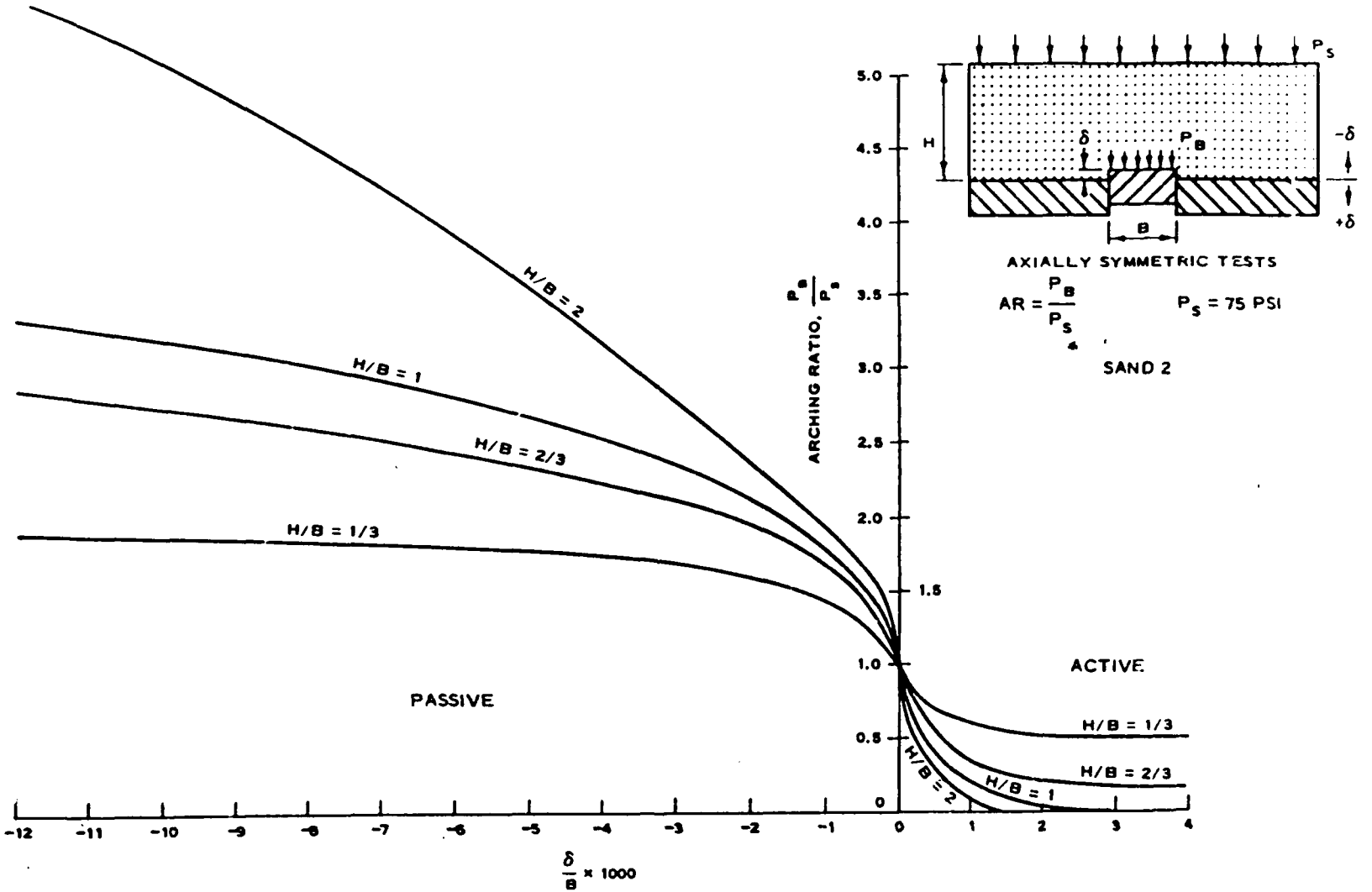

Figure 2-7: Active and passive arching curves (from McNulty, 1965)

mm and average $\phi = 38°$. The results for the active arching experiments with a surface pressure of 75 psi are summarized in Figure 2-8. The top plot shows that, throughout the range of comparable tests, sand 2 (the stronger soil) was capable of transferring more load than was sand 1. For H/B equal to 4, the ultimate arching ratios were almost the same, but it took sand 1 to reach this ratio twice the door deflection it did sand 2 (middle plot). For the shallower depths of cover ($\frac{H}{B} = \frac{1}{3}, \frac{2}{3}$), the ultimate arching ratios differed by about 10%, sand 2 exhibiting the lower value, although the trapdoor underwent the same displacement for both sands to develop the ultimate arching ratio. The similar behavior of the two sands at small values of H/B was attributed to the immediate attainment of a state of plastic equilibrium caused by a slight door deflection with shallow soil depths. The disparity at greater burial depths was then explained as due to the difference in the angle of internal friction, which was higher for sand 2.

2.3.4 Tests by Ladanyi and Hoyaux

Ladanyi and Hoyaux (1969) carried out an experimental program involving an ideal granular mass in plane strain overlying a model trapdoor (Figures 2-9 through 2-10). The geomaterial was simulated by a stack, 40" (1.02 m) high and 80" (2.03 m) wide, of aluminum rods supported by a U-shaped rigid steel frame. The rods were 2.5" (6.35 cm) long and of circular cross section, with two different diameters, viz. $\frac{1}{8}$" (3.18 mm) and $\frac{3}{16}$" (4.76 mm), mixed in equal proportions. After being cut to the required length, the aluminum rods were sanded in a sand drum in order to increase their roughness. The resulting granular medium had a unit weight γ of about 0.079 lb/in^3 (21.5 kN/m^3) and a friction angle ϕ of around $29 - 30°$ at the anticipated stress levels. (No surface pressure was applied, and so these stress levels were relatively low.) The "trapdoor" was actually a buried structure, 3" (7.62 cm) in width and 2.5" (6.35 cm) in length, represented by a rectangular rigid metallic box, which could be displaced up or down as a piston inside another larger box. In the tests, the pressure on the trapdoor was measured as a function of the vertical door movement, and the rod displacement trajectories were

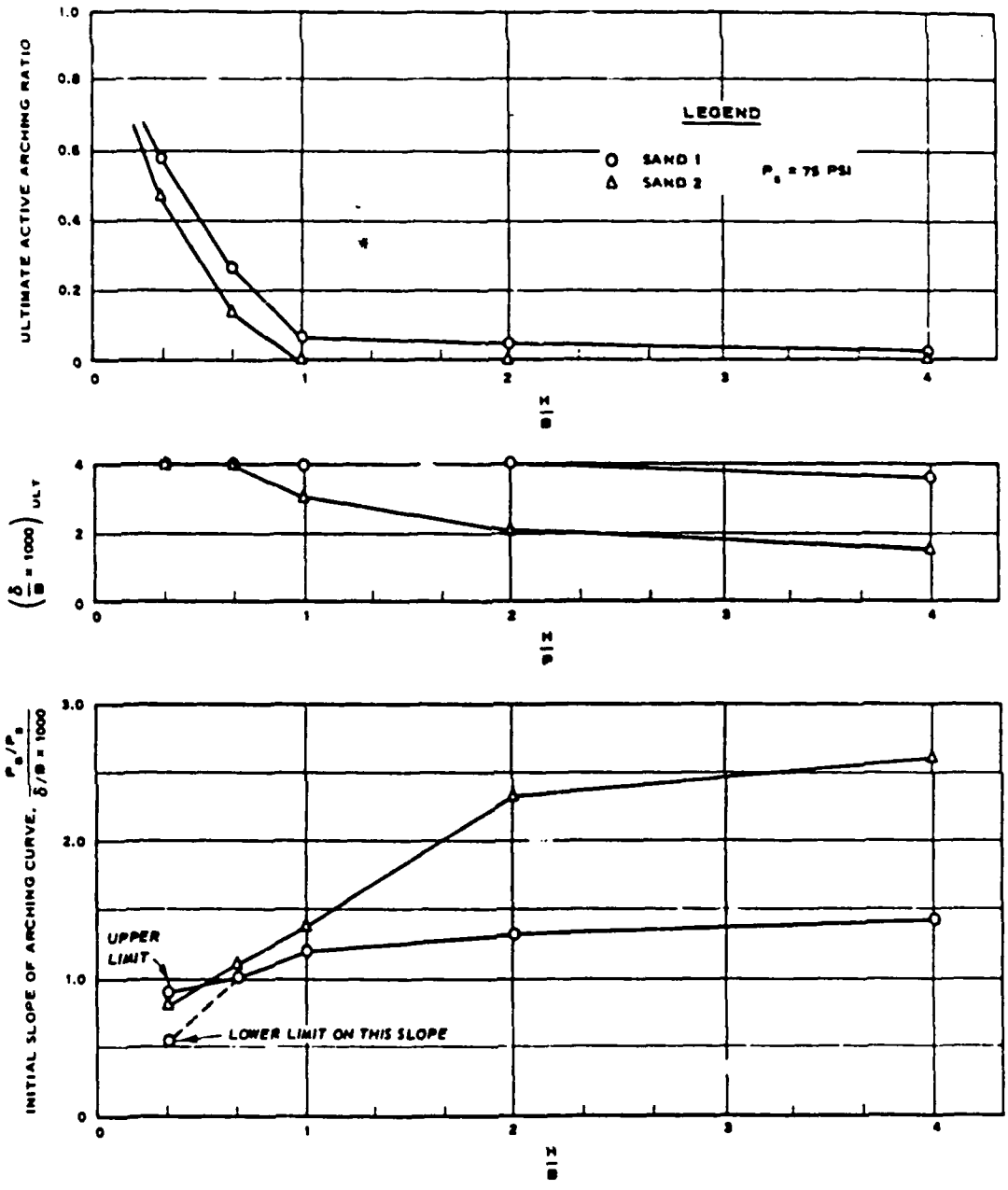

Figure 2-8: Influence of soil properties and depth of cover on active arching (from McNulty, 1965)

photographically recorded.

Photographic recording was executed in two different manners: either with a camera stationary with respect to the trapdoor, or with a camera fixed to the outside piston (and, thus, moving simultaneously with the door). Figures 2-9a and 2-9b are actual photographs taken with a stationary camera during one active arching case (Figure 2-9a) and one passive arching experiment (Figure 2-9b), both of which had the trapdoor starting from about the same original position. The moving granular mass can be seen to have a similar shape in both instances, though wider in the passive arching case. Figures 2-9c and 2-9d were shot with the camera moving simultaneously with the structure. A fixed wedge or "arch" formed in both door raising and lowering, but appeared more pointed in the latter.

By painting a 6" (15.24 *cm*) square mesh grid on the rod arrangement, a picture of the overall deformation pattern could be snapped after the door had translated by a certain amount [about 3.6" (9.14 *cm*) downward in Figure 2-10a]. It was observed that the deformation of the grid was well limited to a narrow tapering band overlying the trapdoor. Some lateral movement of the granular material towards the centerline was also visible near the structure, the mass tending to fill the space created by the settlement of the trapdoor.

The results obtained from four active arching simulations are shown in Figure 2-10b. The original depths of burial were 6" (15.2 *cm*), 8.5" (21.6 *cm*), 13" (33.0 *cm*), and 16" (40.6 *cm*), and the maximum displacement was 4" (10.2 *cm*). Like the earlier tests performed by the other experimenters, there was a rapid decrease of door pressure from its original geostatic value shortly after the lowering began. A minimum load was attained after a door yield of about 8% to 10% of the trapdoor width. With further door translation there was a gradual increase in pressure up to a sensibly constant ultimate value, which occured at a displacement of about half the door width. As in McNulty's experiments, the reduction in pressure due to active arching increased as the soil cover became deeper.

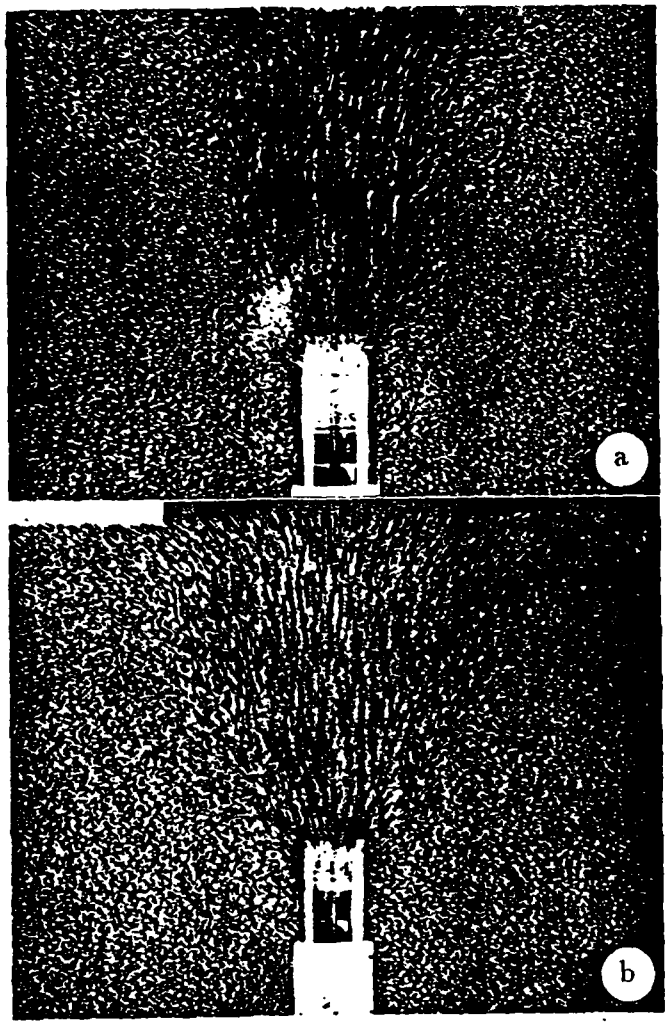

View of the displacement trajectories for (a) downward and (b) upward movement of the structure

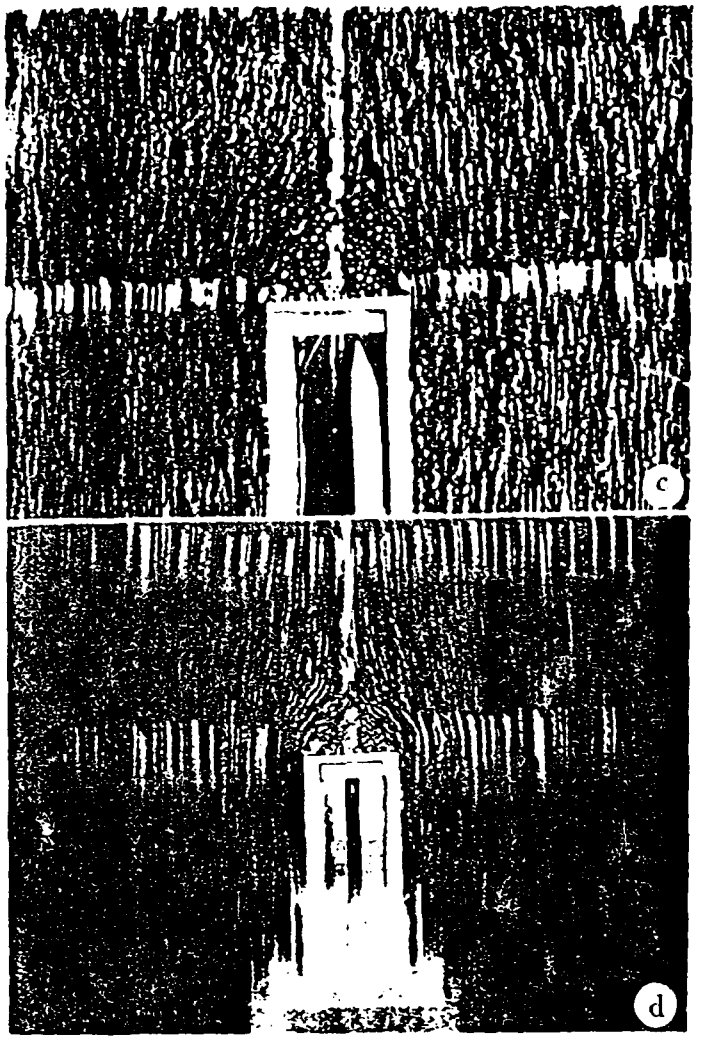

Wedge formation at the contact with structure during (c) downward and (d) upward movement of the structure

Figure 2-9: Ladanyi and Hoyaux's (1969) trapdoor experiments

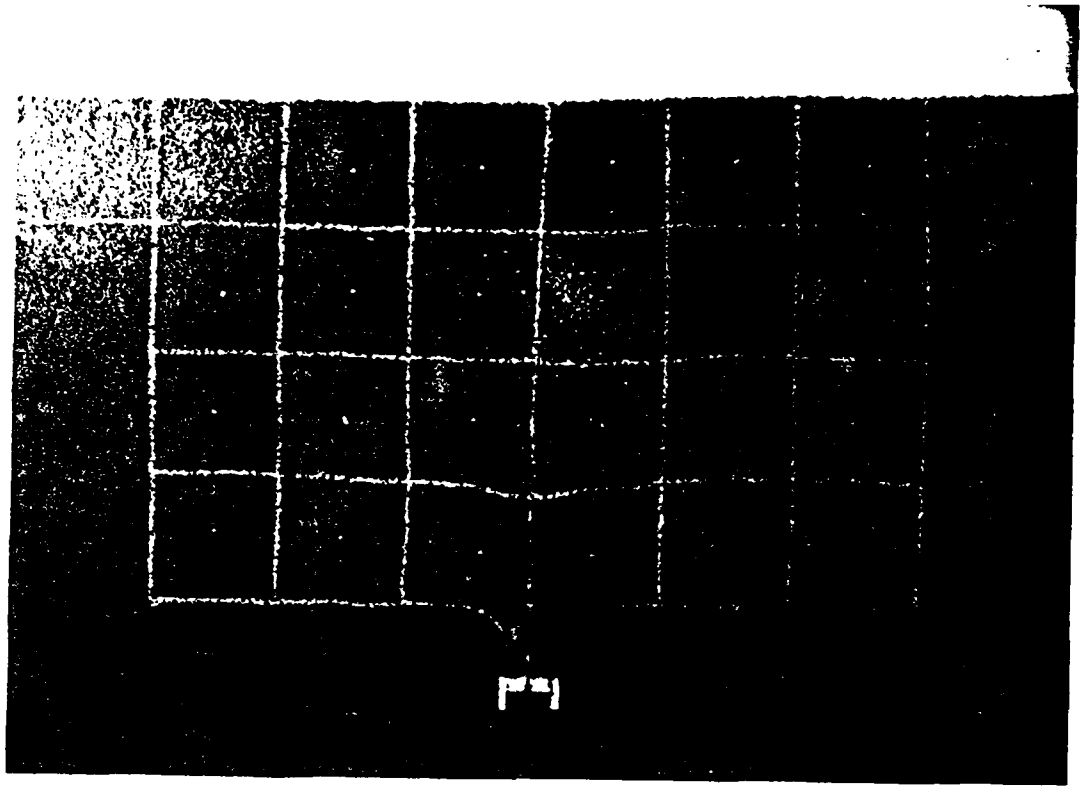

(a) Deformed square grid after a large downward movement of the structure

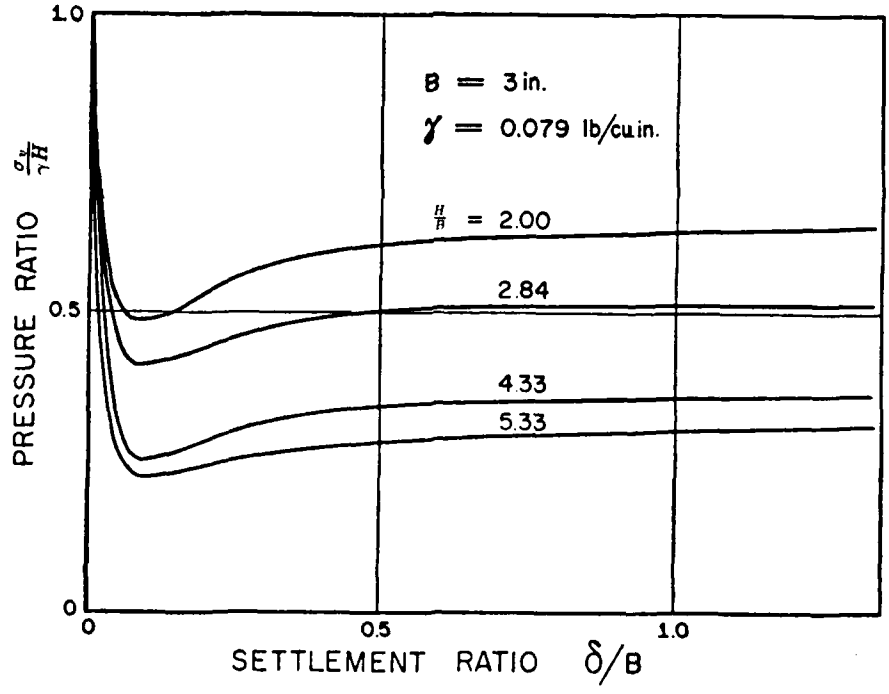

(b) Normalized pressure vs. settlement curves

Figure 2-10: Overall deformation pattern and active arching curves (from Ladanyi and Hoyaux, 1969)

2.3.5 Experiments by Vardoulakis et al.

In another plane strain setup, Vardoulakis et al. (1981) installed a trapdoor at the bottom of a box, 100 cm long, 15 cm wide, and 50 cm high, with parallel glass walls. Karlsruhe medium-grained sand ($d_{50} = 0.33\ mm$, $\phi = 34°$) was used, and both active and passive modes of arching were considered in the absence of surface pressures. Forces on the trapdoor, however, were not measured at all since wall friction was deemed difficult to eliminate and size effects due to progressive failure were expected. Only the deformation and failure mechanisms were then monitored in the tests by using thin horizontal colored sand layers deposited in the sand body. The displacement and failure patterns were recorded photographically.

Representative results are furnished in Figures 2-11a through 2-11d. Under active arching conditions, just soon after the initiation of trapdoor movement, a small dilatant zone – or "arch" – above the door was observed. Boundaries which separate the dilatant zone from the remaining material were clearly discernible. These boundaries started vertically at the edges of the trapdoor and converged successively to the symmetry axis (Figure 2-11a). With further lowering of the door, the dilatant zone expanded upwards to the free surface. The ultimate state was characterized by the formation of a failure region bounded by two vertical shear bands extending up to the free surface (Figure 2-11b).

For the passive arching mode, even a very small upward displacement of the trapdoor yielded a localization of the deformation into shear bands. Primarily two shear bands, which were almost symmetrical with each other about the centerline, proceeded from the edges of the door (Figure 2-11c) into the sand mass. Progressive shear band propagation was inferred from the gaps occurring at the thin colored sand layers due to the localization of deformations. Whether the shear band tip reaches the free surface or comes to a dead stop in the soil interior depended on the depth of overburden relative to the width of the trapdoor. After the shear bands have reached one of these final states, a new set of steeper shear bands was on the verge of moving upwards from the edges of the trapdoor (Figure 2-11d). These mechanisms reportedly excluded rigid body motions; for reasons

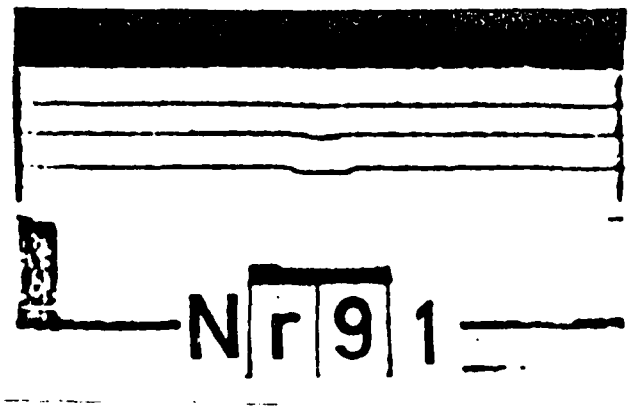

(a) Active mode, after small trapdoor displacements

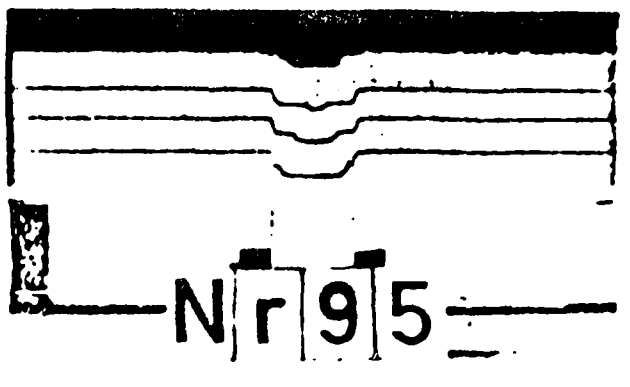

(b) Active mode, after large trapdoor displacements

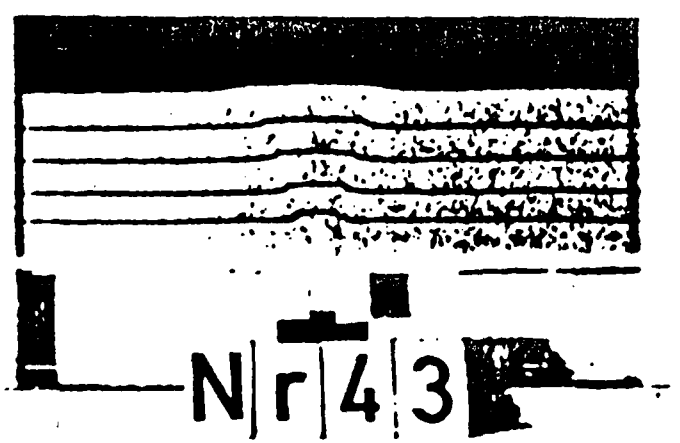

(c) Passive mode, after small trapdoor displacements

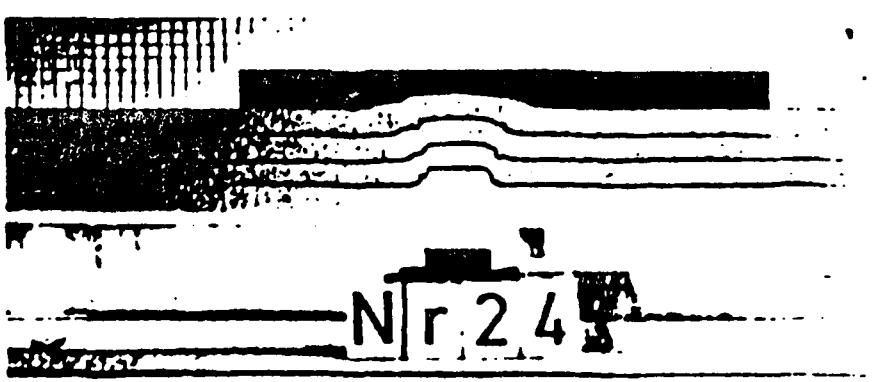

(d) Passive mode, after large trapdoor displacements

Figure 2-11: Vardoulakis et al.'s (1981) trapdoor tests

of kinematical compatibility there must have been a volume increase in the geomaterial. Vardoulakis et al. then claimed the consistency of continued dilatation in the sand mass with the formation of steeper secondary shear bands. In the final condition was the presence of vertical shear bands, implying a constant-volume deformation of the soil at failure.

2.3.6 Evans's Tests

To further explore the load redistribution process in buried structures, Evans (1983) conducted an extensive series of experiments involving: (1) active arching above a circular trapdoor, (2) active and passive arching above a rectangular trapdoor with plane strain boundary conditions, and (3) active arching above a row of trapdoors lowered in succession so as to simulate an advancing tunnel. Four types of sands were used, namely: (1) fine Leighton Buzzard (120/200) sand ($D_{60} = 0.120\ mm$, $\phi = 33°$), (2) coarse Leighton Buzzard (20/30) sand ($D_{60} = 0.905\ mm$, $\phi = 34°$), (3) medium tan sand ($D_{60} = 0.445\ mm$, $\phi = 38°$), and (4) fine white sand ($D_{60} = 0.165\ mm$, $\phi = 43°$). No overpressures were applied, but door pressure and displacement measurements were recorded, and the deformation patterns were photographed.

Figure 2-12a features the evolution of soil displacement patterns with increasing door settlement in a plane strain active arching test. A triangular shaped zone expanded vertically with noticeable dilation present. There was some lateral contraction, but it was largely compensated for by dilation. The door load vs. door displacement curve plotted in figure 2-12b typifies the active arching behavior observed. Vertical stresses decreased rapidly as door movement began, until they reached a minimum value. As door motion proceeded, the stresses increased somewhat up to a point where the displacement approached about 10% of the trapdoor width, at which the stresses became relatively constant afterwards. The overall behavior for the circular trapdoor experiments was consistent with that for the plane strain case, although the level of displacement necessary to mobilize full active arching was generally larger in the axisymmetric tests (3.5% vs.

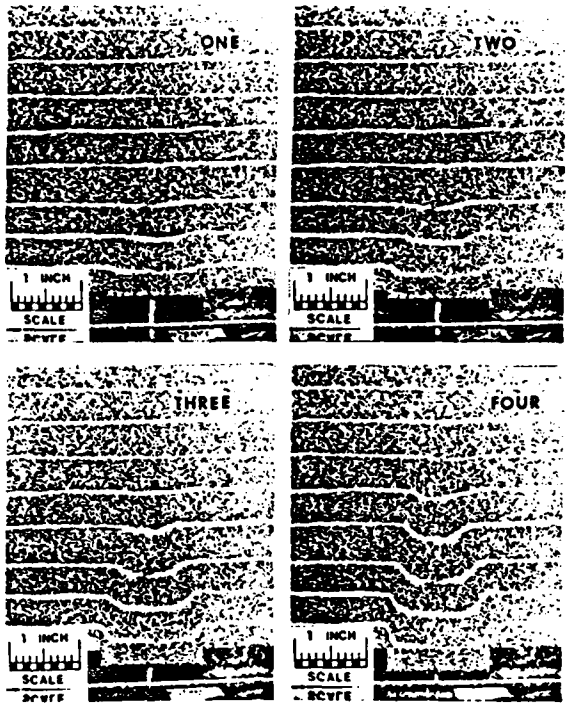

(a) Typical patterns of soil deformation

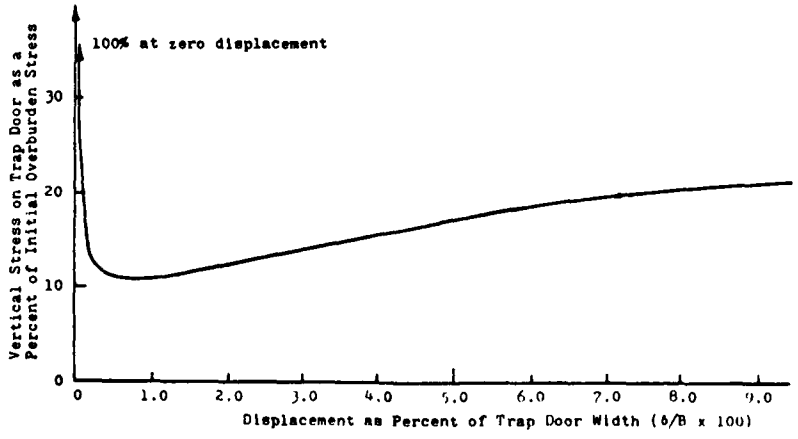

(b) Normalized stress vs. displacement plot

Figure 2-12: Evans's (1983) active arching tests

1.8% of the door width).

For the passive arching case, figure 2-13a exhibits the soil deformation patterns, while figure 2-13b presents typical data. Stress values rose swiftly as upward translation of the door started, eventually reaching a maximum before gradually decreasing. The amount of door displacement needed to obtain the largest stress change was practically the same for both active and passive modes (1.8% of the door width for active, 2.3% for passive). No constant threshold stress value, however, was achieved in the passive arching experiments for the range of displacements considered.

The tests with different sands produced generally similar results. The level of arching obtained was, however, affected by the value of the ratio of the overburden depth, H, to the trapdoor width, B. The percentage change in the door load increased as the H/B value increased.

A few tests to determine the coefficient of lateral earth pressure (K) were also performed by installing pressure transducers to measure both horizontal and vertical stresses just above the trapdoor. The at-rest coefficient, K_0, was found to be 0.51; then, as door displacement commenced, the vertical stress decreased rapidly while the horizontal stress remained nearly constant with only a slight decrease. This caused K to increase to a maximum value of about 1.2, occuring at a displacement of approximately 1% of the trapdoor width (corresponding, in general, to the displacement at which the stress reduction is a maximum in active arching tests). As displacements increased further, vertical stresses increased somewhat and horizontal stresses decreased, yielding lower K values. At large displacements K became constant at a value larger than K_0. Based on his observations, Evans recommended that a value of $K = 1.2$ be used for analyses purposes.

The simulations of an advancing tunnel by successive lowering of a series of trapdoors also yielded interesting results. Even at shallow depths, the "tunnelling" process caused redistribution of stresses more than one diameter in advance, at least $\frac{1}{2}$ diameter to each side, and $1\frac{1}{2}$ diameters behind the face. The results clearly showed that approaches which do not account for three-dimensional behavior will incorrectly model the stress

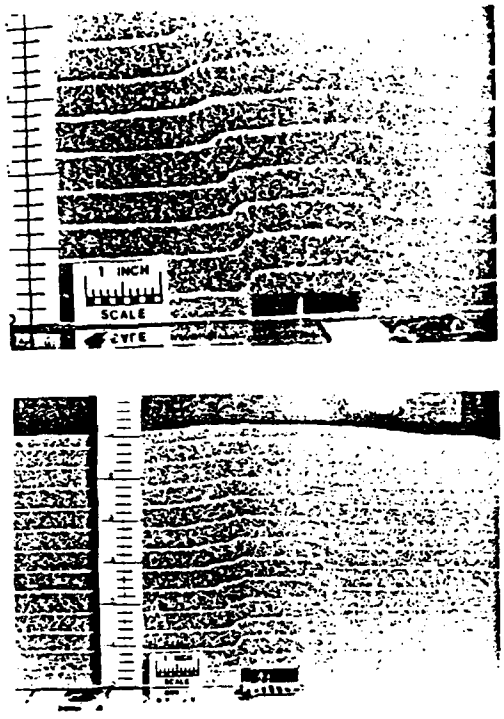

(a) Typical patterns of soil deformation

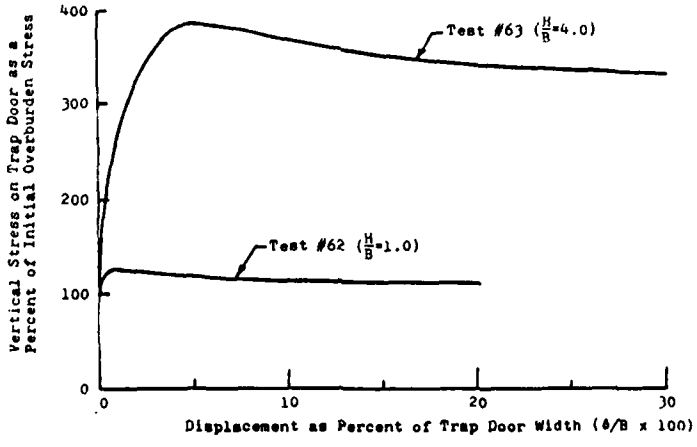

(b) Normalized stress vs. displacement plot

Figure 2-13: Evans's (1983) passive arching tests

redistribution in the vicinity of a tunnel's face.

2.3.7 Stone's Experiments

Stone (1988) was the very first to conduct trapdoor-type (plane strain) tests on a centrifuge. Leighton Buzzard sand in different sets of particle sizes was used in investigating the development of rupture in soils as well as scale effects. Deformation patterns were monitored in flight by obtaining film measurement data and photographs while the "trapdoor" underneath the geomaterial containing horizontal colored sand layers was displaced. Both active and passive arching situations were simulated, but no load measurements were taken. Experiments under normal gravity were also carried out, in which soil strain data were deduced from radiographs.

Typical results from the centrifuge tests are shown in Figures 2-14 through 2-16. The development of regions of localized deformation, shown through contours of maximum shear strain (Figure 2-14) and vertical displacement (Figure 2-15) for various increments of base translation, can be observed from these results. The initial stages of the experiment saw the formation of an inclined localization A (Figure 2-16b) associated with initial trapdoor settlement. During this phase, the maximum shear strain and vertical displacement contours resembled an arch-like shape. Subsequently, a secondary region of localized deformation (localization B, Figure 2-16b) developed which inclined steeply above the door. These results clearly show the developme t of an arch (which appears to be triangular) in the early stages of the test and the reorientation of the failure surfaces, approaching verticality, at larger door displacements. In the passive arching mode, on the other hand, no significant reorientation of the rupture surfaces was observed, and the final model configuration, as in Figure 2-17, reveals the formation of only one distinct rupture surface on each side of the trapdoor.

In general, the tests involving the finer particle sizes exhibited more complex patterns of localized deformation for the same degree of door movement. The formation of localizations in the finer sands was associated with smaller door displacements rather than

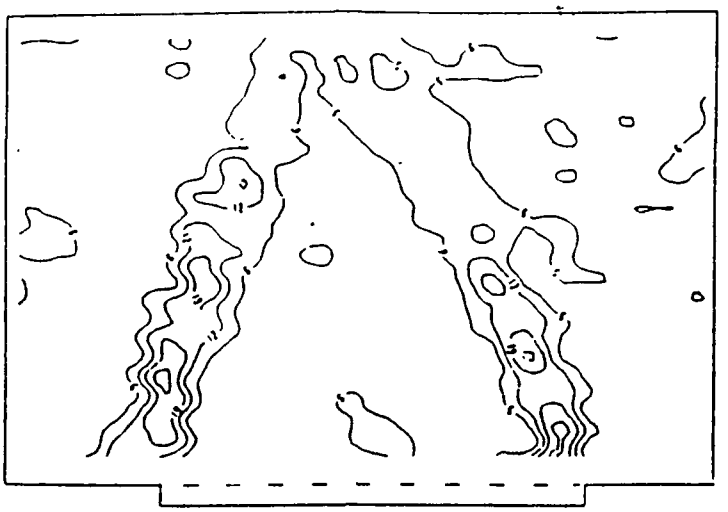

a) Test KS10, 14/25 sand; Δ_B=4.6 to 8.6 mm.

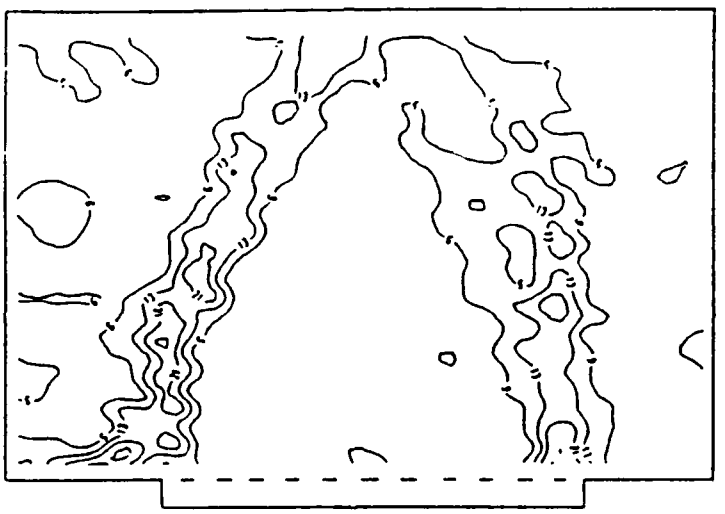

b) Test KS10, 14/25 sand; Δ_B=8.6 to 13.1 mm.

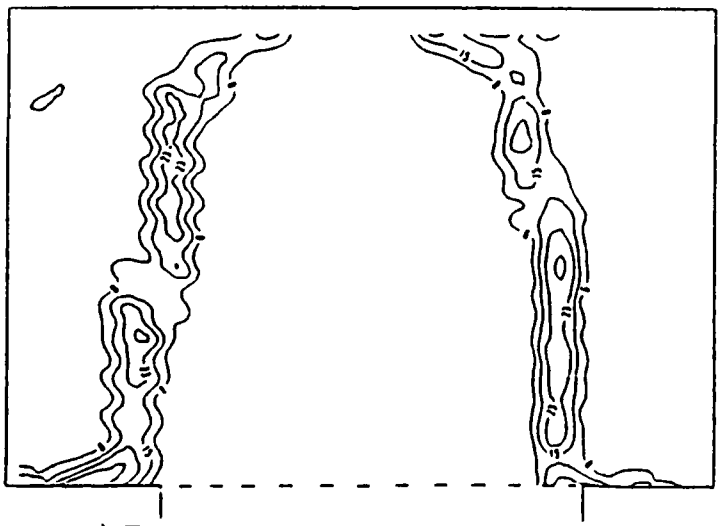

c) Test KS10, 14/25 sand; Δ_B=20.9 to 25.6 mm.

Figure 2-14: Maximum shear strain contours (from Stone, 1988)

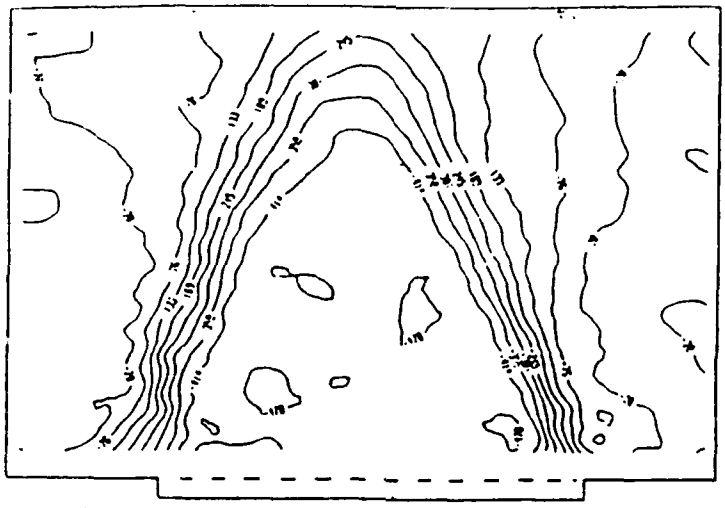

a) Test KS10, 14/25 sand; Δ_B=4.6 to 8.6 mm.

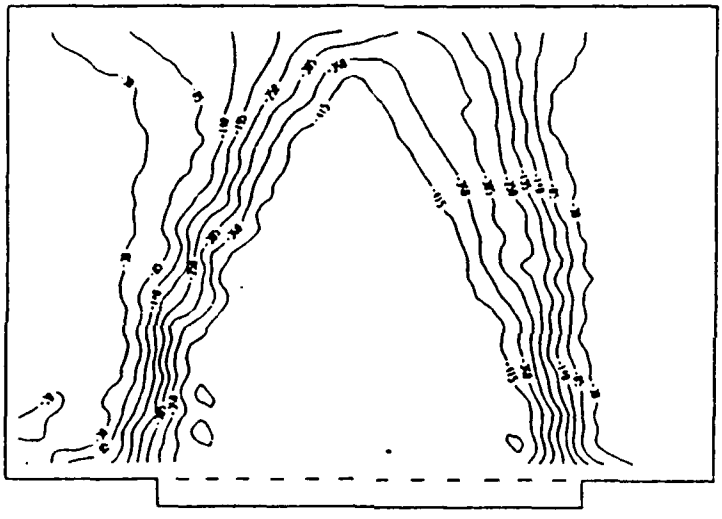

b) Test KS10, 14/25 sand; Δ_B=8.6 to 13.1 mm.

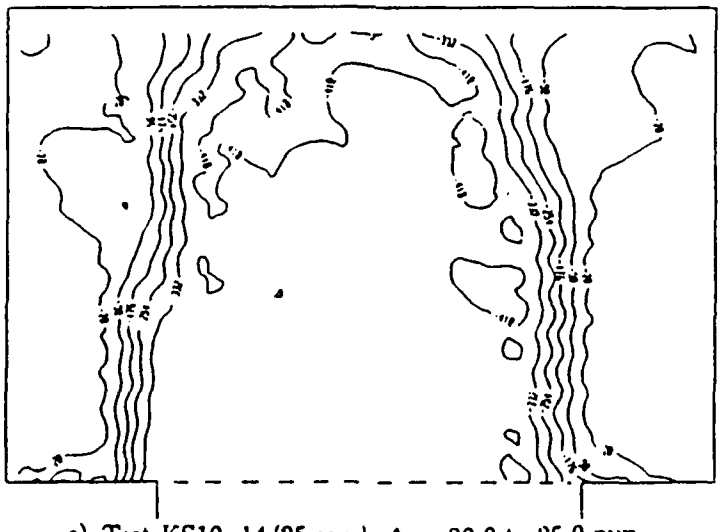

c) Test KS10, 14/25 sand; Δ_B=20.9 to 25.0 mm.

Figure 2-15: Vertical displacement contours (from Stone, 1988)

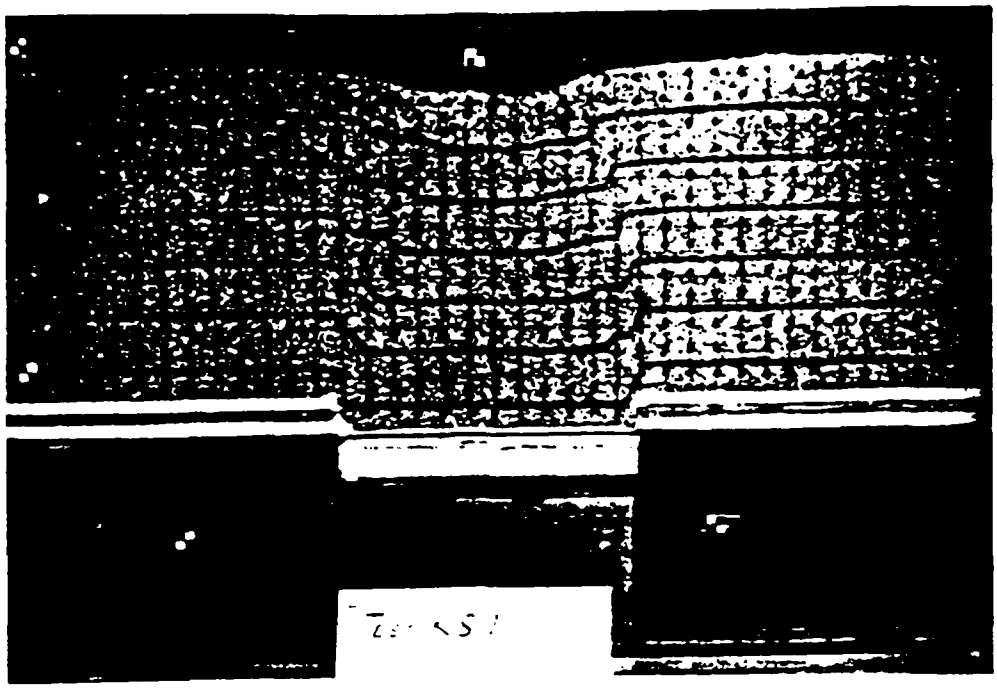

(a) Post-flight photograph

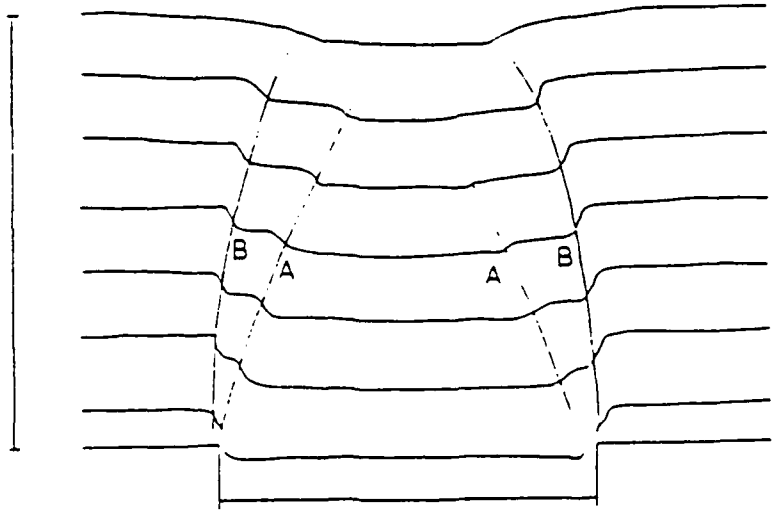

(b) Trace from final in-flight photograph

Figure 2-16: Overall deformation patterns (from Stone, 1988)

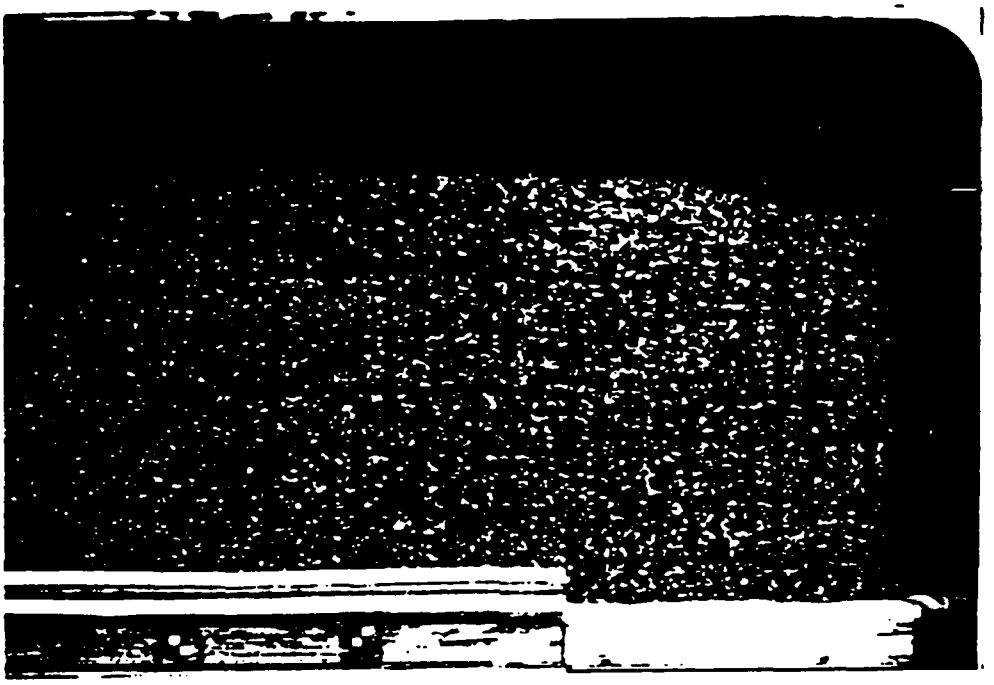

(a) Post-flight photograph

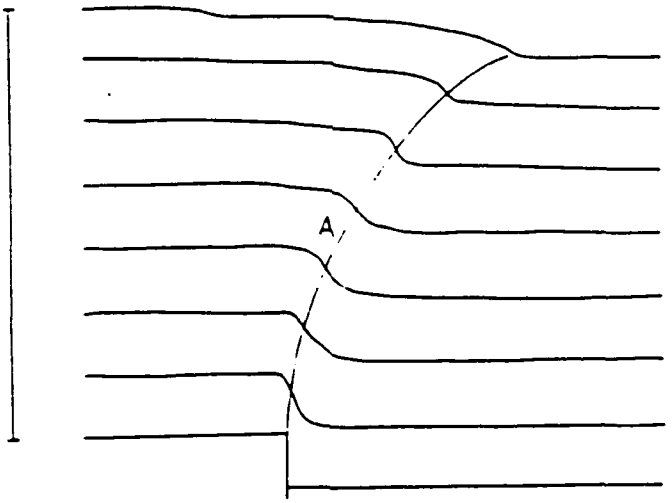

(b) Trace from final in-flight photograph

Figure 2-17: Passive arching test (from Stone, 1988)

with a similarity in behavior between fine and coarse sands. One can then expect that the fine sands would show deformation patterns similar to those of coarse sands only at the earliest stages of the experiments.

When the results from the centrifuge and single gravity tests were compared, the effect of stress level was seen to manifest itself in the directions and number of localizations that developed. (There were more rupture surfaces observed in the experiments performed at $1g$.) While the centrifuge can adequately scale the effects of stress level, Stone suggested, however, that the only satisfactory way to preserve similarity between the localization patterns in the model and prototype is to directly scale the grain size.

2.4 General Comments

The previous trapdoor experiments have supplied fascinating results about arching in soils. There is no question that arching – whether active or passive – occurs even with minute relative displacements in the ground mass. The load reduction in active arching can be quite substantial (up to about 95% of the geostatic stress), which can be beneficial for underground structures. The diminished loads are brought about by the localization of soil deformation around a relatively small region at sufficiently low values of displacement. In contrast, the passive mode involves pushing against the soil mass, mobilizing a larger deforming zone and thereby bringing about a load increase.

A comparative summary based on the past trapdoor tests is provided in Tables 2.3 (active arching) and 2.4 (passive arching). Soil arching behavior seems to be alike for most granular materials, as McNulty (1965) and Evans (1983) have found out, although Stone (1988) has observed this to be true only for small relative displacements. There is a wide disparity among the various test results in the magnitudes of door displacement ($\sim$0.11 mm to $\sim$7 mm) at which the load reaches its extremum value – even if these displacements were normalized with respect to the corresponding door widths. (This may be attributed to the difficulties involved with load measurements in trapdoor experiments,

Table 2.3: Previous trapdoor experiments, active arching mode

Geomaterial	B[a]	H[b]	Stress level	P_{min}[c]	δ_{min}[d]	P_{ult}[e]	δ_{ult}[f]
Engesser (1882): 1g, plane strain tests							
Sand, $\phi = 36.5°$	4 cm	40 cm	~4.0 kPa	0.031	NO DATA		
		6 cm	~0.6 kPa	0.25			
		2.2 cm	~0.2 kPa	0.20			
Terzaghi (1936): 1g, plane strain tests							
Loose sand	7.3 cm	31 cm	~2.7 kPa	0.10	1.6 mm	0.128	8.5 mm
Dense sand, $\phi = 44°$			~3.0 kPa	0.063	0.7 mm	0.128	8.5 mm
McNulty (1965): 1g, axisymmetric tests with applied surface pressure							
Sand 1, D_{10}=0.16 mm, $\phi = 33°$	15.2 cm	61.0 cm	~524 kPa	0.02	0.53 mm	0.02	0.53 mm
		30.5 cm	~521 kPa	0.03	0.61 mm	0.03	0.61 mm
		15.2 cm	~519 kPa	0.05	0.69 mm	0.05	0.69 mm
		10.2 cm	~519 kPa	0.25	0.61 mm	0.25	0.61 mm
		5.08 cm	~518 kPa	0.55	0.61 mm	0.55	0.61 mm
Sand 2, D_{10}=0.22 mm, $\phi = 38°$	15.2 cm	61.0 cm	~511 kPa	0.00	0.23 mm	0.00	0.23 mm
		30.5	~507 kPa	0.00	0.30 mm	0.00	0.30 mm
		15.2 cm	~706 kPa	0.02	0.53 mm	0.02	0.53 mm
			~513 kPa	0.00	0.46 mm	0.00	0.46 mm
			~274 kPa	0.00	0.38 mm	0.00	0.38 mm
		10.2 cm	~743 kPa	0.10	0.61 mm	0.10	0.61 mm
			~503 kPa	0.15	0.61 mm	0.15	0.61 mm
			~264 kPa	0.05	0.61 mm	0.05	0.61 mm
		5.08 cm	~760 kPa	0.40	0.69 mm	0.40	0.69 mm
			~500 kPa	0.45	0.61 mm	0.45	0.61 mm
			~259 kPa	0.45	0.53 mm	0.45	0.53 mm
	7.62 cm	15.2 cm	~502 kPa	0.00	0.23 mm	0.00	0.23 mm
		5.08 cm	~498 kPa	0.15	0.30 mm	0.15	0.30 mm
Ladanyi and Hoyaux (1969): 1g, plane strain tests							
Al rods, $\frac{1}{8}''\varnothing$ and $\frac{3}{16}''\varnothing$, $\phi = 30°$	7.62 cm	40.6 cm	~5.8 kPa	0.23	6.6 mm	0.30	76.2 mm
		33.0 cm	~4.7 kPa	0.25	6.6 mm	0.36	76.2 mm
		21.6 cm	~3.1 kPa	0.41	6.6 mm	0.52	76.2 mm
		15.2 cm	~2.2 kPa	0.48	6.6 mm	0.63	76.2 mm
Evans (1983): 1g, plane strain (PS) and axisymmetric (AS) tests							
PS							
Medium tan sand, $\phi = 38°$	11.4 cm	22.8 cm	~2.2 kPa	0.16	1.43 mm	0.221	13.2 mm
		11.4 cm	~1.2 kPa	0.315	0.11 mm	0.869	7.7 mm
	3.81 cm	19.1 cm	~2.0 kPa	0.091	1.0 mm	0.130	3.8 mm
		11.8 cm	~1.2 kPa	0.093	1.0 mm	0.217	3.4 mm
		7.62 cm	~0.8 kPa	0.16	0.19 mm	0.190	0.38 mm
AS							
Fine white sand, $\phi = 43°$	5.72 cm	18.3 cm	~1.6 kPa	0.054	2.51 mm	0.078	7.0 mm
		10.3 cm	~1.4 kPa	0.082	4.97 mm	0.148	14.0 mm
Fine LB sand, $\phi = 33°$	5.72 cm	9.14 cm	~1.2 kPa	0.096	1.83 mm	0.170	15.6 mm
		5.14 cm	~0.7 kPa	0.157	1.71 mm	0.258	15.4 mm

[a] Width of trapdoor
[b] Depth of cover
[c] Minimum door load as a fraction of the initial geostatic force
[d] Door displacement at which the minimum load is attained
[e] Ultimate door load attained, as a fraction of the initial geostatic force
[f] Door displacement at which the ultimate load is attained

Table 2.4: Previous trapdoor experiments, passive arching mode

Geomaterial	B^a	H^b	Stress level	$P_{max}{}^c$	$\delta_{max}{}^d$	$P_{ult}{}^e$	$\delta_{ult}{}^f$
McNulty (1965): $1g$, axisymmetric tests with applied surface pressure							
Sand 2, D_{10}=0.22mm, $\phi = 38°$	15.2 cm	30.5 cm	~504 kPa	10.0	7.62 mm	10.0	7.62 mm
		25.4 cm	~507 kPa	6.00	3.05 mm	6.00	3.05 mm
		20.3 cm	~503 kPa	4.50	2.29 mm	4.50	2.29 mm
		15.2 cm	~508 kPa	3.60	2.29 mm	3.60	2.29 mm
		10.2 cm	~510 kPa	3.00	1.98 mm	3.00	1.98 mm
		5.08 cm	~502 kPa	1.95	1.52 mm	1.95	1.52 mm
	7.62 cm	15.2 cm	~502 kPa	10.0	3.81 mm	10.0	3.81 mm
		5.08 cm	~505 kPa	3.00	0.99 mm	3.00	0.99 mm
Evans (1983): $1g$, plane strain tests							
Medium tan sand, $\phi = 38°$	3.81 cm	15.2 cm	~1.4 kPa	3.43	2.74 mm	2.76	11.4 mm
		11.4 cm	~1.3 kPa	2.56	2.86 mm	—	—
		7.62 cm	~0.8 kPa	2.01	2.49 mm	—	—
		4.95 cm	~0.4 kPa	1.27	0.63 mm	1.12	5.23 mm
		4.57 cm	~0.4 kPa	1.14	0.23 mm	1.08	4.11 mm
		3.81 cm	~0.4 kPa	1.33	0.69 mm	1.17	7.62 mm
Fine LB sand, $\phi = 33°$		5.33 cm	~0.5 kPa	1.28	0.06 mm	1.17	7.52 mm
		4.95 cm	~0.5 kPa	1.24	0.29 mm	1.08	5.23 mm

[a] Width of trapdoor
[b] Depth of cover
[c] Maximum door load as a fraction of the initial geostatic force
[d] Door displacement at which the maximum load is attained
[e] Ultimate door load attained, as a fraction of the initial geostatic force
[f] Door displacement at which the ultimate load is attained

such as friction at the door edges, relative stiffnesses, etc.)

Conflicting statements have also been made regarding the effect of stress levels. According to McNulty (1965), the influence of stress levels (overpressures) on soil arching is minimal, but Stone (1988) has reported otherwise. There seems to be a distinct difference in the overall shape of the arching curves between those with high stress levels and with low stress levels. In the experiments with applied surface pressures, the load on the door tends to remain constant when the extremum value is reached. In the tests without overpressures, the load increases after the minimum (active arching) value is attained, while it decreases to an ultimate value after the maximum (passive arching) value is reached.

Finally, there are no known trapdoor experiments with jointed media preceding this investigation. Beyond the *modeling-of-models* exercise, therefore, the quantitative results obtained from the tests with simulated jointed rock should add to the better understanding of shearing along planar surfaces.

Chapter 3

Experimental Arrangement

The trapdoor apparatus in the present study is basically similar to the plane strain arrangements used in the other studies described in Chapter 2. It consists of a horizontal strip, or trapdoor, underneath the geomaterial, with a vertical downward movement of the door simulating the deflection of a flexible support relative to the adjacent mass. The resulting change in the load on the door with increasing displacement is then observed in the test. Unlike the past setups, however, the trapdoor load and displacement in this research are measured while the apparatus is spinning at a predetermined speed on board the centrifuge. In the following, the details of the test packages at MIT and RUB are described.

3.1 MIT Setup

The essential features of the experimental apparatus at MIT are presented in Figure 3-1. The movement of the trapdoor is achieved by means of a system of wedges. The lower wedge is pulled by a motor-driven rod through a gear box assembly, causing the upper wedge, which is restrained laterally, to slide down at a vertical displacement rate of $\sim 0.018\ mm/sec$.

The vertical force on the trapdoor is measured by load cells installed between the

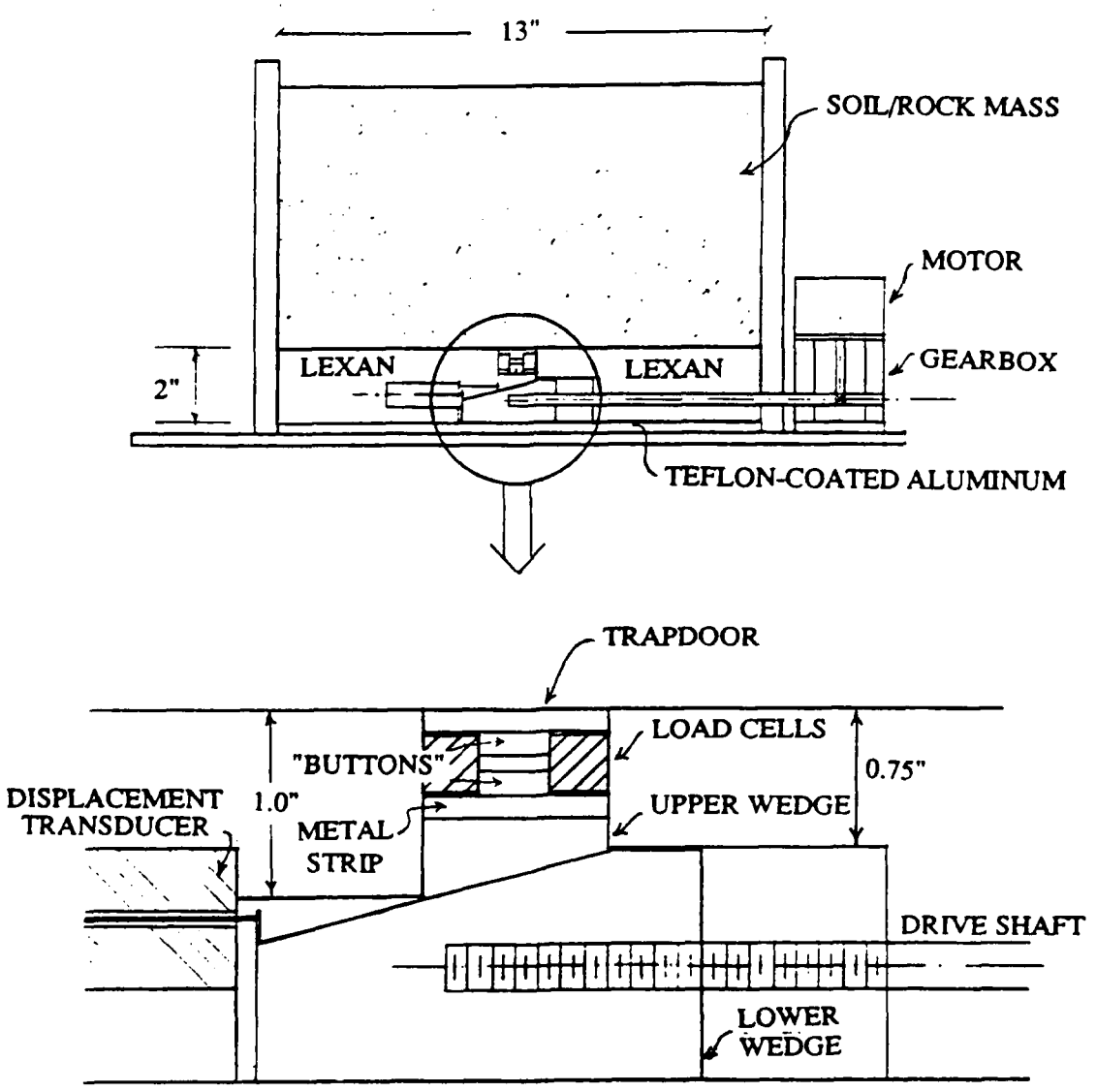

Figure 3-1: MIT trapdoor apparatus

trapdoor and the upper wedge. These load cells are of the (commercially available) washer type, as shown in Figure 3-2, and have a capacity of 1000 lb (4.45 kN). Inside each washer is a thin tube, around which four (4) strain gages are placed 90° apart. One diametrically opposite pair of these strain gages is designed to measure the vertical load, and the other pair, the horizontal load.

The displacement of the door is monitored by a transducer, the probe of which is attached to the lower wedge through a tiny connector which protrudes vertically at the toe of the wedge (Figure 3-1). (Note that the measured displacement is the horizontal movement of the lower wedge; the vertical translation of the trapdoor can be computed from simple geometric relations.)

In the course of the construction and completion of the apparatus, several modifications were deemed necessary for the reliable performance of the motor-gear-shaft system and the measurement devices. Initially, the upper wedge was created from the same lexan piece – to reduce weight – as the lower wedge and the general substructure. The lower wedge was supposed to slide over a $\frac{1}{8}''(3.18\ mm)$-thick teflon sheet – having relatively low friction – on top of a $\frac{1}{4}''(6.35\ mm)$-thick aluminum plate. The problem with the teflon sheet was that the material compressibility and gross non-uniformities in the plate thickness caused alignment difficulties which hampered system operation at high g's. Eventually, the teflon/aluminum base was replaced by a $\frac{3}{8}''(9.52\ mm)$-thick teflon-coated aluminum plate. The upper wedge material was then changed from lexan to teflon-coated aluminum – to ease up the sliding between wedges. The most significant alteration, however, involved the rearrangement of the load cells and the manner in which the trapdoor is supported and transmits the load onto the force transducers, as discussed below.

3.1.1 Original Load Cell Setup

Three (3) steel (flat ground die stock) segments originally comprised the trapdoor. In the early stages, one (1) 6-$inch$(152.4-mm)-long segment was placed in between two (2) 2-$inch$(50.8-mm)-long segments. (Refer to Figure 3-3.) Load Cells 1 and 4 were

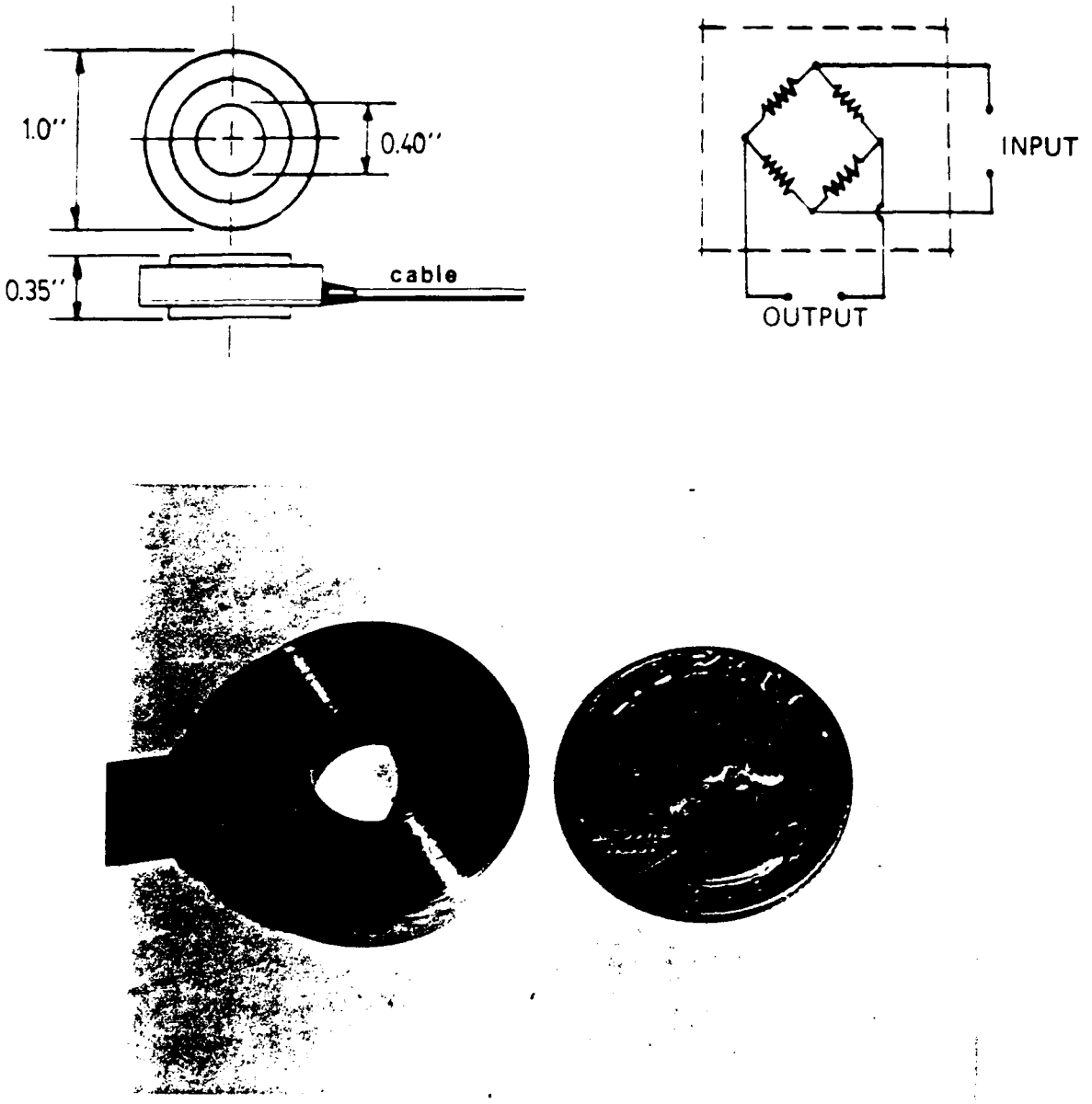

Figure 3-2: Load cell used at MIT

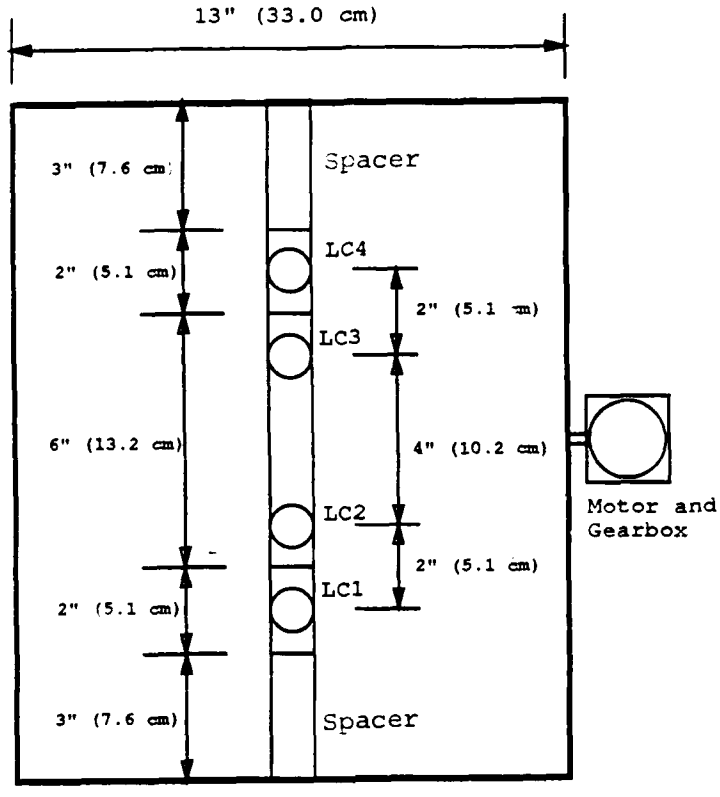

Plan view

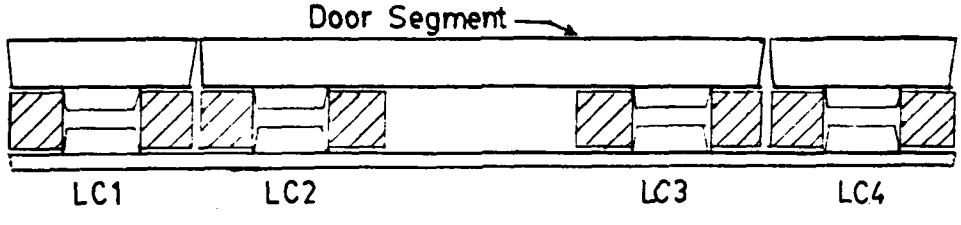

Figure 3-3: Original load cell setup @ MIT

respectively placed beneath each of the two end segments, while Load Cells 2 and 3 were symmetrically positioned to support the middle segment. The force transducers were aligned, as well as stabilized, by means of "buttons" (Figure 3-1) mounted to the trapdoor and also to a steel strip screwed down on the upper wedge. Both this steel strip and the trapdoor had tapered edges to minimize friction with the side walls of the trench.

Several tests were carried out with this arrangement (see Appendix A, Tests GI1-GI66), but the data obtained from these runs turned out to be either quantitatively unacceptable or very difficult to interpret. For example, consider the load cell data from Test *GI*57 (empty package), presented in Figure 3-4. The graph shows the variation of the load cell readings with time as the apparatus is gradually spun up to $80g$ with a pause or hold for every $20g$ increment. Shortly after $80g$ was attained, the trapdoor was lowered and a considerable drop was observed in the force transducer readings even though there was no soil above the door. Furthermore, when data from tests with soil fill obtained with the original load cell setup were reduced, the minimum loads on the trapdoor, after the door self-weight was deducted, were very low (in some cases, even negative!).

The main cause of the irregularities is believed to be the extremely high sensitivity of the force transducers to eccentricity of load application. That is, a load cell subjected to a concentrated force not acting along its annular center will give a different voltage output than when it is concentrically loaded with a force of the same magnitude. Thus, when fairly large moments are present, the transducer measurements will be affected. The manufacturer prescribes special load cell caps which ensure concentric loading on the transducers, but these could not be used due to space constraints.

Figure 3-5a shows the principal forces acting on the "lip" of a load cell. When the forces on each side are not equal, i.e., $P_1 \neq P_2$, the resultant load will not be concentric, and there will be an error in the measured load cell output. The use of the trapdoor segments with "buttons", in lieu of the manufacturer's caps, potentially causes some

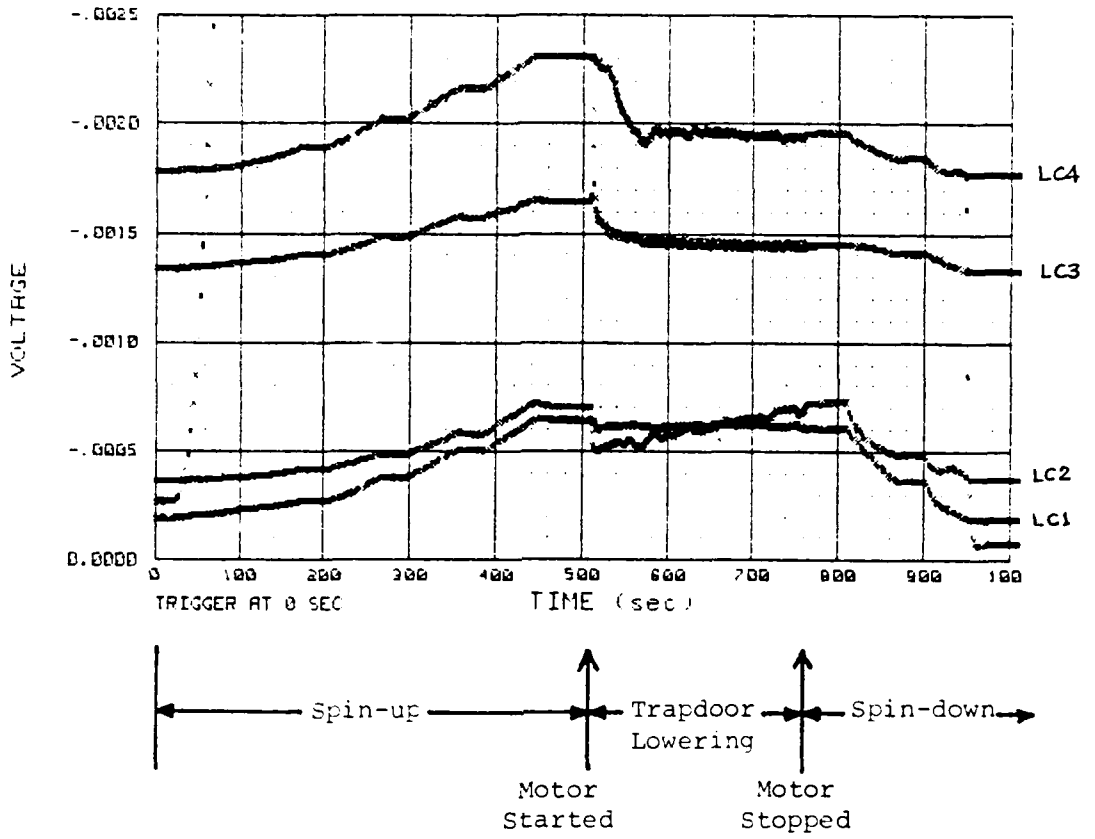

Figure 3-4: Test *GI57* – Empty package with original setup

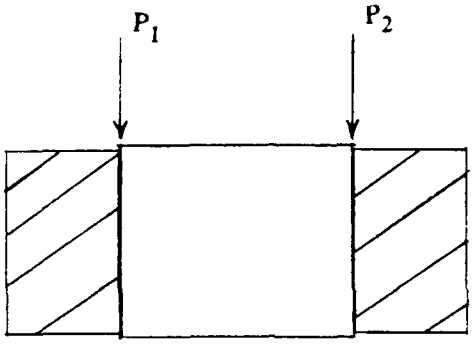

(a) Load Cell

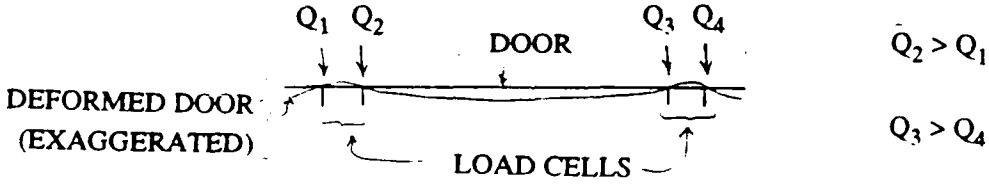

(b) Middle Door Segment (Original Setup)

Figure 3-5: Principal forces on load cells

eccentricity of loading on each force transducer. This unfavorable situation is exacerbated on the relatively long middle segment, especially at higher g-levels (or greater loads) when substantial bending, as shown in Figure 3-5b, is more likely to occur. A tendency of the trapdoor to rock in the lateral direction will also pose some problems.

Most of the tests conducted with the aforementioned force transducer setup have been with sand and have yielded qualitative results at best. Since the accuracy of load measurements is of paramount importance in this research, the load cell assembly has subsequently been redesigned.

3.1.2 Modified Load Cell Setup

The modified arrangement of the load washers and trapdoor segments is displayed in Figure 3-6. Each segment is now supported by a ball and a roller, for greater stability. The balls transmit part of the door load onto the load cells through cylindrical steel caps, and they are positioned right at the center of each washer. To ensure a truly concentric loading, another set of balls and steel caps is placed underneath the center of each load cell. The roller should take care of the problems associated with the rocking of the door in the lateral direction.

The middle segment has been shortened from 6" (152.4 mm) to 4" (101.6 mm) to make the placement of the new type of supports on the end segments possible; the end segments have been lengthened from 2" (50.8 mm) to 3" (76.2 mm). As usual, the edges of the trapdoor segments have been tapered so as to minimize friction with the side walls of the trench. The roller support is located almost at the end of each segment, while the ball support (atop a load washer) is situated at a third of the segment span from the other end.

In order to compensate for an increase in vertical space occupied by the new door-transducer-wedge system, the adjacent base is correspondingly elevated by placing $\frac{1}{2}''$(12.7 mm)-thick aluminum plates on top of the lexan pieces. (See Figure 3-7.) The trapdoor strip itself has been fabricated from a $\frac{1}{4}''$(6.35 mm)-thick aluminum plate, while the

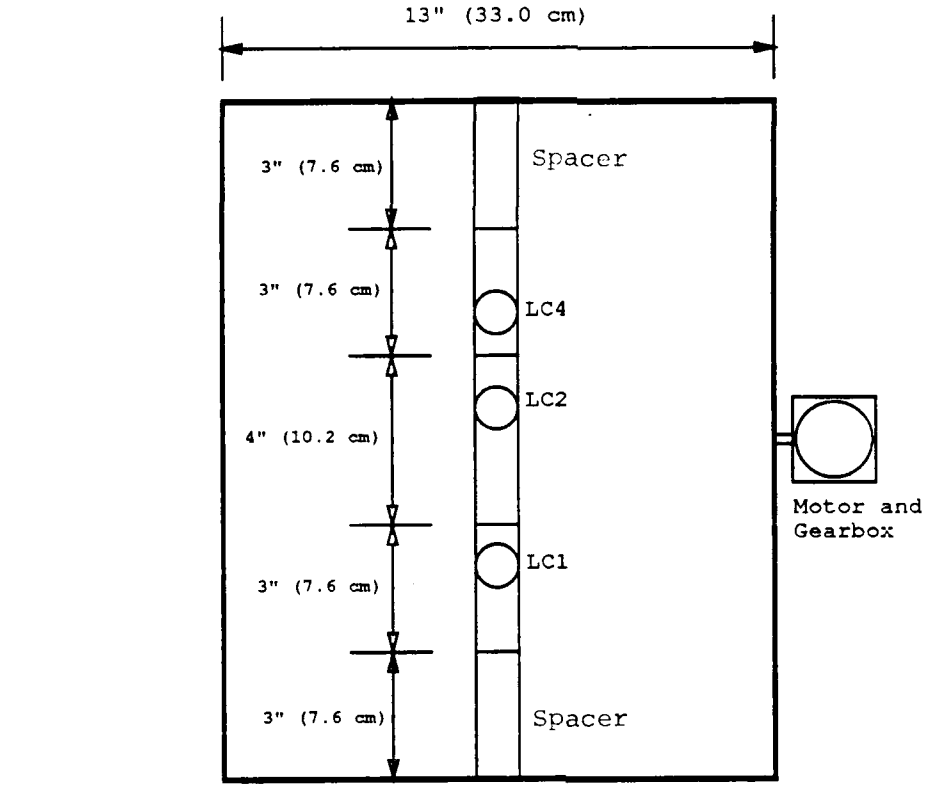

Plan view

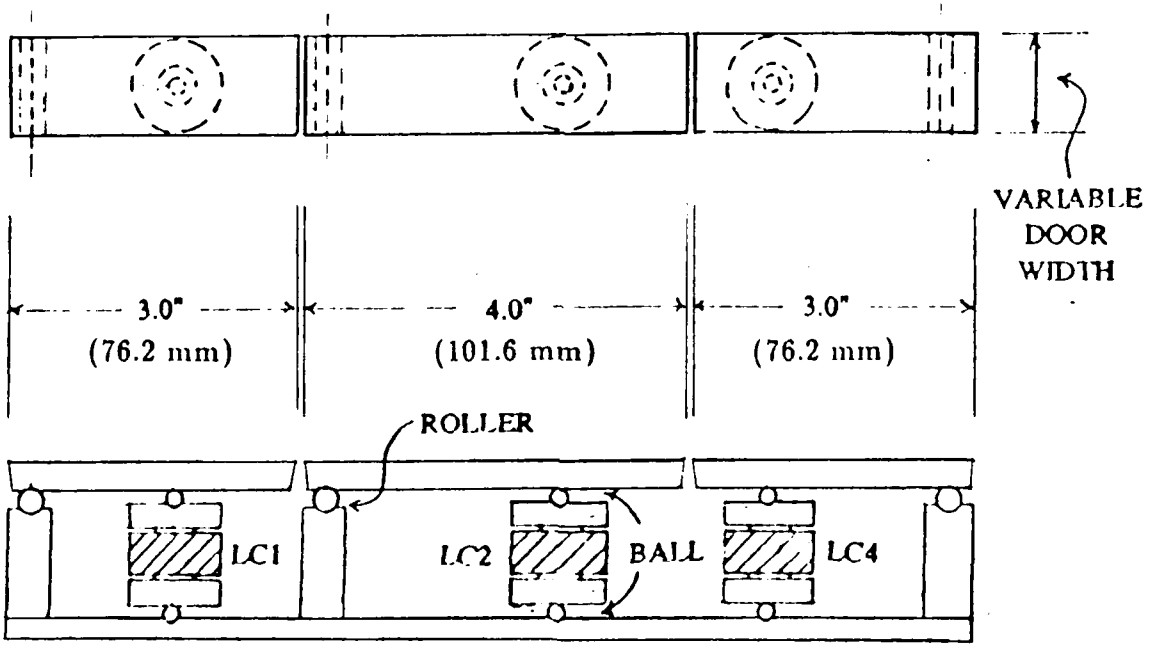

Figure 3-6: Modified MIT load cell setup

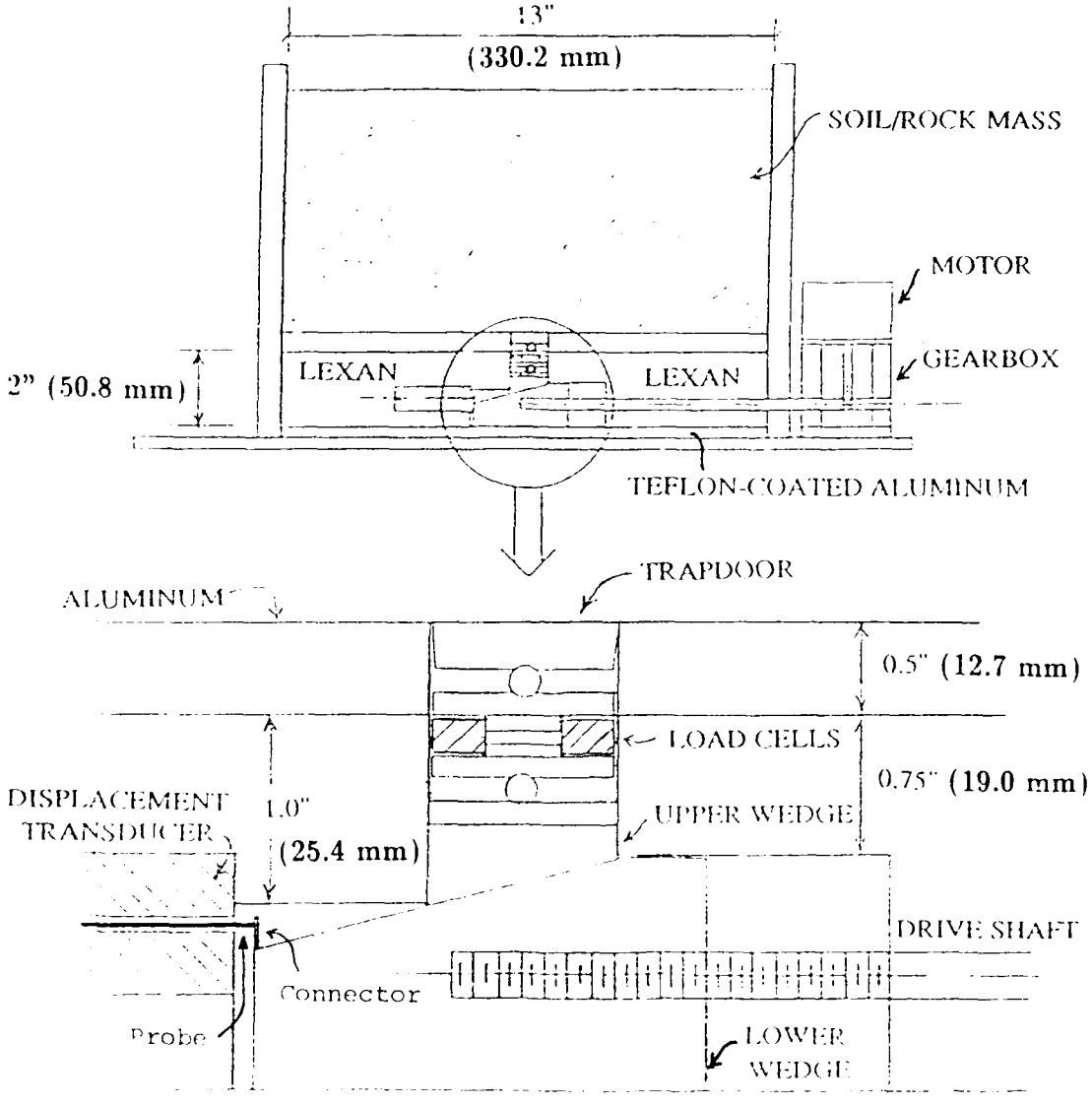

Figure 3-7: MIT trapdoor apparatus with modified setup

$\frac{1}{4}$"(6.35 mm)-$\oslash$ roller and $\frac{3}{16}$"(4.76 mm)-$\oslash$ ball supports are made of steel. Installation of different widths of trapdoor is made possible by providing room for spacers alongside the $\frac{1}{2}$"(12.7 mm)-thick aluminum top plates, as exhibited in Figure 3-8.

The new setup employs only three (3) load cells instead of the previous four (4). (Load Cell 3 of the old arrangement has been taken out, but the original numbering has been retained. Hence, the end load cells are LC1 and LC4, and the middle load cell is LC2.) This new load cell arrangement has also been checked for any considerable variation in force readings as soon as the trapdoor is lowered. Figure 3-9 depicts the results from Test $GI91$, a run with the new setup and no material on the 1"(25.4 mm)-wide trapdoor. Note that there is virtually no change in load readings as soon as the door is moved down – a significant improvement over the original setup.

In the absence of other measurements pertinent to the door load, a critical assumption in the data reduction process is that the resultant force due to the earth pressure acts at the center of each door segment.

3.1.3 Load Cell Calibration and Data Reduction

The force transducers have been calibrated by spinning up the trapdoor package containing known masses aboard the centrifuge. The desired maximum acceleration level is achieved in steps, and the voltage outputs for the computed weights (i.e., the masses multiplied by the corresponding acceleration) are recorded. The known masses are either those of the trapdoor segments, ball supports, and load cell caps, or these plus metal blocks placed on top of the door segments. Calibration tests have been performed with the different trapdoor widths [2" (50.8 mm), 1" (25.4 mm), and $\frac{1}{2}$" (12.7 mm)] and at various acceleration levels.

Hysteresis of the load measurements can be observed from the calibration data. For instance, looking at Figure 3-9, the initial and final voltage values are not always the same, even though both represent normal gravity readings. Hence, to get around this problem, calibration curves are plotted separately for loading and for unloading of each

(a) 2"(50.8 mm)-wide door

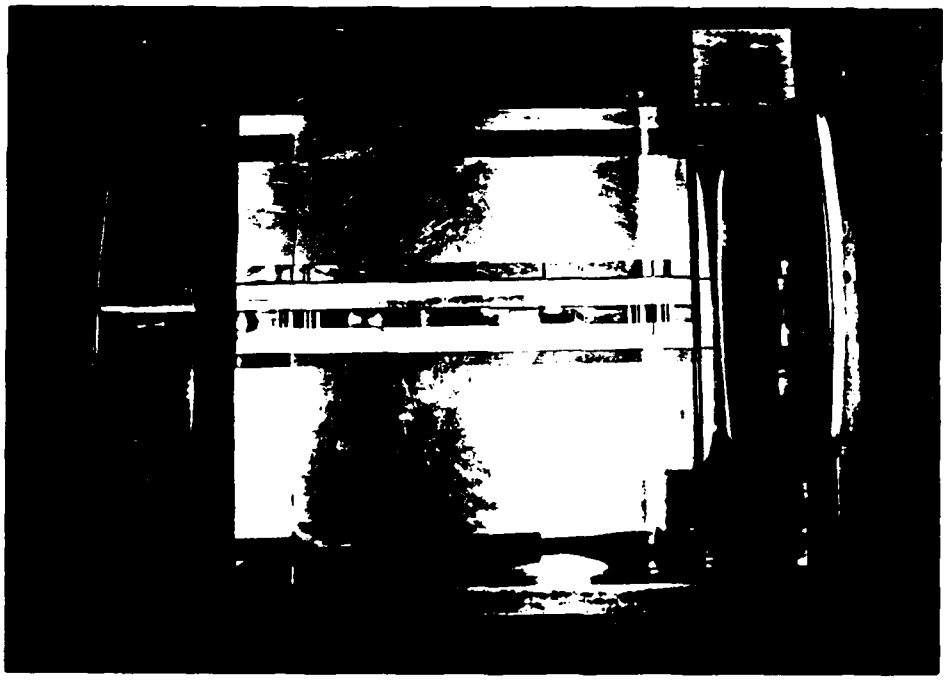

(b) $\frac{1}{2}$"(12.7 mm)-wide door

Figure 3-8: Arrangement to accomodate variable trapdoor widths

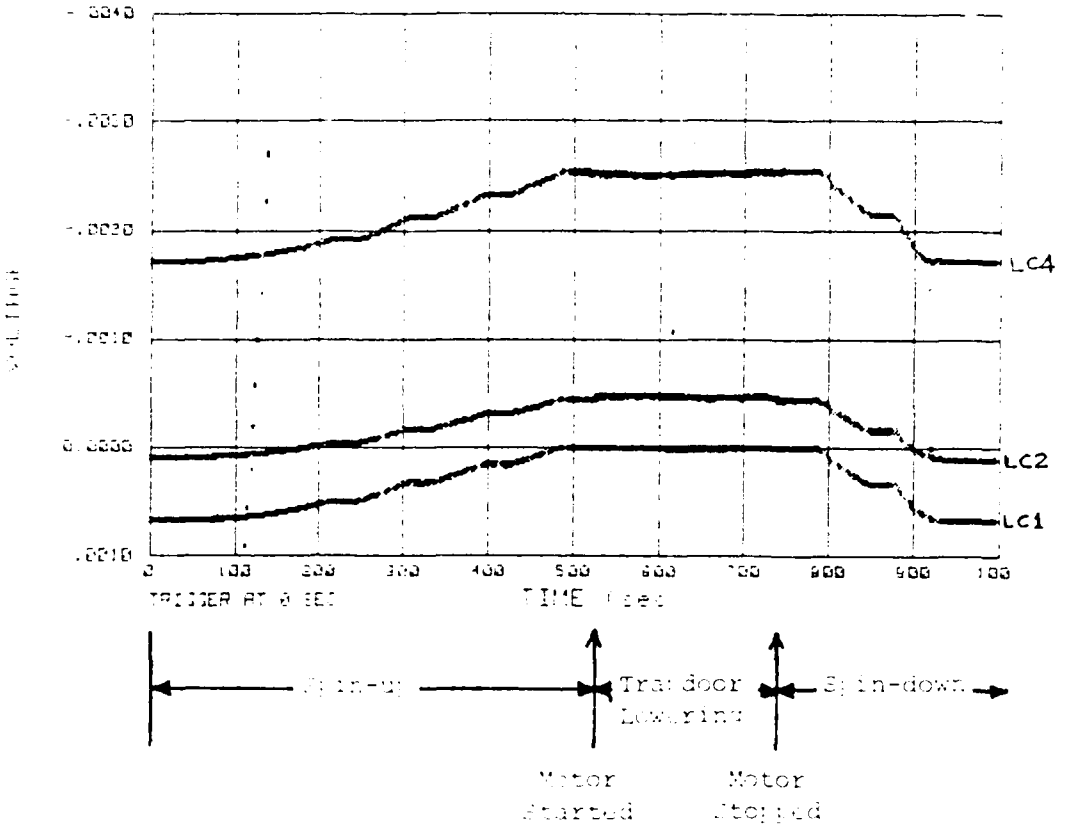

Figure 3-9: Test *G791* - Empty package with modified setup

load cell. (Loading in this case refers to the spin-up phase, with initial $1g$ values as datum; unloading, the spin-down phase, with final $1g$ readings as datum.) These are presented in Figures 3-10 through 3-12.

By means of regression analysis, it is possible to fit smooth curves through the calibration data. Included in Figures 3-10 through 3-12 are two of the best fit curves through each data set. While the straight-line "curve" provides the best fit throughout the entire range of voltage outputs, the slightly non-linear curve fits the data better at low loads. Since during active arching the load can become fairly small, the non-linear curve is adopted for processing the data obtained from the trapdoor experiments.

Due to the hysteretic behavior of the force-measuring system, a special treatment of the zero or datum values for the loads is required such that different zero values are utilized for loading and for unloading. These zero values are determined from the spin-up and spin-down data for loading and unloading, respectively. The basic procedure is described below.

Since the non-linear calibration curve is used, the force F detected by a load cell during a test can be expressed in the form

$$F = A \cdot (\psi - \psi_0)^B \tag{3.1}$$

where A and B are the regression coefficients, and ψ is the voltage output due to the force F, with ψ_0 being the voltage reading at zero force. Then, at Ng, say,

$$F_N = A \cdot (\psi_N - \psi_0)^B. \tag{3.2}$$

This equation can be written for two values of N, e.g., N_1 and N_2:

$$F_{N_1} = A \cdot (\psi_{N_1} - \psi_0)^B \tag{3.3}$$

$$F_{N_2} = A \cdot (\psi_{N_2} - \psi_0)^B. \tag{3.4}$$

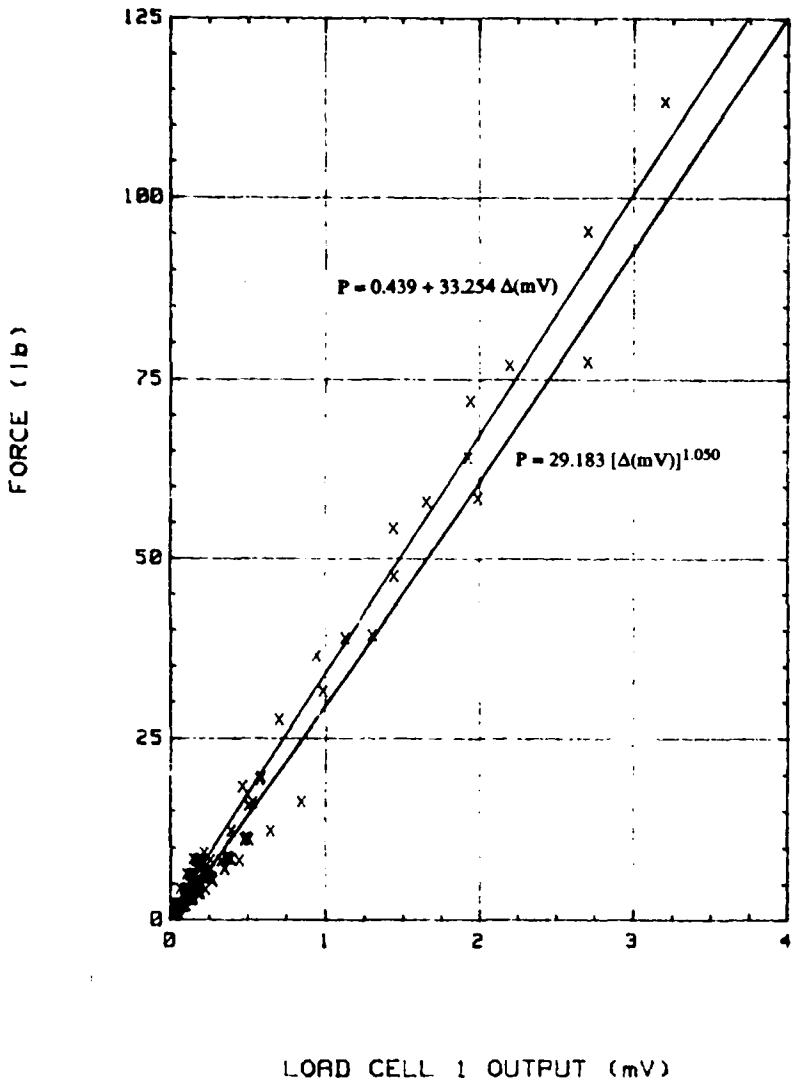

(a) Loading

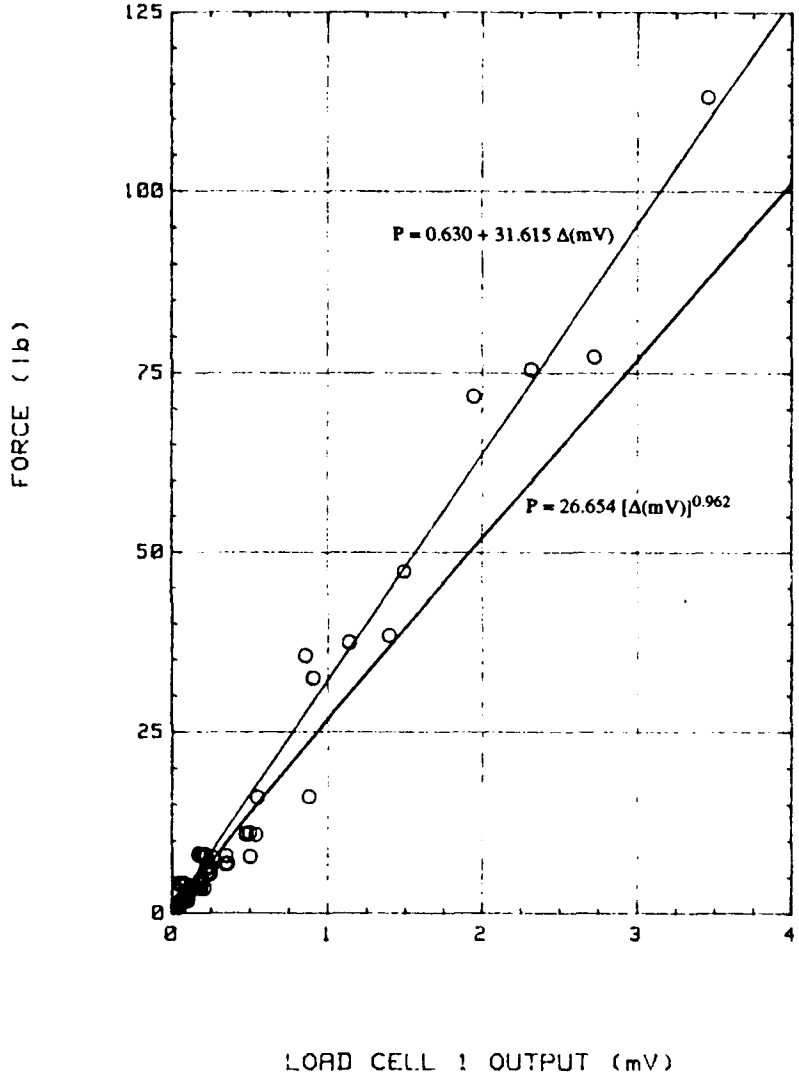

(b) Unloading

Figure 3-10: Calibration data, Load Cell 1

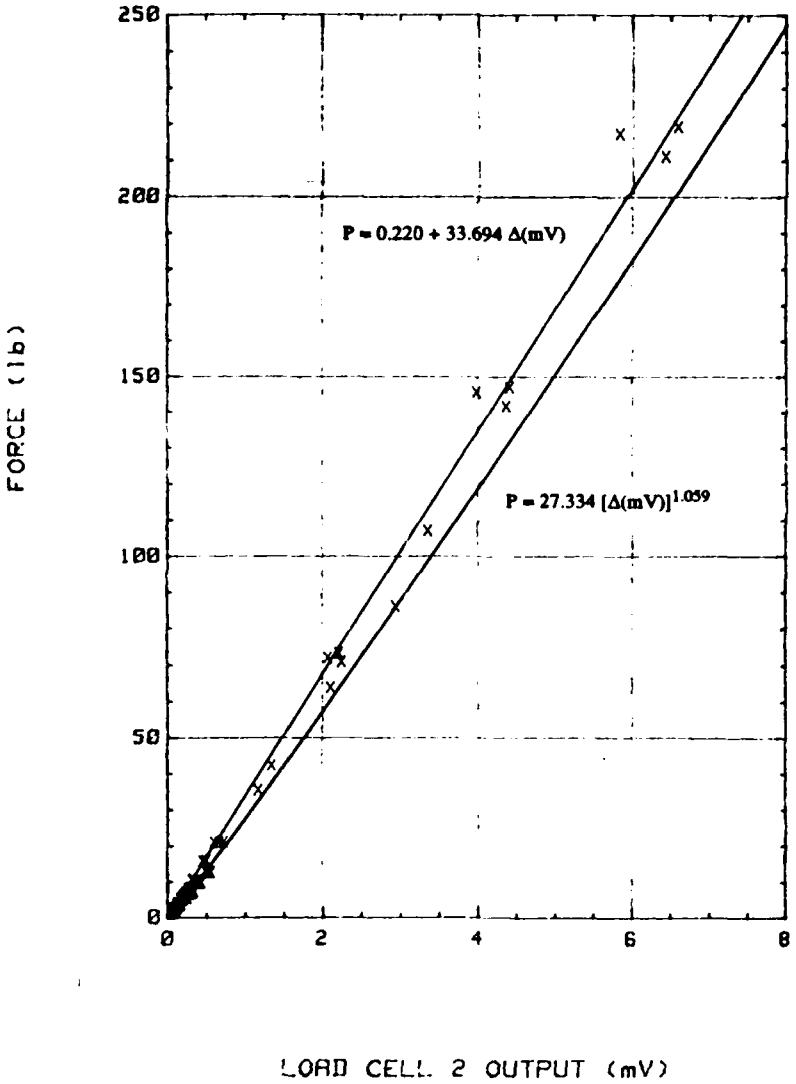

(a) Loading

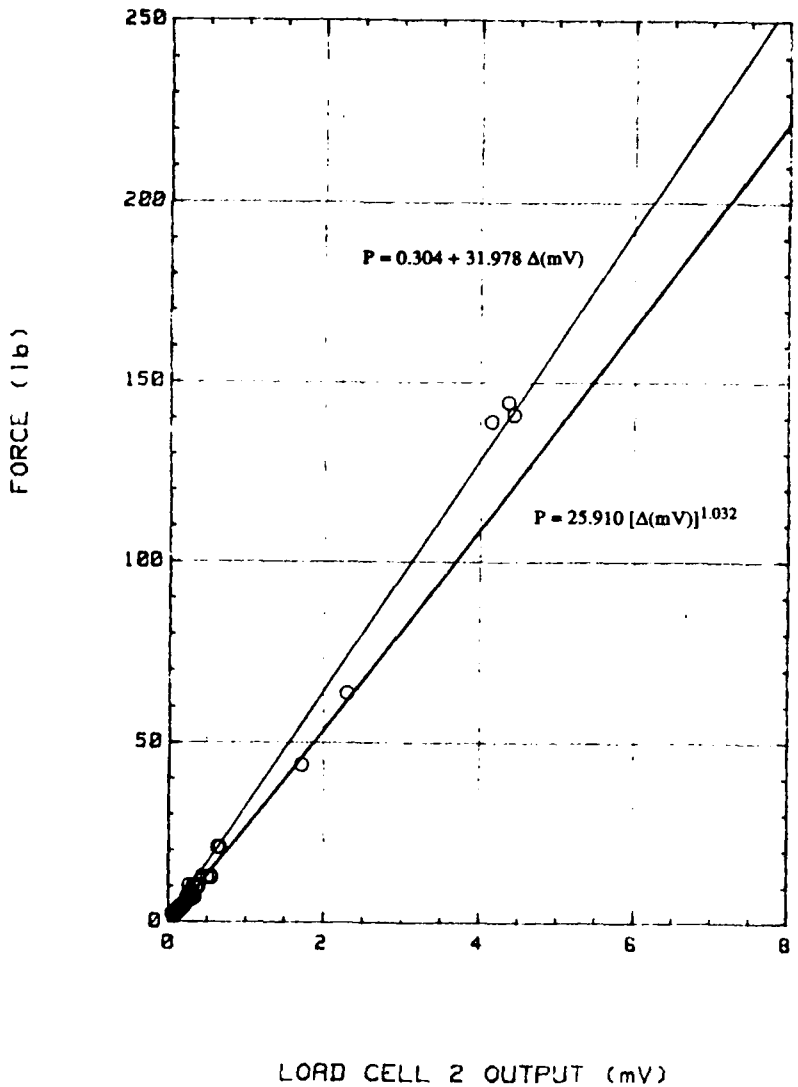

(b) Unloading

Figure 3-11: Calibration data, Load Cell 2

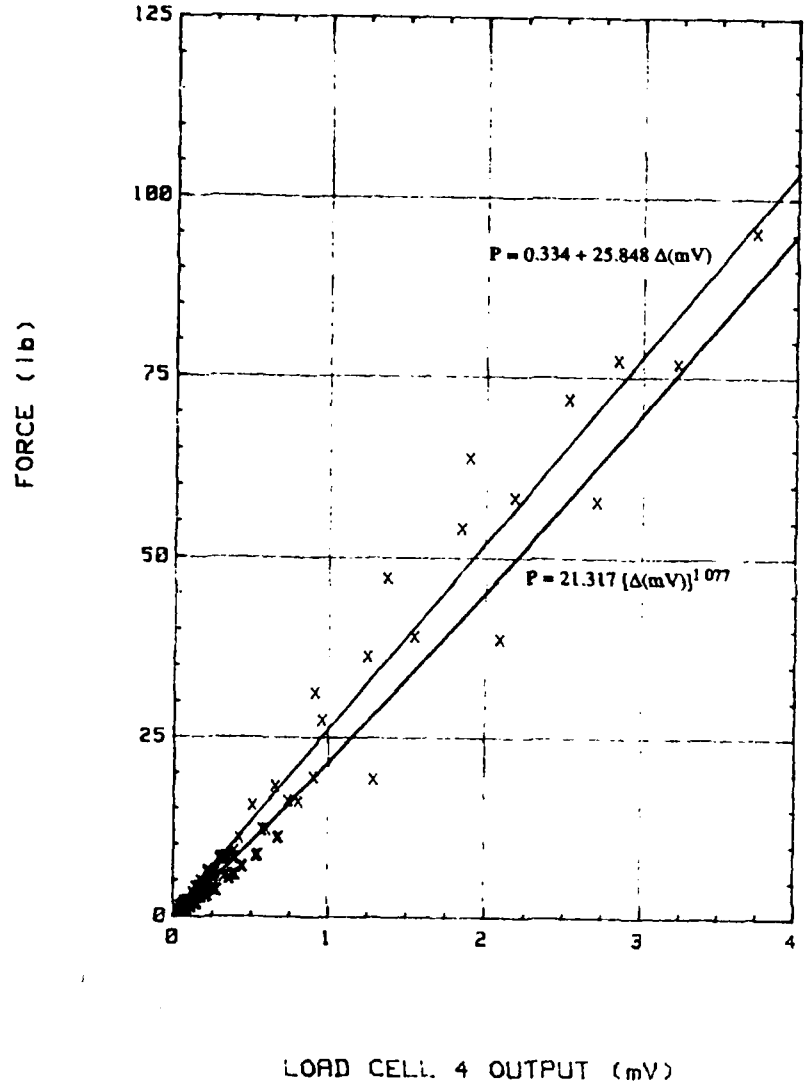

(a) Loading

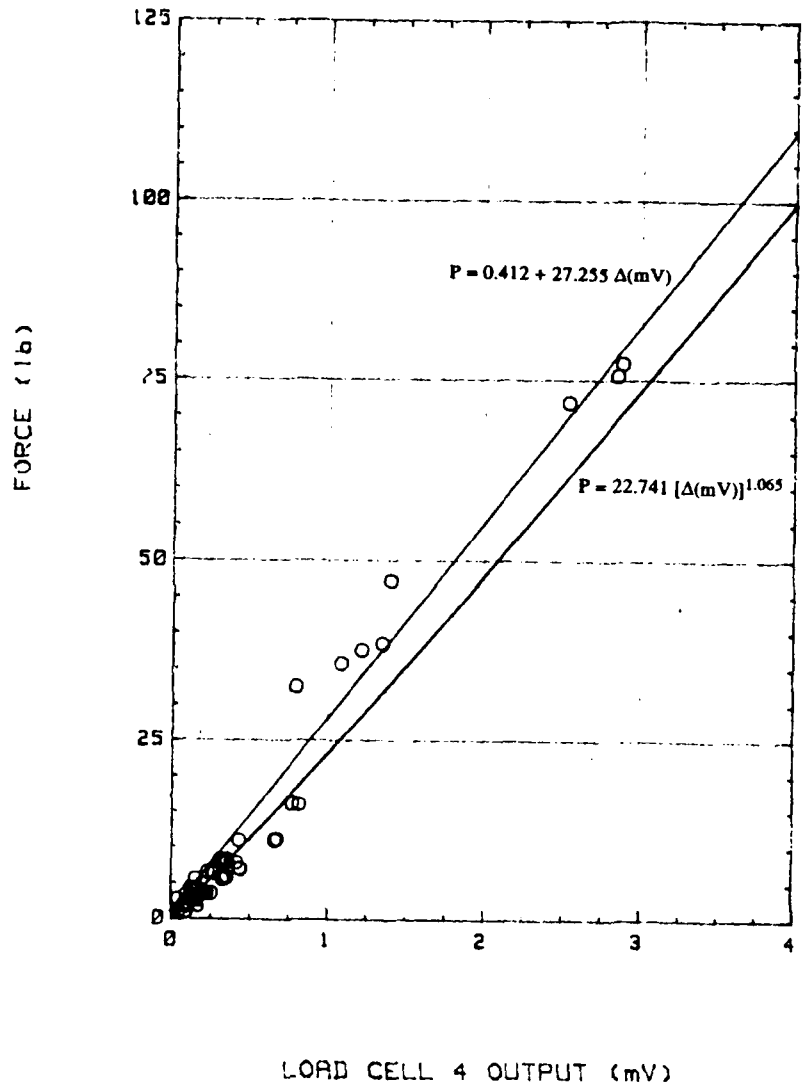

(b) Unloading

Figure 3-12: Calibration data, Load Cell 4

Since

$$\frac{F_{N_2}}{F_{N_1}} = \frac{N_2}{N_1}, \tag{3.5}$$

$$\left(\frac{\psi_{N_2} - \psi_0}{\psi_{N_1} - \psi_0}\right)^B = \frac{N_2}{N_1}. \tag{3.6}$$

Solving for ψ_0, one obtains

$$\psi_0 = \frac{(\frac{N_2}{N_1})^{\frac{1}{B}}\psi_{N_1} - \psi_{N_2}}{(\frac{N_2}{N_1})^{\frac{1}{B}} - 1}. \tag{3.7}$$

Equation (3.7) is employed in determining the datum values for the conversion of voltage readings into force quantities. For the loading phase, N_1 is usually 1 and $N_2 g$ is the top acceleration level; for unloading, N_1 is also 1 and $N_2 g$ is the acceleration at the first step down from the top g-level on the way back to normal gravity conditions. Most of the time, ψ_1 for loading is not the same as ψ_1 for unloading, and because of unequal calibration exponents B, the ψ_0's are often different. This introduces an incongruence in the measured force at the top acceleration level, prior to door lowering, between "loading" and "unloading" computations. The discrepancy, however, is within 10% of the average of both force magnitudes. (This is significantly lower than the error from ignoring the hysteresis of the load-measuring system, especially at the all-important low loads due to active arching.)

3.2 RUB Setup

The trapdoor system at the Ruhr-Universität Bochum (RUB) [Stone and Güttler (1989), Jessberger and Scherbeck (1990)], illustrated in Figure 3-13, is slightly different from the MIT arrangement. Movement is controlled by a hydraulic system connected to a piston which supports the trapdoor. To prevent premature piston settlement as the acceleration is increased prior to door lowering, back pressure is applied to the piston through a column of water contained in a 1.2-m-high pressure vessel. Before dropping the piston, the back pressure is cut off by closing the solenoid valve 1, and the piston is

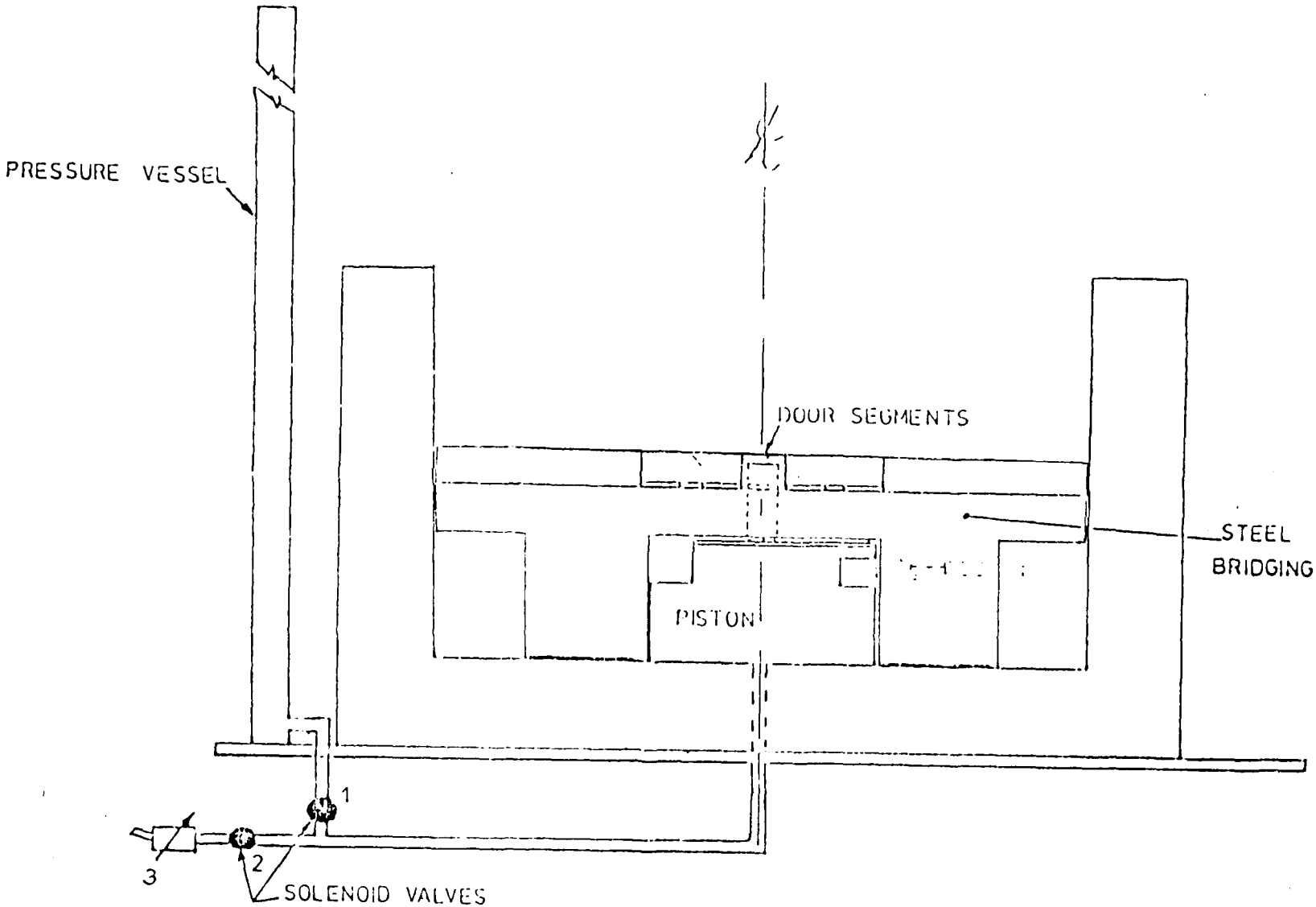

Figure 3-13: RUB trapdoor apparatus

subsequently lowered by opening valve 2. The rate of piston descent is governed by the needle flow control valve 3 and can be pre-set to a desired dropping rate if the pressure drop across the valve is known.

The centrifuge model tests at RUB are performed in a strong box using the arrangement shown schematically in Figure 3-13. The internal dimensions of the strong box are 395 *mm* in depth, 658 *mm* in length, and 395 *mm* in width. Mounted on the base and extending through the full width of the box is a central rectangular tank filled with water. This serves as the movable piston that has a maximum displacement of 25 *mm*.

The front of the strong box is formed by a 70-*mm* thick perspex face through which deformations of the model can be recorded on video cassette. In the RUB test package, there are four trapdoor segments, each 10 *mm* thick, 97.5 *mm* long, and also made of aluminum. (See Figure 3-14.) During an experiment the lowering of the piston causes the uniform settlement of all four trapdoor segments. The segments are designated number 1 through 4 from the front face to the back wall of the strong box. Only three of these – segments 1, 2, and 4 – are equipped with load cells, because segment 3 is instrumented with a displacement transducer to monitor the trapdoor movement. The load cells used in the door segments are of varying capacities, as given in Table 3.1 below. Each segment is simply supported as in the MIT setup, except that a "knife edge" is used instead of a roller.

Table 3.1: RUB load cell capacities

Door Segment	Load Cell Capacity
1	5 *kN*
2	10 *kN*
3	Inactive
4	20 *kN*

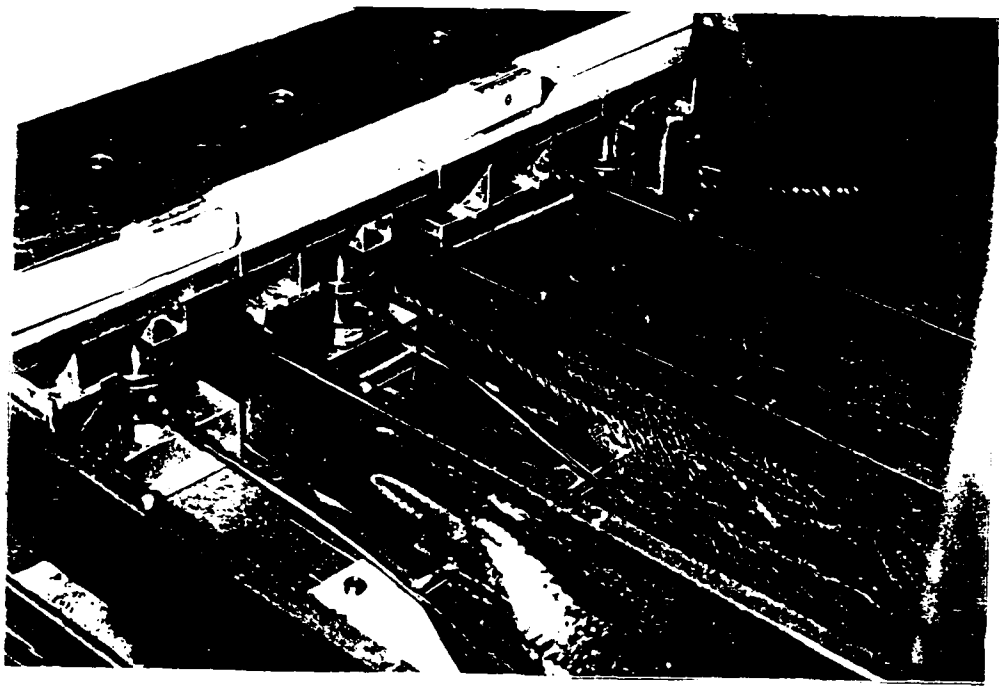

Figure 3-14: RUB load cell setup

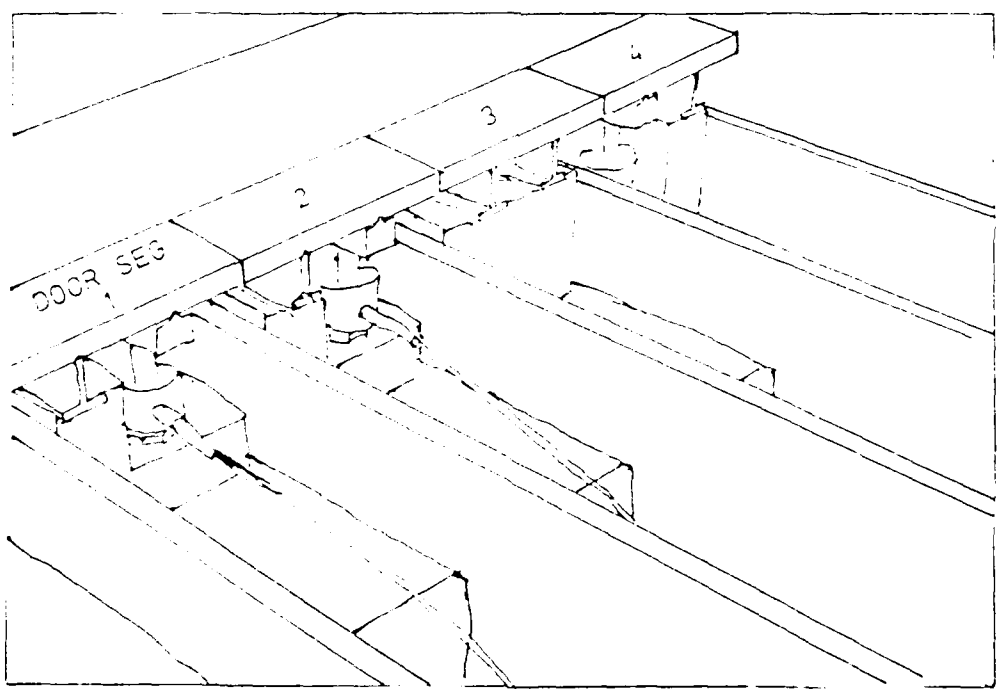

3.3 Measurement of Pre-lowering Door Displacement

The theoretical geostatic force P_0 at N gravities on a trapdoor segment with loaded area A underneath a geomaterial of depth h and unit weight γ is equal to $N\gamma hA$. Due to inherent differences between the stiffness of the door/load-cell assembly and that of the adjacent base, the forces measured in the trapdoor experiments before any actual door translation may deviate from the theoretical geostatic loads. If the door/transducer system is stiffer than the neighboring base, for instance, the load measurements tend to be on the high side.

A few tests have been carried out to check whether the MIT trapdoor arrangement is stiffer or more flexible than the adjacent base by measuring the displacement of the base relative to the trapdoor. The salient features of the setup for measuring this relative displacement are shown in Figure 3-15. The probe of a proximity sensor is mounted on a lexan bracket piece and oriented in such a way that deformations on the aluminum trapdoor or base plate can be detected as the package spins up to higher gravity levels in the centrifuge. In one test, the probe is positioned over the center of the trapdoor; in another, the probe is placed above a nearby point on the adjacent base. (See Figures 3-16 and 3-17.) In both cases, the legs of the bracket piece are standing on the surface of the base adjacent to the trapdoor so as to have a common reference. The difference in the readings for the test with the probe over the door and that with the probe over the adjacent base should correspond to the relative displacement between the trapdoor and the base.

A typical set of results from spin-up tests with the package containing the deflection-measuring gadgetry is presented in Figure 3-18. The positive ordinate refers to the decrease in the distance between the probe face and the "target" surface with respect to its initial value. On inspection of the data from tests with the proximity sensor probe both over the door and over the base, it is clear that, except for some initial "seating," as

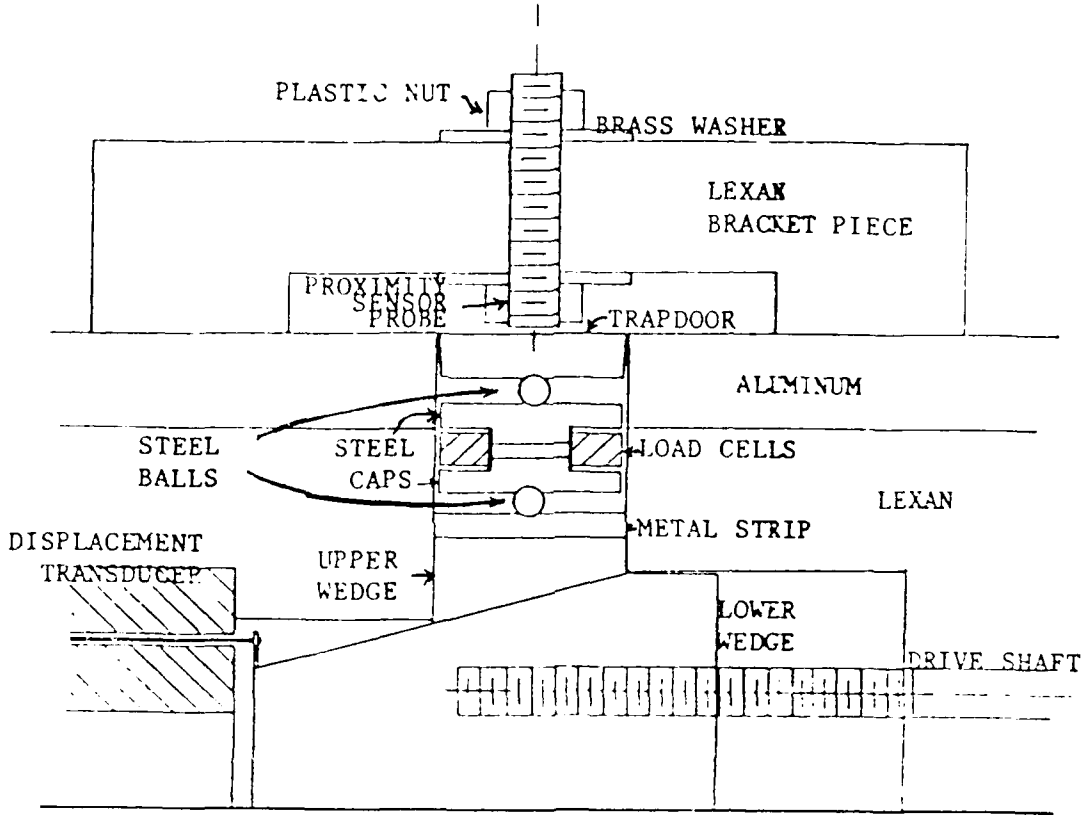

Figure 3-15: Setup for measuring pre-lowering displacement of trapdoor relative to adjacent base

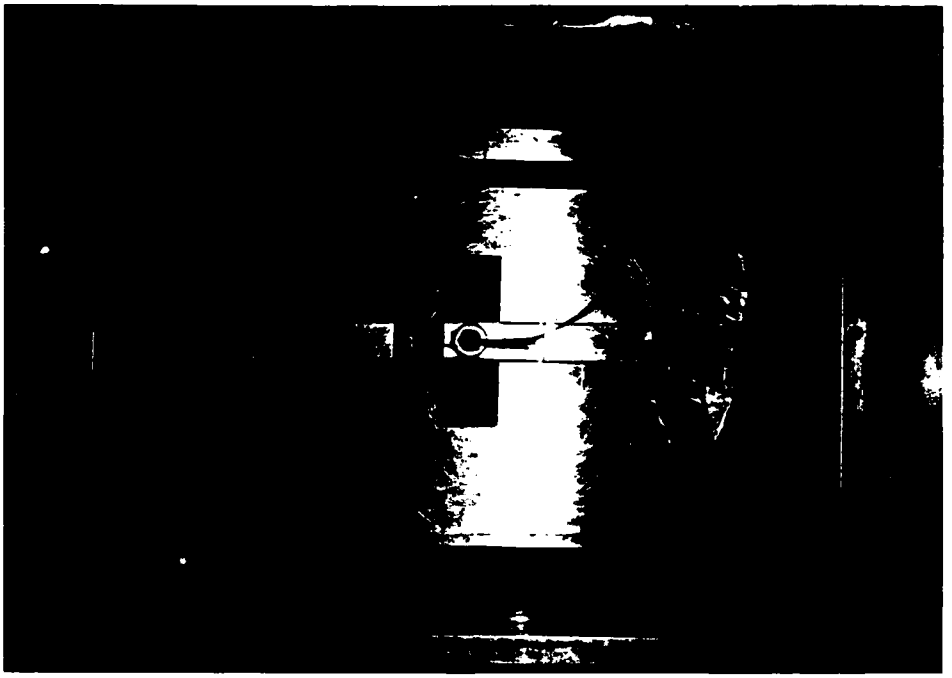

(a) Plan View

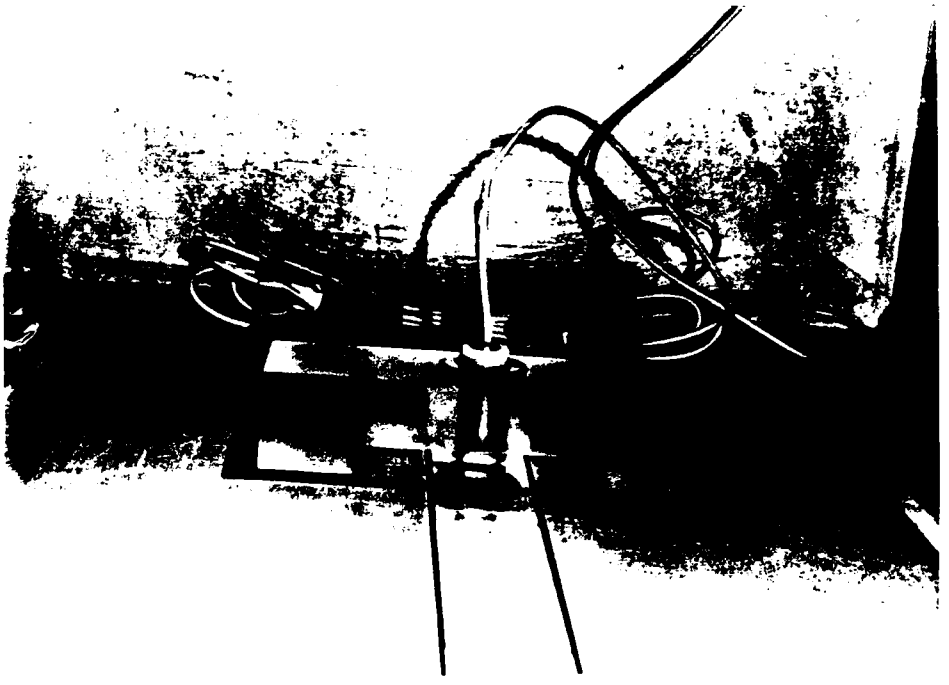

(b) Elevation View

Figure 3-16: Displacement test with probe @ door

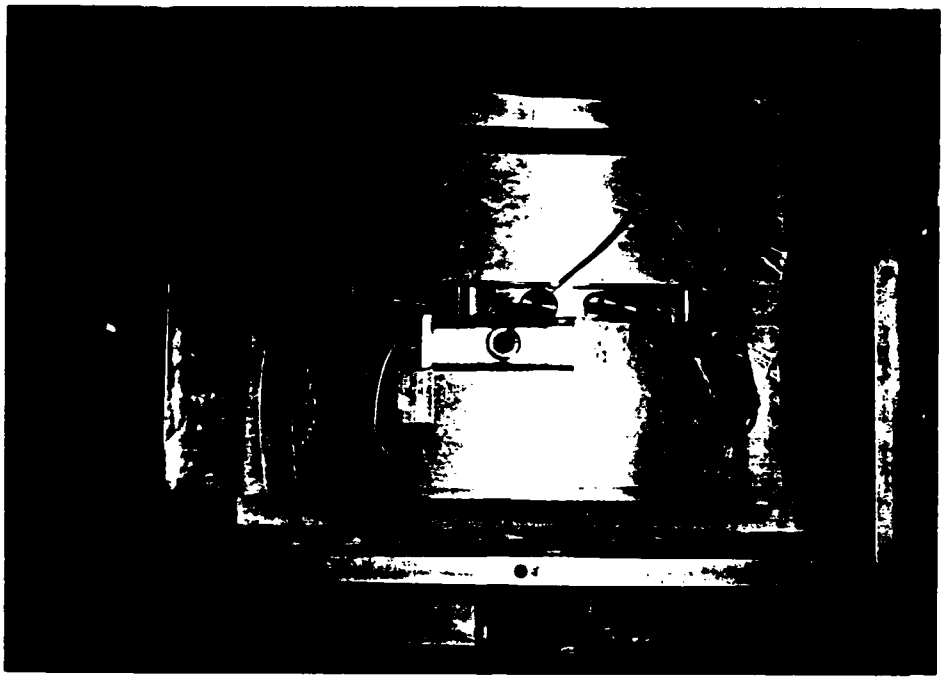

(a) Plan View

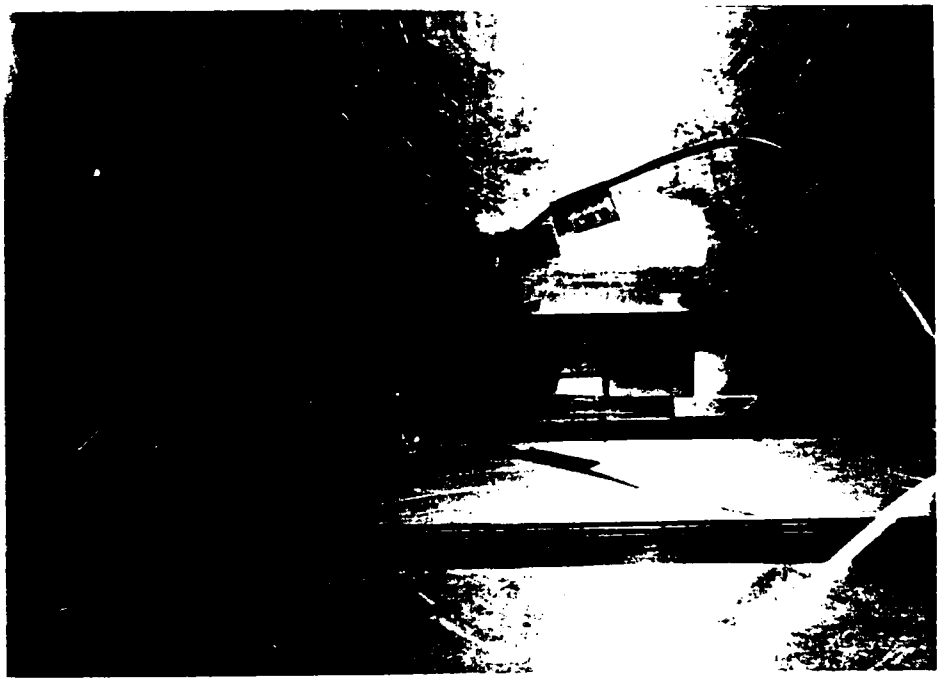

(b) Elevation View

Figure 3-17: Displacement test with probe 9 adjacent base

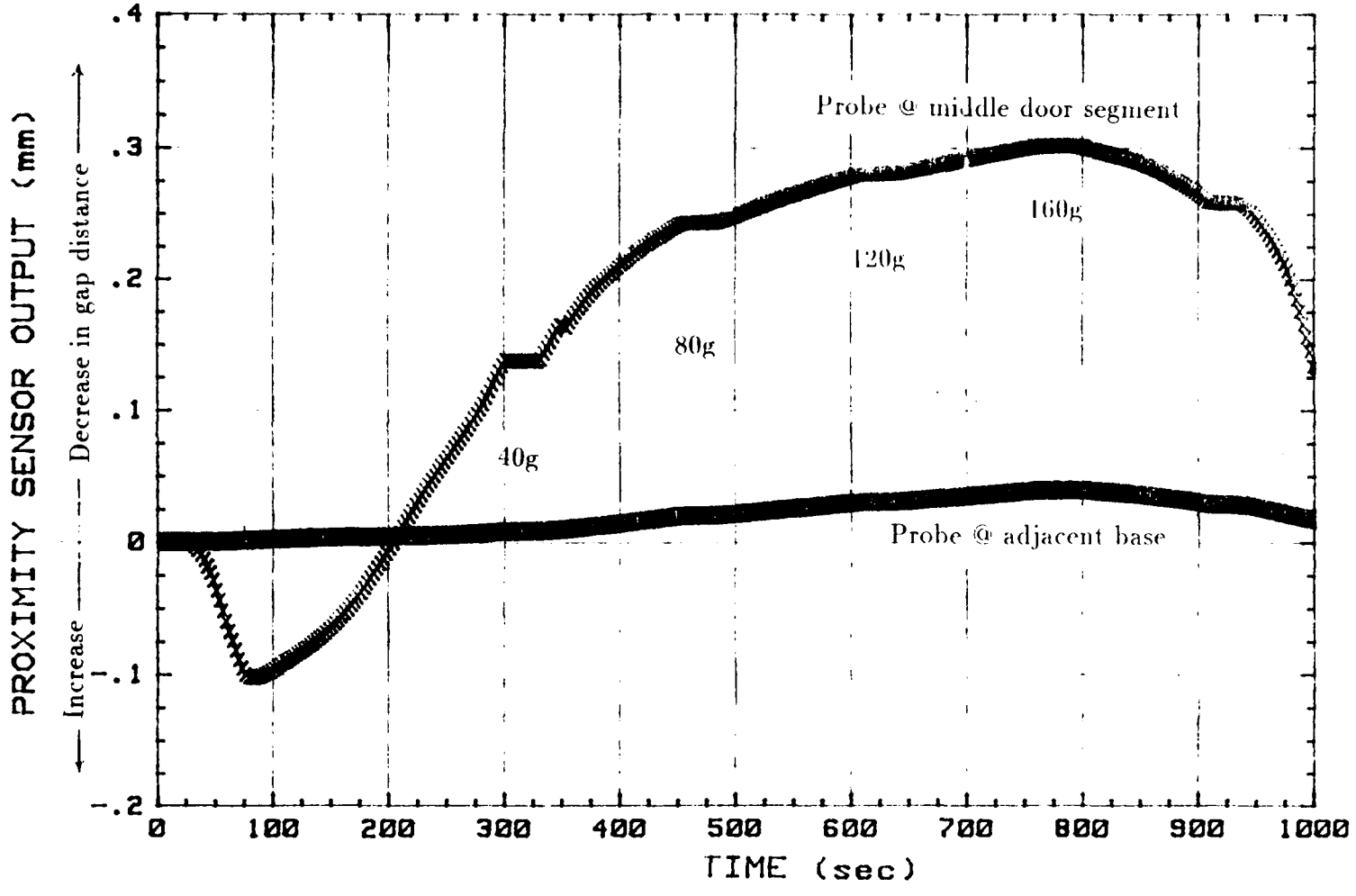

Figure 3-18: Proximity sensor measurements (MIT middle trapdoor segment)

the centripetal acceleration increases, the gap distance generally decreases. This implies that the base deflects more with larger loads than the door itself, and, hence, that the trapdoor/load-cell assembly is stiffer than the contiguous base. The relative displacement is obtained by subtracting the output for the base test from the corresponding output for the door segment test, and average values from various runs are summarized in Table 3.2. (These are for the MIT trapdoor only; no relative displacement measurements have been

Table 3.2: Relative displacement values (MIT middle trapdoor segment)

Gravity Level	Relative Displacement
10g	-0.054 mm
20g	0.020 mm
40g	0.128 mm
60g	0.191 mm
80g	0.222 mm
120g	0.248 mm
160g	0.261 mm

made for the trapdoor at RUB.)

In the door segment tests, there is a "dip" in the proximity sensor curves (Figure 3-18) as the centrifuge rotation starts to pick up some speed. This is attributed to a "seating" problem associated with the transmission of the trapdoor load onto the force transducer via a ball support. Initially, there is hardly any load on the door, and the ball supports may not be properly seated in their grooves until the load becomes greater through an increase in the centrifugal acceleration. No such "dip" is observed in the test where the probe is aimed at a nearby point on the adjacent base.

As the gravity level is stepped up from one level to the next, the change in the measured displacement diminishes with higher g-levels. This can be explained by the inevitable presence of air gaps between surfaces which do not completely touch each other to begin with (i.e., imperfections in at least one of the contacting surfaces underneath the trapdoor assembly would leave some spaces unfilled under initial conditions). With these air gaps, deformations appear to be large initially, then the incremental magnitudes decrease as the surfaces come into full contact with each other at high values of pseudo-

gravitational acceleration.

Chapter 4

Experiments with Granular Materials

Tests with granular media above the trapdoor have been conducted aboard the MIT centrifuge so that the results can be compared with those of previous arching experiments. In this regard, the effects of varying door widths, burial depths, gravities, and particle sizes are evaluated.

4.1 Tests with Coarse Sand

4.1.1 Material Description and Test Procedure

For these experiments, New Jersey 4/14[1] (coarse) sand with subangular grains (specific gravity $G_s = 2.66$) having an average size of 2.1 mm is used. Figure 4-1 presents the grain size distribution curve. One notes from this curve that the uniformity coefficient C_u ($= D_{60}/D_{10}$) is around 1.7; hence, the sand model material may be considered uniform. The friction angle ϕ of this soil (void ratio $e \approx 0.70$) has been determined from direct

[1]These numbers indicate the U.S. Standard sieve sizes through which the sand particles pass and on which they are retained. Thus, the sand used passes through the #4 (4.76 mm) sieve and is retained on the #14 (1.41 mm) sieve.

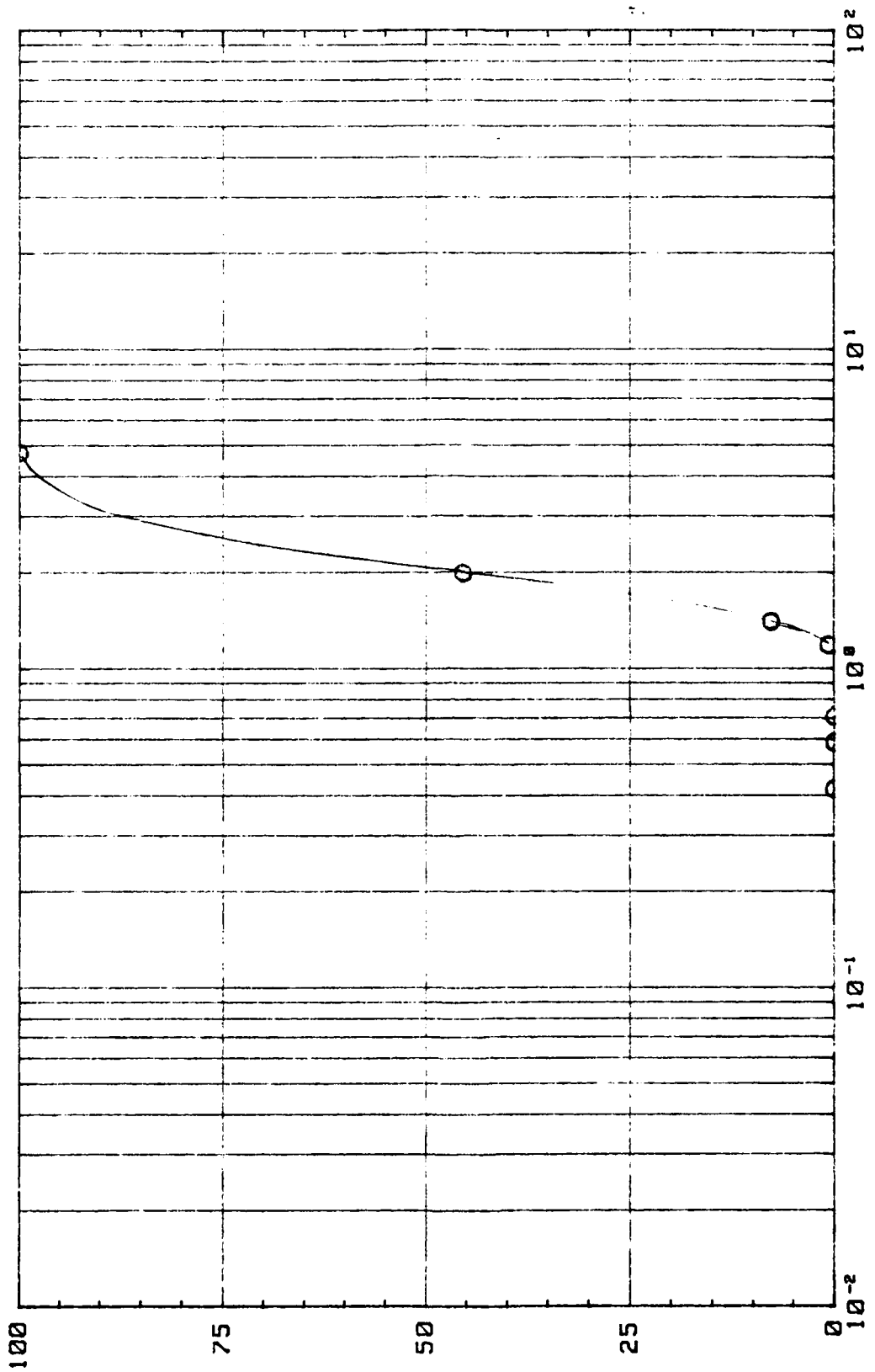

Figure 4-1: Grain size distribution of sand used

shear tests (with normal stress levels at 49 and 98 kPa) as $\sim 39°$.

In constructing the model, the coarse sand is poured and scattered manually over the trapdoor setup, occupying the full 13" (33 cm) width of the strongbox.[2] When the desired depth is attained, the top surface is levelled by scraping the particles from the higher portions over to the lower areas. The average soil density achieved using this procedure is reasonably consistent at around 100 lb/ft^3 (1604 kg/m^3)[3]. This corresponds to a void ratio e of about 0.66 and a relative density D_r of about 57%.

In the early stages of the experimental program, transparent tape was stuck to the edges of the door segments with a slight overhang (sticky side coated with graphite powder) to prevent soil grains from falling through the gaps. Later on, this became unnecessary along the edges where the spacers (Figure 3-8) were moved inward to narrow down the gap.

To illustrate how each trapdoor experiment on the MIT centrifuge proceeds, the pertinent data collected in a typical test are shown in Figure 4-2. The pseudo-gravitational acceleration in the centrifuge at which the trapdoor is displaced downward is arrived at in four major increments. That is, the package is spun up gradually from 1g to the top g-level, with the speed of rotation held constant momentarily at three intermediate stages. Each major increment is roughly a quarter of the highest acceleration level. The load cell measurements for the entire duration of the centrifuge run are reflected as in Figure 4-2a. Shortly after the desired acceleration is reached, the door is moved down. Figure 4-2b shows a typical vertical door displacement versus time plot. (All this while, the rotational speed – and, thus, the effective gravitational field – of the package is maintained.) When the maximum possible door translation [$\sim$0.16 $in.$ (4 mm)] is attained, the package is subsequently brought down from the top g-level to earth's gravity. The

[2]Initially, the sand filled the entire 13"x16" (33 cm x 40.6 cm) inside area of the strongbox. In the later tests, $\frac{1}{8}$"x5.5"x13" (0.32 cm x 14 cm x 33 cm) glass plates were mounted vertically at each outer edge of the trapdoor strip to permit partial viewing of the model from the sides. This reduced the "field" area of the model to 13"x10" (33 cm x 25.4 cm).

[3]The density of the sand varies from test to test and is determined from knowing the package mass and the soil volume.

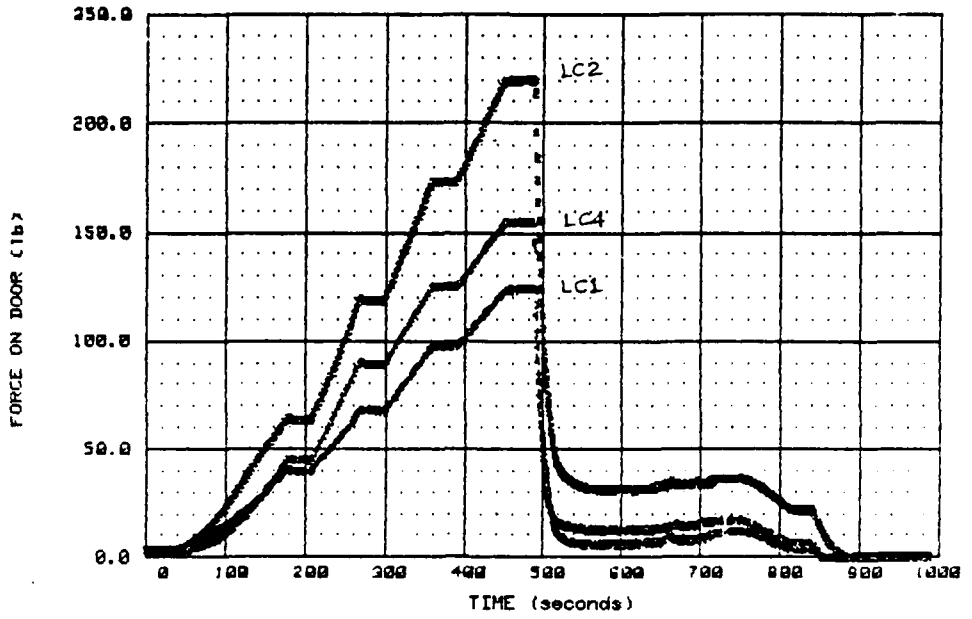

(a) TEST GI106: DOOR LOAD DATA

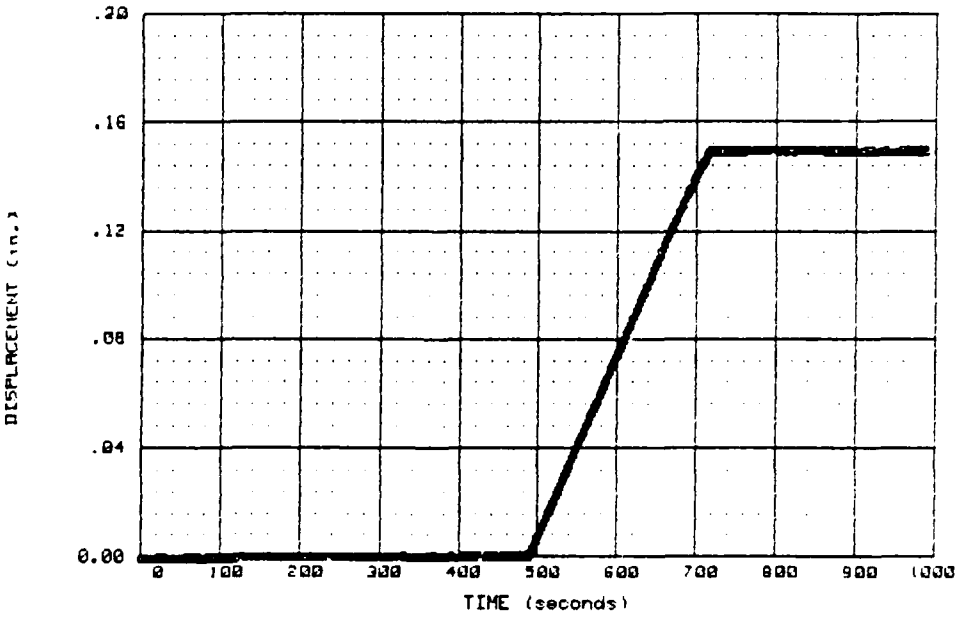

(b) TEST GI106: DOOR DISPLACEMENT DATA

Figure 4-2: Typical trapdoor test data

rotational speed of the centrifuge is pre-programmed in the controller so that it varies automatically according to the spin-up sequence described above.

Theoretically, the loads should be proportional to the g-level, and so, for equal g-level increments, the load increments should also be the same. Due to the difference in stiffness between the trapdoor and the adjacent base (as discussed in Chapter 3), however, the measured incremental loads (Figure 4-2a) do not tally with the theoretical values. Since the measured relative displacements between the door and the adjacent base reveal a non-linear trend as the g-level varies, the measured force increments are not equal.

Although the data from all three load cells are exhibited, one should bear in mind that the outer segments (LC1 and LC4) are probably affected by uncontrollable factors associated with end conditions; thus, only the force measurements in the middle segment (LC2) are regarded to be reliable. In the following, then, observations are made solely on the basis of data obtained from the middle segment.

4.1.2 Results

From data similar to Figure 4-2, the load on the trapdoor can be plotted against the door displacement while the package is under the desired acceleration level. Such results are presented in the following.

4.1.2.1 Repeatability of Tests

The results from two tests both with 2"(50.8 mm)-deep coarse sand overlying a 1"(25.4 mm)-wide trapdoor, lowered at $80g$ are shown in Figure 4-3. One (GI119) is among the tests wherein graphite-coated tape has been attached along the longitudinal edges of the trapdoor, while the other (GI198) has the spacers squeezed in to eliminate the need for the tape on the edges.

The computed densities of the manually deposited specimens are 105.5 pcf (1692 kg/m^3) and 106.3 pcf (1705 kg/m^3) for GI119 and GI198, respectively. While both tests are assumed to be conducted at $80g$ (nominal), the acceleration (as inferred from

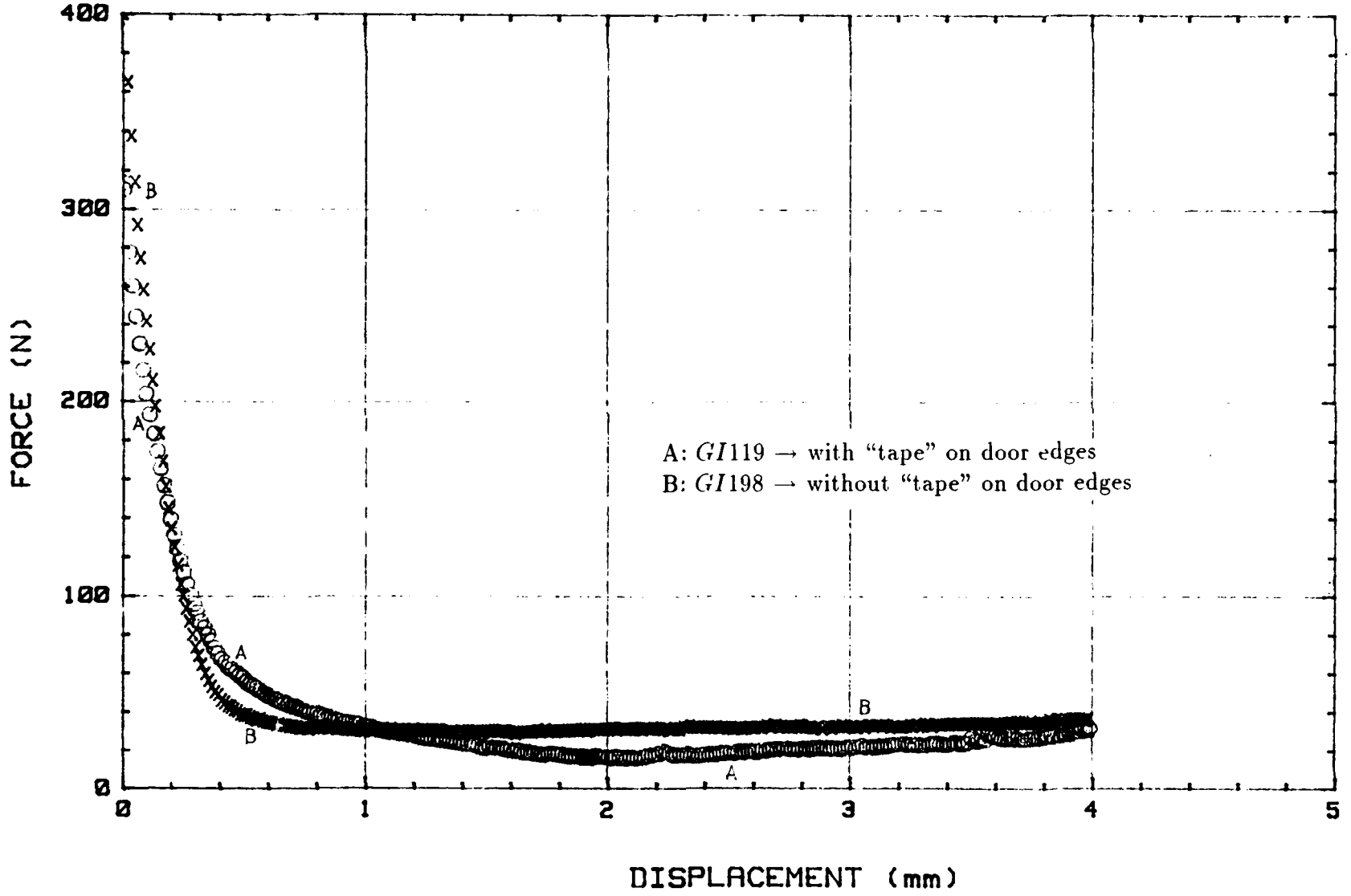

Figure 4-3: Tests with coarse sand, 2" (50.8 *mm*) deep, on 1" (25.4 *mm*) @ 80*g*

the accelerometer data) at a third of the height from the bottom of the soil along the centerline of the package is a little bit different in GI119 (80.6g) from that in GI198 (87.3g). Moreover, the presence of the graphite-coated tape in GI119 may cause a little bit of the load on the door to be carried by the tape itself. Thus, the measured loads in the two experiments do not start out at the same value (343 N vs. 400 N). Note that these measured loads prior to any door translation are greater than the theoretical geostatic force of $\sim$178 N, due to the stiffer door relative to its adjacent base.

As can be seen more clearly in the "tape-less" test (GI198), the force on the door approaches a minimum ($\sim$37 N) at a door displacement of $\sim$0.5 mm and stays approximately constant thereafter. The more curved appearance of the load vs. displacement plot in GI119 is attributed to the presence of the graphite-coated tape. Overall, nevertheless, these results indicate that the trapdoor experiments with granular media are fairly repeatable.

4.1.2.2 Effect of Soil Depth

The effect of overburden depth on trapdoor arching is well known. The deeper the soil, the greater the percent reduction in the load, relative to its geostatic value, as the door displaces. Engesser (1882), McNulty (1965), Ladanyi and Hoyaux (1969), among others, have corroborated this in their experiments. The trends from the present tests are also in agreement with the tests of these researchers.

Figure 4-4 displays the results from experiments with coarse sand of varying depths on the 1"(25.4 mm)-wide trapdoor, moved down at 80g. The measured forces are normalized with respect to the theoretical geostatic force and are plotted against the vertical door displacement. At zero door displacement, the initial measured forces are 50% to 120% larger than the overburden, the discrepancy tending to increase as the soil becomes deeper. This is again related to the trapdoor being relatively stiffer than the adjacent substratum. Upon lowering of the door, the normalized minimum door load attained is smaller as the depth of cover increases. The door displacement at which this minimum

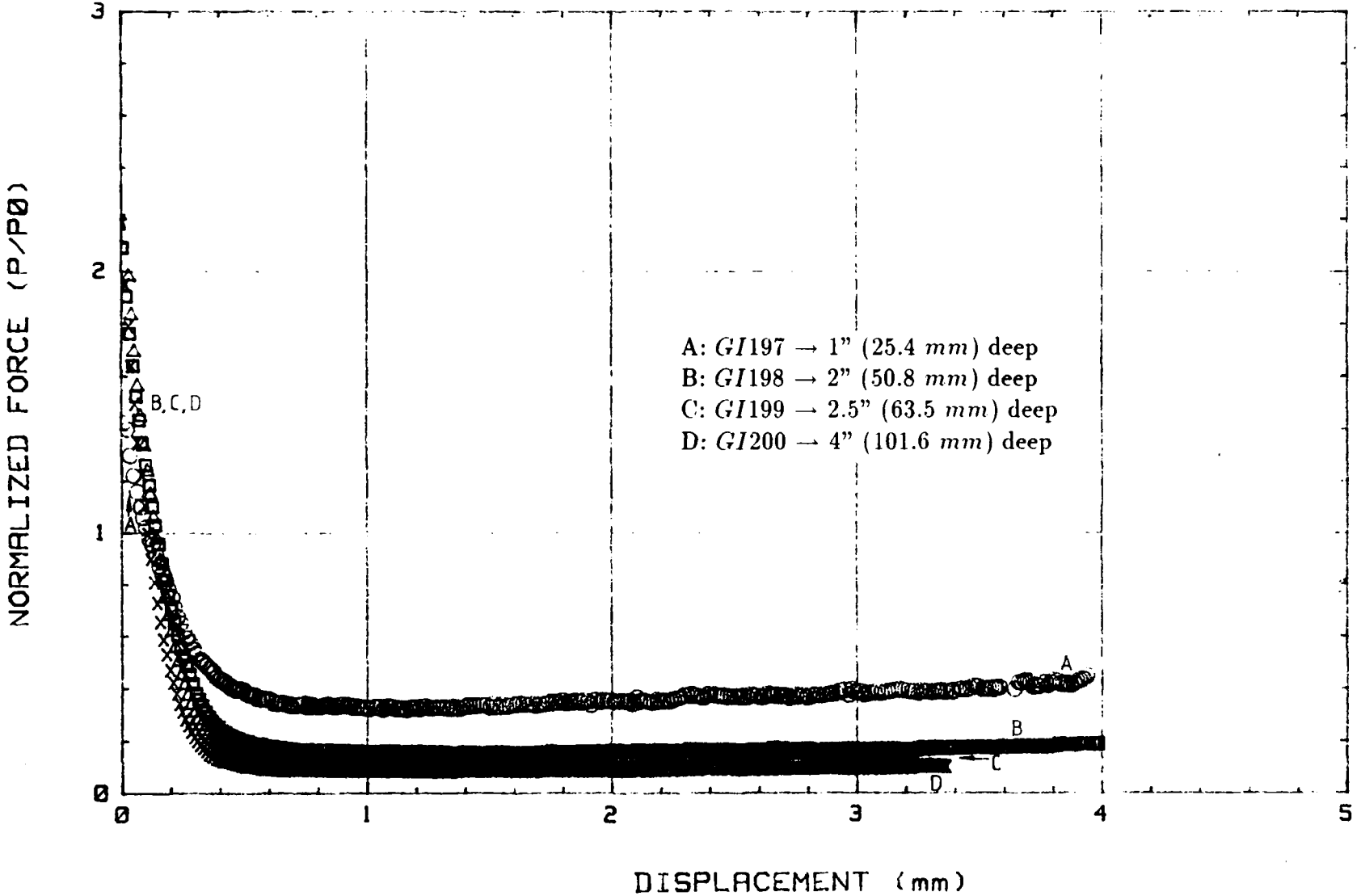

Figure 4-4: Tests with coarse sand of varying depths on 1" (25.4 mm) door @ $80g$

load occurs is about the same ($\sim$1 mm) in these 1"(25.4 mm)-door/80g tests with coarse sand and different burial depths.

4.1.2.3 Modelling of Models

A *modelling of models* program of experiments with coarse sand is conducted to verify the centrifuge scaling relations for granular media. In this regard, two sets of tests are performed: one set with the 1"(25.4 mm)-wide trapdoor lowered at 80g, and the other with 2"(50.8 mm) door at 40g. For each set, the depths of cover are varied but are related by a factor of 2 to those in the other set, in compliance with geometric similarity requirements. Table 4.1 describes in concise terms the experiments carried out as part of this *modelling of models* exercise.

Table 4.1: *Modelling of models* with coarse sand

Depth of Cover	Door Width	Gravity Level
First Set		
1. 1.0 $in.$ (25.4 mm)	1.0 $in.$ (25.4 mm)	80g
2. 2.0 $in.$ (50.8 mm)		
3. 2.5 $in.$ (63.5 mm)		
Second Set		
4. 2.0 $in.$ (50.8 mm)	2.0 $in.$ (50.8 mm)	40g
5. 4.0 $in.$ (101.6 mm)		
6. 5.0 $in.$ (127.0 mm)		

The results are presented in Figures 4-5 through 4-11. The force on the door normalized with respect to the theoretical geostatic load is plotted in Figure 4-5 for each of the tests as a function of the vertical door displacement. As before, the measured forces prior to any door movement are larger than the theoretical geostatic loads. The normalized initial forces are generally greater for the 1"(25.4 mm)-door/80g tests than for the 2"(50.8 mm)-door/40g tests. This is, again, a direct consequence of the difference in the stiffness between the door and the adjacent base.

With a finite door displacement the load in each test drops to a minimum value. This

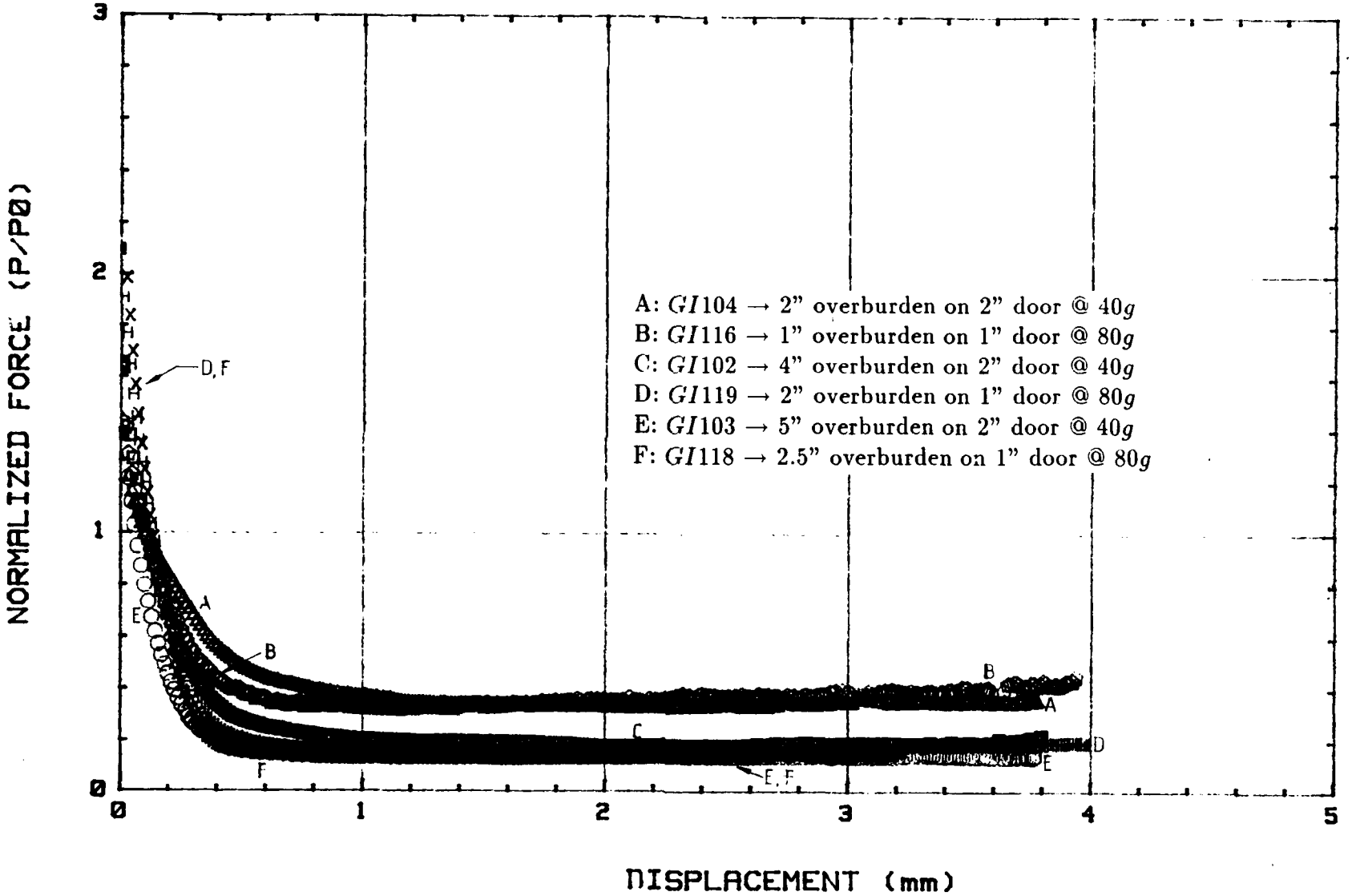

Figure 4-5: *Modelling of models* with coarse sand: Normalized force vs. door displacement

minimum force, normalized with respect to the theoretical geostatic load, is about the same for each pair of geometrically similar setups. Figure 4-6 shows the absolute (i.e., not normalized) force on the trapdoor versus the downward translation of the door for the 1"(25.4 mm)-door/80g and the 2"(50.8 mm)-door/40g experiments; to provide more detaila, only the portion of the curve where the force approaches the minimum value is shown. Not only do the plots group together for each set of tests carried out with the same door width at the same gravity level; they also tend to coincide in the vicinity of the minimum loads. This indicates the formation of an actual physical arch in the centrifuge trapdoor experiments. If the force on the trapdoor represents the weight of soil below the stable arch, then the volume of soil underneath the arch is roughly constant for each set of experiments with the same door size under the same gravitational field, regardless of the depth of overburden.

At N gravities, the minimum force P_{min} on the door is approximately equal to $N\gamma V$, where V is the volume of soil (unit weight γ) below the arch. From Figure 4-6, the minimum door load for the 2"(50.8 mm)-door/40g tests is about twice that for the 1"(25.4 mm)-door/80g tests. It follows then that the below-the-arch volume for the the 2"(50.8 mm)-door/40g tests is four times that for the 1"(25.4 mm)-door/80g tests. With the trapdoor lengths the same for both sets of tests and assuming plane strain conditions, a generic cross-section through the soil below the arch has an area which is four times larger in the 2"(50.8 mm)-door/40g tests than in the 1"(25.4 mm)-door/80g tests. This conforms with the geometric scaling factor of 2 for the door widths, wherein the scaling factor for planar areas should be $2^2 = 4$.

The fact that no noticeable subsidence on the surface has been observed in the tests supports the "physical arch" hypothesis. Photographs of the soil models taken at the end of some of the experiments are presented in Figure 4-7. Although the presumed physical arch is not so obvious from these pictures, they do show hardly any deformations on the surface of the samples.

Since this *modelling of models* is aimed at verifying the scaling laws, the results

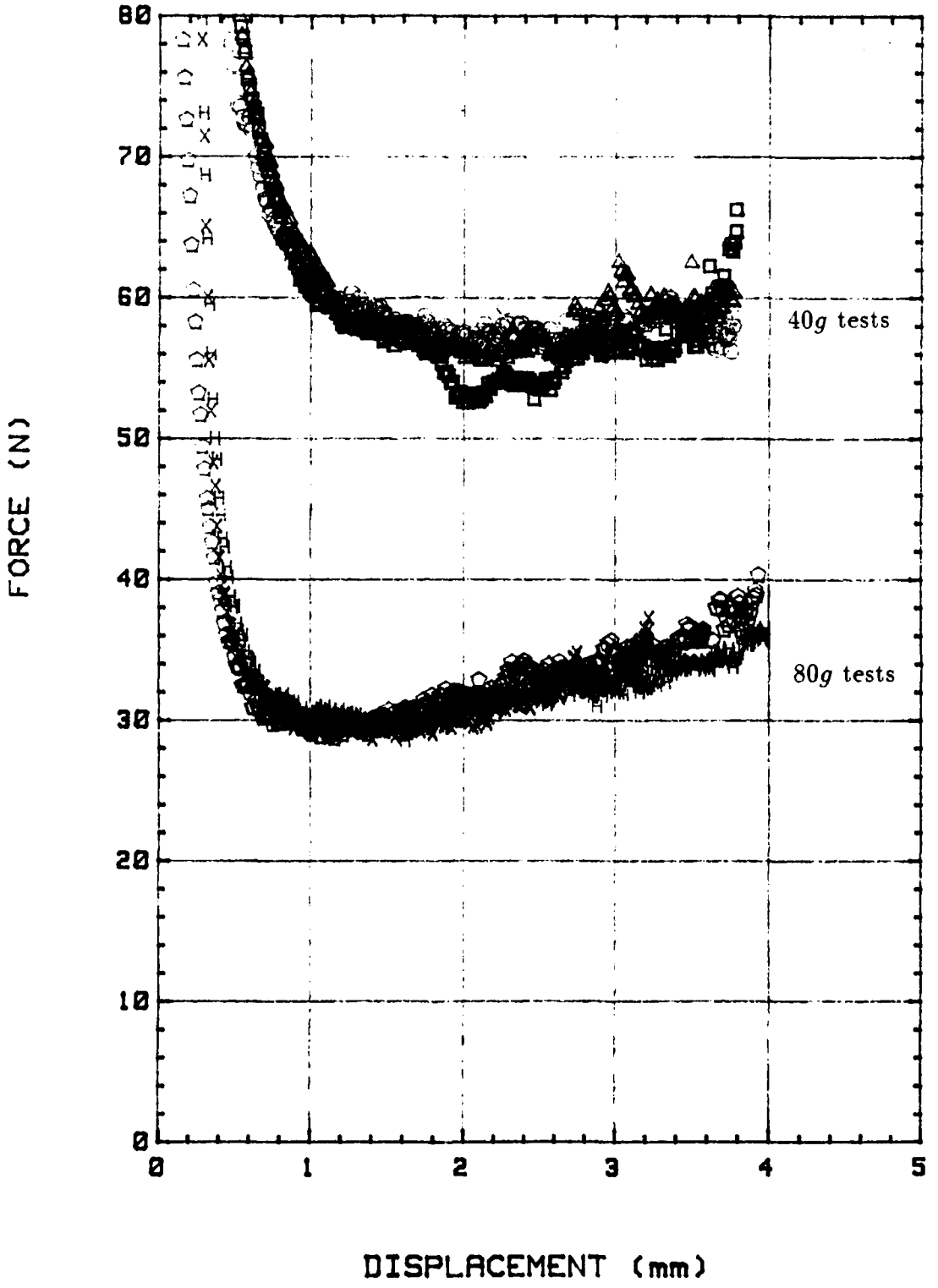

Figure 4-6: *Modelling of models* with coarse sand: Minimum (absolute) loads vs. door displacement

(a) Test $GI197$ - 1"(25.4 mm)-deep coarse sand on 1" (25.4 mm) door @ 80g

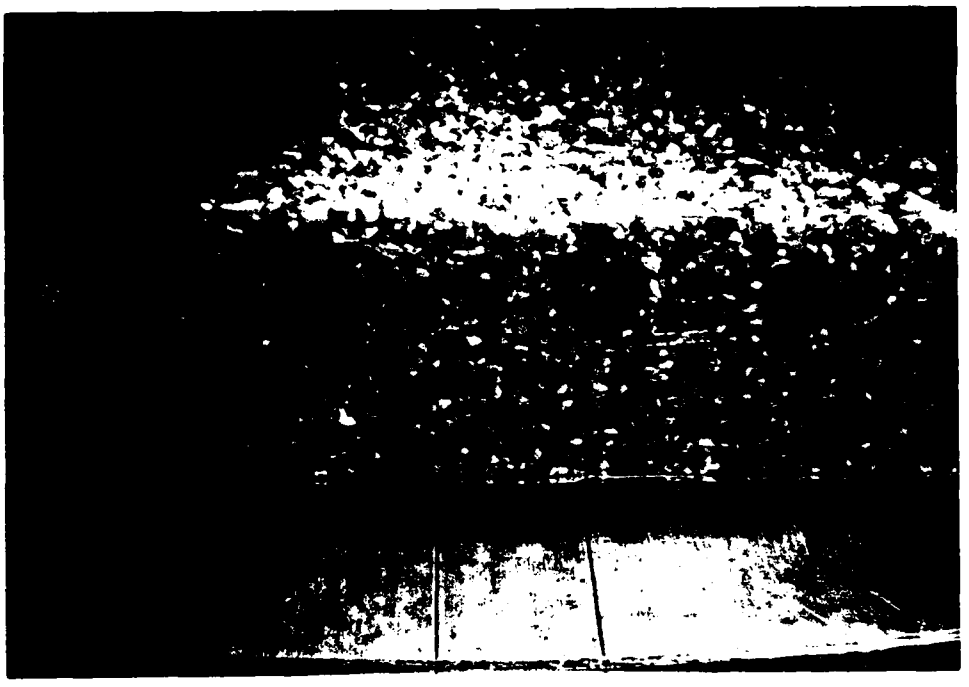

(b) Test $GI198$ - 2"(50.8 mm)-deep coarse sand on 1" (25.4 mm) door @ 80g

Figure 4-7: Test with coarse sand: Final configuration

should be examined in terms of dimensionless parameters. This is done in Figure 4-8, which looks like Figure 4-5 except that the abscissa is the door displacement normalized with respect to the door width. If similitude exists between the 1"(25.4 mm)-door/80g experiments and the correspondingly scaled 2"(50.8 mm)-door/40g cases, the normalized results for geometrically similar pairs should coincide. The curves in Figure 4-8 imply that the results apparently do not fulfill such a necessary condition. While the normalized minimum loads are about the same for analogous pairs, the corresponding dimensionless displacements at which these minimum forces occur do not seem to tally, especially for the specimens simulating deeper prototypes. (The match is actually a little bit better in Figure 4-5, where the displacement is not normalized at all.)

The slopes of the normalized force vs. normalized displacement curves (Figure 4-8) for geometrically similar arrangements do, however, appear to be parallel. A major reason, of course, why the dimensionless plots do not coincide is that the starting points are not the same. To correct for this difference, the data are adjusted such that zero displacement occurs where the normalized force ratio equals unity (or where the measured load equals the theoretical geostatic value). This correction scheme essentially shifts the curves in Figure 4-5 horizontally to those in Figure 4-9. The portion of the load-deformation plots in Figure 4-9 below the line $P/P_0 = 1$ may be considered to be the truly active arching mode and is then blown up, yielding Figure 4-10. When the adjusted displacement is normalized with respect to the width of the trapdoor, the resulting curves are those shown in Figure 4-11. This time, the data from each pair of analogous cases superpose nicely almost into one template. In other words, the shifted curves reasonably adhere to the similitude requirement that dimensionless ratios match for appropriately scaled systems.

4.1.2.4 Effect of g-level

Tests have also been run whereby identical models (i.e., same soil, depth of cover, and door width) are subjected to different pseudo-gravitational fields. These have been

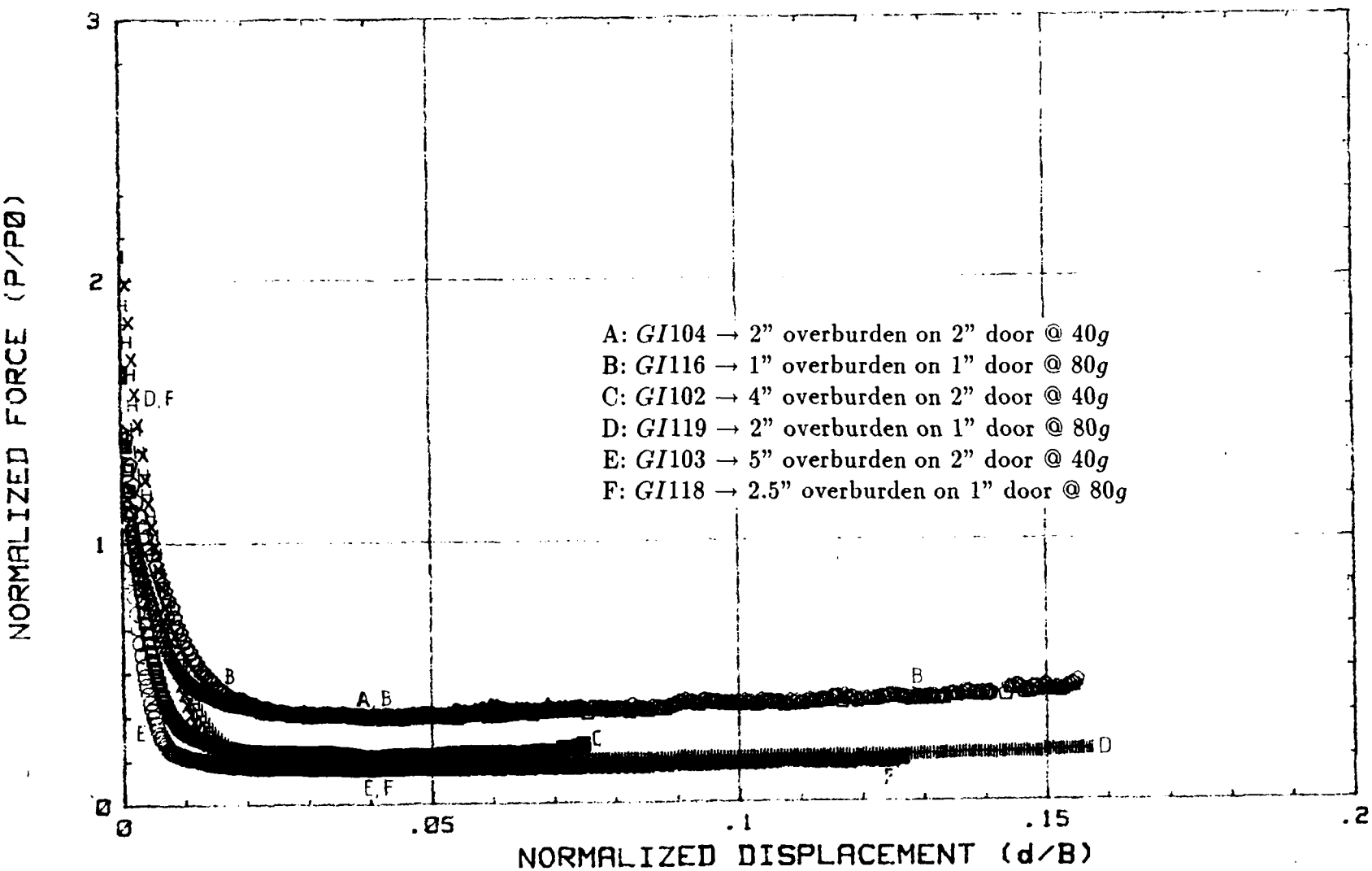

Figure 4-8: *Modelling of models* with coarse sand: Normalized force vs. displacement d normalized with respect to the door width B

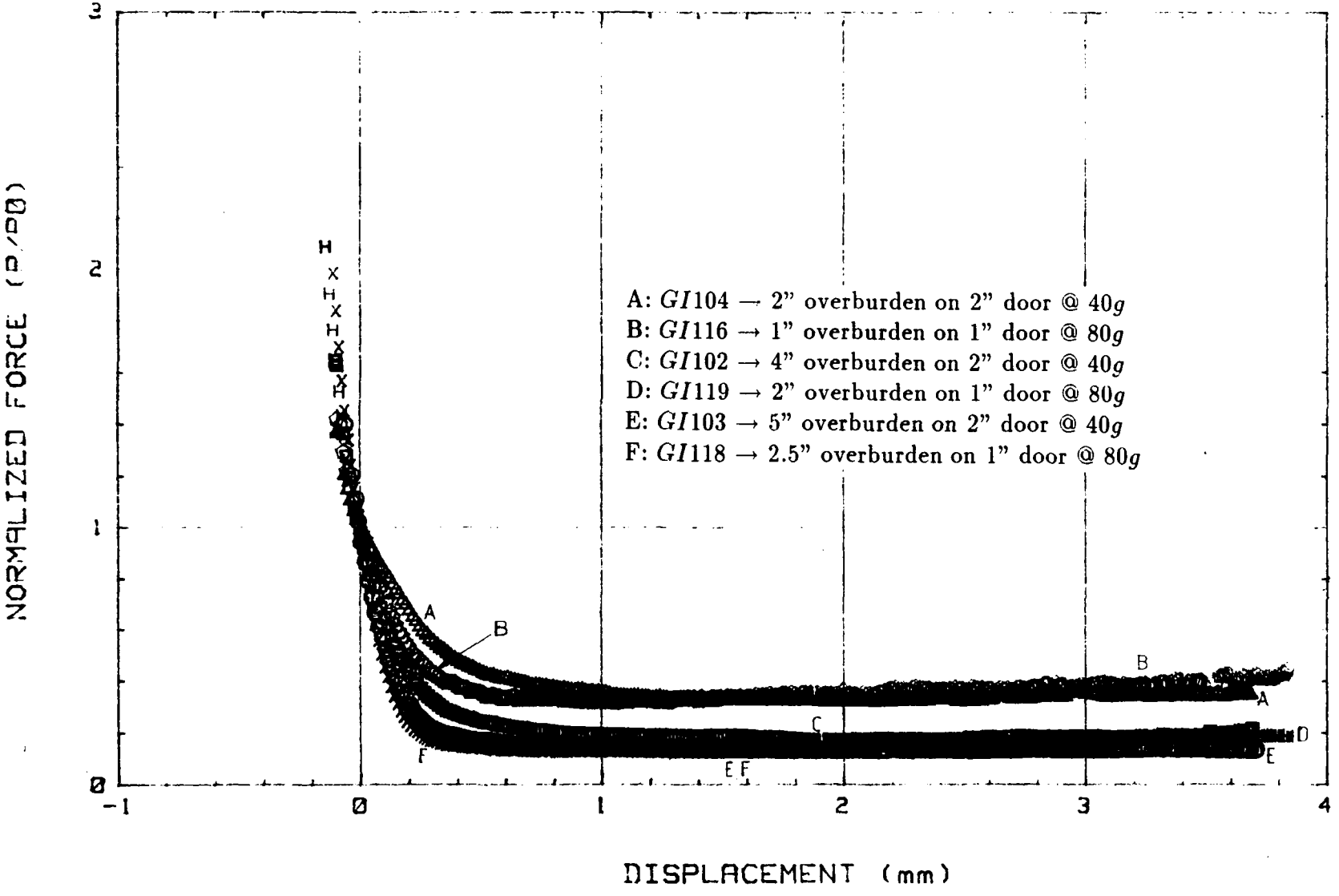

Figure 4-9: *Modelling of models* with coarse sand: Normalized force vs. adjusted displacement

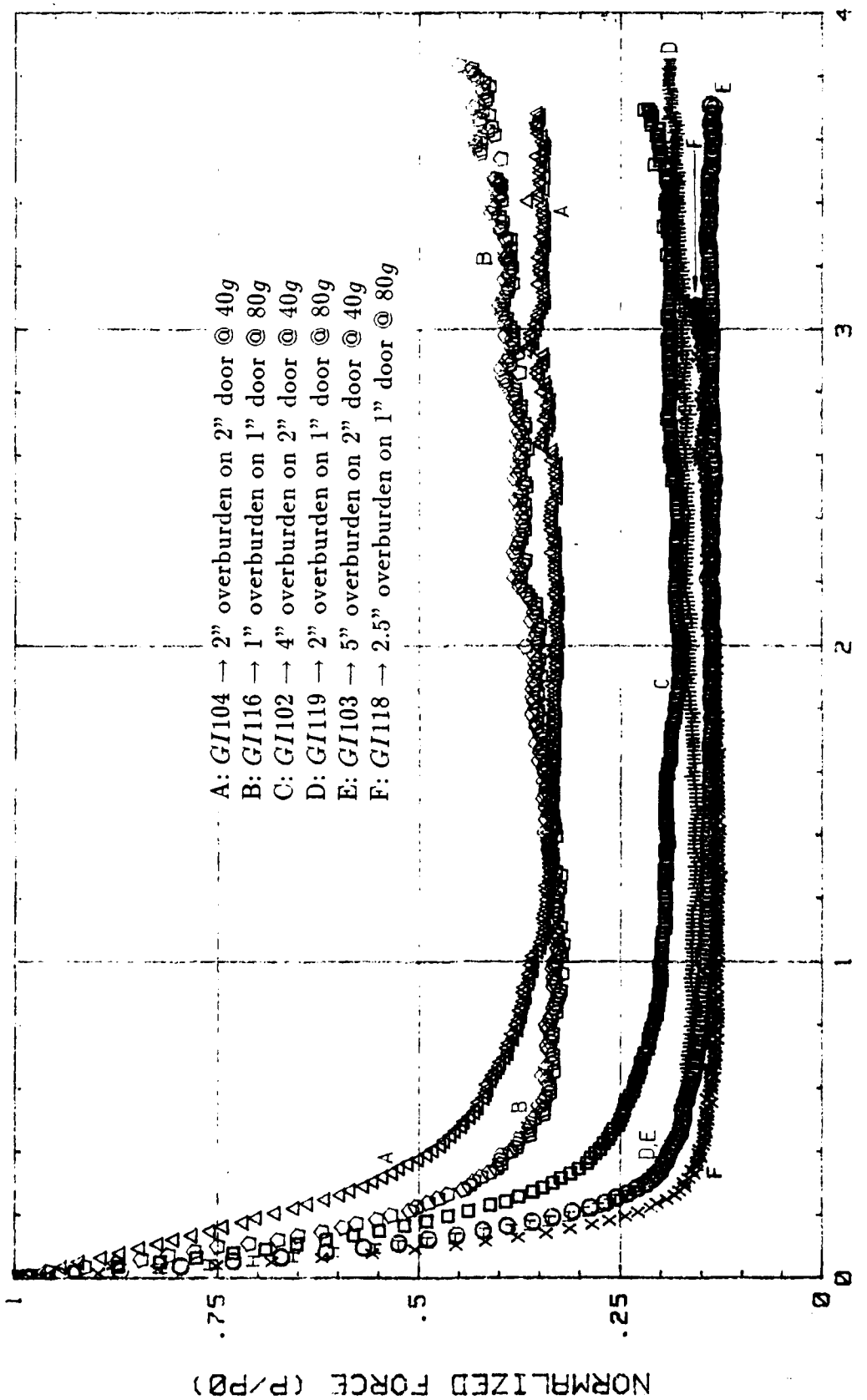

Figure 4-10: *Modelling of models* with coarse sand: Normalized force vs. adjusted displacement, active arching mode

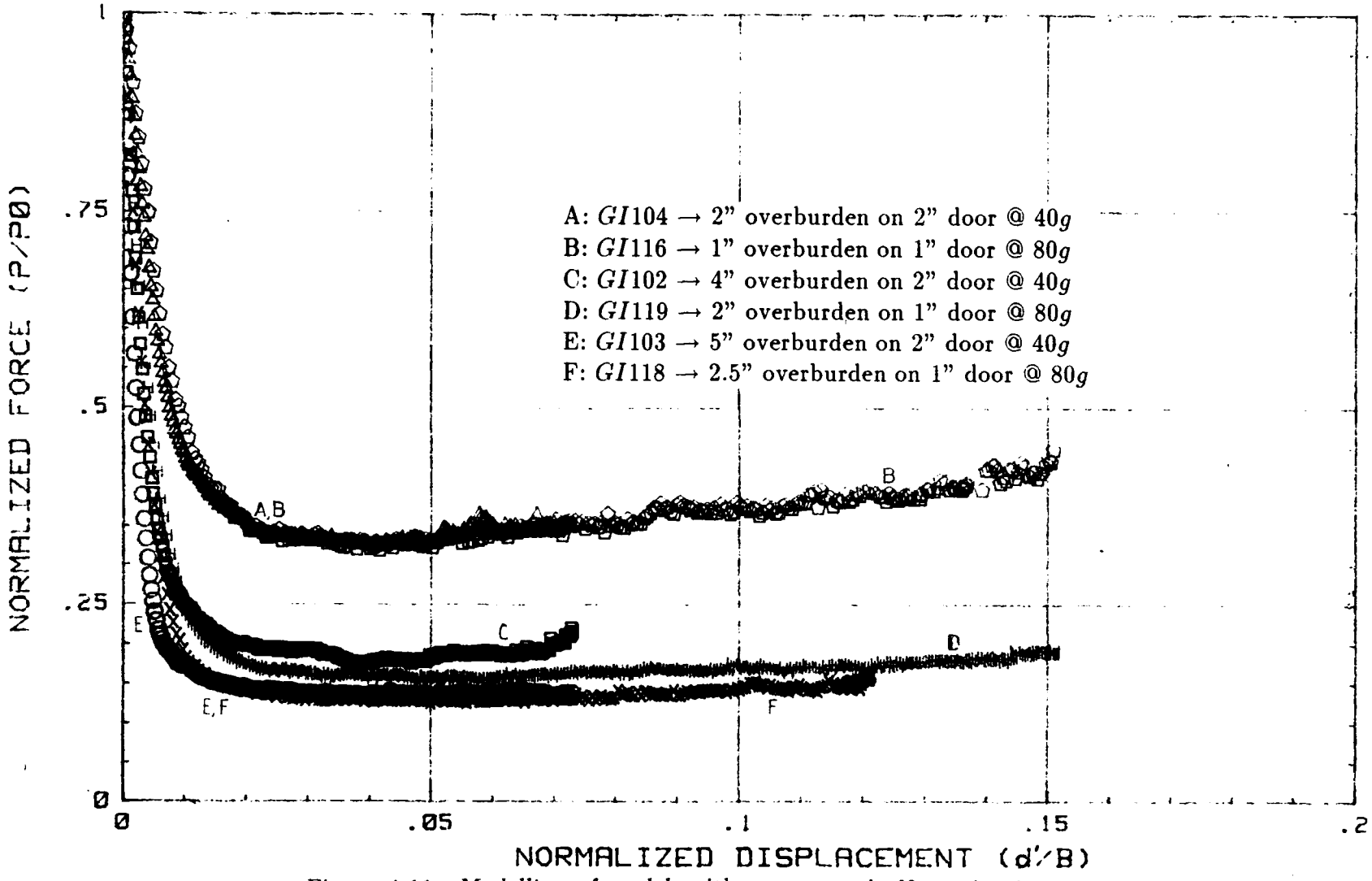

Figure 4-11: *Modelling of models* with coarse sand: Normalized force vs. adjusted displacement d' normalized with respect to the door width B, active arching mode

carried out with two different depths of coarse sand [2" (50.8 mm) and 4" (101.6 mm)] overlying the 2"(50.8 mm)-wide trapdoor at two acceleration levels ($40g$ and $80g$).

The results displayed in Figure 4-12 show that the normalized force vs. (unadjusted) door displacement curves coincide for the tests with 4" (101.6 mm) overburden but do not for the tests with 2" (50.8 mm) overburden. The 4" (101.6 mm) depth-of-cover test data support the "physical arch" hypothesis and imply that the same volume of soil travels with the trapdoor regardless of the g-level. In the experiments with 2" (50.8 mm) burial depth, the "below-the-arch" volume is apparently not the same in the $40g$ and $80g$ tests. As has been noted previously [e.g., Engesser (1882), Terzaghi (1943)], there is a lower limit to the depth of overburden for which a full redistribution of soil pressures can occur above the trapdoor. This lower limit is around 1.5 times the width of the door, while in the experiments with 2" (50.8 mm) burial depth $H/B = 1$.

4.1.3 Comparison with Previous Trapdoor Experiments

It is only fitting to compare the results from the centrifuge trapdoor tests in this study with those from previous experiments with a plane strain setup carried out under normal gravity. Specifically, Table 4.2 provides a comparison of the present data with the results obtained by Terzaghi (1936) and by Evans (1983).

For $\frac{H}{B} \approx 4$, the three sets of experiments produce more or less the same minimum load ratios (~ 0.09) and normalized displacements $\frac{\delta_{min}}{B}$ (~ 0.02) at which these minimum values occur. The minimum load ratios for the other overburden depths at $1g$ are comparable with those at $80g$, although the forces tend to be larger in the latter as $\frac{H}{B} < 2$. Moreover, Evans (1983) has obtained a trend that the the minimum load occurs at smaller displacements as the overburden becomes shallower; an opposite trend is observed in the centrifuge tests. Presumably, the higher stress levels induced by the elevated gravity field allow the formation of the arch more rapidly as the door is displaced for cases with relatively deep soils.

A major difference between the single gravity and centrifuge experimental results is

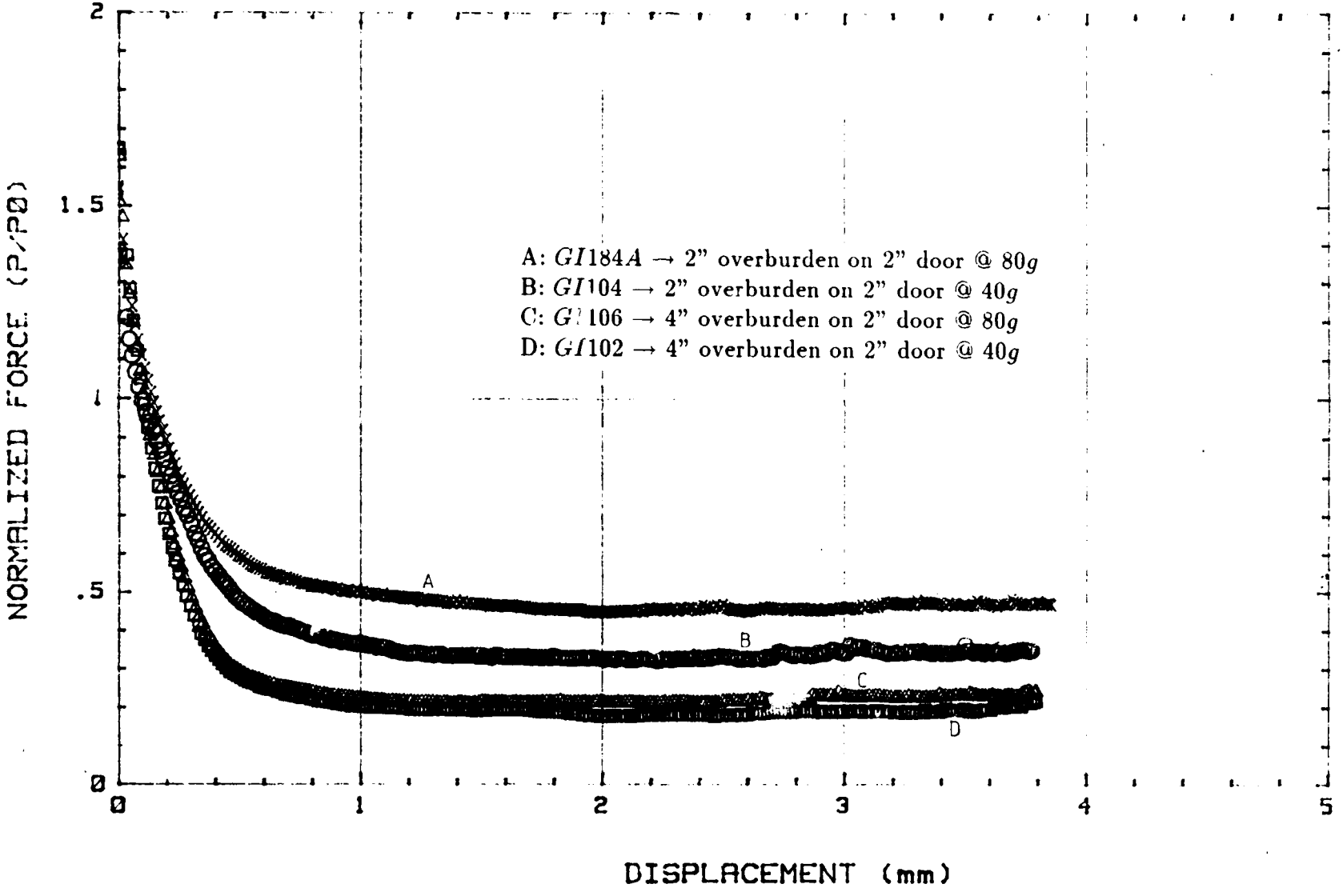

Figure 4-12: Tests with identical coarse sand setups at different g's

Table 4.2: Comparison of Past and Present Trapdoor Experiments with Sand

Sand type	$\frac{H}{B}$	$\frac{\delta_{min}}{B}$	$\frac{P_{min}}{P_0}$	$\frac{\delta_{ult}}{B}$	$\frac{P_{ult}}{P_0}$	λ^a
Terzaghi (1936)						
Loose sand	4.25	0.022	0.10	0.116	0.128	0.298
Dense sand, $\phi = 44°$	4.25	0.0096	0.063	0.116	0.128	0.611
Evans (1983)						
Medium tan sand, $\phi = 38°$	5	0.026	0.091	0.10	0.130	0.527
	3.1	0.026	0.093	0.089	0.217	1.968
	2	0.013	0.16	0.116	0.221	0.592
	1	0.0028	0.315	0.068	0.869	8.497
Iglesia (1991)[b]: Tests with 1"(25.4 mm)-wide door @ 80g						
NJ coarse sand, $\phi = 39°$	4	0.020	0.09	0.12	0.11	0.20
	2	0.025	0.18	0.15	0.19	0.16
	1	0.032	0.36	0.15	0.40	0.34

[a] Load Increase Index: $\lambda = \frac{\frac{P_{ult}}{P_0} - \frac{P_{min}}{P_0}}{\frac{\delta_{ult}}{B} - \frac{\delta_{min}}{B}}$

[b] Displacement values have been adjusted so that zero displacement is where the measured force equals the theoretical overburden load.

the slope of the load-deformation curve after the minimum force is reached. In order to evaluate this difference quantitatively, a parameter called the *load increase index* is introduced. It is essentially the average slope of the normalized force vs. normalized displacement plot after the minimum door load occurs and is defined as

$$\lambda = \frac{\frac{P_{ult}}{P_0} - \frac{P_{min}}{P_0}}{\frac{\delta_{ult}}{B} - \frac{\delta_{min}}{B}} \tag{4.1}$$

The parameter λ is, thus, a measure of the rate of increase of the load on the trapdoor as it is continually displaced after its minimum is achieved. One sees in Table 4.2 that the load in the centrifuge tests does not increase as much as in the experiments at 1g.

4.2 Tests with Glass Beads

The experiments with coarse sand have been performed at different gravity levels without scaling the particle size; i.e., the same soil has been used throughout. To investigate the effects of proportioning the grain size with g-level, glass beads in uniform sizes have been utilized as the geomaterial overlying the trapdoor. Compared to natural soil, glass beads have the advantage of being commercially available in spherical shapes of various sizes, with relatively minimal variation in particle properties.

4.2.1 Material Description and Test Procedure

Four (4) major sizes have been ordered: 0.5 $mm\varnothing$ (size range 350 - 710 $microns\varnothing$), 1.5 $mm\varnothing$ (1.4 - 1.6 $mm\varnothing$ range), 3.0 $mm\varnothing$ (2.5 - 3.5 $mm\varnothing$ range), and 6.0 $mm\varnothing$ (5.5 - 6.5 $mm\varnothing$ range). The glass beads procured for the trapdoor tests are grinding media used in high speed mills by manufacturers of dyes, paints, pharmaceuticals, carbon paper and ribbon, and the like. The chemical composition of the glass beads as provided by the supplier is itemized in Table 4.3. Other properties determined by the glass bead manufacturer include the specific gravity (~ 2.55), modulus of elasticity ($\sim$14.3 GPa), Poisson's ratio (~ 0.27), and Rockwell hardness (~ 47). At MIT, direct shear tests have been performed with the glass beads using an applied normal stress of 98 kPa; the measured friction angle values have ranged from $\sim 27°$ for the 1.5 $mm\varnothing$ beads ($e \approx 0.54$) to $\sim 30°$ for the 6.0 $mm\varnothing$ beads ($e \approx 0.50$).

Table 4.3: Chemical composition of glass beads

Silica	(SiO_2)	67%
Soda	(Na_2O)	10%
Potassium Oxide	(K_2O)	7%
Barium Oxide	(BaO)	6%
Lime	(CaO)	5%
Boric Oxide	(B_2O_3)	2%
Aluminum Oxide	(Al_2O_3)	1%
Magnesium Oxide	(MgO)	1%

The specimen preparation technique is basically the same as for the coarse sand experiments. The glass beads are poured by hand into the trapdoor package until the desired depth is attained. The surface is then evened out horizontally by carefully scraping the excess particles at the elevated sites over to the deficient locations. This process yields a density of $\sim 110\ lb/ft^3$ ($1764\ kg/m^3$), corresponding to a void ratio e of 0.45 or a relative density D_r of about 83%.

The spin-up and trapdoor-lowering routines in the glass bead tests are the same as in the centrifuge experiments with coarse sand.

4.2.2 Results

As with the sand tests, the load vs. door displacement curve can be drawn. The relevant data are the measurements during the monitored settlement of the trapdoor at the top rotational speed of the centrifuge. The results presented in the following are again from the middle segment (LC2), which is least influenced by end effects. [Results from all three segments can be found in Iglesia's (1991) thesis.]

4.2.2.1 Modelling of Models

The scaling relations (covered in Chapter 2) for length dimensions stipulate that, for complete similitude between model and prototype, the particle size of granular media should be proportioned according to the gravity level. To verify this, a *modelling of models* scheme is implemented using the various glass bead sizes and the trapdoor apparatus (with different door widths) in the centrifuge. The series of tests involved are shown in Table 4.4.

The main results obtained from the *modelling of models* experiments with glass beads are presented in Figures 4-13 through 4-15. Figure 4-13 shows the force on the trapdoor, normalized with respect to the theoretical geostatic load, plotted against the downward door movement for each of the three arrangements (Table 4.4). As in the sand tests, the measured forces start out greater than the theoretical values, with the difference

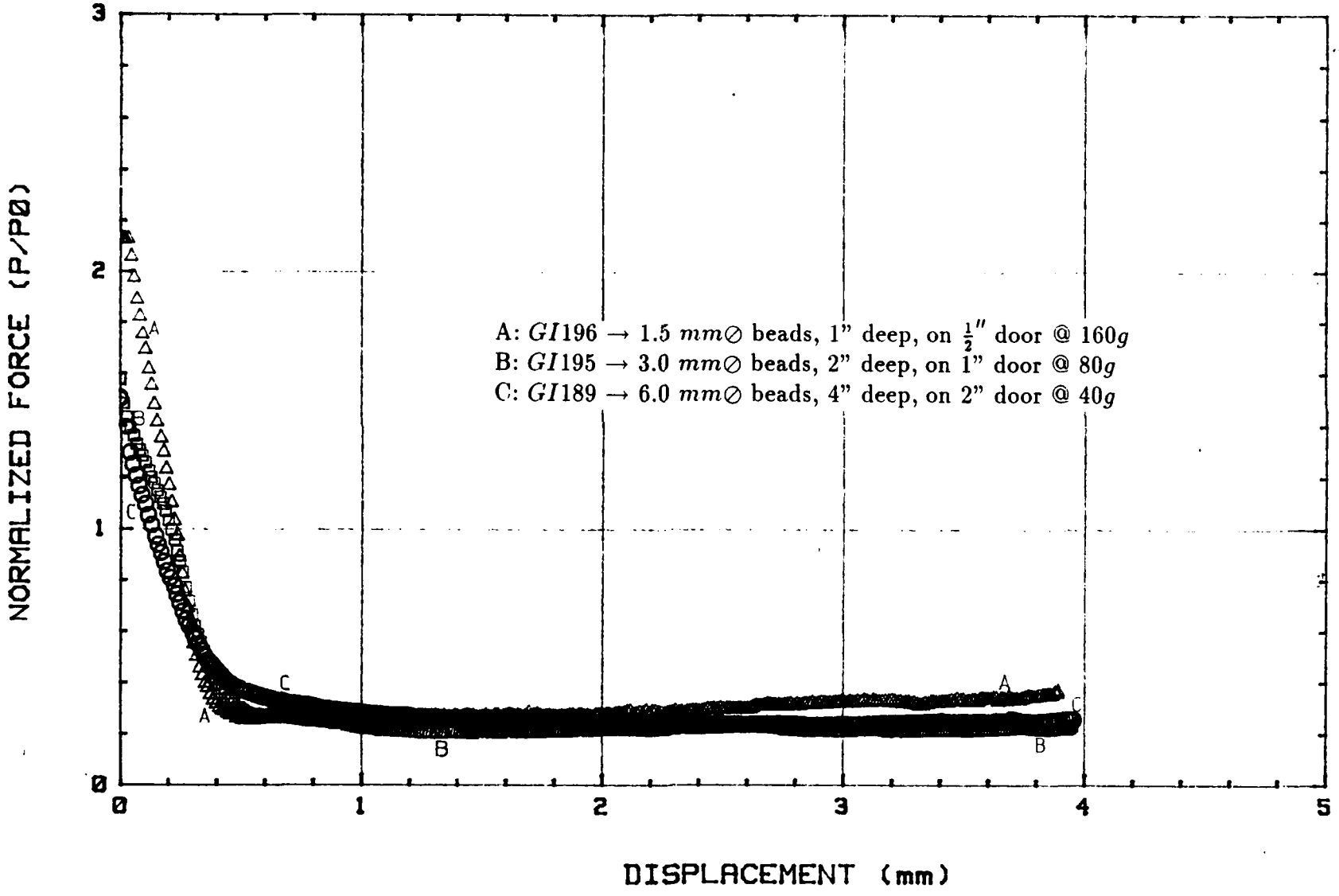

Figure 4-13: *Modelling of models* with glass beads: Normalized force vs. door displacement

Table 4.4: *Modelling of models* with glass beads

	Bead Diameter	Depth of Cover	Door Width	Gravity Level
1.	6.0 *mm*	4.0 *in.* (101.6 *mm*)	2.0 *in.* (50.8 *mm*)	40*g*
2.	3.0 *mm*	2.0 *in.* (50.8 *mm*)	1.0 *in.* (25.4 *mm*)	80*g*
3.	1.5 *mm*	1.0 *in.* (25.4 *mm*)	0.5 *in.* (12.7 *mm*)	160*g*

greater at the higher gravities. After the door is put into motion, the load decreases to about the same minimum normalized value of ~ 0.25 in all three cases. This minimum value appears to occur at about the same door displacement. Due to different starting points, however, the initial segments of the normalized force vs. displacement curves in Figure 4-13 do not coincide.

When the data are adjusted such that the displacement starts at the point where the measured force matches the theoretical overburden load, the resulting graphs look as shown in Figure 4-14. (The scale has been expanded to display only the portion where $P/P_{0t} \leq 1$.) It is evident that the door loads in the smaller-scale/higher-g models drop to the minimum values at relatively smaller displacements.

The interesting part is that the (adjusted) displacements at which the minimum forces are attained seem to be related as 1:2:4 from the 160g tests to the 80g tests to the 40g tests. (These displacement values, thus, obey the scaling rules for length dimensions.) This is confirmed when the data in Figure 4-14 are re-plotted in dimensionless space by normalizing the adjusted displacement with respect to the door width (Figure 4-15). The three curves in Figure 4-15 tend to follow exactly the same pattern. This nice superposition indicates that proper similitude is achieved when the grain size is appropriately scaled together with the overall model dimension and gravity level.

The extent to which the door can be lowered is the same for all the tests. Even after the data are corrected so that the normalized forces start out at unity, the maximum door displacement is still roughly the same in the three geometrically similar cases. Hence, the normalization of displacements would inevitably compress the curves from the tests with

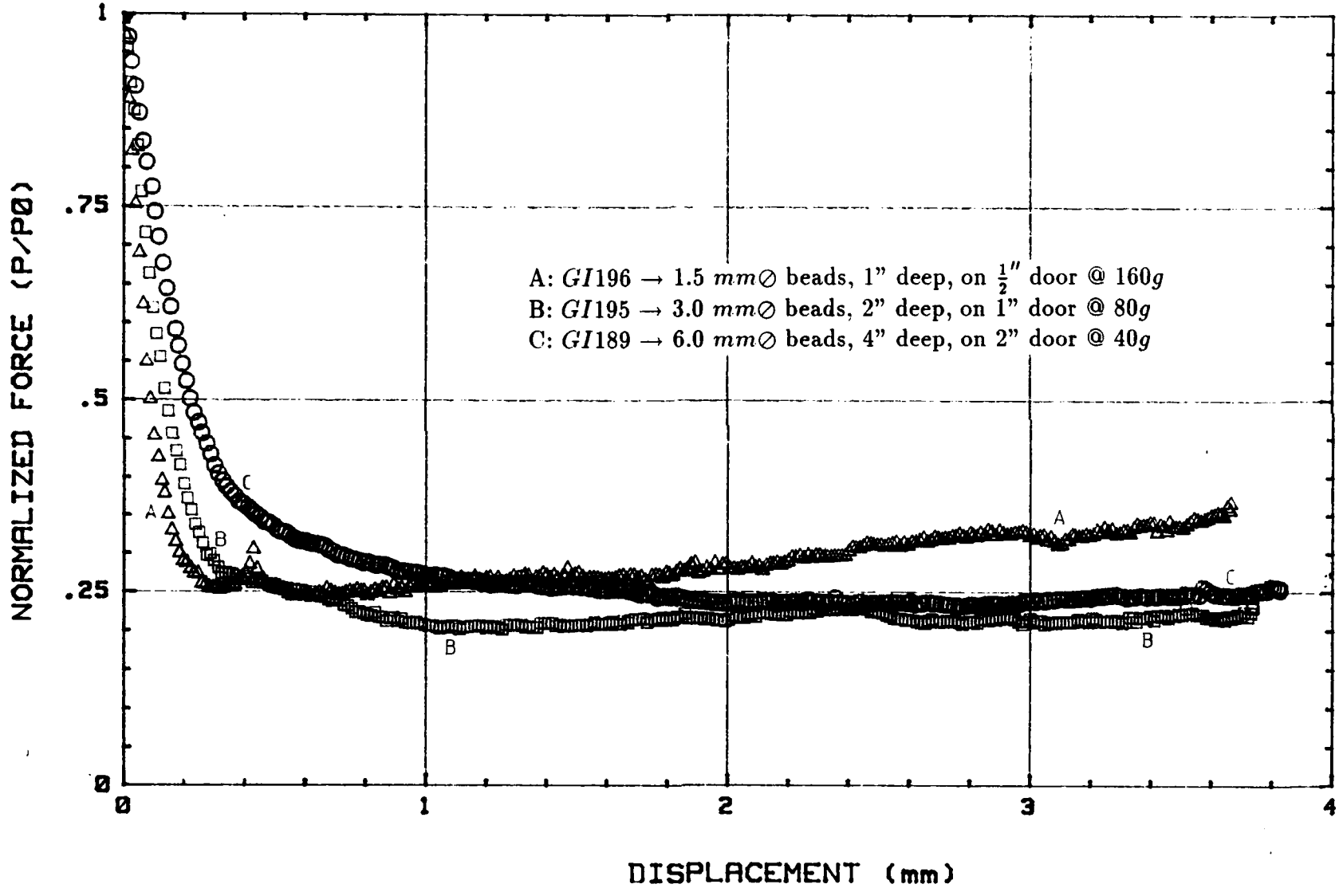

Figure 4-14: *Modelling of models* with glass beads: Normalized force vs. adjusted displacement (active arching mode)

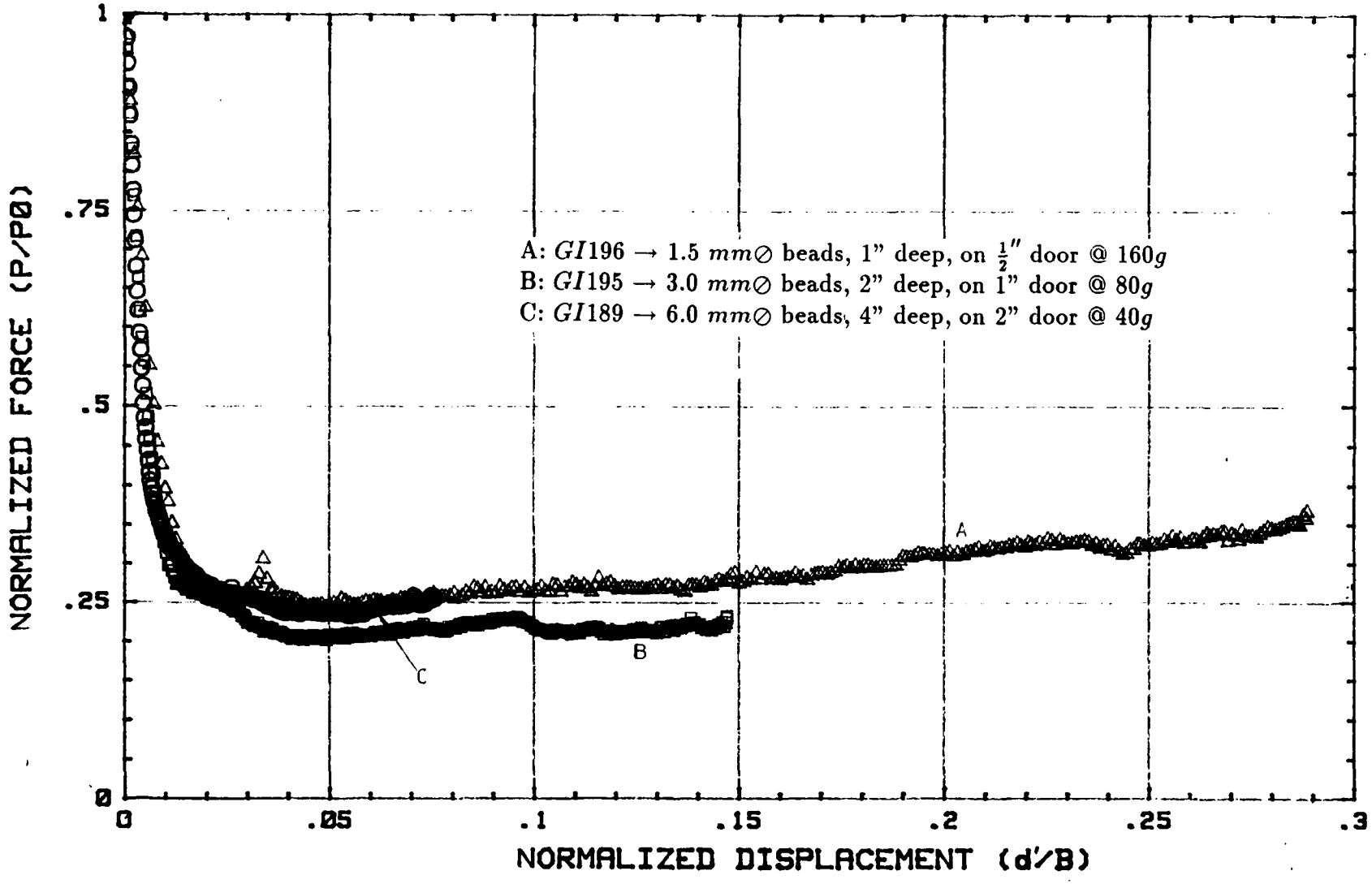

Figure 4-15: *Modelling of models* with glass beads: Normalized force vs. adjusted displacement d' normalized with respect to the door width B (active arching mode)

wider doors. Presumably, from Figure 4-15, if the 2"(50.8 mm)-wide and 1"(25.4 mm)-wide doors can be displaced further, the resulting curves would also exhibit a gradual increase in the load similar to the test with the 0.5"(12.7 mm)-wide door.

In some of the tests, colored glass beads have been placed in horizontal layers so that the deformation of the soil after each experiment may be observed. Figure 4-16 shows photographs of the post-test appearance typical of the glass bead setups. Surface deformations are practically unnoticeable, and the formation of a physical arch is quite evident. Only a volume of material within a limited zone just above the trapdoor has clearly followed the downward movement of the door. This corresponds to the force measurements, which indicate that the load remains approximately constant after the minimum value is reached. It should also be noted that the shape of the arch at the end of each experiment appears to be curved in the 2"(50.8 mm)-door/40g tests and tends to become triangular in the $\frac{1}{2}$"(12.7 mm)-door/160g tests. Since the final door displacements are the same in each case, this implies that the shape of the arch changes as the door settles more in proportion to the door width (or the grain size, for these scaled tests).

4.2.2.2 Tests with Compensatory Lowering of Door During Spin-up

A few tests have been conducted to compensate for the stiffer door relative to the neighboring substratum – without making structural changes in the trapdoor setup. The scheme entails an incremental lowering of the trapdoor during the spin-up phase so that, before the "main event" of continuous door displacement, the measured force is approximately equal to the theoretical overburden load. The distance to which the door is moved down incrementally can be estimated from the relative displacement data obtained from the tests with the proximity sensor setup (see Chapter 3).

For example, Test *GI*202 has the package filled with 3-$mm\oslash$ glass beads, 2" (50.8 mm) deep, overlying the 1"(25.4 mm)-wide door with the "main event" at 80g. From the proximity sensor data of Table 3.2, the relative displacement at 80g between the door

(a) Test $GI201$ – 3-$mm\oslash$ glass beads, 2" (50.8 mm) deep, on 1" (25.4 mm) door @ $80g$

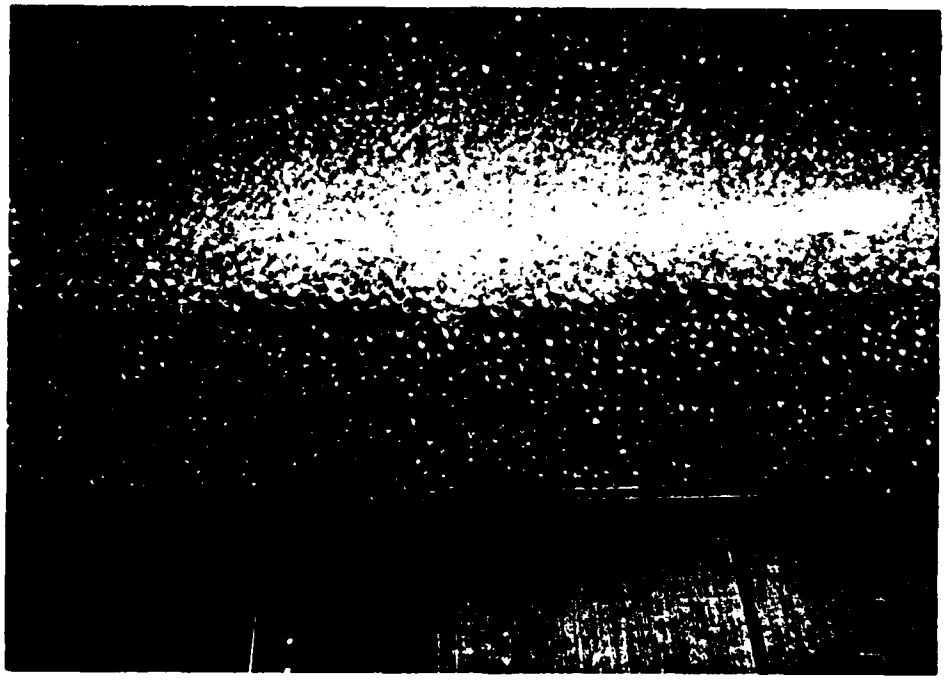

(b) Test $GI196$ – 1.5-$mm\oslash$ glass beads, 1" (25.4 mm) deep, on $\frac{1}{2}$" (12.7 mm) door @ $160g$

Figure 4-16: Experiments with glass beads: Final configuration

and the adjacent base is 0.222 mm. Thus, this is the total distance to which the trapdoor is to be pre-lowered, i.e., before the "main event." The door is incrementally displaced 0.028 mm, 0.083 mm, and 0.11 mm, respectively, at the intermediate acceleration levels $20g$, $40g$, and $60g$. Figure 4-17 illustrates the variation of the measured force on the middle segment as the centrifuge experiment proceeds for Test $GI202$.

The results shown in Figure 4-18 are for the Test $GI202$, if the measured force during the "main event" is normalized with respect to the theoretical geostatic load and is plotted against the displacement of the door from its pre-lowered position. For comparison with a similar test without any pre-lowering, the normalized force vs. (adjusted) displacement data from Test $GI201$ are also plotted in Figure 4-18. It can be seen that the "pre-lowering" procedure does not completely neutralize the effect of the non-uniform stiffness at the bottom of the soil since the measured force is still greater (by about 20%) than the theoretical overburden load. More importantly, however, the results from the tests with pre-lowering and without pre-lowering, but with the displacement data adjusted in the latter such that the origin is where the measured and theoretical geostatic forces match, are practically the same. This holds true even if the displacement values for the test with pre-lowering are "corrected" in a similar fashion, as can be observed in Figure 4-19. These results justify the adjustment of the displacement data as was done in the earlier sections.

4.2.2.3 Different "Soils" on Same Trapdoor

The *modelling of models* series of tests carried out with coarse sand and glass beads have demonstrated that $\frac{1}{N}$ scale models of granular media, when brought up to an Ng environment, simulate the prototype. It is not clear, however, whether it is absolutely necessary to proportion the particle size depending on the g-level to achieve reasonable similitude. The glass bead experiments strongly indicate that, to obtain similarity, a completely-scaled system is necessary; the coarse sand experiments imply that it might be possible to obtain sensibly analogous behavior without having to scale the grain size.

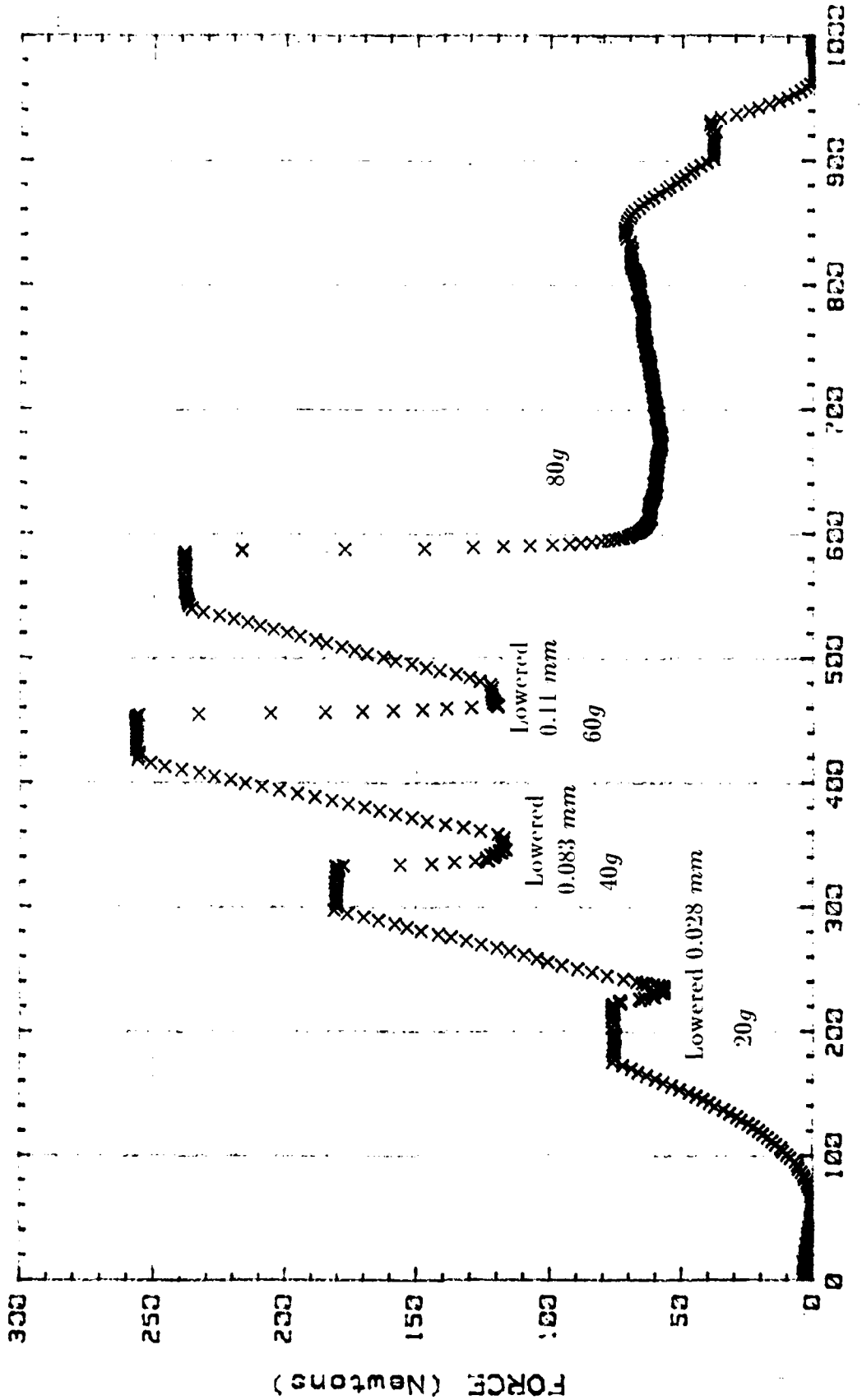

Figure 4-17: Test *GI202*: 3-*mm*∅ glass beads, 2" (50.8 *mm*) deep, on 1" (25.4 *mm*) door @ 80*g* *with pre-lowering*

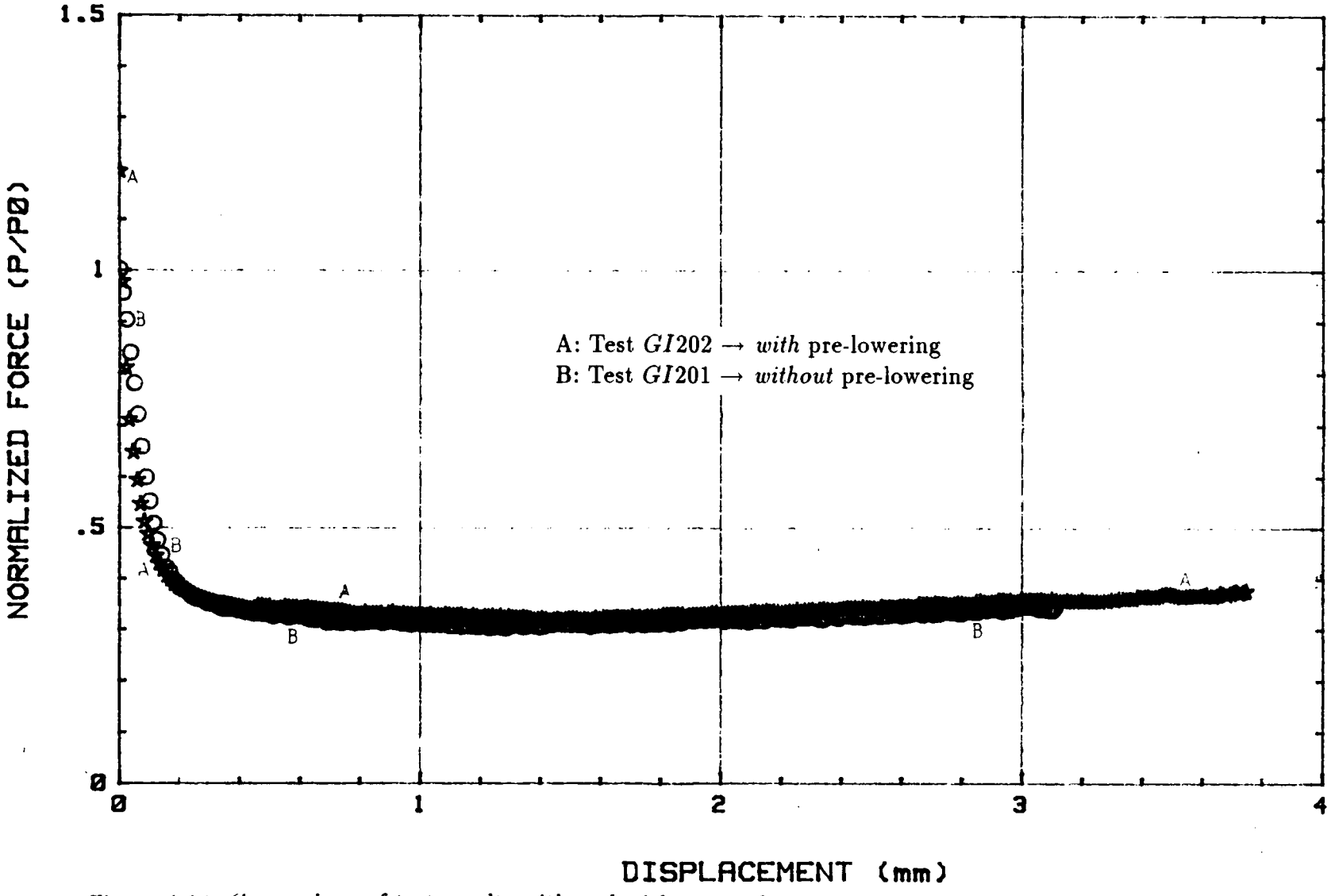

Figure 4-18: Comparison of test results with and without pre-lowering (displacement data adjusted in the latter)

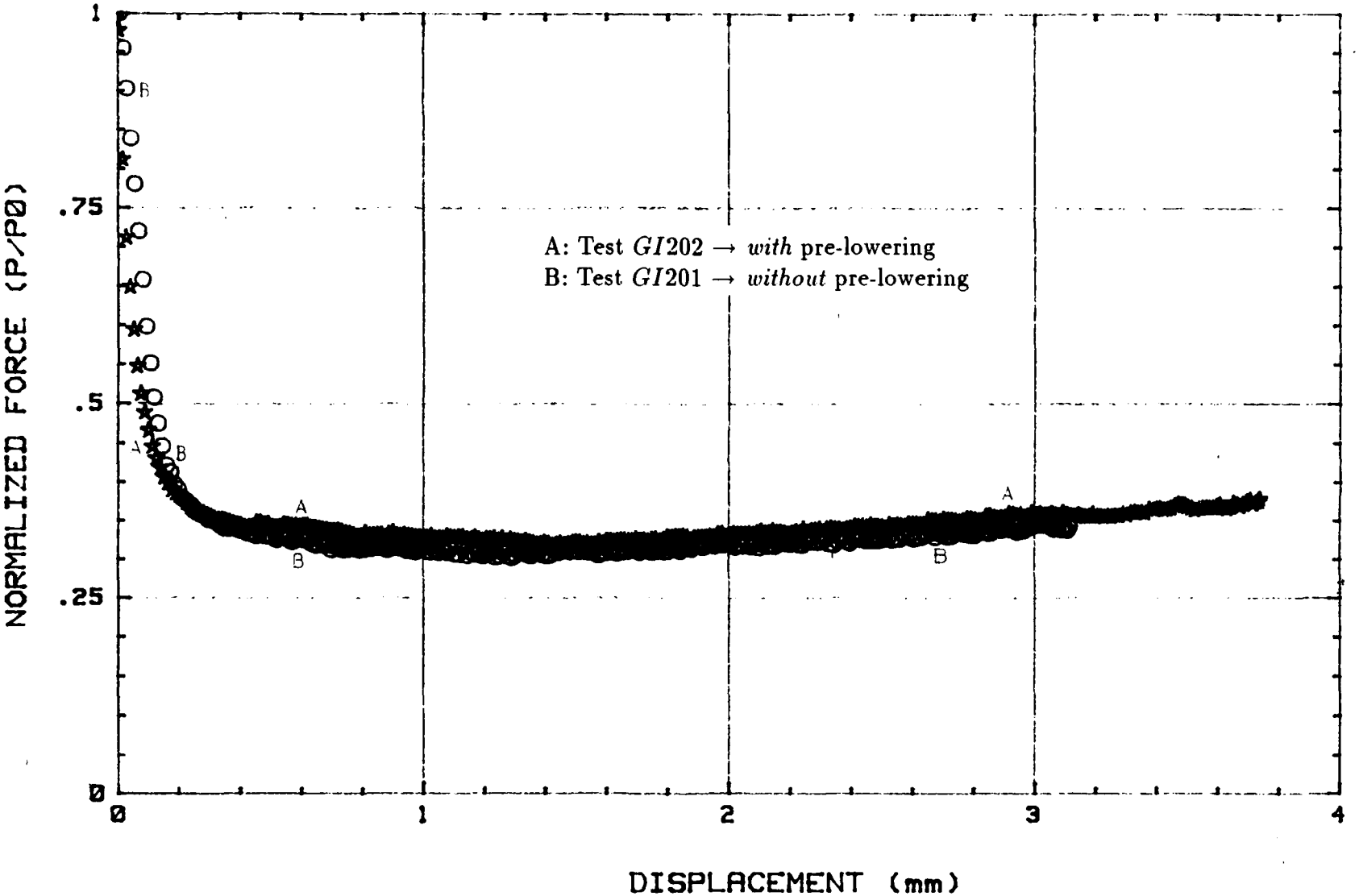

Figure 4-19: Comparison of test results with and without pre-lowering (displacement data adjusted in both)

In attempting to resolve this issue of particle size scaling, several tests, utilizing glass beads of a different nominal diameter and deposited to the same depth over the same trapdoor under the same g-field, have been conducted. Specifically, the experiments are run with the 2"(50.8 mm)-wide trapdoor underneath the granular mass, 2"(50.8 mm) deep, at $80g$, using all the glass bead sizes and coarse sand.

The data from these experiments are shown in Figures 4-20 and 4-21. The displacement values in Figure 4-20 have already been adjusted so that the starting point is where the measured force equals the theoretical geostatic load before door lowering. As usual, the ordinate represents the force on the door normalized with respect to the theoretical geostatic value. Qualitatively, the results follow the same trend; i.e., the load drops steeply with displacement until a minimum value is attained, followed by a gradual increase in the door force with continued door settlement. The curves tend to coincide, however, only at small displacements up to $\sim$0.2 mm, after which they begin to diverge.

Regarding the tests with glass beads, the minimum loads range from $\sim$ 50% to $\sim$ 60% of the theoretical overburden and occur at smaller displacements for the finer grains. Moreover, the normalized forces at the maximum door displacement (roughly the same at about 3 mm, before data adjustment, for all cases) turn out to be greater for the tests with smaller particles. Considering, however, that the range of particle sizes used covers about an order of magnitude, the effect of varying grain sizes does not appear to be very significant, especially at small door displacements.

The normalized load vs. displacement curve for the coarse sand experiment is almost parallel to that for the 6-$mm\oslash$ glass bead test. The load values in the former, however, are generally lower, due to the greater friction angle of the sand (39°) compared to the glass beads ($\sim$ 28.5°).

In order to examine further the effects of particle size, the displacement data are normalized with respect to the grain size, as portrayed in Figure 4-21. The resulting curves in the dimensionless plane do not quite match, especially where the load tends to increase after the minimum load occurs. The minimum normalized force also does not

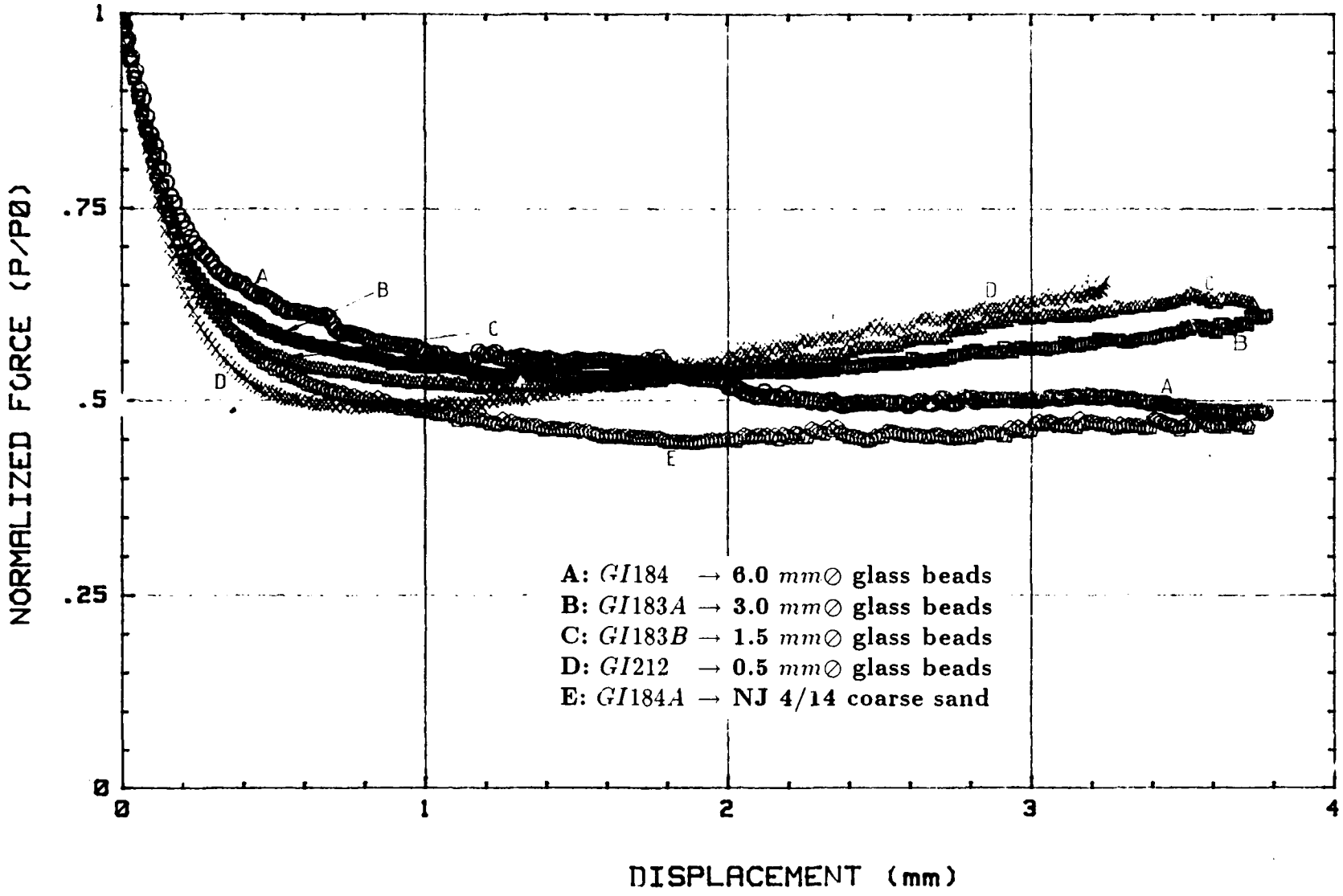

Figure 4-20: Different "soils," 2" (50.8 *mm*) deep, on 2" (50.8 *mm*) door @ 80*g*: Normalized force vs. adjusted displacement

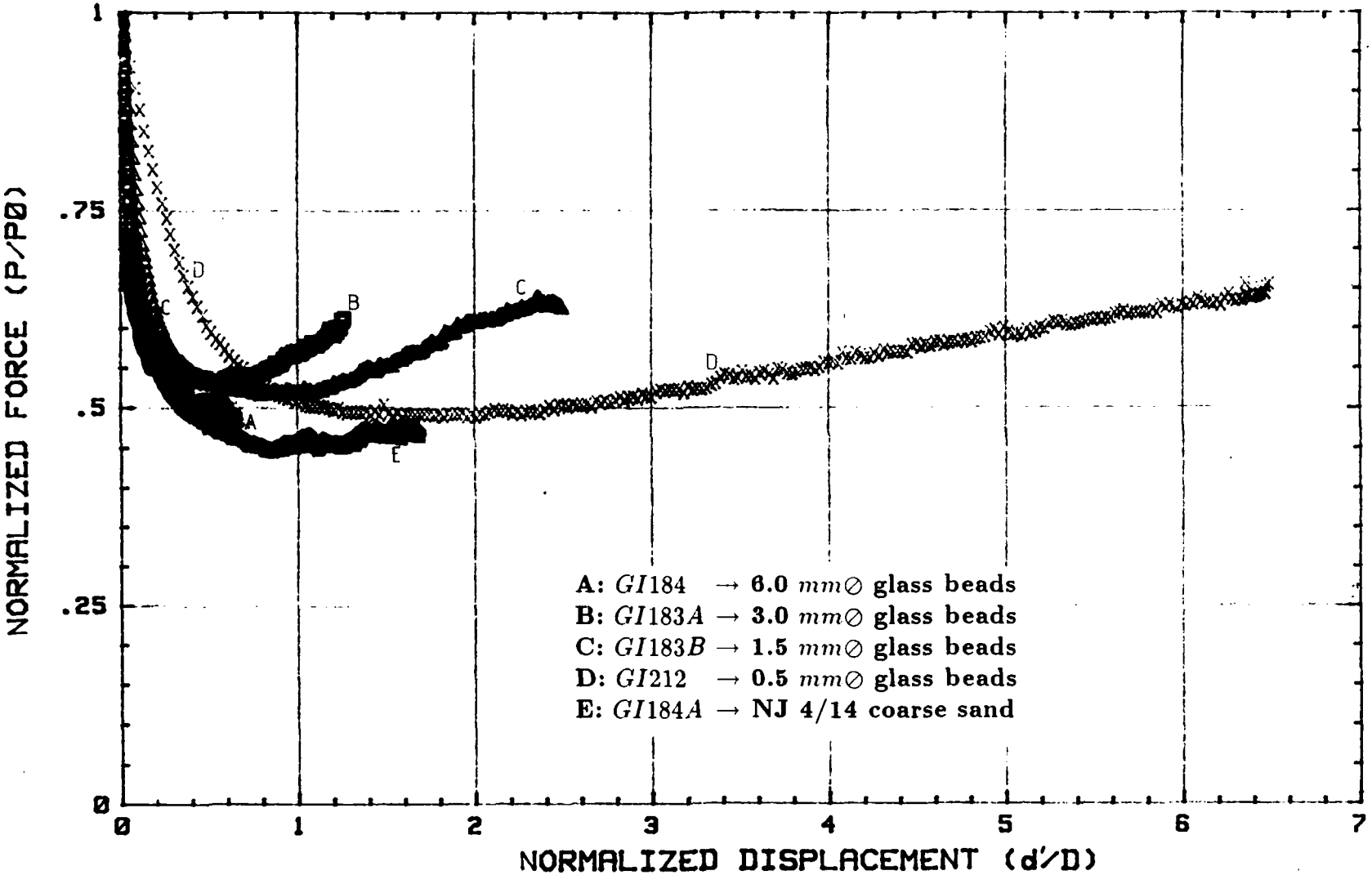

Figure 4-21: Different "soils," 2" (50.8 *mm*) deep, on 2" (50.8 *mm*) door @ 80*g*: Normalized force vs. adjusted displacement *d'* normalized with respect to grain size *D*

take place at the same normalized displacement for the different experiments. Thus, it is clear that, to model a prototype behavior over a wide range of displacements, the grain size will have to be scaled.

4.2.2.4 Same Soil on Different Door Widths

The effect of the trapdoor width on arching is examined further by considering the results from the experiments performed at the same g-level with the same granular medium (i.e., same grain size and overburden depth) overlying different trapdoor widths. One such set of results is exhibited in Figure 4-22, which is extracted from tests conducted at $80g$ with 6-$mm\oslash$ glass beads, 2" (50.8 mm) in depth using two door widths: 2" (50.8 mm) [Test $GI184$] and $\frac{1}{2}$" (12.7 mm) [Test $GI211$]. Clearly, the minimum loads and the displacements at which they take place are not the same in the two cases, implying the dependence of arching on the door width. An interesting observation is that the minimum load (as a percentage of the geostatic value) and the displacement at which it occurs are greater as the ratio H/B decreases.

One can infer from these results that, at small door displacements, the arching behavior is controlled more by the width of the trapdoor than by the grain size. An order of magnitude variation in the grain size brings about only a slight change in the load vs. displacement curve, while altering the width of the trapdoor by less than half an order of magnitude causes a significant difference both in the load reduction and in the displacements at which the minimum load is reached.

4.3 Summary of Observations

Lowering of the trapdoor underneath a granular mass causes an "arch" to develop just above the door, reducing the load carried by the door by 70%-90% from its initial geostatic value. Although the arch appears to be curved at the outset, a triangular shape has been observed at the end of some centrifuge experiments performed with glass beads.

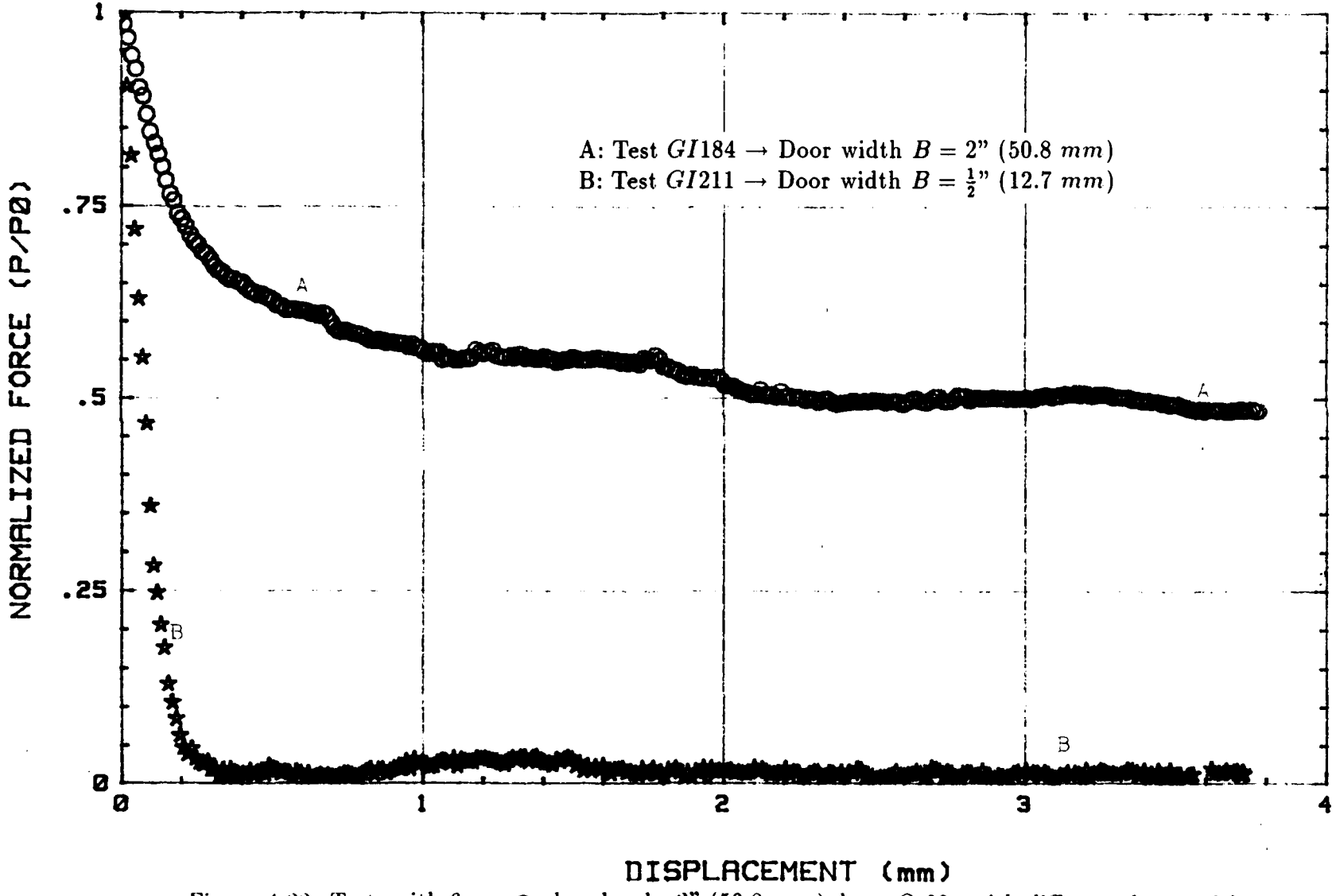

Figure 4-22: Tests with 6-$mm\oslash$ glass beads, 2" (50.8 mm) deep, @ 80g with different door widths

The amount of load reduction depends primarily on the friction angle of the soil, the depth of overburden, and the door width. At displacements in the order of about 1%-2% of the door width, the force on the door approaches a minimum and remains low over considerable door displacements in the centrifuge tests. The point at which the load begins to climb is a function of the particle size, in addition to the three factors mentioned above.

The centrifuge scaling laws for granular materials have been validated in the trapdoor experiments with NJ coarse sand as well as with glass beads. The results from appropriately scaled setups superpose nicely in the dimensionless space of normalized force (with respect to the theoretical overburden) versus normalized displacement (with respect to the door width). From a series of tests with varying grain sizes, it is seen that a scaling of particle size is necessary in order to achieve full similitude between model and prototype.

Significant differences have been observed between the $1g$ and Ng test results. Aside from the larger displacements over which the loads remain close to the minimum, the centrifuge can produce higher stress levels which accelerate the redistribution of soil pressures in relatively deeper samples. That is, the deeper the sample, the less displacement it takes to reach the minimum load in the high-gravity environment.

Chapter 5

Experiments with Jointed Media

As cited in Chapters 1 and 2, trapdoor tests with simulated jointed rock are conducted in a centrifuge environment to try to resolve the scaling issue confronting discontinuous systems. The emphasis, therefore, is on a *modelling of models* type of experimentation, whereby different door widths with corresponding model sizes are subjected to (inversely) proportionate gravity levels. In addition, the effects of varying number of discontinuity planes (represented by the interface between neighboring square rods), lateral confinement, and g-field are examined.

5.1 Jointed Medium Layout

The jointed rock models consist of rods, square in cross-section, which are juxtaposed side by side and on top of each other to simulate joint sets with uniform spacing. Ideally the rods should be made of a rock-like material, but it is cumbersome to cast or cut such a material into small pieces uniform in size. Instead, balsa wood (initially at MIT) and aluminum (at both MIT and RUB) rods have been used since they are readily available in sizes small enough such that a reasonable number of pieces fit on the relatively narrow trapdoor strip. Also, if the main concern is the shearing between planar surfaces of semi-rigid elements and not the fracturing phenomena, experiments with solid rods should

already provide meaningful results.

Two basic types of stack-up schemes have been implemented: one in which the rods are directly placed on top of one another (Figure 5-1a), and the other, in a staggered fashion like bricks (Figure 5-1b). Hence, the first arrangement is consequently referred to as "direct stack"; the second is called "brick stack." Following these two basic schemes, the door widths, the size and number of rods over the door[1], the lateral confinement, and the centrifuge speed can be altered from one test to another.

5.2 Tests with Balsa Wood Rods

5.2.1 Material Description and Test Procedure

Experiments with balsa wood have been conducted primarily as preliminary runs for investigating similitude in centrifuge models of discontinua. Two balsa wood rod sizes – $\frac{1}{4}$"(6.35 mm)□ and $\frac{1}{2}$"(12.7 mm)□ – have been procured to go along with two trapdoor widths – 1" (25.4 mm) and 2" (50.8 mm). The balsa wood used has a density of 0.0075 lbs/in^3 (208 kg/m^3). In complying with the requirements of the *modelling of models* technique, the tests with $\frac{1}{4}$"(6.35 mm)□ rods on 1"(25.4 mm)-wide door are performed at 80g, and the $\frac{1}{2}$"(12.7 mm)□-rods/2"(50.8 mm)-door tests, at 40g.

Initially, lateral confining stress has been applied to the stack of balsa wood rods (see Appendix A, Test $GI58$) by filling the sides of the strongbox with $\frac{1}{4}$"(6.35 mm)-sized aluminum rods hexagonal in cross section. When the trapdoor underneath the rods has been lowered in this setup, however, the force on the door abruptly drops to zero, i.e., the rods above the door are held in place by the shearing resistance between the rods. This is a demonstration of the arching effect; but the load measurements in this arrangement hardly provide any significant information, especially in regard to assessment of similitude in models of various scales. Thus, the confining stress has been removed in the subsequent

[1]Since the displacements along the length of the trapdoor are presumed to be the same, the dimensions parallel to this direction are considered to be irrelevant and are, thus, unchanged.

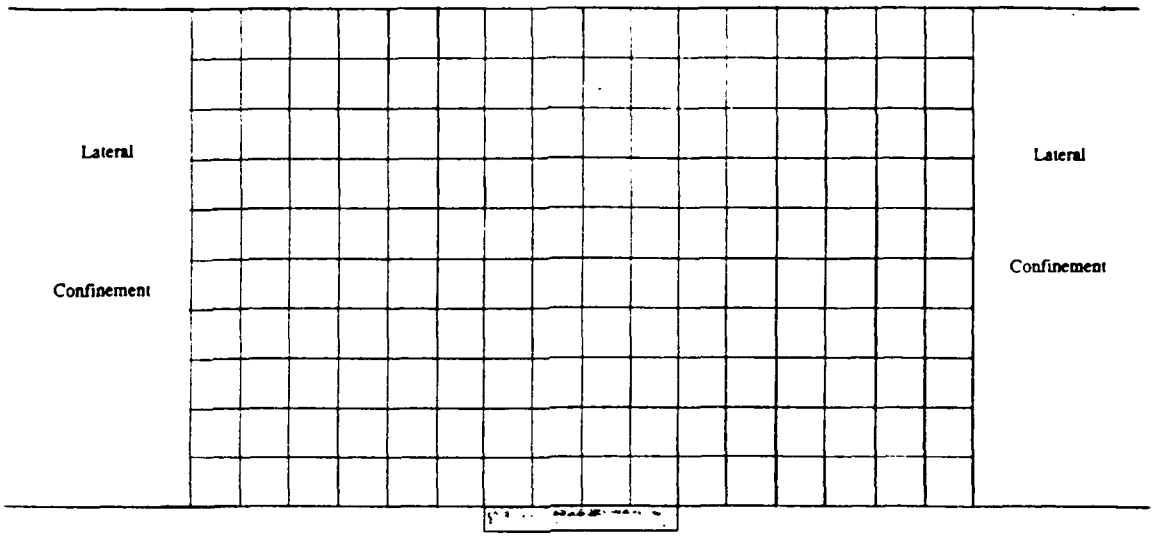

(a) Direct stack

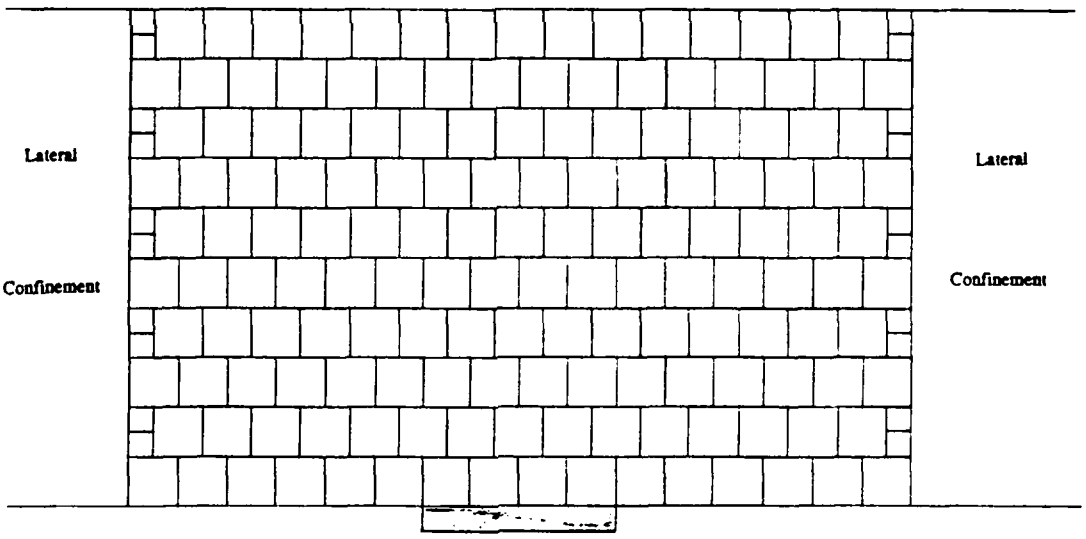

(b) Brick stack

Figure 5-1: Basic types of stack patterns

balsa wood tests.

Only one load cell (LC2) has been used in the experiments with balsa wood rods, 10"(254 mm) in length, centrally placed over the 4"(101.6 mm)-long middle segment. (This is done to maximize the force from the weight of the low-density balsa wood to be measured by the high-capacity load cell.) In general, the rods are laid out by row, starting in the middle of the strongbox, i.e., just above the trapdoor, and travelling symmetrically outward. The completed model has a height equivalent to ten times the width of the fundamental square rod used in each test. The jointed medium assembly is specifically constructed as follows:

(a) For the arrangements with $\frac{1}{4}$"(6.35 mm)$\square$ rods on a 1"(25.4 mm)-wide trapdoor, the bottom $\frac{1}{2}$"(12.7 mm)-high layer is composed of three pairs of $\frac{1}{4}$"(6.35 mm)$\square$ rods centered over the width of the door, eight pairs [2" (50.8 mm) wide] of $\frac{1}{4}$"(6.35 mm)$\square$ rods on each side, and three $\frac{1}{2}$"(12.7 mm)$\square$ rods farther out on each of the sides. (See, e.g., Figures 5-2a, 5-3a.)

- In the direct stack (Figure 5-2a), the next $\frac{1}{2}$"(12.7 mm)-high layer is placed in the same manner as the first layer, with the rods of the new layer positioned right on top of those of the previous layer. This is repeated in the succeeding layers until the desired height [2.5" (63.5 mm)] is attained.
- In the (semi-)brick stack (Figure 5-3a), the next group of $\frac{1}{4}$"(6.35 mm)$\square$ rods is staggered over the previous set of $\frac{1}{4}$"(6.35 mm)$\square$ rods, forming an alternating pattern up to the desired height. [$\frac{1}{8}$"(3.18 mm)$\square$ rods are used to fill up the space that comes about at the sides due to the staggering, and the next layer of $\frac{1}{2}$"(12.7 mm)$\square$ rods are directly placed on top of the previous row of $\frac{1}{2}$"(12.7 mm)$\square$ rods.]

(b) For the setups with $\frac{1}{2}$"(12.7 mm)$\square$ rods on a 2"(50.8 mm)-wide trapdoor, the bottom 1"(25.4 mm)-high layer consists of three pairs of $\frac{1}{2}$"(12.7 mm)$\square$ rods centered over the door width, and three pairs [1.5" (38.1 mm) wide] of $\frac{1}{2}$"(12.7 mm)$\square$ rods

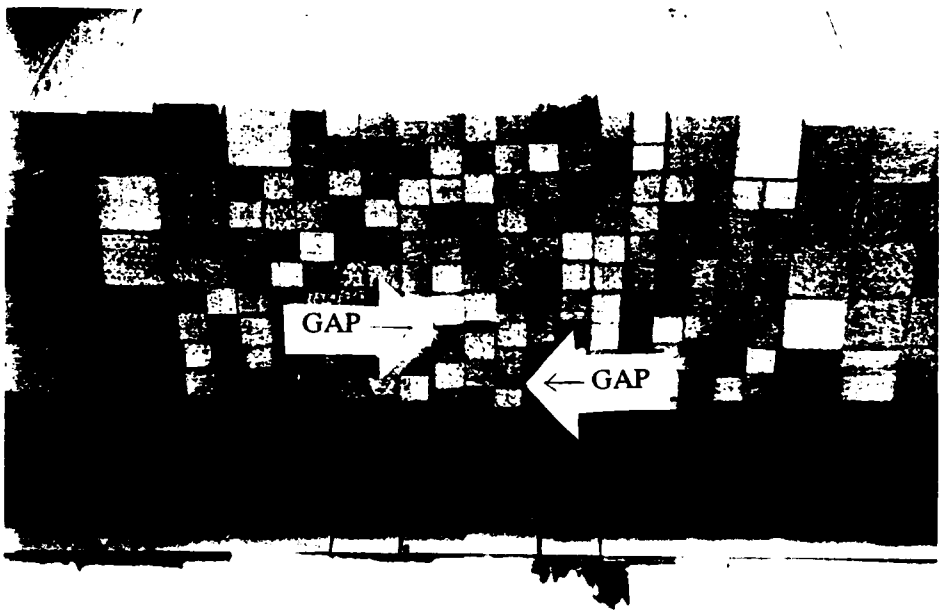

(a) Test $GI112$ - $\frac{1}{4}$"(6.35 mm)□ rods, 2.5" (63.5 mm) high, on 1" (25.4 mm) door
(Hang-ups occured in bottom three layers.)

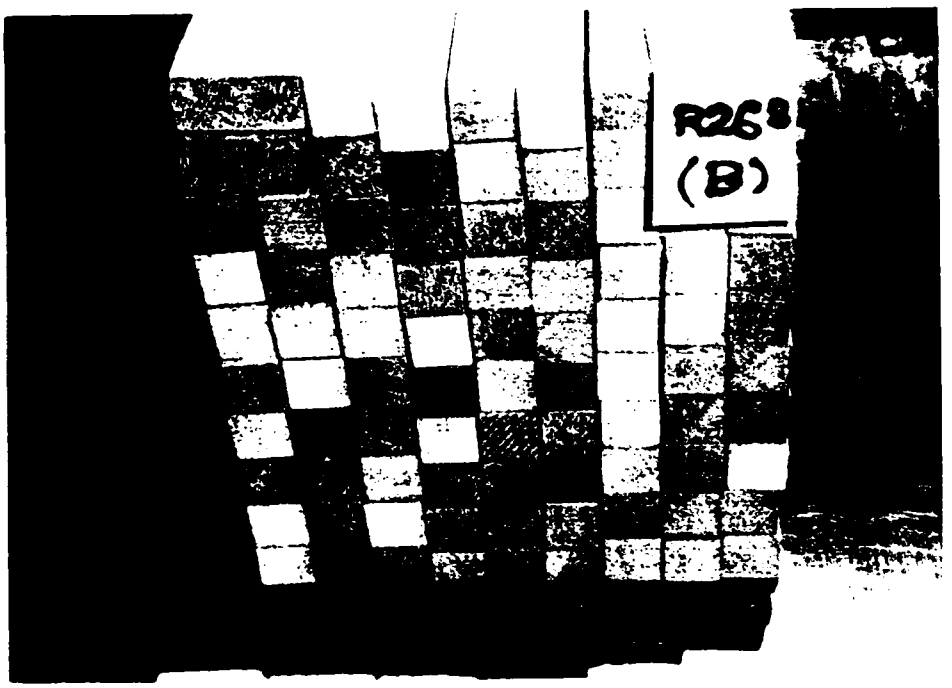

(b) Test $GI125$ - $\frac{1}{2}$"(12.7 mm)□ rods, 5" (127 mm) high, on 2" (50.8 mm) door
(Rods followed movement of door.)

Figure 5-2: "Three-on-door" direct stack of balsa wood rods, tested @ $80g$:
Final configuration

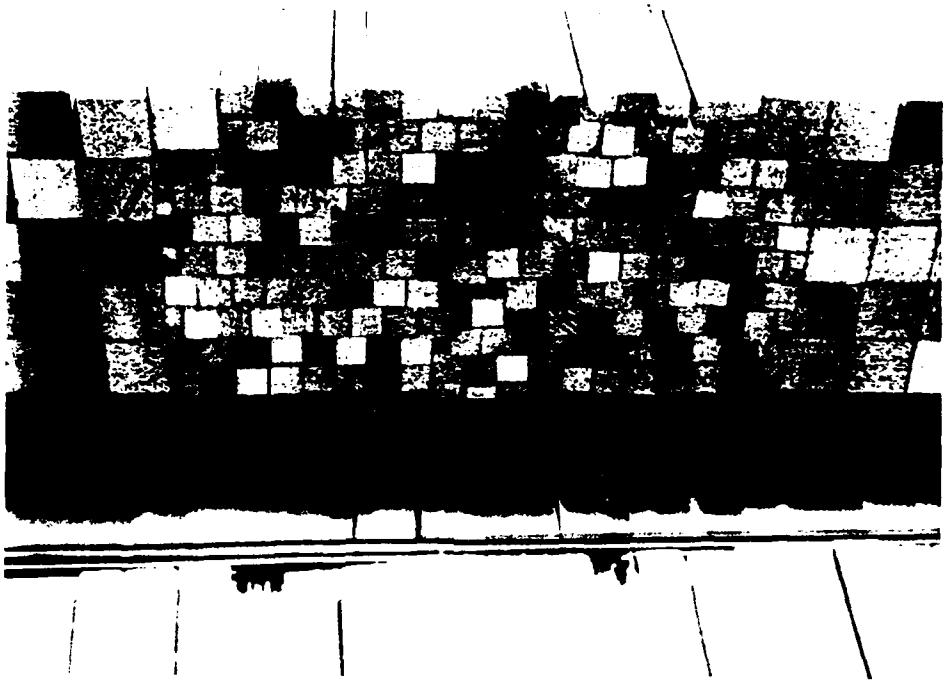

(a) Test $GI114$ - $\frac{1}{4}$"(6.35 mm)□ rods, 2.5" (63.5 mm) high, on 1" (25.4 mm) door @ 80g

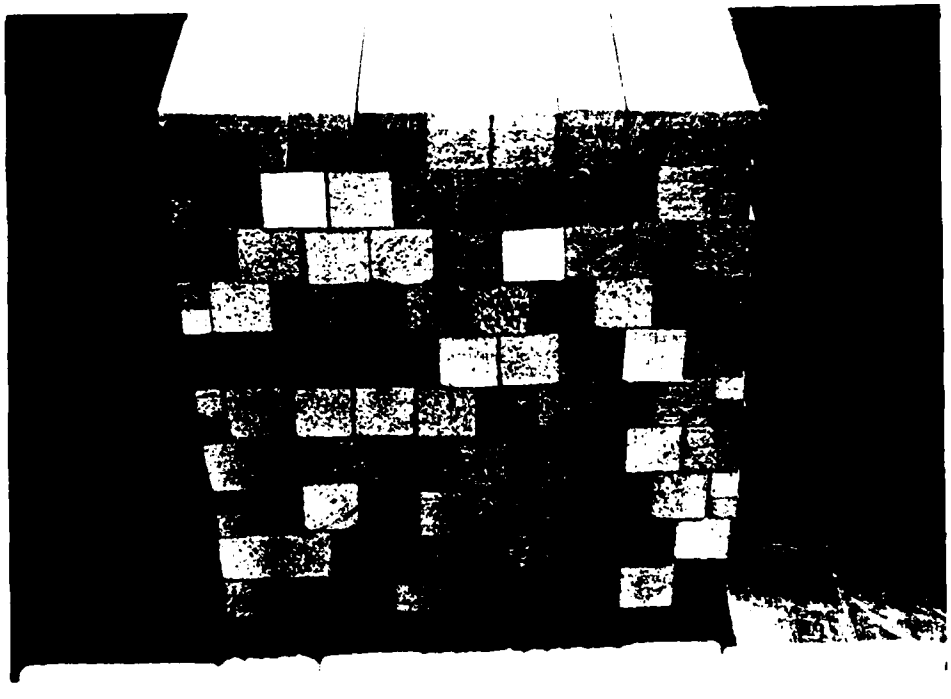

(b) Test $GI122$ - $\frac{1}{2}$"(12.7 mm)□ rods, 5" (127 mm) high, on 2" (50.8 mm) door @ 40g

Figure 5-3: "Three-on-door" (semi-)brick stack tests with balsa wood rods: Final configuration

on each side (as in Figures 5-2b, 5-3b, 5-4).

- In the direct stack (Figures 5-2b, 5-4), the next 1"(25.4 mm)-high layer is placed in the same manner and right on top of the previous layer, and so on, until the desired height [5" (127 mm)] is achieved.
- In the (semi-)brick stack (Figure 5-3b), the next group of $\frac{1}{2}$"(12.7 mm)$\square$ rods is staggered over the previous set of $\frac{1}{2}$"(12.7 mm)$\square$ rods, forming an alternating pattern up to the desired height. [$\frac{1}{4}$"(6.35 mm)$\square$ rods are utilized to fill up the space at the sides brought about by the staggering.]

Note that, while there are the same number of rods centered just above the trapdoor in analogous setups, the total number of balsa wood rods used in the $\frac{1}{4}$"(6.35 mm)$\square$-rods/1"(25.4 mm)-door and $\frac{1}{2}$"(12.7 mm)$\square$-rods/2"(50.8 mm)-door tests are different. Hence, there may be anomalies in the corresponding forces acting along the "joints" in the discontinuum above the trapdoor from one to another scaled arrangement.

The centrifuge spin-up sequence, including the door-lowering phase, is basically identical to that in the tests with granular materials, as discussed in Chapter 4. In particular, the package is brought up to speed at the premeditated g-level in four increments; before long the trapdoor is displaced downward; and, soon after the door movement reaches its limit, the centrifuge is spun back down to normal gravity.

5.2.2 Results

The final configuration, i.e., the appearance of the blocky system at the end of each experiment, in the various tests can be observed in Figures 5-2 through 5-4. The quantitative results are summarized in Figures 5-5 and 5-6.

5.2.2.1 Direct Stack Tests

In Figure 5-5, the normalized force [with respect to the weight (at Ng) of the 40 rods that can be placed straightway above the door] versus door displacement graphs are

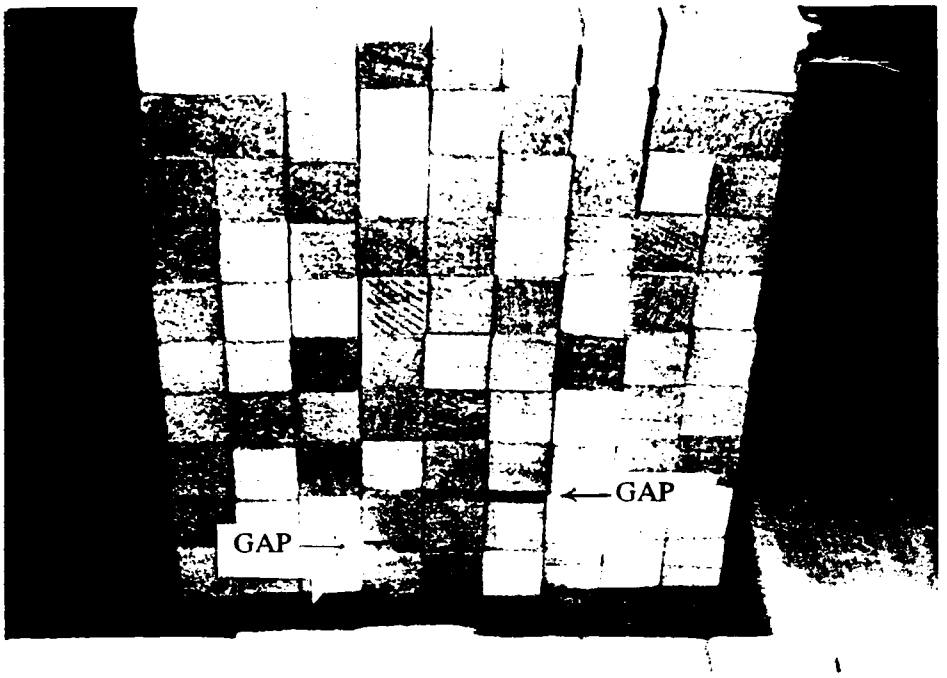

(a) Test $GI123$ – Hang-ups occured in bottom two layers

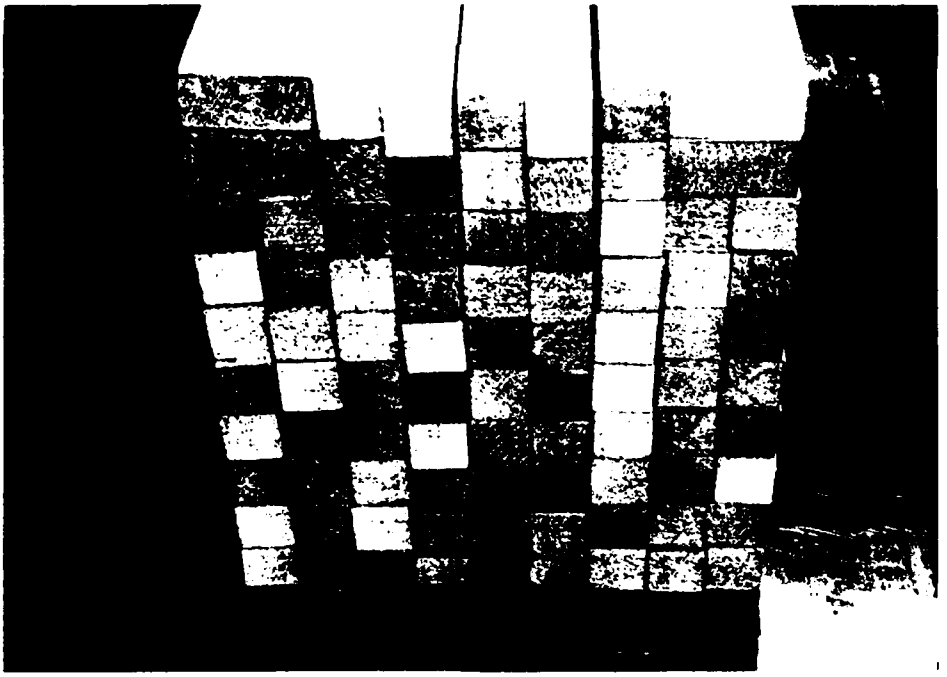

(b) Test $GI124A$ – Rods followed movement of door

Figure 5-4: "Three-on-door" direct stack of $\frac{1}{2}$"(12.7 mm)□ balsa wood rods, 5" (127 mm) high, on 2"(50.8 mm)-wide door @ 40g: Final configuration

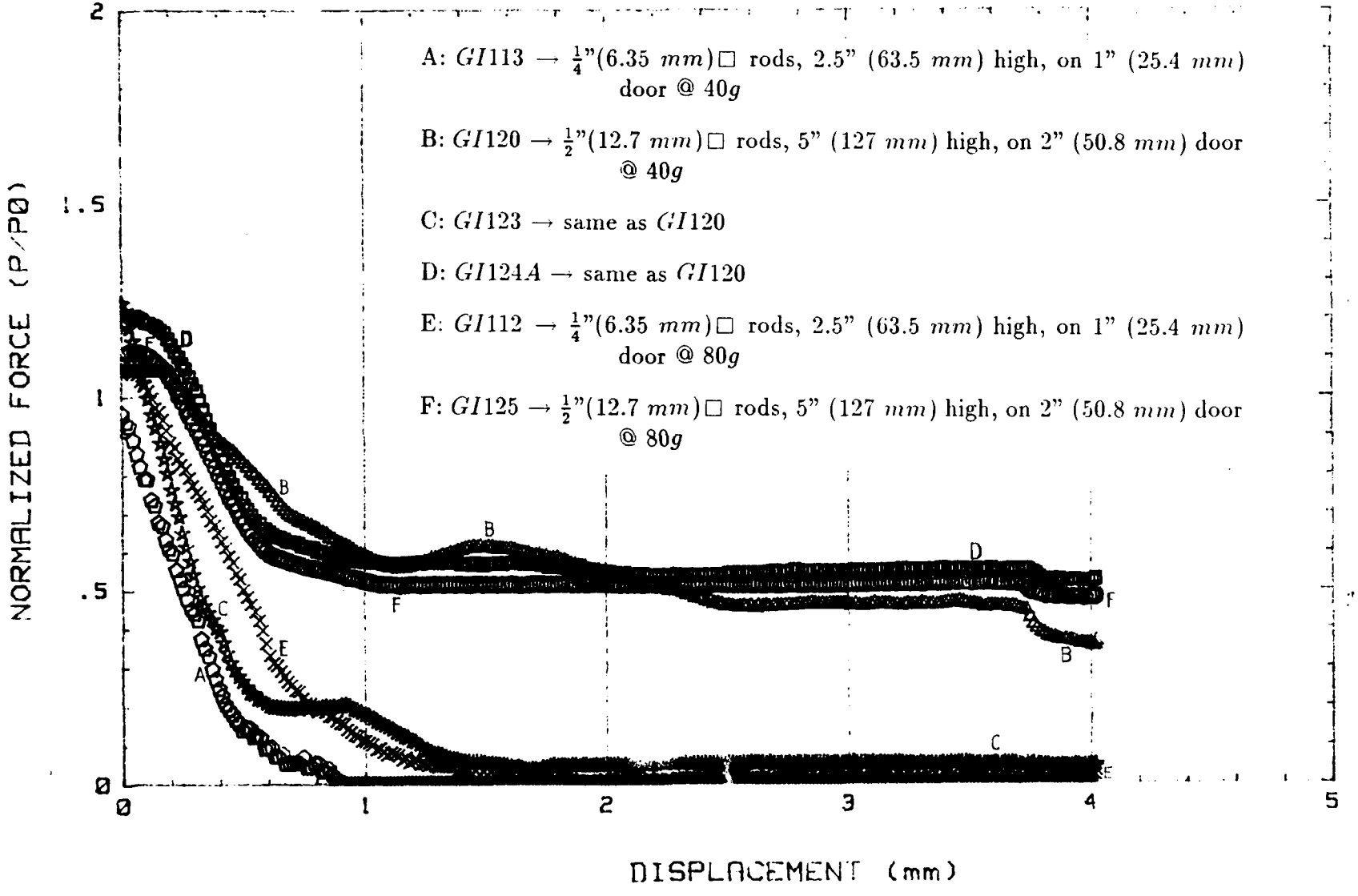

Figure 5-5: "Three-on-door" direct stack tests with balsa wood rods: Normalized force vs. displacement

shown for the direct stack setups with balsa wood rods. Qualitatively, the results show a reduction in the load on the trapdoor upon lowering, i.e., arching occurs, and this load eventually approaches a minimum ($\sim$ constant) value. Quantitatively, however, the data have a tendency to be highly irregular, and Figure 5-5 indicates that the tests are only moderately repeatable at best. While the normalized force values start out (i.e., at zero door displacement) close to unity, in general, they do not end up (i.e., with a finite door displacement) consistently at reasonably similar values.

Due to inherent imperfections in the size and non-uniform frictional properties of the balsa wood rods, the potential for "hang-ups" is there. The low density of balsa wood aggravates the situation further, since a light material may not provide the necessary driving force to mobilize the rods. In the tests with $\frac{1}{2}$"(12.7 mm)$\square$ rods on a 2"(50.8 mm)-wide door, for instance, when there is no apparent "hang-up" (Tests $GI120$, $GI123$, $GI124A$ in Figure 5-5), the the minimum load attained is about half the weight of the 40 rods, or about two-thirds of the weight of the three columns of rods centered over the width of the door; when there is a "hang-up" (e.g., Test $GI123$), the minimum door load is considerably lower. The likelihood of getting "hang-ups" is greater in the experiments with $\frac{1}{4}$"(6.35 mm)$\square$ rods on a 1"(25.4 mm)-wide trapdoor (Tests $GI112$ and $GI112$), where the smaller imperfections are harder to notice and are, thus, more difficult to remedy. This is attested to by the results, as in Figures 5-2a and 5-5.

The data in Figure 5-5 do show that the onset of the minimum door load in each test occurs at approximately the same amount of downward door movement ($\sim$1 mm). This then tends to concur with the notion that the shearing behavior of joints is dependent on absolute displacements, not strains.

It is also worth noting that the gravity level does not seem to affect the normalized behavior of the jointed-medium-on-a-trapdoor arrangement. This can be inferred from the results of the tests with $\frac{1}{4}$"(6.35 mm)$\square$ rods on a 2"(50.8 mm)-wide trapdoor conducted at 40g (e.g., $GI124A$) and at 80g ($GI125$). The normalized force vs. displacement data from these experiments tend to coincide. Of course, there is no lateral confining stress

in both cases; hence, the frictional characteristics are, most probably, not very different from one to the other.

5.2.2.2 Brick Stack Tests

In the tests where the rods are stacked in a staggered fashion like bricks, the arching effect is observed both visually (Figure 5-3) and from trapdoor load measurements (Figure 5-6). The $80g$ experiment ($GI114$) with $\frac{1}{4}$"(6.35 mm)$\square$ rods on a 1"(25.4 mm)-wide door exhibits some similarity with the $40g$ tests ($GI121$, $GI122$) with $\frac{1}{2}$"(12.7 mm)$\square$ rods on a 2"(50.8 mm)-wide door regarding the final geometric configuration and the *absolute* displacement at which the minimum trapdoor load is attained. [Some "hang-up" was observed in the $\frac{1}{4}$"(6.35 mm)$\square$-rods/1"(25.4 mm)-door/$40g$ test.] This minimum load remains practically constant once its value is reached. The weight (at Ng) of the (9) rods that follow the trapdoor as a fraction of the weight of the 40 rods that can be placed directly on top of the door is $9/40 = 0.225$. The normalized measured minimum load (~ 0.17) is only about 75% of that figure, with the discrepancy presumably being due to friction.

The initial measured loads are consistently greater than the theoretical geostatic force on the trapdoor. This is attributed to the stiffer door relative to the adjacent base. As far as the minimum loads are concerned, the experiments with the brick-like arrangement provide more consistent results than their direct stack counterparts. In the former, only the lower three or four layers of rods can follow the displacement of the trapdoor since the downward movement of the upper layers is prevented by the interlocking layout of the rods. A possible explanation is that with fewer sliding sliding surfaces directly involved, the results from the brick stack tests tend to be less variable.

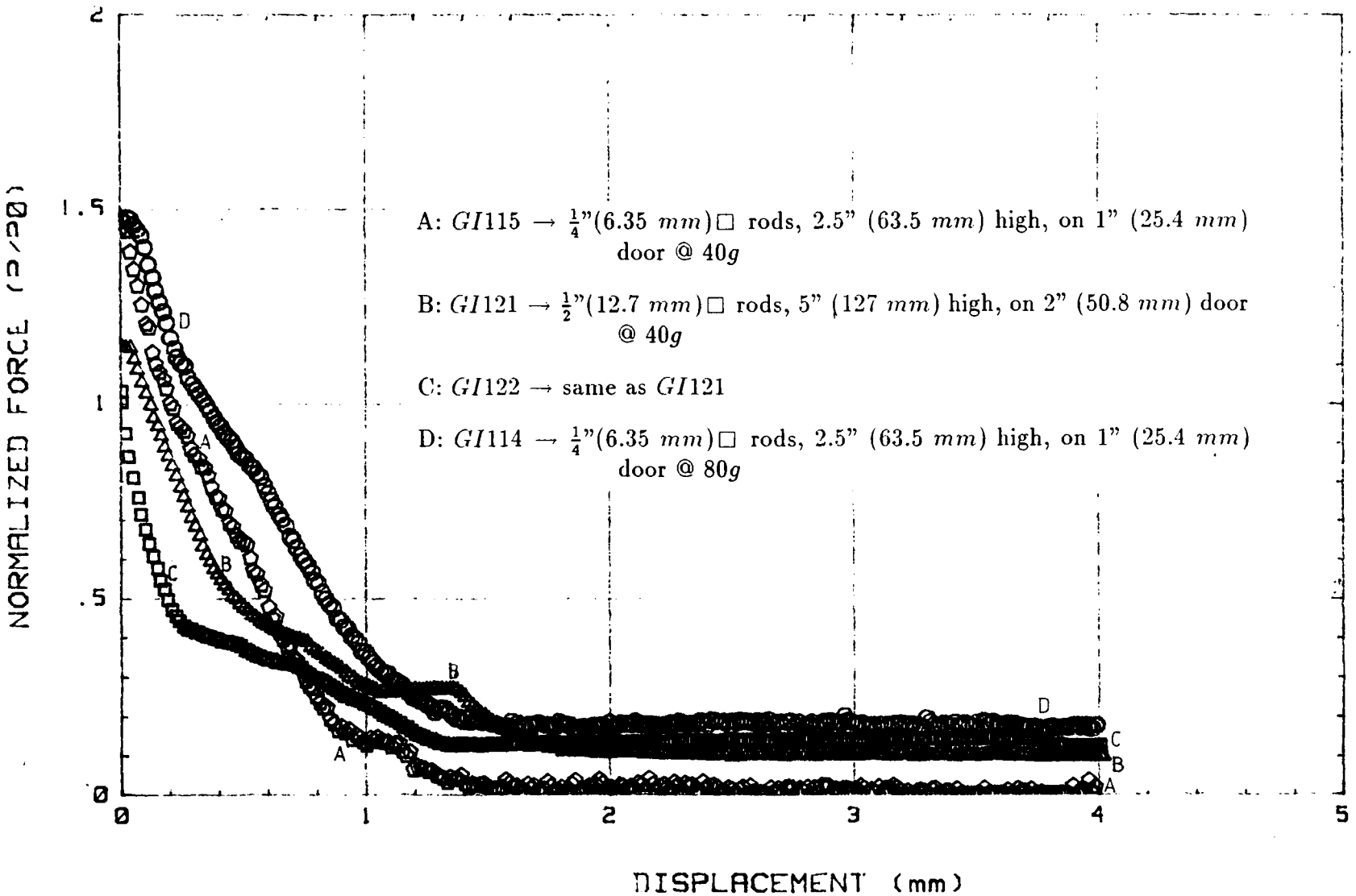

Figure 5-6: "Three-on-door" (semi-)brick stack tests with balsa wood rods: Normalized force vs. displacement

5.3 Tests with Aluminum Rods

5.3.1 Material Description

Aluminum is well suited for simulating rock due to its high strength-to-weight ratio (ideal for modelling semi-rigid components) and a density that is not too different from that of rock. The aluminum material utilized is of Grade 6061-T6 (according to the American Aluminum Association designation system), which is a wrought aluminum alloy containing additions of magnesium (1%), silicon (0.6%), copper (0.28%), and chromium (0.2%). It has a unit weight of 0.098 lbs/in^3 (26.64 kN/m^3), a modulus of elasticity of $\sim$60 GPa, and a shear modulus of $\sim$25 GPa.

At MIT, three sizes of square aluminum rods have been procured: $\frac{1}{8}$"(3.18 mm)$\square$, $\frac{1}{4}$"(6.35 mm)$\square$, and $\frac{1}{2}$"(12.7 mm)$\square$. At RUB, two sizes are used: 10 $mm\square$ and 20 $mm\square$. From a simple "tilting base" test, the friction angle between the aluminum rods is estimated to be $\sim 25°$.

5.3.2 Tests at MIT

As in the balsa wood experiments, the two basic types of arrangements – direct stack and brick stack – are adopted in the tests with aluminum rods. The centrifuge spin-up procedure, as well as the synchronism of the trapdoor descent, is also similar to the balsa wood and granular media tests.

All three trapdoor segments are used this time; in each of the experiments with aluminum rods, three stacks of "jointed" mass are assembled, one stack over each segment. The outer segments (LC1 and LC4) are still, however, susceptible to end effects; thus, the results presented here are solely from the middle segment (LC2). [Results from all three segments are provided in the appendices of Iglesia's (1991) thesis.] Several schemes have been tried out in regard to the number of rods placed above the door and the method of lateral confinement, as expounded in the following subsections.

5.3.2.1 "Three-on-door" Layout

During the early stages of experimentation, the "three-on-door" setup in the balsa wood case was adopted in the tests with aluminum rods. That is, in the bottom-most row of rods, there are three rods centered over the width of the trapdoor. Unlike in the balsa wood experiments, however, a lateral confining stress is imposed on the sides of the aluminum discontinuum by means of $\frac{1}{4}$"(6.35 mm)-sized aluminum rods, hexagonal in cross-section, piled up to simulate a granular mass under K_0 conditions. [A trial run without any lateral confining stress, i.e., no hexagonal aluminum rods on the sides, was carried out (Test *GI*92, Appendix A), but the stack of rods collapsed during spin-up. No other aluminum rod tests without lateral confinement have been performed since.] In these series of tests, $\frac{1}{4}$"(6.35 mm)□ rods are used with the 1"(25.4 mm)-wide trapdoor, and $\frac{1}{2}$"(12.7 mm)□ rods, with the 2"(50.8 mm)-wide door. The experiments are again conducted at $40g$ and at $80g$.

As usual, the rods are laid out by row, starting in the middle of the strongbox and travelling symmetrically outward. The finished structure has, in general, ten such rows of rods. The "three-on-door" jointed medium setup is described in detail below:

(a) For the arrangements with $\frac{1}{4}$"(6.35 mm)□ rods on a 1"(25.4 mm)-wide trapdoor, the bottom $\frac{1}{2}$"(12.7 mm)-high layer, for a stack over each door segment, contains three pairs of $\frac{1}{4}$"(6.35 mm)□ rods centered over the width of the door, eight pairs [2" (50.8 mm) wide] of $\frac{1}{4}$"(6.35 mm)□ rods on each side, and three $\frac{1}{2}$"(12.7 mm)□ rods farther out on each of the sides. (See, e.g., Figures 5-7 and 5-8.) Three more $\frac{1}{2}$"(12.7 mm)□ rods, 10" (254 mm) in length, are placed on each side of the three stacks, and $\frac{1}{4}$"(6.35 mm)-sized hexagonal aluminum rods, each 6" (152.4 mm) long, are laid out in two bundles to obtain a total length of 12" (304.8 mm), filling up the remaining space on the sides.

- In the direct stack (Figure 5-7), the following $\frac{1}{2}$"(12.7 mm)-high layers are placed in the same manner as the first layer, with the rods of the new layer

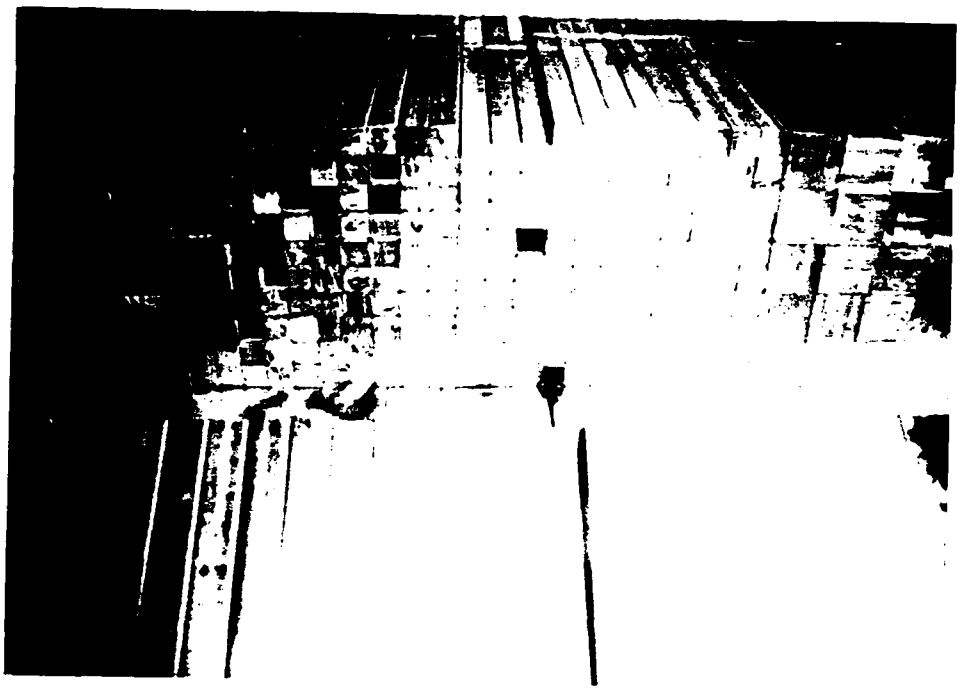

Figure 5-7: MIT "three-on-door" direct stack of $\frac{1}{4}$"(6.35 mm)□ Al rods, 2.5" (63.5 mm) high, on 1" (25.4 mm) door @ 80g: Final configuration

(The rods have followed the downward movement of the trapdoor.)

positioned right on top of those of the previous layer, until the desired height [2.5" (63.5 mm)] is attained.

- In the (semi-)brick stack (Figure 5-8), the next group of $\frac{1}{4}$"(6.35 mm)$\square$ rods is staggered over the previous set of $\frac{1}{4}$"(6.35 mm)$\square$ rods, forming an alternating pattern up to the desired height. [$\frac{1}{8}$"(3.18 mm)$\square$ rods are used to fill up the space created at the sides due to the staggering, while the next layer of $\frac{1}{2}$"(12.7 mm)$\square$ rods are directly placed on top of the previous row of $\frac{1}{2}$"(12.7 mm)$\square$ rods.]

(b) For the setups with $\frac{1}{2}$"(12.7 mm)$\square$ rods on a 2"(50.8 mm)-wide trapdoor, the bottom 1"(25.4 mm)-high layer is composed of three pairs of $\frac{1}{2}$"(12.7 mm)$\square$ rods centered over the door width, and a pair of $\frac{1}{2}$"(12.7 mm)$\square$ rods on each side. Farther out, three pairs of $\frac{1}{2}$"(12.7 mm)$\square$ rods, 10" (254 mm) in length, are placed on each side of the three stacks, and $\frac{1}{4}$"(6.35 mm)-sized aluminum rods, each 6" (152.4 mm) long, are arranged in two bundles to obtain a total length of 12" (304.8 mm), filling up the remaining space on the sides.

- In the direct stack, the following 1"(25.4 mm)-high layers are placed in the same manner as the first layer, with the rods of the new layer positioned right on top of those of the previous layer, until the desired height [5" (127 mm)] is achieved.

- In the (semi-)brick stack, the next group of $\frac{1}{2}$"(12.7 mm)$\square$ rods is staggered over the previous set of $\frac{1}{2}$"(12.7 mm)$\square$ rods, forming an alternating pattern up to the desired height. [$\frac{1}{4}$"(6.35 mm)$\square$ rods are utilized to fill up the space at the sides brought about by the staggering, while the next layer of $\frac{1}{2}$"(12.7 mm)$\square$ rods, 10" (254 mm) long, are directly placed on top of the previous layer of $\frac{1}{2}$"(12.7 mm)$\square$ rods.]

Note, again, that the total number of rods used in the $\frac{1}{4}$"(6.35 mm)$\square$-rods/1"(25.4 mm)-door and the $\frac{1}{2}$"(12.7 mm)$\square$-rods/2"(50.8 mm)-door cases are not the same. Thus,

Figure 5-8: MIT "three-on-door" (semi-)brick stack of $\frac{1}{4}$"(6.35 mm)$\square$ Al rods, 2.5" (63.5 mm) high, on 1" (25.4 mm) door @ $80g$: Final configuration

(Note triangular pattern formed at the bottom four layers.)

there may be discrepancies between analogous arrangements in the corresponding forces acting along the "joints."

Typical final configurations in the different experiments are depicted in Figures 5-7 and 5-8. For the direct stack (Figure 5-7), the three columns of rods centered over the width of the trapdoor, in general, follow the downward displacement of the door. For the (semi-)brick stack (Figure 5-8), a symmetrical pattern resembling an isosceles triangle with terraces can be observed just above the door in the bottom four layers of the discontinuum.

Figures 5-9 and 5-10 display the normalized load (with respect to the theoretical geostatic force) versus displacement curves representative of the various "three-on-door" experiments with aluminum rods. The results in Figure 5-9 are for direct stack cases, while those in Figure 5-10, for (semi-)brick stack arrangements. Both Figures 5-9 and 5-10 show data obtained from repeated tests and do clearly demonstrate the reproducibility of results.

For the direct stack setup (Figure 5-9), both the $\frac{1}{4}$"$(6.35\ mm)\square$-rods/$80g$ and $\frac{1}{2}$"$(12.7\ mm)\square$-rods/$40g$ tests have measured forces starting out slightly higher than the theoretical values. As the trapdoor is lowered in each case, the measured load drops, as in the balsa wood experiments, but before it reaches its minimum value, there is a stage where the load stays approximately constant. While the normalized forces at this intermediate stage are not the same (~ 1.01 vs. ~ 0.83) for the $\frac{1}{4}$"$(6.35\ mm)\square$-rods/$80g$ and $\frac{1}{2}$"$(12.7\ mm)\square$-rods/$40g$ tests, the minimum load ratios roughly are (~ 0.55). An equally, if not more, significant result is the similar range at which the intermediate plateau ($\sim$0.1 $mm < d <\sim$0.55 mm) and the onset of minimum load ($d >\sim$0.65 mm) occur in these appropriately scaled situations.

In the brick stack layout (Figure 5-10), the loads at the top gravity level prior to any activated door movement are considerably higher than the theoretical geostatic forces. This is attributed to the fair number of rods involved in the transmission of forces due to the interlocking arrangement of the brick stack, coupled with the stiffer trapdoor

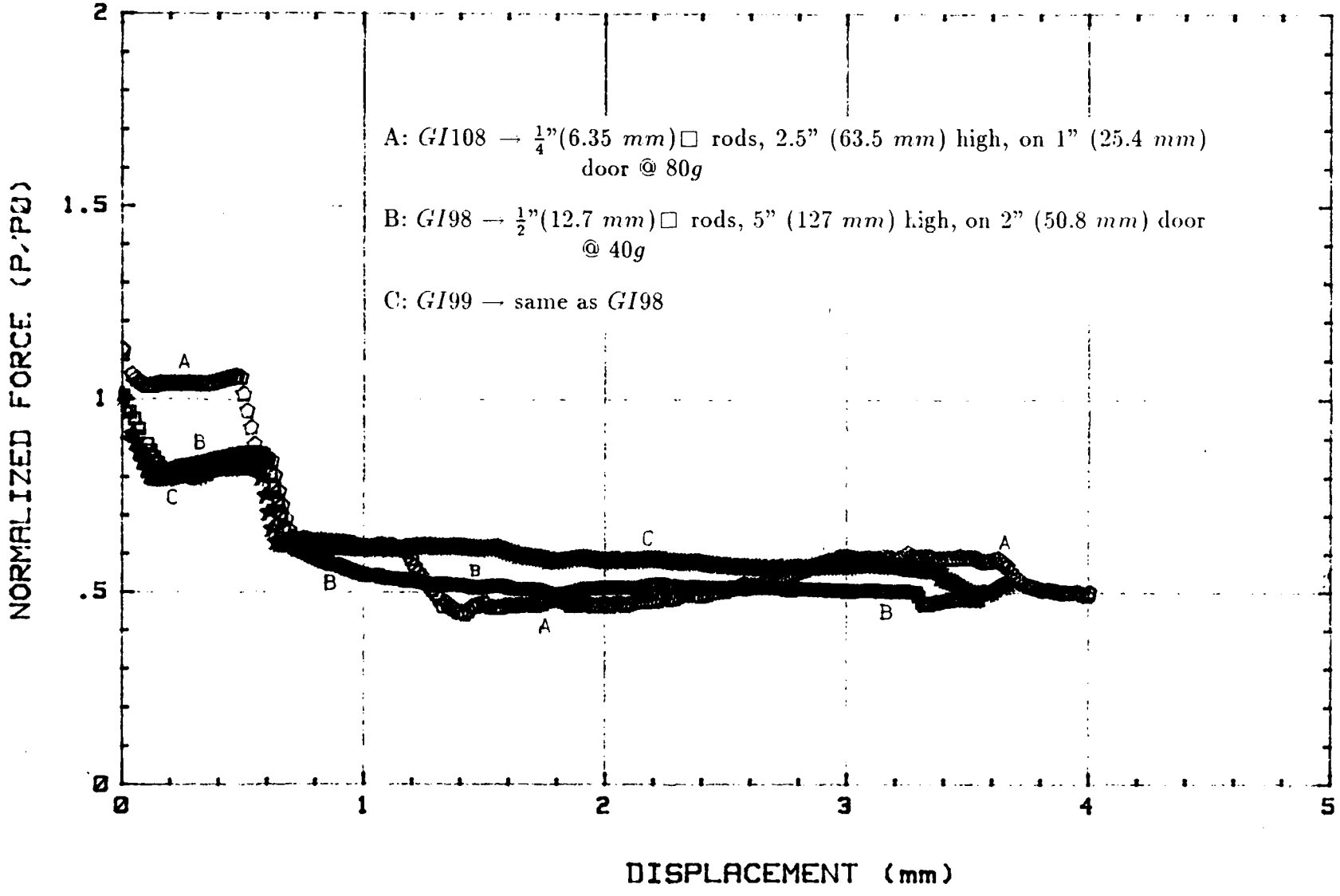

Figure 5-9: MIT "three-on-door" direct stack tests with *Al* rods: Normalized force vs. displacement

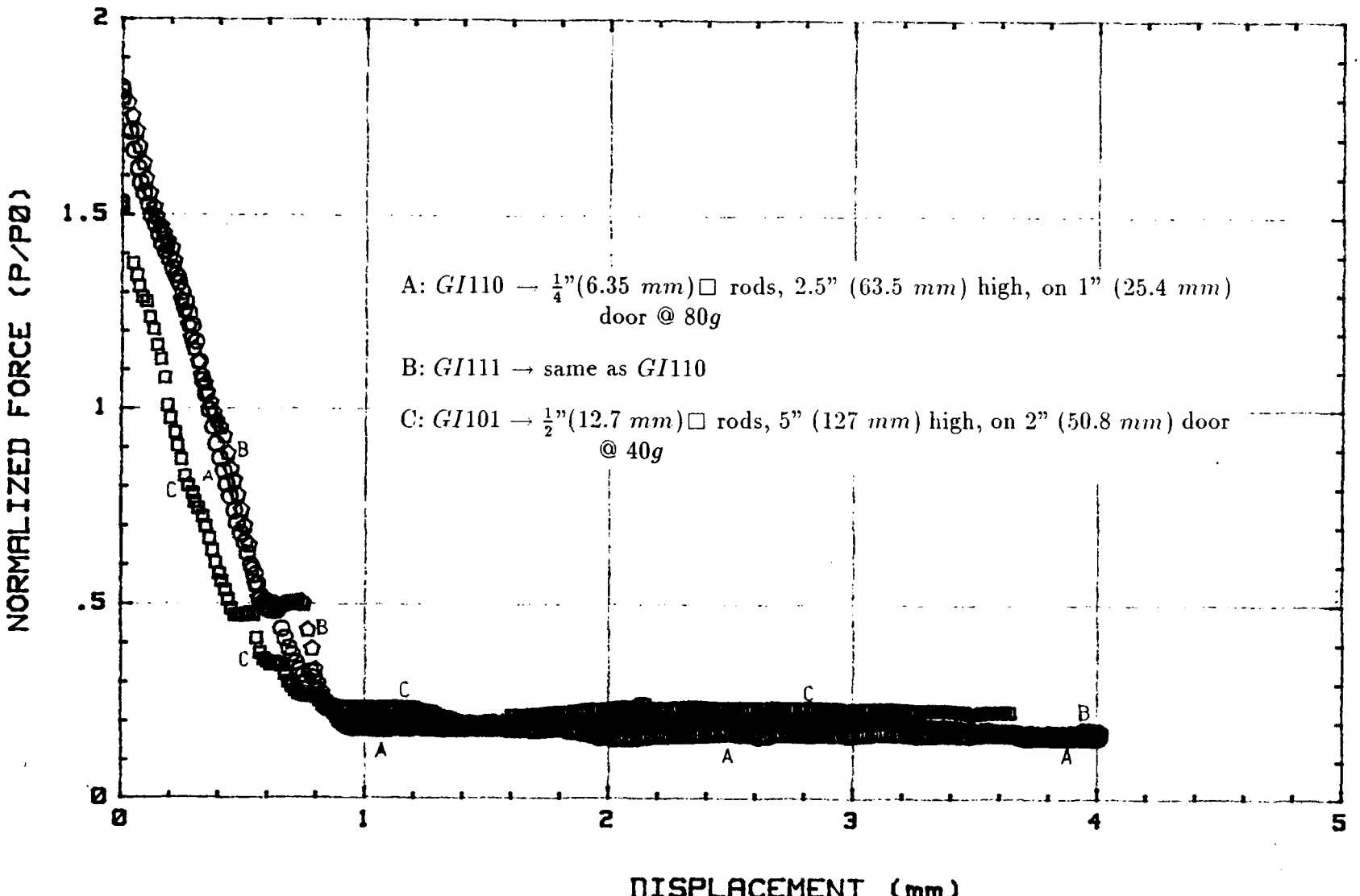

Figure 5-10: MIT "three-on-door" (semi-)brick stack tests with *Al* rods: Normalized force vs. displacement

relative to the adjacent base. It is, therefore, not surprising that the $\frac{1}{4}$"(6.35 mm)□-rods/80g tests exhibit greater initial normalized forces than the $\frac{1}{2}$"(12.7 mm)□-rods/40g tests ($\sim$ 1.8 vs. $\sim$ 1.55). Also, because of the presence of lateral confinement from the hexagonal rods on the sides, the initial normalized forces in the brick stack tests with aluminum rods are greater than those in the corresponding tests with balsa wood rods (Figure 5-5).

As downward door displacement proceeds in each experiment, the force on the trapdoor decreases almost continually until the minimum value is attained. Roughly equal minimum values of the normalized door load are found for the $\frac{1}{4}$"(6.35 mm)□-rods/80g and $\frac{1}{2}$"(12.7 mm)□-rods/40g cases. These minimum load ratios ($\sim$ 0.2) tally approximately with the weight of the material that move down with the trapdoor [9 rods (see Figure 5-3)] divided by the total weight of the aluminum rods bounded by two vertical planes through the edges of the trapdoor (40 rods), or 9/40 = 0.225. It is again worth noting that the minimum door loads occur at more or less the same amount of door displacement ($\sim$0.9 mm) in the analogous arrangements.

5.3.2.2 "Four-on-door" Layout

In order to form a full alternating pattern in the brick stack, a "four-on-door" layout is subsequently adopted. In other words, the modified basic assembly – for both direct and brick stacks – has four rods, instead of only three, centered in the bottom-most row over the width of the trapdoor, as illustrated in Figure 5-11. Moreover, so as to standardize the lateral confinement of the aluminum discontinuum at MIT and RUB, uniform-sized glass beads are placed on the sides. (These are the same glass beads used in the granular media experiments.) The use of glass spheres also allows one to vary the diameter of the beads in accordance with the scaling of the rod and door sizes. With the basic setup shown in Figure 5-11, the plan is to use corresponding rod sizes, door widths, glass bead diameters, and gravity levels as listed in Table 5.1.

As before, assembly starts at the middle of the package and goes symmetrically out-

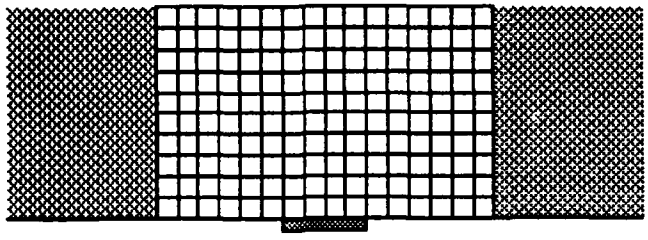

(a) Direct stack

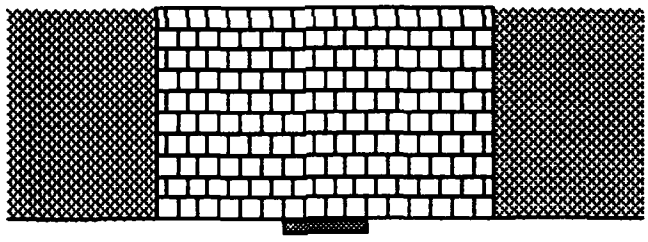

(b) Brick stack

Figure 5-11: Basic "four-on-door" assembly

Table 5.1: MIT tests with "four-on-door" setup

	Rod Size	Total Height	Door Width	Glass Bead Size	Gravity Level
1.	$\frac{1}{2}$ *in*□ (12.7 *mm*□)	5.00 *in* (127 *mm*)	2.0 *in* (50.8 *mm*)	6.0 *mm*	40*g*
2.	$\frac{1}{4}$ *in*□ (6.35 *mm*□)	2.50 *in* (63.5 *mm*)	1.0 *in* (25.4 *mm*)	3.0 *mm*	80*g*
3.	$\frac{1}{8}$ *in*□ (3.18 *mm*□)	1.25 *in* (31.8 *mm*)	0.5 *in* (12.7 *mm*)	1.5 *mm*	160*g*

ward by row. As can be seen in Figure 5-11, each row consists of four rods above the trapdoor and six rods on each side, for a sum of sixteen (= 16) rods. The glass beads are not poured until all ten rows have been stacked up. The total number of rods that comprise each model are then the same (= 160) in the "four-on-door" tests. (In the brick stack, some "half-rods" are utilized at the ends to fill the space that comes about from the staggering of rods, providing a vertically flat surface on the sides.)

The results from the "four-on-door" direct stack experiments at MIT are presented in Figures 5-12 through 5-16. Configurations of the model assembly at the end of the tests are depicted in Figures 5-12a, 5-13a, and 5-14a. In general, the four columns of rods directly above the trapdoor simply follow the vertical door movement.

In Figures 5-15 and 5-16 the measured force on the trapdoor, normalized with respect to the weight (at Ng) of the material directly above the door, has been plotted against the vertical door displacement for the various tests. (Figure 5-16 is just a blown-up version of Figure 5-15.) The data shown are for two runs each of the experiments listed in Table 5.1. There are inevitable discrepancies in the force measurements among the different direct stack tests due to friction along the shearing surfaces that extend vertically from the bottom of the stack all the way to the top surface. The most significant aspect of the results, however, is the similarity in the overall behavior. As the door is displaced downward, an immediate reduction in the load ensues; this is followed by a stage of roughly constant load ($P/P_0 \approx 0.6 \rightarrow 0.9$) up to a door displacement of ~1-1.25 *mm*, a further decrease in load ($P/P_0 \approx 0.4 \rightarrow 0.6$) to about 1.5 *mm* displacement, and then a gradual measured force increase toward another fairly constant value ($P/P_0 \approx 0.4 \rightarrow 0.8$).

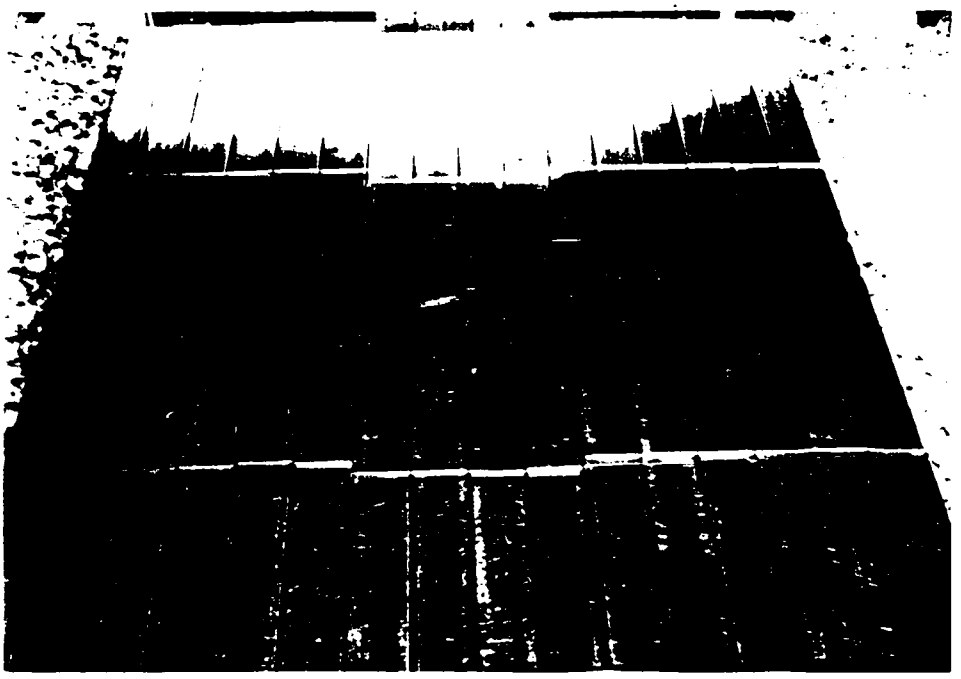

(a) Test $GI190$ – Direct stack

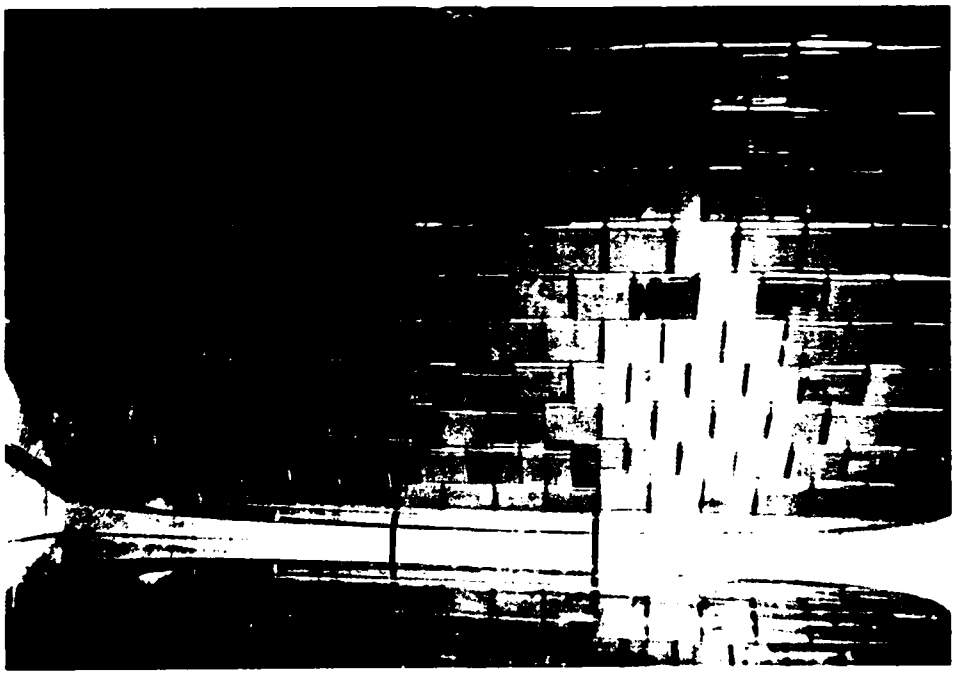

(b) Test $GI192$ – Brick stack

Figure 5-12: MIT "four-on-door" direct stack of $\frac{1}{2}$"(12.7 mm)□ Al rods, 5" (127 mm) high, on 2" (50.8 mm) door @ 40g: Final configuration

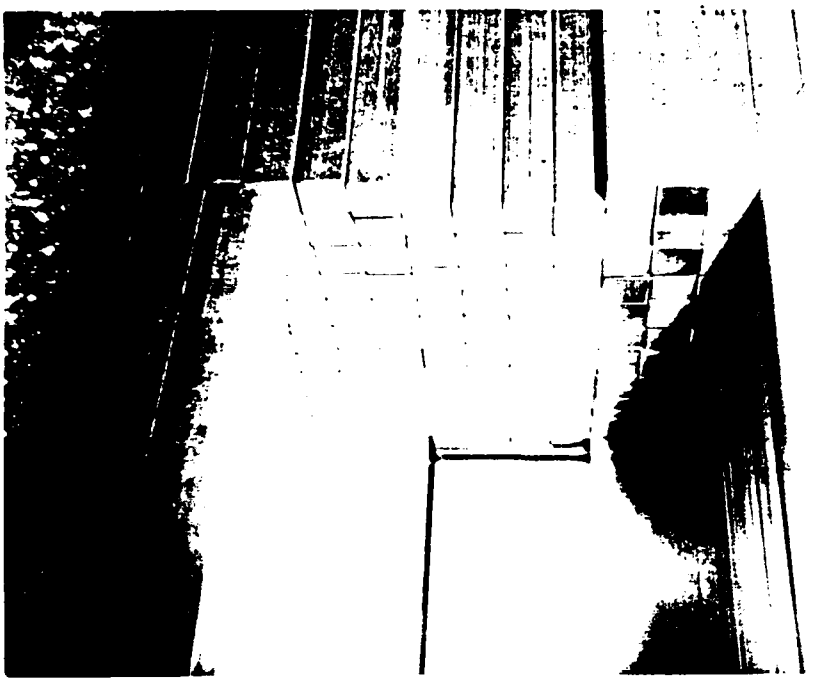

(a) Test $GI187$ – Direct stack

(b) Test $GI188$ – Brick stack

Figure 5-13: MIT "four-on-door" direct stack of $\frac{1}{4}$"(6.35 mm)□ Al rods, 2.5" (63.5 mm) high, on 1" (25.4 mm) door @ 80g: Final configuration

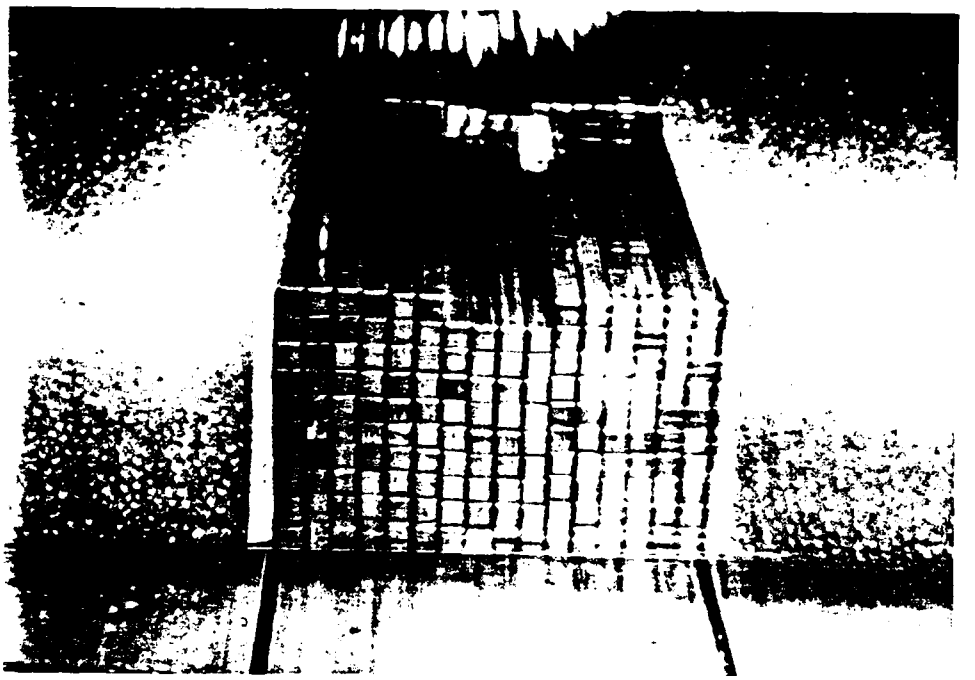

(a) Test $GI193$ – Direct stack

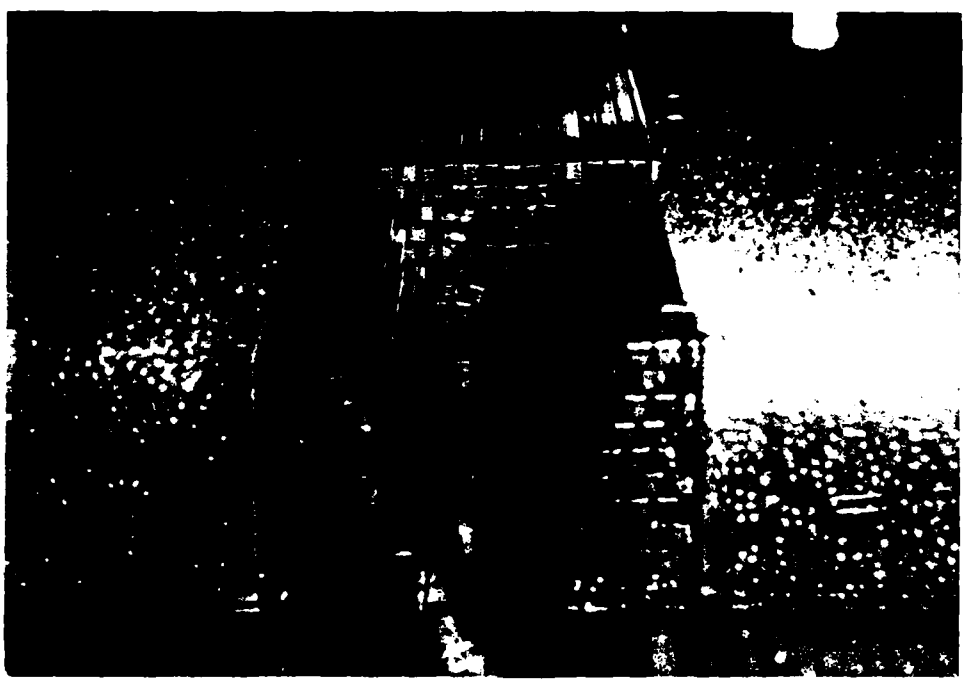

(b) Test $GI209$ – Brick stack

Figure 5-11: MIT "four-on-door" direct stack of $\frac{1}{8}$"(3.18 mm)□ Al rods, 1.25" (21.8 mm) high, on $\frac{1}{2}$" (12.7 mm) door @ 160g: Final configuration

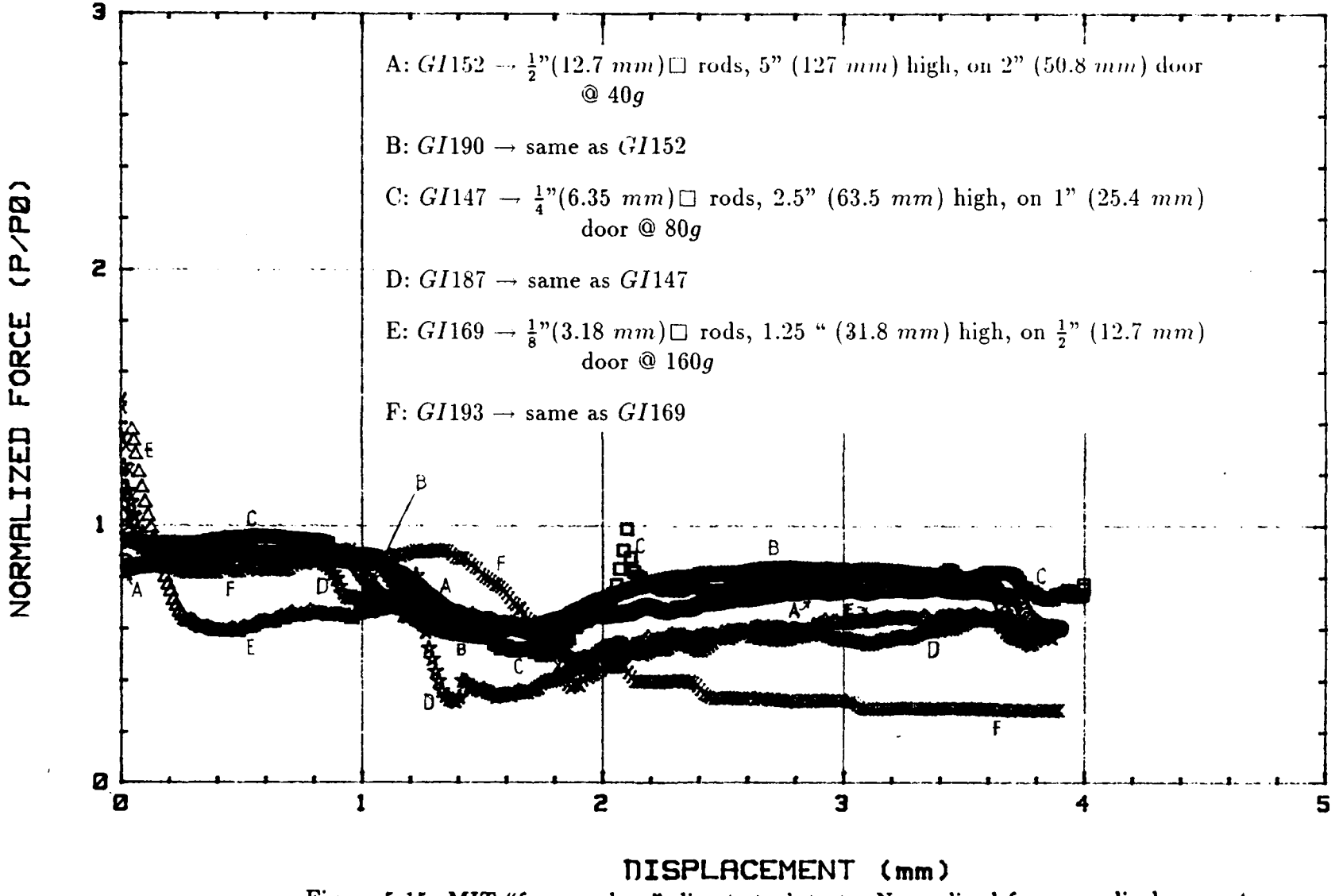

Figure 5-15: MIT "four-on-door" direct stack tests: Normalized force vs. displacement

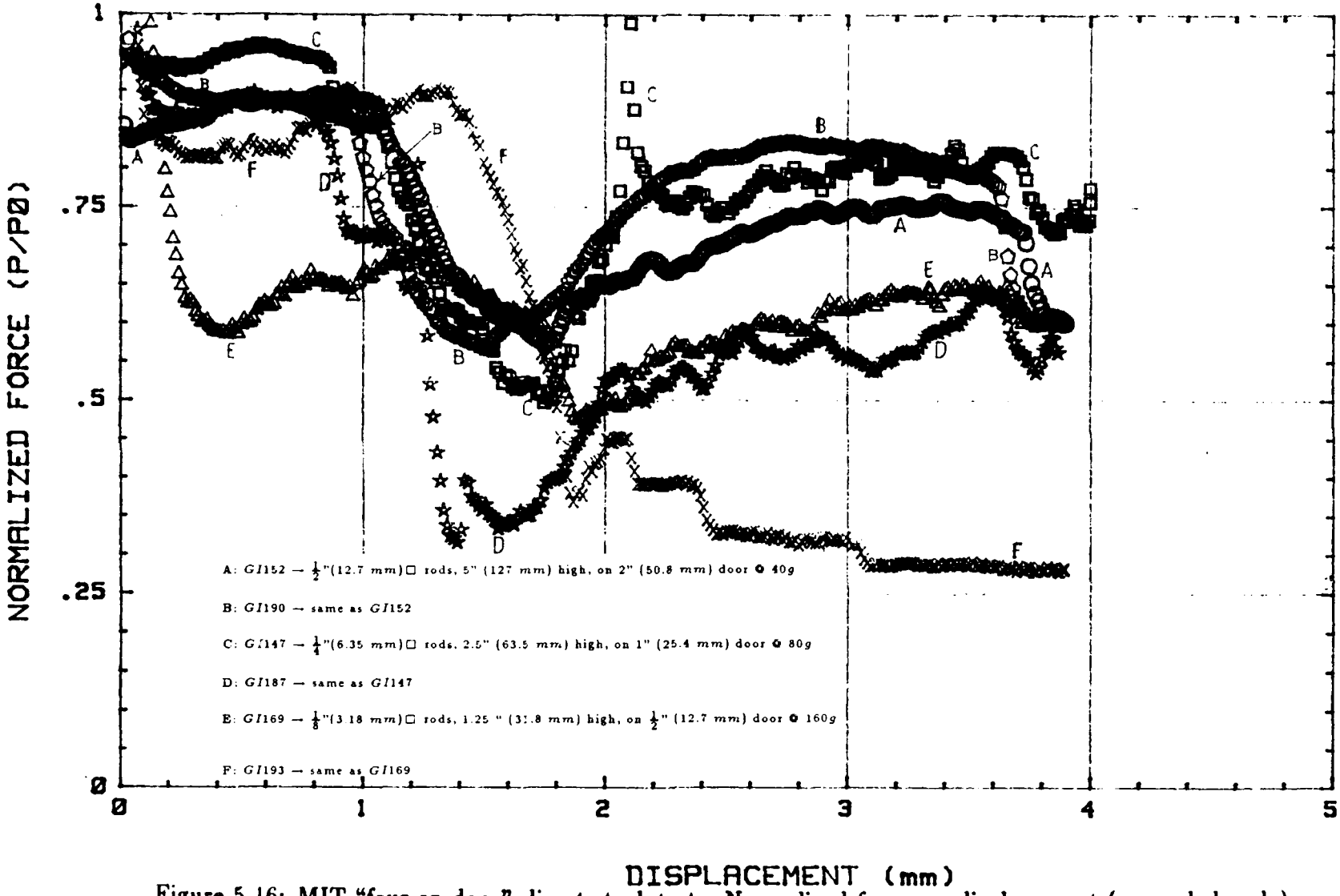

Figure 5-16: MIT "four-on-door" direct stack tests: Normalized force vs. displacement (expanded scale)

For the "four-on-door" brick stack cases performed at MIT, the results are given in Figures 5-12b, 5-13b, 5-14b, 5-17 through 5-19. In the final configuration (Figures 5-12b, 5-13b, and 5-14b), a triangular pattern is typically formed in the bottom four layers just above the trapdoor. This is also reflected in the measured loads (Figures 5-17 through 5-19), which become constant towards the end of each experiment. Since there are a maximum possible 40 blocks that can be placed above the door, the 10 rods that follow the door movement in each test constitute 25 percent of the theoretical geostatic force. One observes that the minimum normalized force in the brick stack tests is close (though slightly lower, due to friction) to this 25 percent value.

Consistent with the fact that the trapdoor is stiffer than the adjacent base, the initial load ratios prior to any activation of door movement are much greater than unity and are also greater than those in the direct stack tests. The direct stack arrangement shows mobilization of friction along continuous vertical "joints," whereas in the brick stack more elements are involved in the transmission of forces due to interlocking. Hence, the initial load ratio is lower in the former.

As the trapdoor settles in the brick stack setup, the transition from the initial force to the minimum load follows a much smoother curve than in the direct stack experiment. It is evident from Figure 5-17 that the minimum load occurs at about the same amount of door displacement for all the geometrically similar tests. This observation is even more pronounced if the data are adjusted such that zero displacement is set at where the normalized force ratio equals unity, shifting the curves in Figure 5-17 horizontally to those in Figure 5-18. The data in Figure 5-19 are exactly the same as those in Figure 5-18, except that the scale is expanded in the former to "zoom in" on the portion where $P/P_0 < 1$.

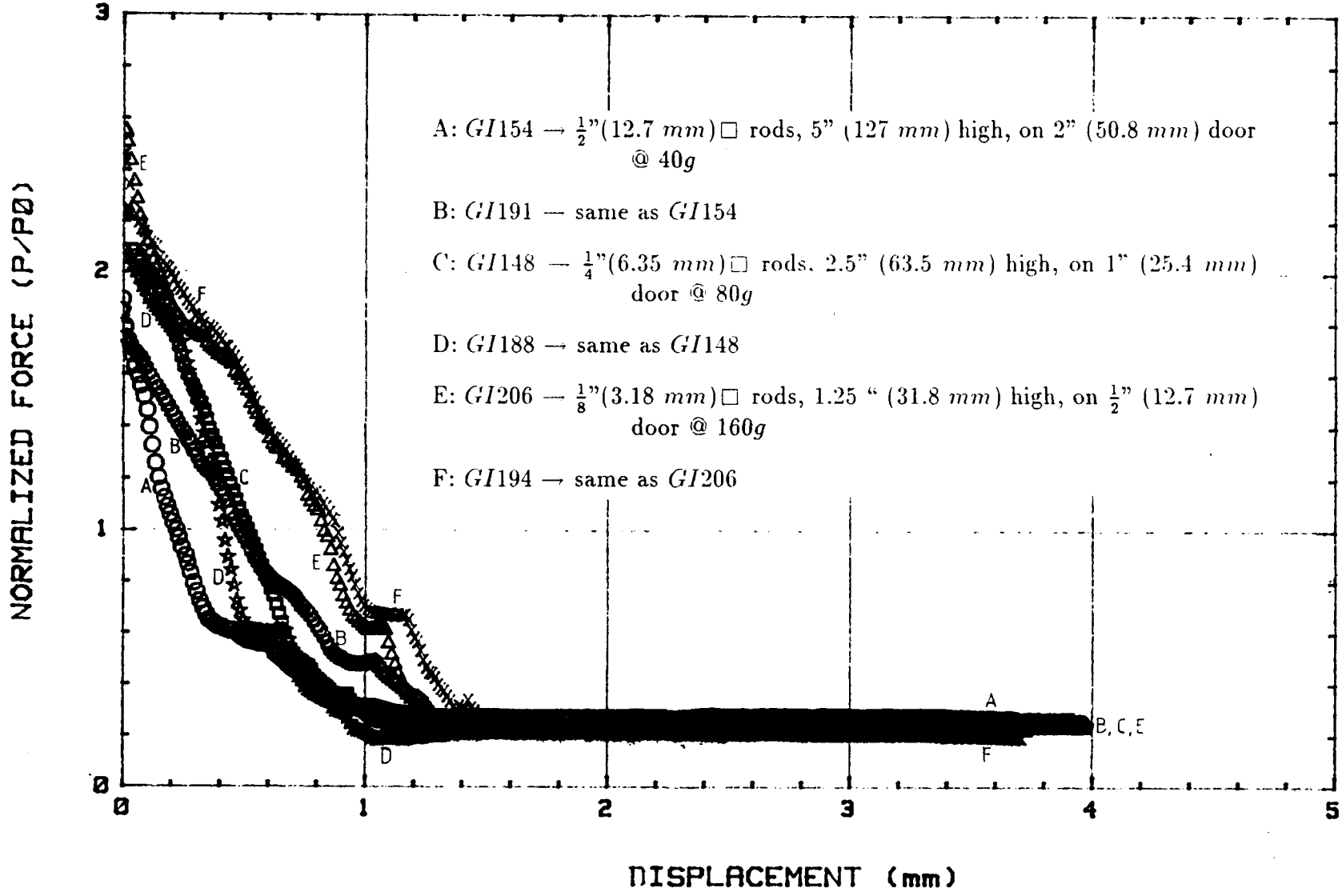

Figure 5-17: MIT "four-on-door" brick stack tests: Normalized force vs. displacement

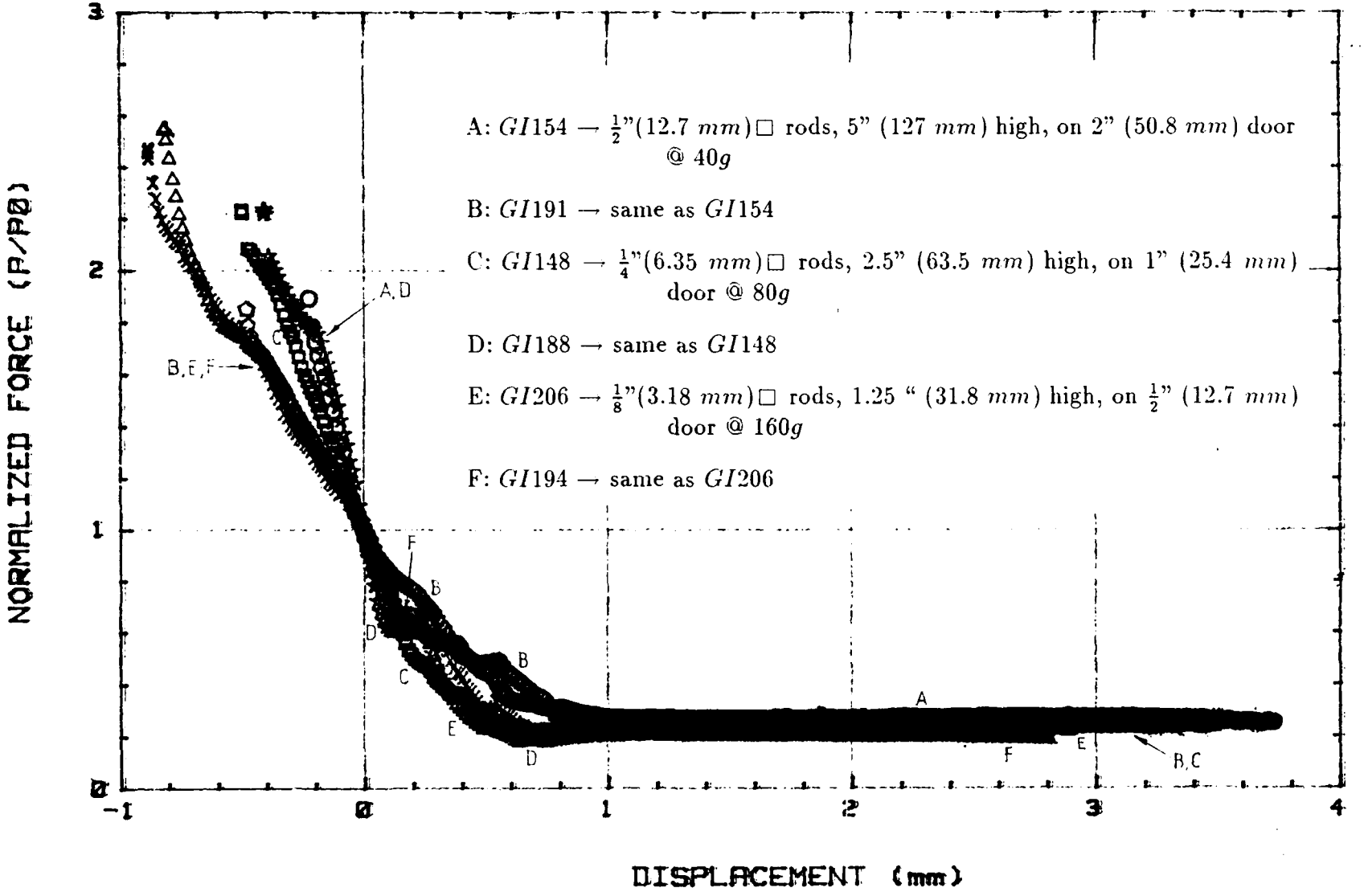

Figure 5-18: MIT "four-on-door" brick stack tests: Normalized force vs. adjusted displacement

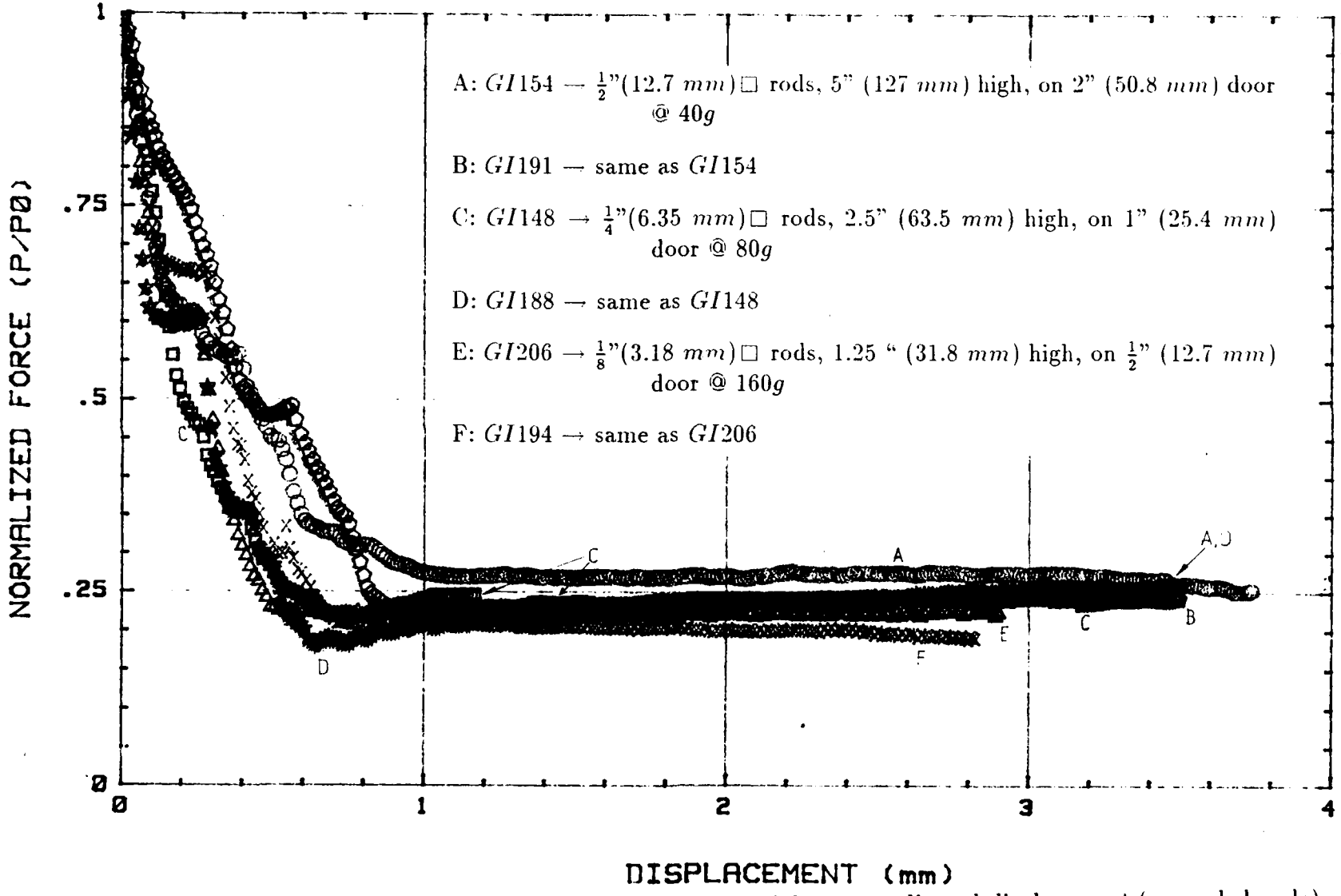

Figure 5-19: MIT "four-on-door" brick stack tests: Normalized force vs. adjusted displacement (expanded scale)

5.3.3 Other Layouts

5.3.3.1 Effect of Lateral Confinement

Some tests have also been performed to determine the influence of different types of lateral confinement. These are done with the "three-on-door" layout, and the results are graphically presented in Figure 5-20.

A direct stack arrangement (Test $GI137$) of $\frac{1}{2}$"(12.7 mm)$\square$ aluminum rods, 2.5" (63.5 mm) high, over the 2" (50.8 mm) door is confined laterally with densely packed $\frac{1}{4}$"(6.35 mm)$\oslash$ circular aluminum rods [with some $\frac{1}{8}$"(3.18 mm)$\oslash$ Al rods] and is tested at $40g$. A similar setup (Test $GI138$), but laterally confined with NJ coarse sand, is also tested at $40g$. As can be seen in Figure 5-20, the resulting load-displacement plots are quite different, with the sand-confined setup obtaining greater measured loads. The difference may be ascribed to the dissimilar friction angles and unit weights (which both affect the lateral stresses) of the confining materials.

Two tests at $80g$ with arrangements geometrically similar to those above, i.e., with $\frac{1}{4}$"(6.35 mm)$\square$ rods, 1.25" (31.75 mm) high, on 1" (25.4 mm) door, have also been conducted. As before, circular Al rods are used in one ($GI139$), while NJ coarse sand is used in the other ($GI140$). The sand-confined setup again tends to result in greater measured loads (Figure 5-20).

The effect of different lateral confinements on the brick stack layout is evaluated by comparing the results from an experiment using hexagonal aluminum rods ($GI111$) with those from a test using glass beads ($GI204$). The load vs. displacement curves (Figure 5-20) obtained from these two tests tend to coincide. Unlike in the direct stack case, then, varying lateral confinements apparently have minor effect on the results in the brick stack arrangement.

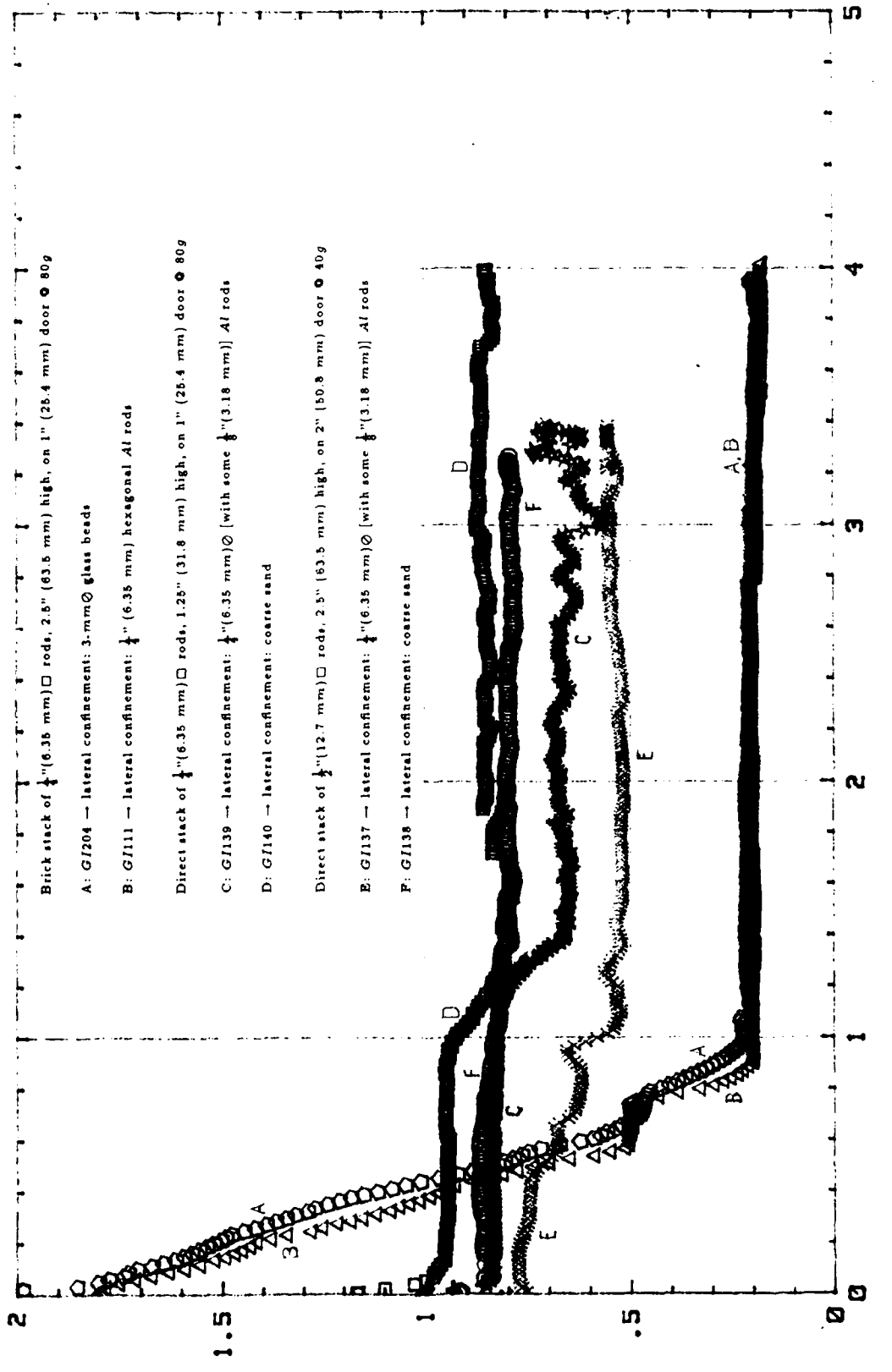

Figure 5-20: Tests to determine effects of lateral confinement

5.3.3.2 Effect of g-level

To determine how much the gravity level affects the results, identical setups are tested at different g's. Experiments with both direct and brick stacks are performed, and the results are displayed in Figure 5-21.

Two direct stack tests - one at $40g$ ($GI109$), and the other at $80g$ ($GI108$) - are carried out with the "three-on-door" arrangement of $\frac{1}{4}$"(6.35 mm)$\square$ Al rods, 2.5" (63.5 mm) high, on 1" (25.4 mm) door. Two brick stack tests - one at $40g$ ($GI191B$), and the other at $80g$ ($GI192$) - are performed with the "four-on-door" layout of $\frac{1}{2}$"(12.7 mm)$\square$ Al rods, 5" (127 mm) high, on 2" (50.8 mm) door. One can see from Figure 5-21 that, in both cases, the g-level does not seem to have any effect on the resulting normalized load vs. displacement plots.

5.3.3.3 "Two-on-door" Arrangement

A few tests have also been conducted wherein the aluminum rods are stacked such that two columns of rods fit directly above the trapdoor. Performing a *modelling of models* type of experimentation, $\frac{1}{2}$"(12.7 mm)$\square$ rods confined laterally by 6-$mm\oslash$ glass beads are used with the 1" (25.4 mm) door to be lowered at $80g$ ($GI177$); $\frac{1}{4}$"(6.35 mm)$\square$ rods surrounded by 3-$mm\oslash$ glass beads are used with the $\frac{1}{2}$" (12.7 mm) door to be lowered at $160g$ ($GI172$). In addition, a test almost identical to $GI177$, with the exception that 3-$mm\oslash$ (instead of 6-$mm\oslash$) glass beads are utilized, have been performed. Table 5.2 summarizes these three sets of experiments.

Table 5.2: MIT tests with "two-on-door" setup

	Rod Size	Total Height	Door Width	Glass Bead Size	Gravity Level
1.	$\frac{1}{2}$ $in\square$ (12.7 $mm\square$)	2.50 in (63.5 mm)	1.0 in (50.8 mm)	6.0 mm	$80g$
2.	$\frac{1}{4}$ $in\square$ (6.35 $mm\square$)	1.25 in (31.8 mm)	0.5 in (25.4 mm)	3.0 mm	$160g$
3.	$\frac{1}{2}$ $in\square$ (12.7 $mm\square$)	2.50 in (63.5 mm)	1.0 in (50.8 mm)	3.0 mm	$80g$

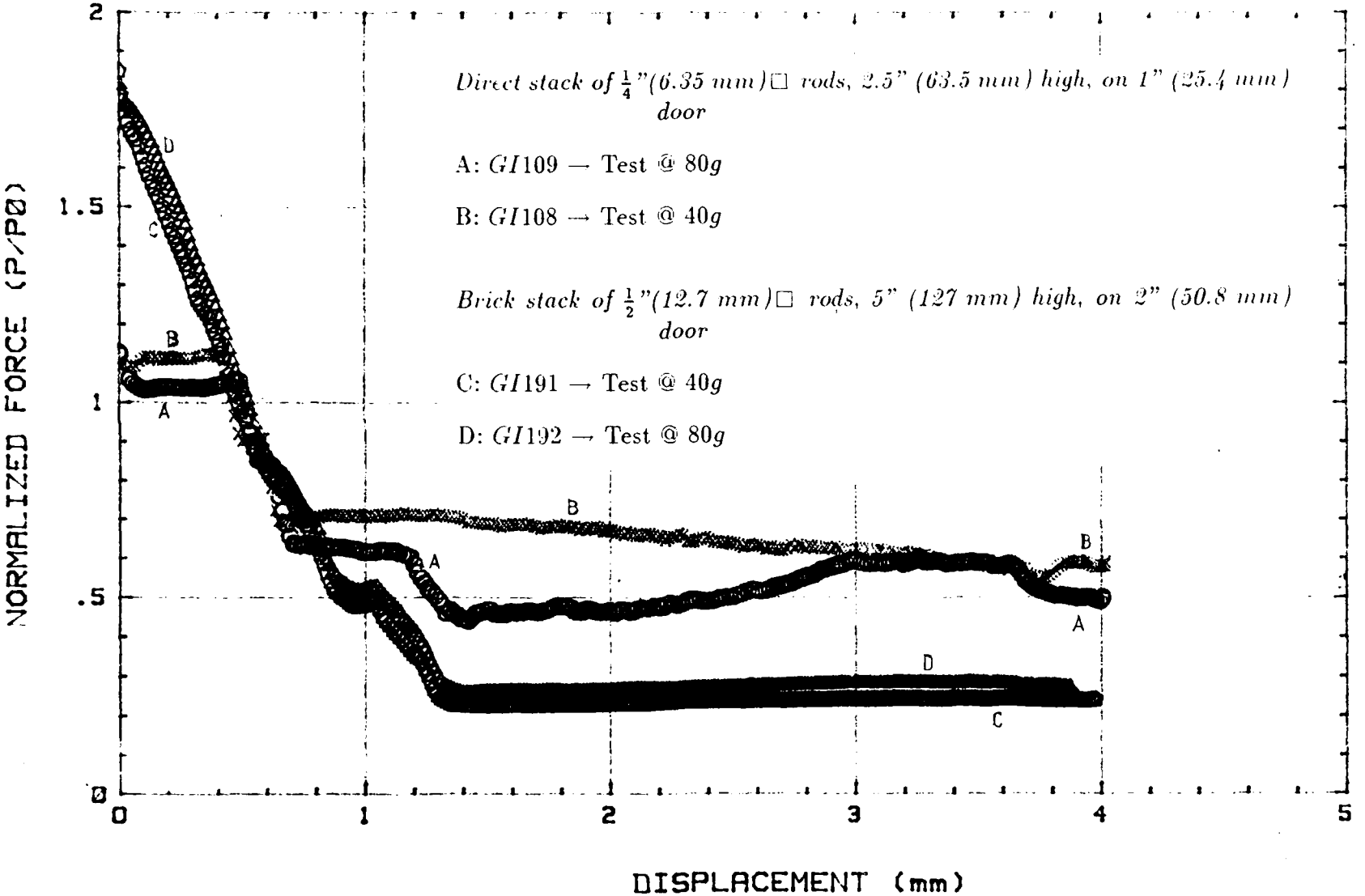

Figure 5-21: Tests to determine effects of g-level

As usual, model assembly starts from the center; row by row the two rods above the trapdoor are placed, followed by six rods laid out individually on each side. When five rows are completed for all door segments, the glass beads are deposited on the sides. The spin-up and door lowering sequence is the same as before.

The final configurations are depicted in Figure 5-22. In all three tests, the two columns of rods above the door simply follow the downward displacement of the trapdoor. Figure 5-23 shows the quantitative results. It should be noted that the data from Test *GI*172 are questionable, considering that, at the start of downward movement of the door, the measured load increases before eventually dropping. [2] Not surprisingly, the normalized force vs. displacement curves from the *modelling of models* pair of tests (*GI*172 and *GI*177) do not match. The effect of different lateral confinements seems to manifest itself in the results from Tests *GI*177 and *GI*203 which do not quite coincide. Possibly, however, this is due to the inherent imperfections in the alignment of the rods which affect the shearing process. Nevertheless, the ultimate values of the measured loads normalized with respect to the weight of the two columns of rods do appear to be comparable (for all three tests).

5.3.3.4 "Eight-on-door" Setup

An "eight-on-door" arrangement has also been tried out in a few runs. Both direct and brick stacks of aluminum rods are implemented, executing, again, a *modelling of models* series of tests. The rod sizes, door widths, diameters of glass beads (for lateral confinement), overall dimensions, and gravity levels involved are detailed in Table 5.3.

There is some slight variation in these "eight-on-door" setups as compared to the other layouts (e.g., "four-on-door") because there are not enough rods in the former to be laid

[2] Recall that a pair of brackets/spacers is used for the tests with $\frac{1}{2}$" (12.7 *mm*) door. It turned out that the roller support of the trapdoor was touching these brackets/spacers, thus, affecting the force measurements, especially prior to and during the initial stages of door lowering. This problem was not discovered until after Test *GI*181. Hence, all experiments *with the* $\frac{1}{2}$" *(12.7 mm) trapdoor* carried out before and including Test *GI*181 had been unreliable. The problem was solved by trimming material off the bracket/spacer pieces, and measurements henceforth were more reasonable. Unfortunately, due to lack of time, Test *GI*172 was never repeated.

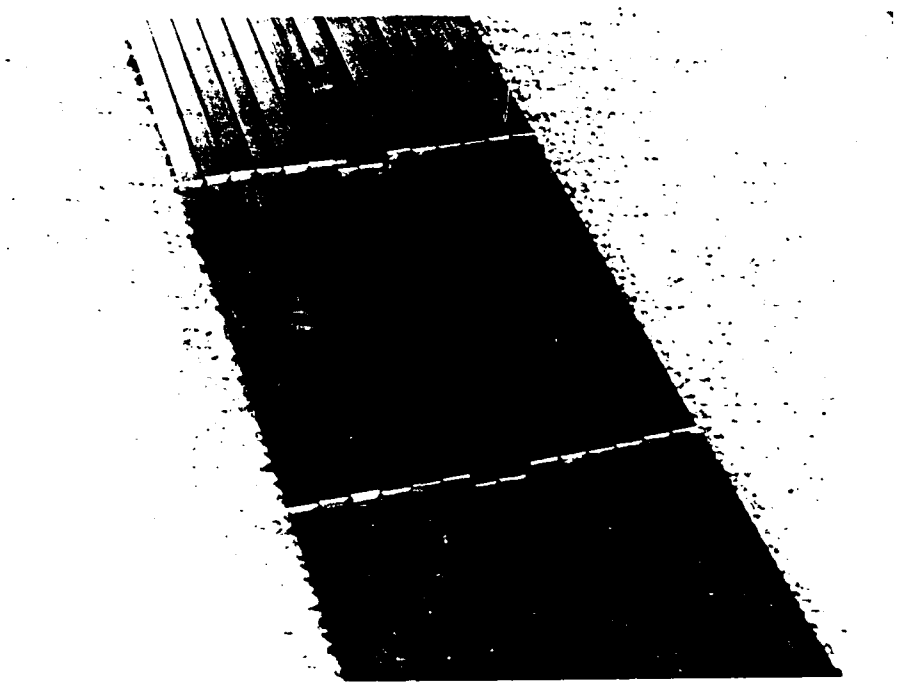

(a) Test $GI172$ - $\frac{1}{4}$"(6.35 mm)□ rods, 1.25" (31.8 mm) high, on $\frac{1}{2}$" (12.7 mm) door @ 160g

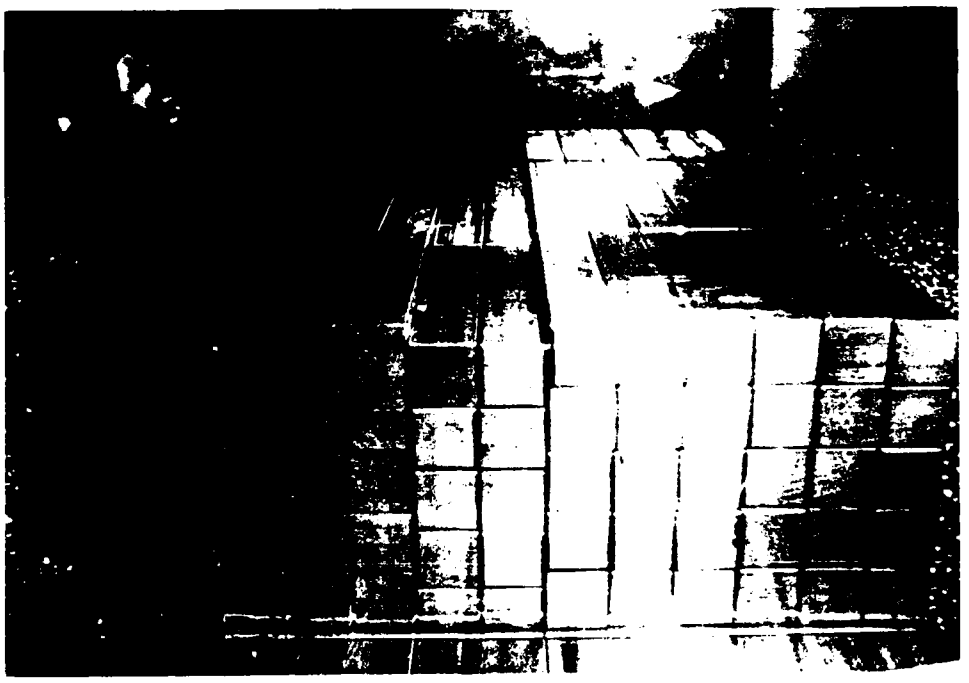

(b) Test $GI203$ - $\frac{1}{2}$"(12.7 mm)□ rods, 2.5" (63.5 mm) high, on 1" (25.4 mm) door @ 80g

Figure 5-22: "Two-on-door" tests with Al rods: Final configuration

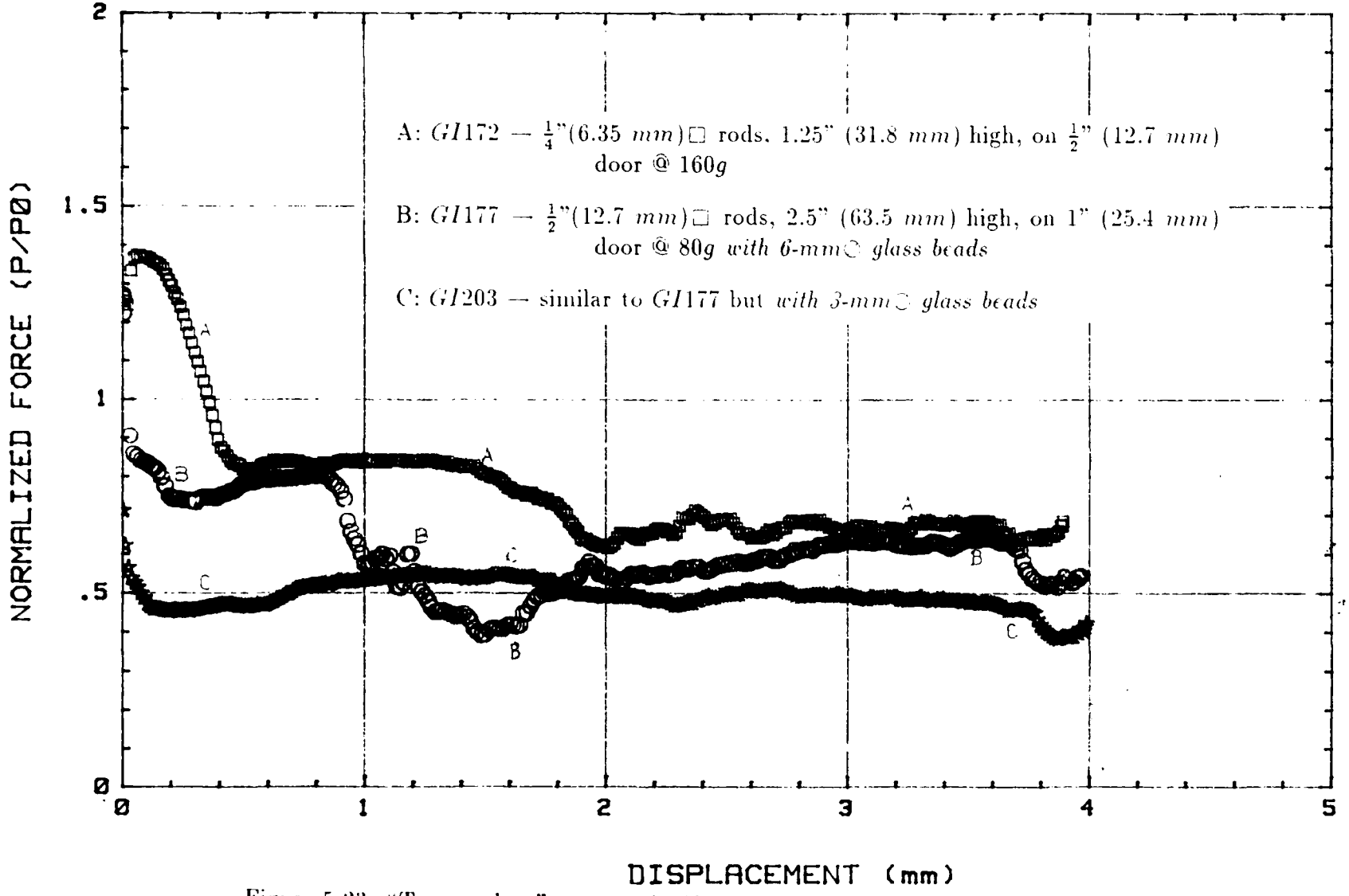

Figure 5-23: "Two-on-door" tests with *Al* rods: Normalized force vs. displacement

Table 5.3: MIT tests with "eight-on-door" setup

	Rod Size	Total Height	Door Width	Glass Bead Size	Gravity Level
1.	$\frac{1}{4}$ *in*□	5.00 *in*	2.0 *in*	6.0 *mm*	40*g*
	(6.35 *mm*□)	(127 *mm*)	(50.8 *mm*)		
2.	$\frac{1}{8}$ *in*□	2.50 *in*	1.0 *in*	3.0 *mm*	80*g*
	(3.18 *mm*□)	(63.5 *mm*)	(25.4 *mm*)		

out to the same height and exact geometric pattern as in the latter. To have the same overall height and width as the "four-on-door" arrangement, some larger-sized rods have been utilized in the tests done with an "eight-on-door" arrangement. The brick stack for the "eight-on-door" assembly is actually a semi-brick and semi-direct arrangement: the lower half of the total height is laid out in a staggered fashion like bricks, and the entire upper half is placed in a direct stack configuration. Nevertheless, in complying with the geometric similarity requirements of the *modelling of models* approach, from one model scale of "eight-on-door setup to another, the overall arrangement has been maintained.

Partial facades of the jointed assemblies at the conclusion of each test are shown in Figure 5-24 for the direct stacks and in Figure 5-25 for the brick stacks. Utilizing more blocks in the model poses added complications in the alignment of the individual elements, leading to some "hang-ups," especially in the direct stack (Figure 5-24).

The measured force on the door normalized with respect to the theoretical overburden load is plotted against the door displacement for the direct stack tests in Figure 5-26, and for the brick stack cases in Figure 5-27. Due to "hang-up" problems in the direct stack, the data in Figure 5-26 may be difficult to interpret. The results from the brick stack experiments (Figure 5-27), however, are generally more consistent. Since the initial measured loads are considerably greater than the theoretical values, the displacement data are "corrected" as in Figure 5-28, where the normalized force ratios are equal to unity at zero (adjusted) displacement. The tendency of the normalized force vs. displacement plots for the brick stack experiments to coincide is evident from these results. This attests to the dependence of the shearing between the rod surfaces on *absolute* displacement.

Comparing the results from the "eight-on-door" brick stack setup with those from

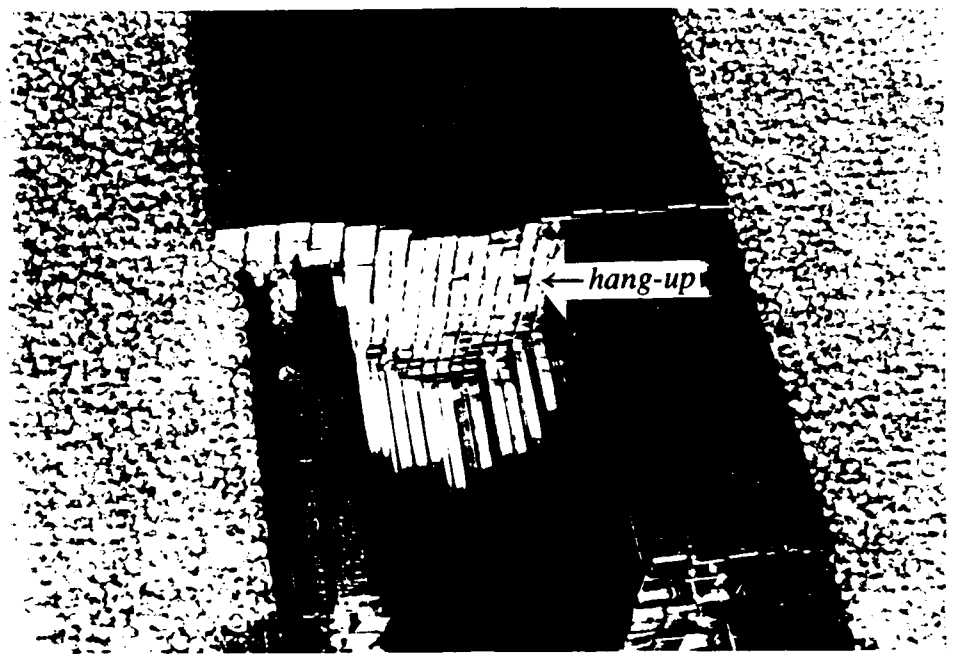

(a) Test $GI149$ - $\frac{1}{8}$"(3.18 mm)□ rods, 2.5" (63.5 mm) high, on 1" (25.4 mm) door @ $80g$
(Most rods followed movement of door; some hung up.)

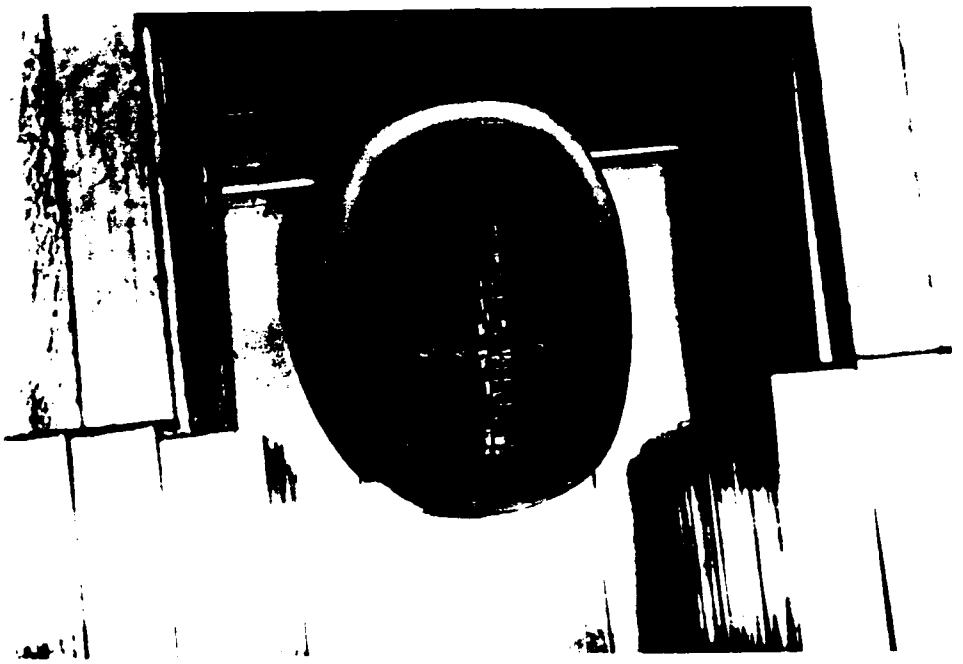

(b) Test $GI155$ - $\frac{1}{4}$"(6.35 mm)□ rods, 5" (127 mm) high, on 2" (50.8 mm) door @ $40g$
(Only 6 [not all 8] columns of rods followed door movement.)

Figure 5.21: "Eight-on-door" direct stack tests with AI rods: Final configuration

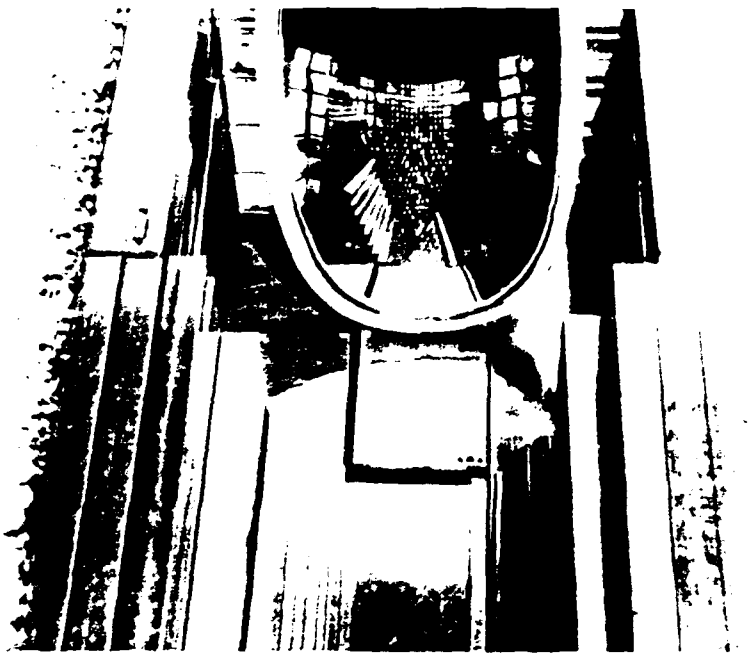

(a) Test $GI150$ - $\frac{1}{8}$"(12.7 mm)□ rods, 2.5" (63.5 mm) high, on 1" (25.4 mm) door @ 80g
(Triangular pattern formed at the bottom seven layers.)

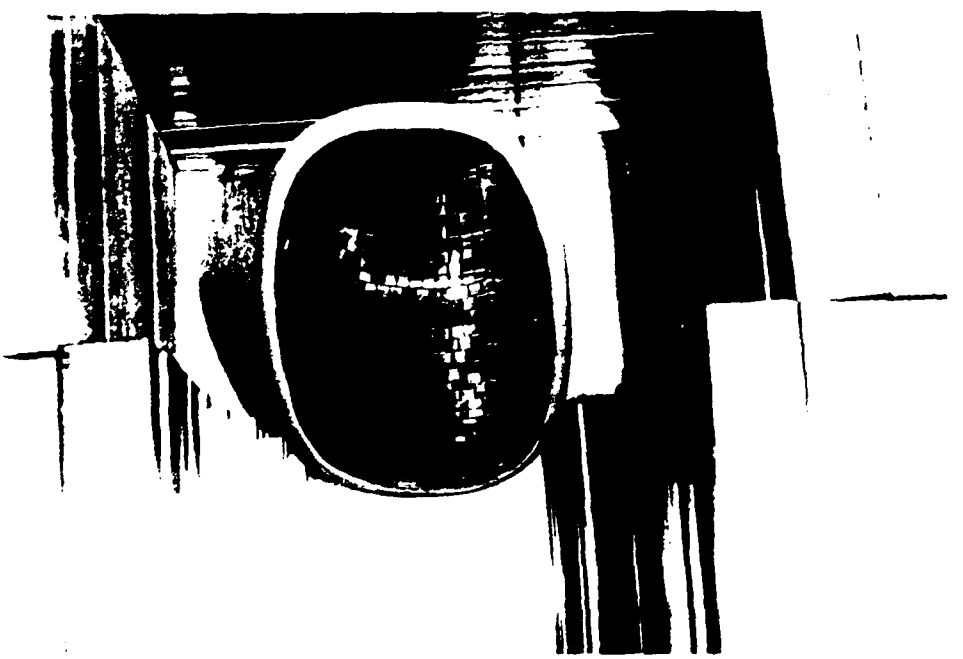

(b) Test $GI156$ - $\frac{1}{4}$"(6.35 mm)□ rods, 5" (127 mm) high, on 2" (50.8 mm) door @ 40g
(Trapezoidal pattern formed at the bottom four layers.)

Figure 5.25: "Eight-on-door" (semi-)brick stack tests with AI rods: Final configuration

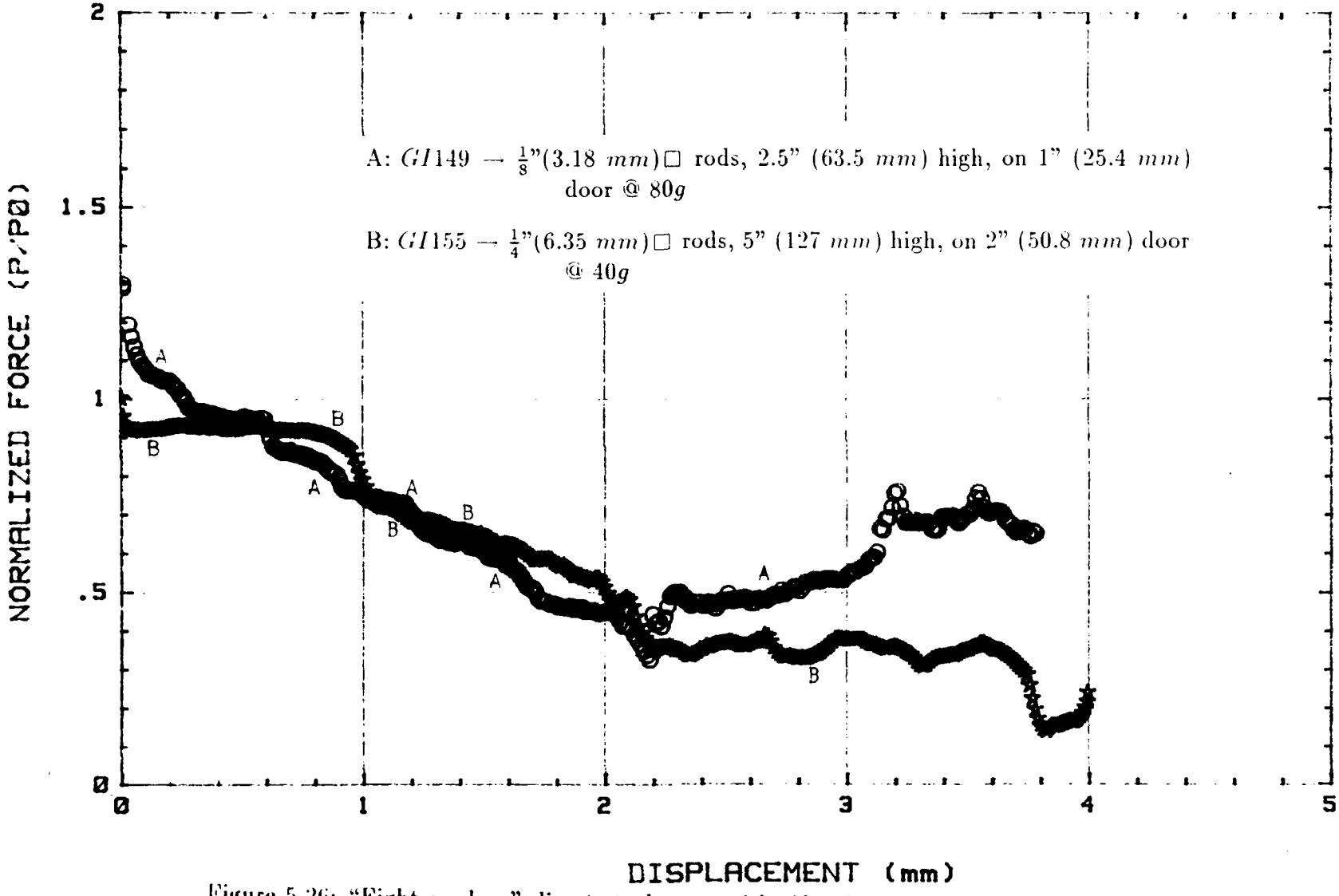

Figure 5-26: "Eight-on-door" direct stack tests with *Al* rods: Normalized force vs. displacement

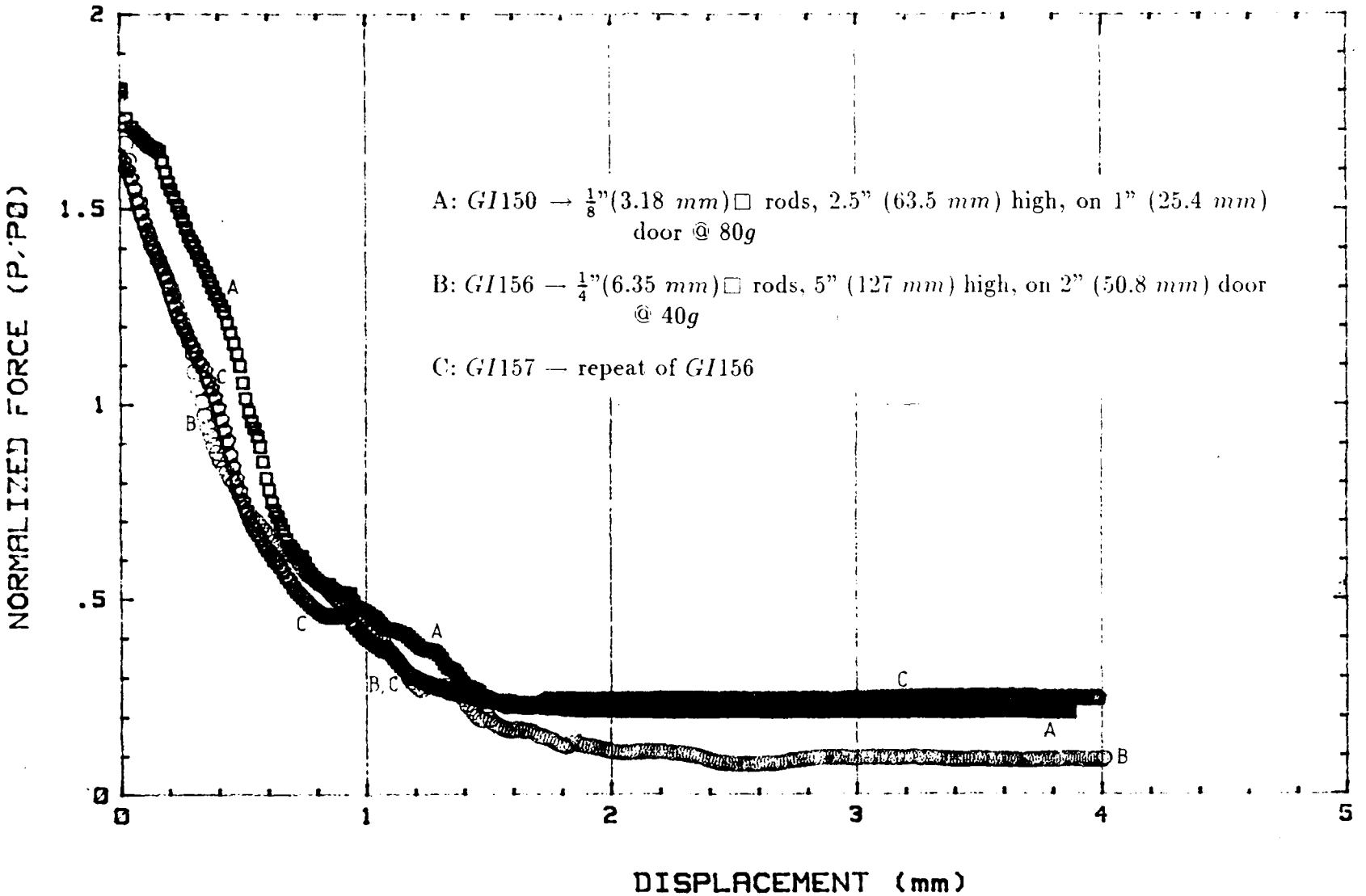

Figure 5-27: "Eight-on-door" (semi-)brick stack tests with *Al* rods: Normalized force vs. displacement

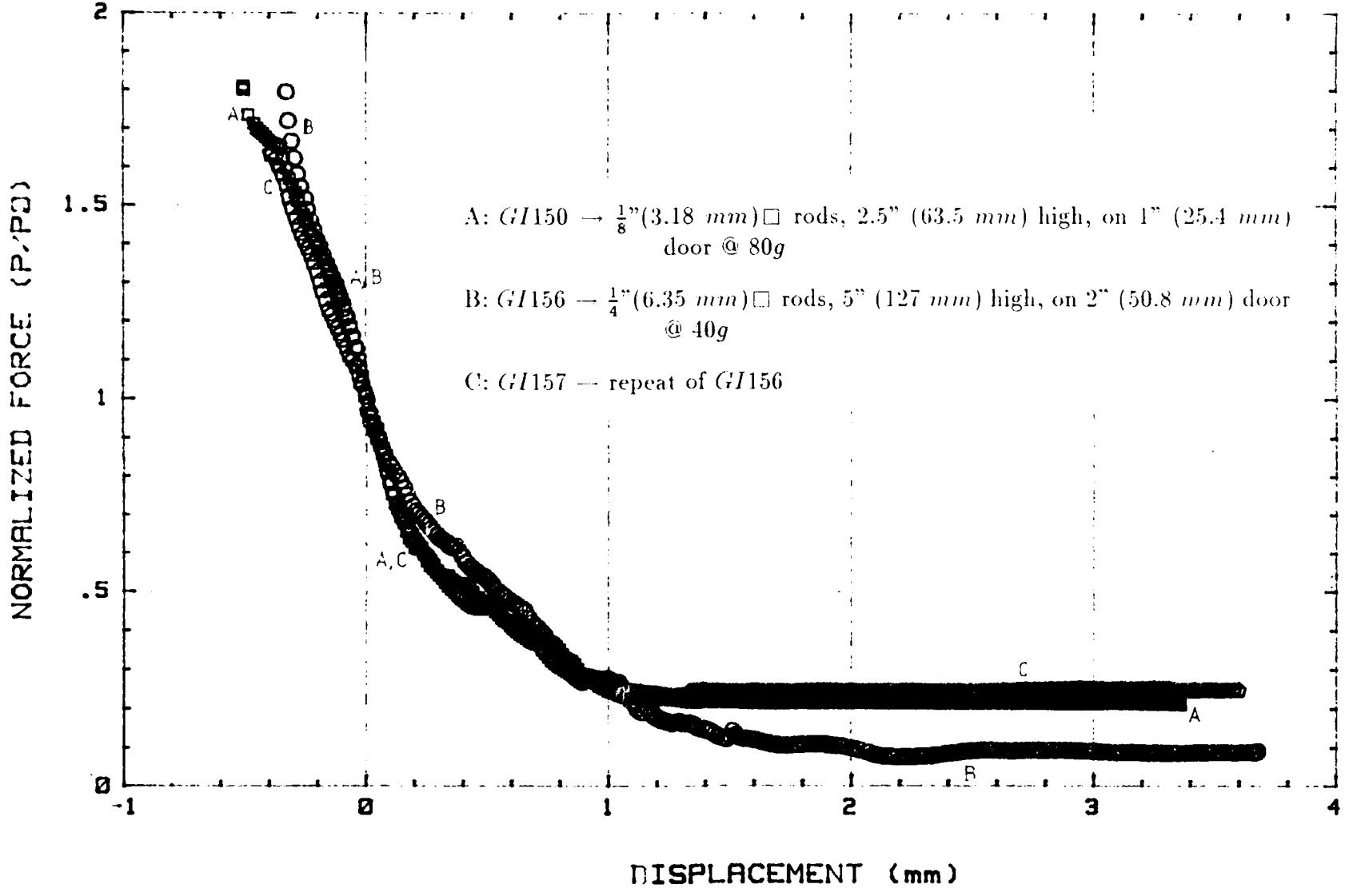

Figure 5-28: "Eight-on-door" (semi-)brick stack tests with *Al* rods: Normalized force vs. adjusted displacement

the "four-on-door" assembly (Figure 5-19), it is seen that the (adjusted) displacement at which the minimum load occurs is greater in the former ($\sim 1\ mm$) than in the latter ($\sim 0.7\ mm$). The overall shape of the force-displacement curve is also smoother in the case with more rods above the door, resembling somewhat the results from the tests with granular media.

5.3.4 Tests at RUB

The *modelling of models* exercise with aluminum rods is extended to other scales with the cooperation of Ruhr-Universität Bochum (RUB) in Germany. In particular, the same stack-up patterns with the "three-on-door" and "four-on-door" setups are implemented but with correspondingly scaled geometric dimensions and gravity levels ($50g$ and $25g$).

The spin-up sequence at RUB is slightly different from that at MIT. Instead of accelerating in four equal increments, the package is typically brought up to the top speed in three steps which are approximately related by 1:2.5:5. For example, the setup to be tested at $50g$ is spun up with "holds" at $10g$, $25g$, and $50g$. Nevertheless, this is of no major consequence when the results are compared.

Although the RUB apparatus has four trapdoor segments (three instrumented), the results in the following subsections present only the results from segment 2, believed to be least influenced by end effects. [Results from all three instrumented segments can be seen in the appendices of Iglesia's (1991) thesis or in the reports by Stone and Güttler (1989) and Jessberger and Scherbeck (1990).]

5.3.4.1 "Three-on-door" Arrangement

Following the initial phase of experimentation at MIT, tests with a "three-on-door" assembly have also been performed at RUB. These tests are carried out at $50g$, using 10 $mm\square$ aluminum rods with a 40-mm-wide trapdoor and laterally confined with fine sand. (When these tests were run, the geometric setup and lateral confinement had not

been standardized.)

Model preparation consists of placing ten rows of 15 aluminum rods, centering three rods over the width of the trapdoor, over all four trapdoor segments. This is followed by the placement of a plastic sheet against the edges of the outermost columns of rods and then by the deposition of fine sand into the remaining vacant spaces of the strong box (Figure 5-29). Pieces of cardboard ($\sim$0.5 *mm* thick) are inserted in the gaps between the stack segments to prevent interlocking/sliding of the rods across door segments during the construction of the model, and these cardboard pieces are left in place during the test.

The final model configurations resemble those in the MIT "three-on-door" tests. In the direct stack, the three columns of rods centered over the door simply follow the downward movement of the door. In the brick stack, a triangular "arch" pattern is clearly visible, as in Figure 5-30, with nine (9) rods going down with the door.

The measured forces, normalized with respect to the weight (at 50g) of the maximum 40 rods that can fit above the door, are plotted against the vertical door displacement as in Figure 5-31. The results are presented vis-a-vis those from the geometrically similar MIT setups in Figures 5-32 and 5-33 It is seen that the RUB direct stack results are quite different from the MIT results. The data for the direct stack case are questionable, since the measured loads turn out to be greater than the weight of the three columns of rods that descend with the door. The RUB brick stack results look more reasonable, although the initial measured loads are less than the normalizing force. When the RUB brick stack data are compared with the MIT data wherein the displacements have been adjusted so that the normalized loads are equal to unity at zero displacement (Figure 5-34), the curves tend to come closer to each other. The displacement at which the minimum load occurs is about the same for the different scaled models - another manifestation of the dependence of shearing between surfaces on *absolute* displacements.

These tests have not been repeated since the researchers at MIT and RUB have agreed to adopt the "four-on-door" layout of aluminum rods laterally confined with glass beads

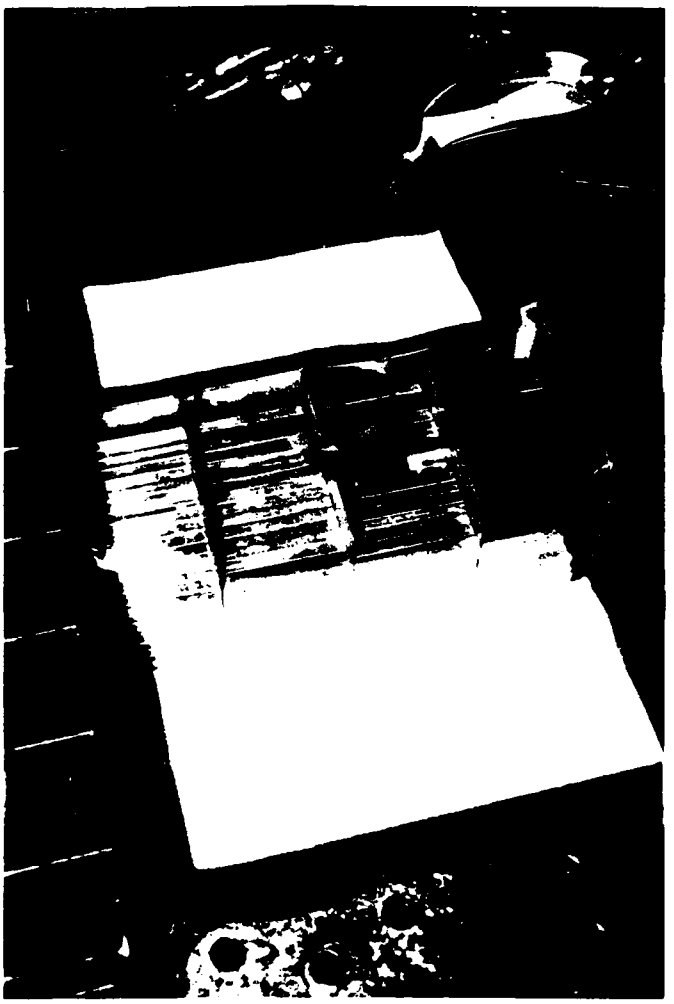

Figure 5-29: RUB "three-on-door" setup

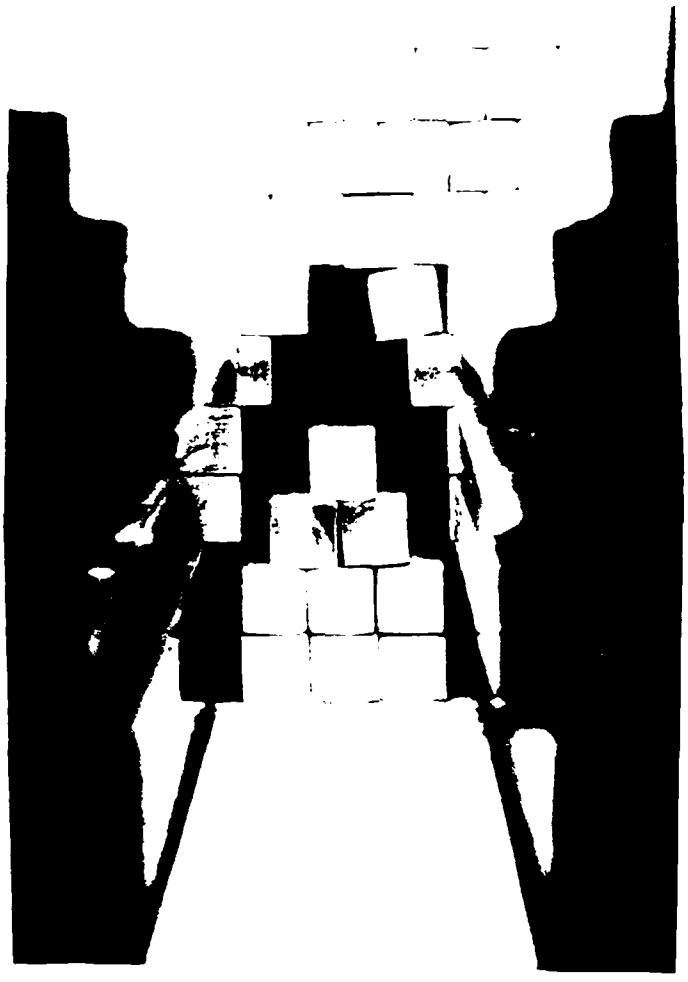

Figure 5-30: RUB "three-on-door" (semi-)brick stack test: Final configuration

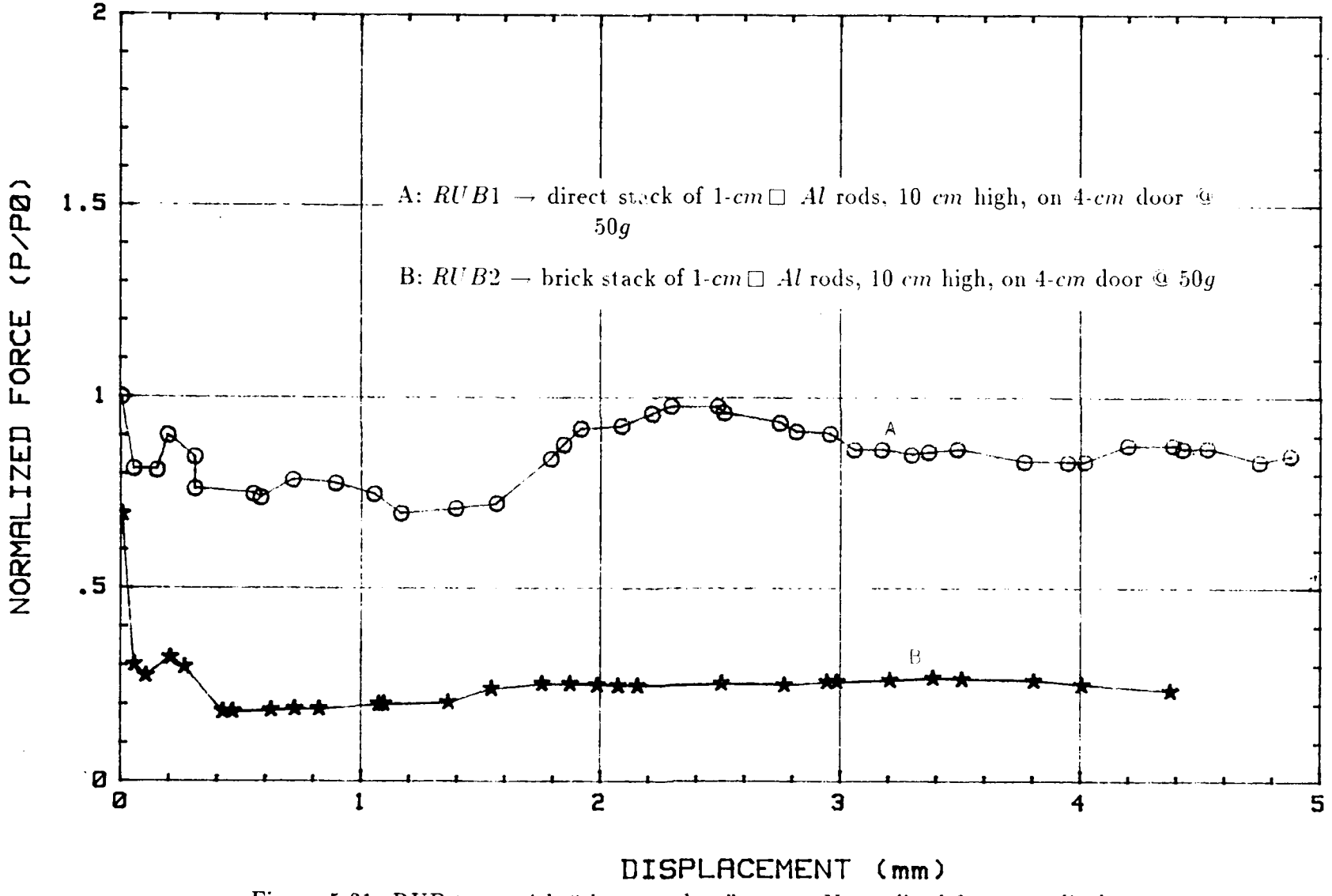

Figure 5-31: RUB tests with "three-on-door" setup: Normalized force vs. displacement

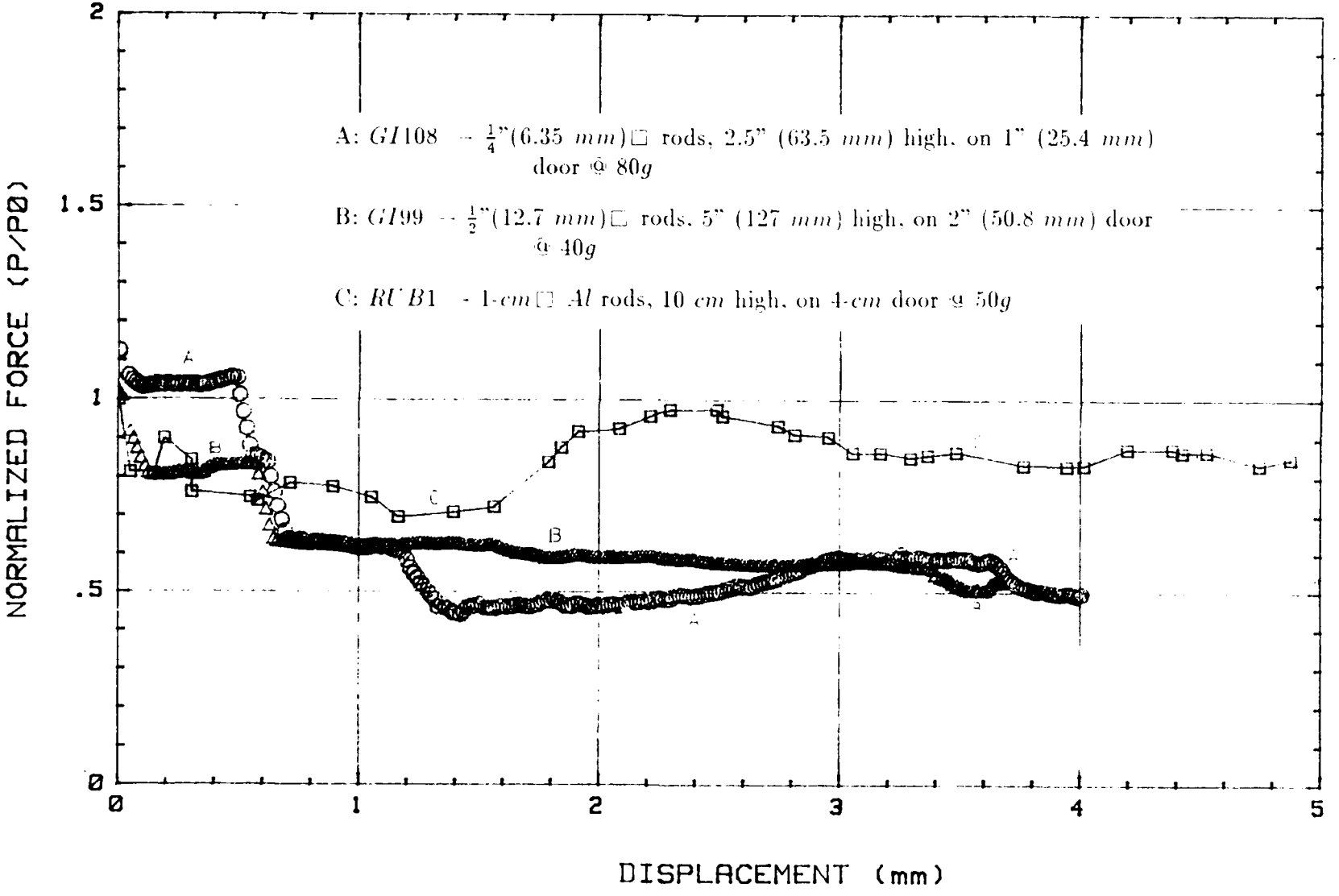

Figure 5-32: "Three-on-door" direct stack tests: Normalized force vs. displacement

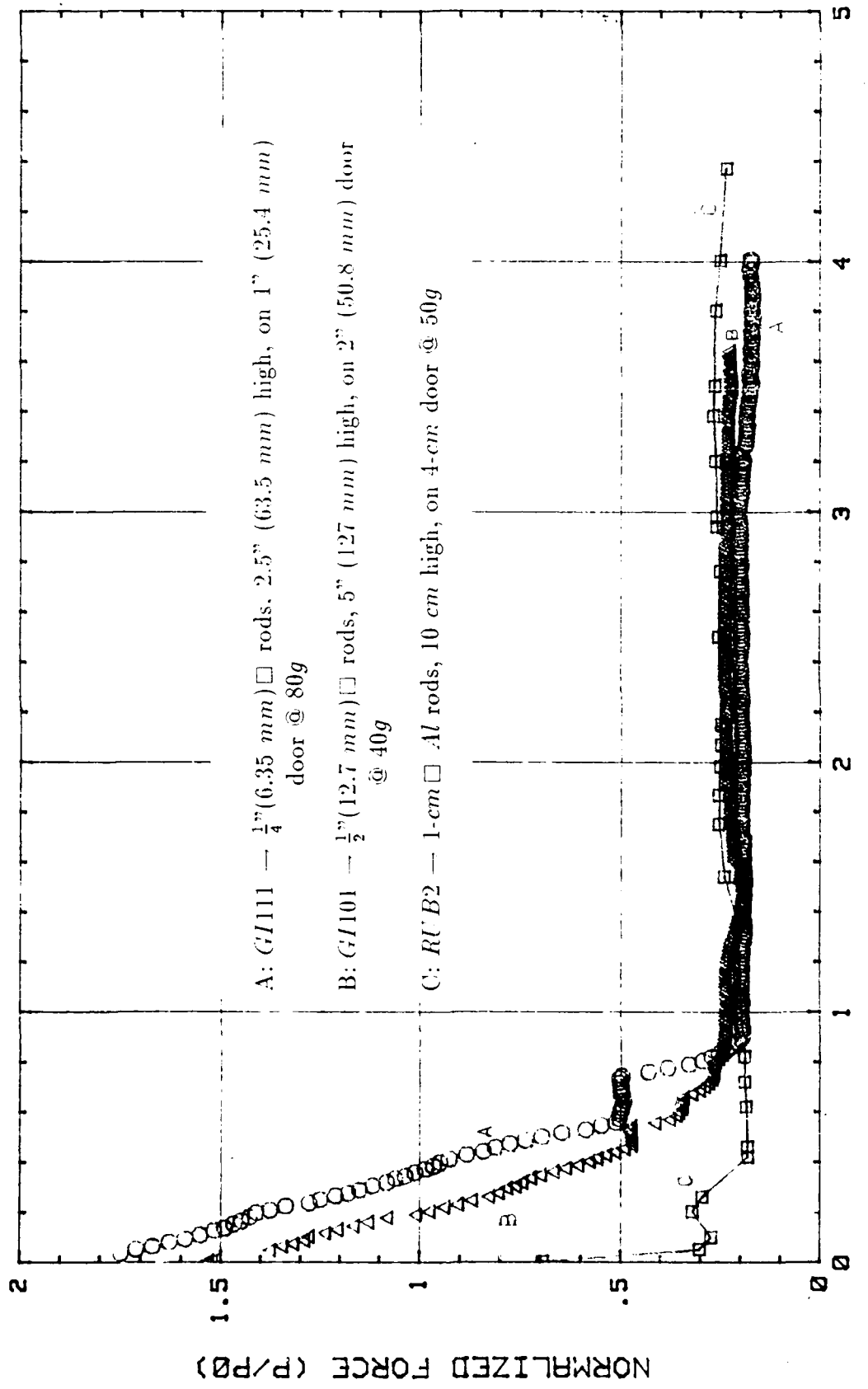

Figure 5-33: Three-on-door" (semi-)brick stack tests: Normalized force vs. displacement

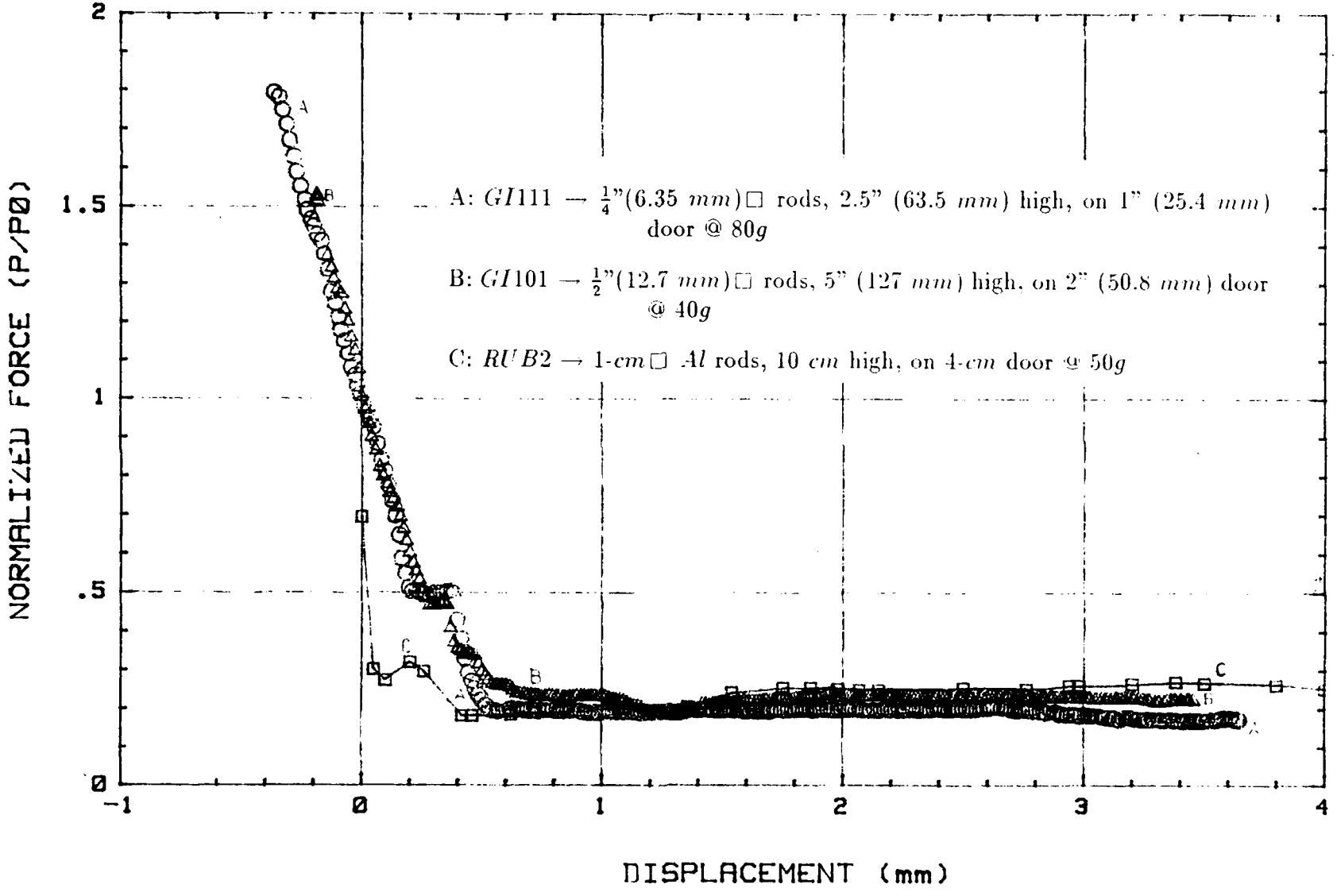

Figure 5-34: "Three-on-door" (semi-)brick stack tests: Normalized force vs. adjusted displacement

as the standard arrangement.

5.3.4.2 "Four-on-door" setup

Using the basic "four-on-door" assembly as in Figure 5-11, experiments are performed at RUB with the aluminum rod and glass bead sizes (and the corresponding model dimensions and gravity levels) shown in Table 5.4. Note that, due to the unavailability

Table 5.4: RUB tests with "four-on-door" setup

	Rod Size	Total Height	Door Width	Glass Bead Size	Gravity Level
1.	10 mm	100 mm	40 mm	5 mm	$50g$
2.	20 mm	200 mm	80 mm	5 mm	$25g$

of 10-$mm\oslash$ glass beads, the same 5-$mm\oslash$ glass beads are used for both the $50g$ and $25g$ tests.

Figures 5-35 and 5-36 display the final configurations in the various tests. For the direct stack arrangement, as in the MIT experiments, the four columns of rods above the door simply follow the settlement of the trapdoor. For the brick stack case, a triangular pattern tends to form above the door.

The quantitative results are shown in Figure 5-37 for the RUB direct stack tests, and in Figure 5-38 for the RUB brick stack arrangements. These plots indicate that the results are fairly reproducible. Collated results from the "four-on-door" experiments at both RUB and MIT are presented in Figures 5-39 through 5-41. It is evident from these results that the normalized force vs. (non-normalized) displacement curves tend to coincide, implying that the displacement values violate the centrifuge scaling rules for length dimensions.

5.4 Summary of Observations

Lowering of the trapdoor underneath a direct stack arrangement of rods causes an abrupt reduction in the load on the door. As door displacement continues, this reduced load

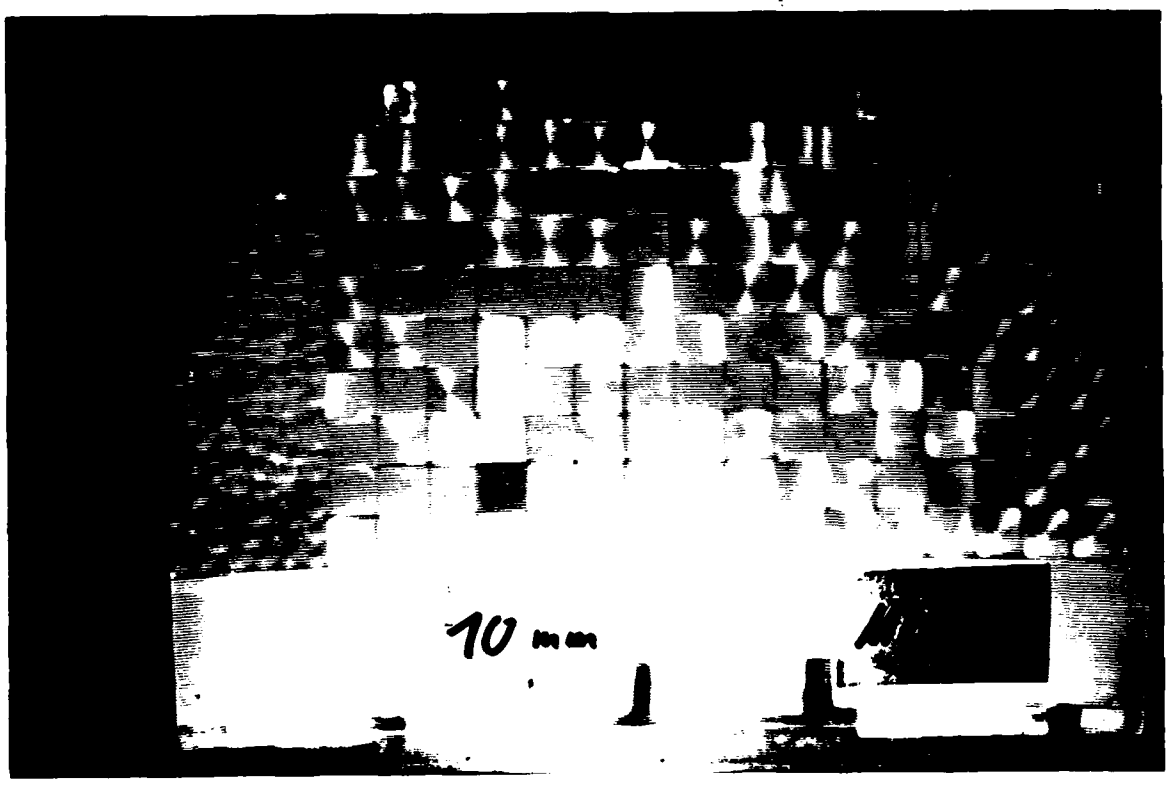

(a) Test *RUB7* – 1-*cm*□ rods, 10 *cm* high, on 4-*cm* door @ 50*g*

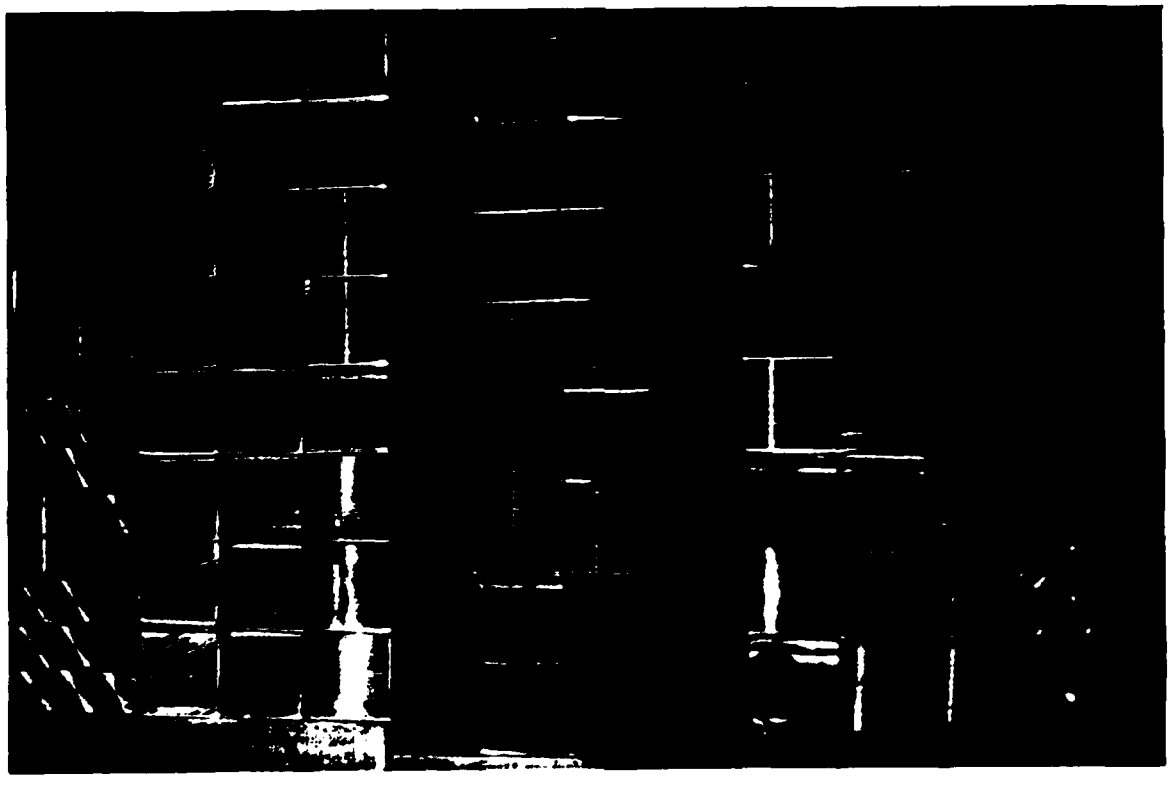

(b) Test *RUB13* – 2-*cm*□ rods, 20 *cm* high, on 8-*cm* door @ 25*g*

Figure 5-35: RUB "four-on-door" direct stack tests: Final configuration

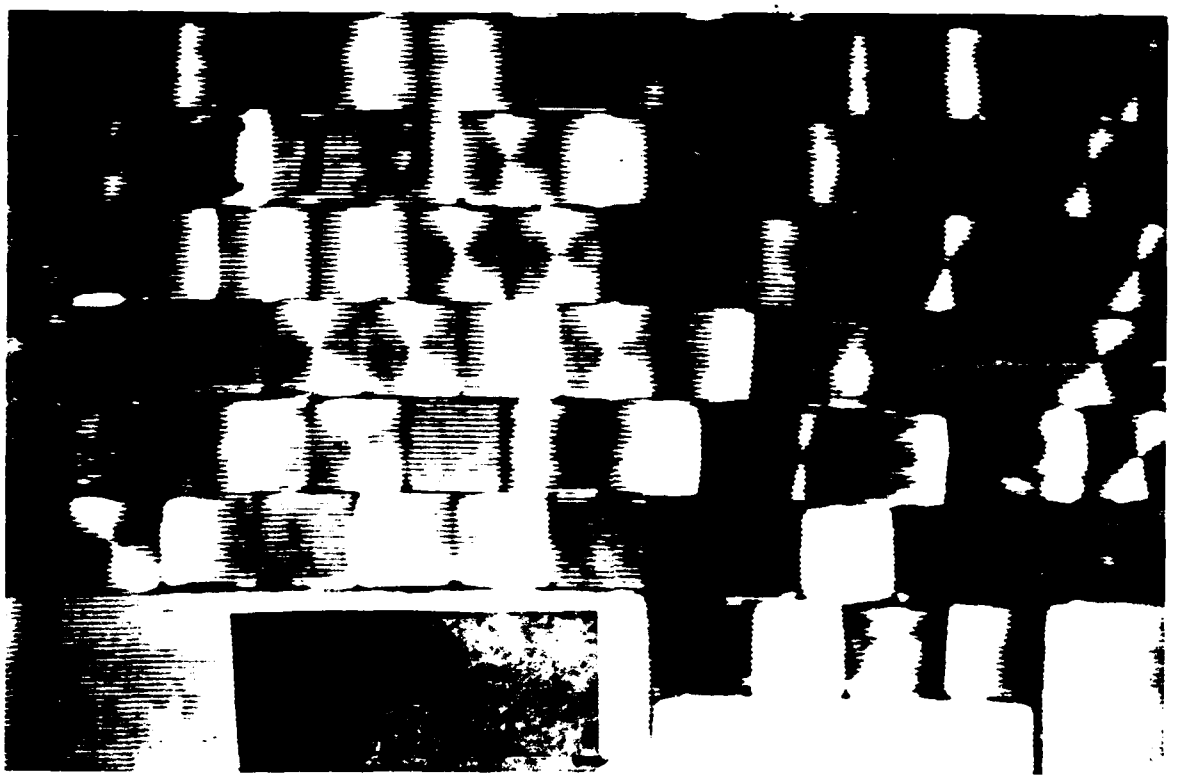

(a) Test $RUB9$ – 1-$cm\square$ rods, 10 cm high, on 4-cm door @ $50g$

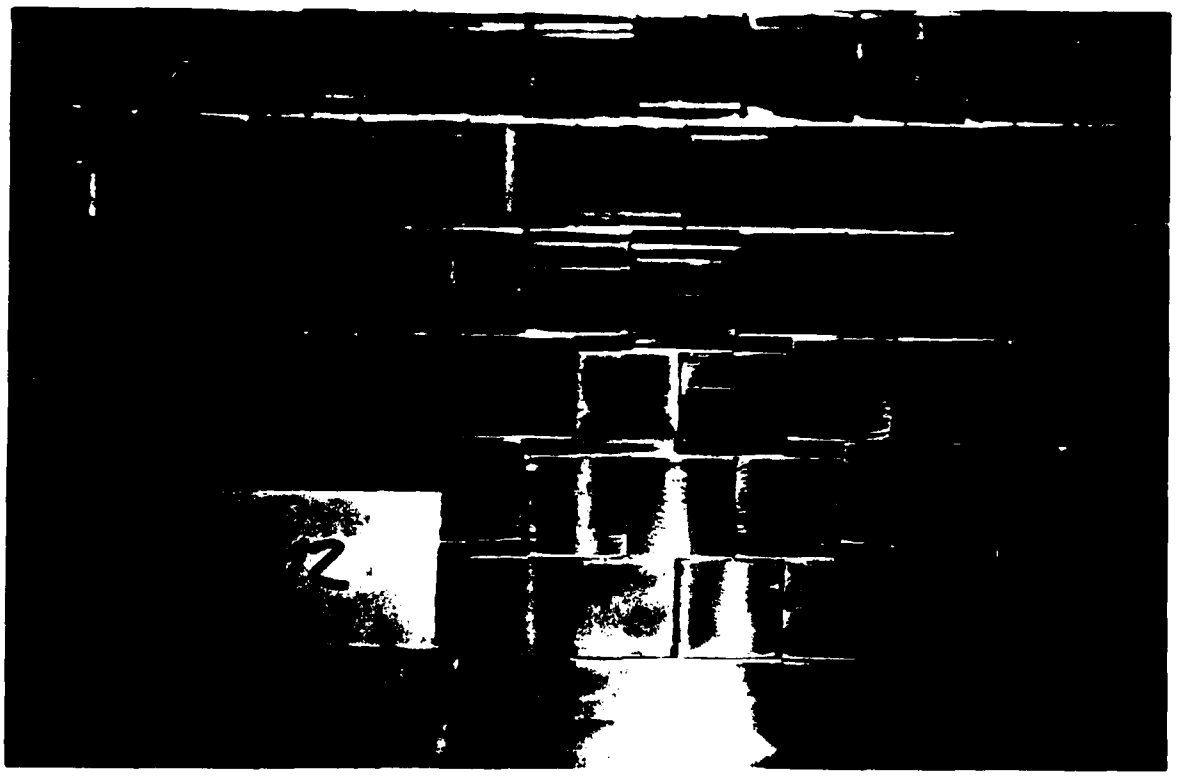

(b) Test $RUB12$ – 2-$cm\square$ rods, 20 cm high, on 8-cm door @ $25g$

Figure 5-36: RUB "four-on-door" brick stack tests: Final configuration

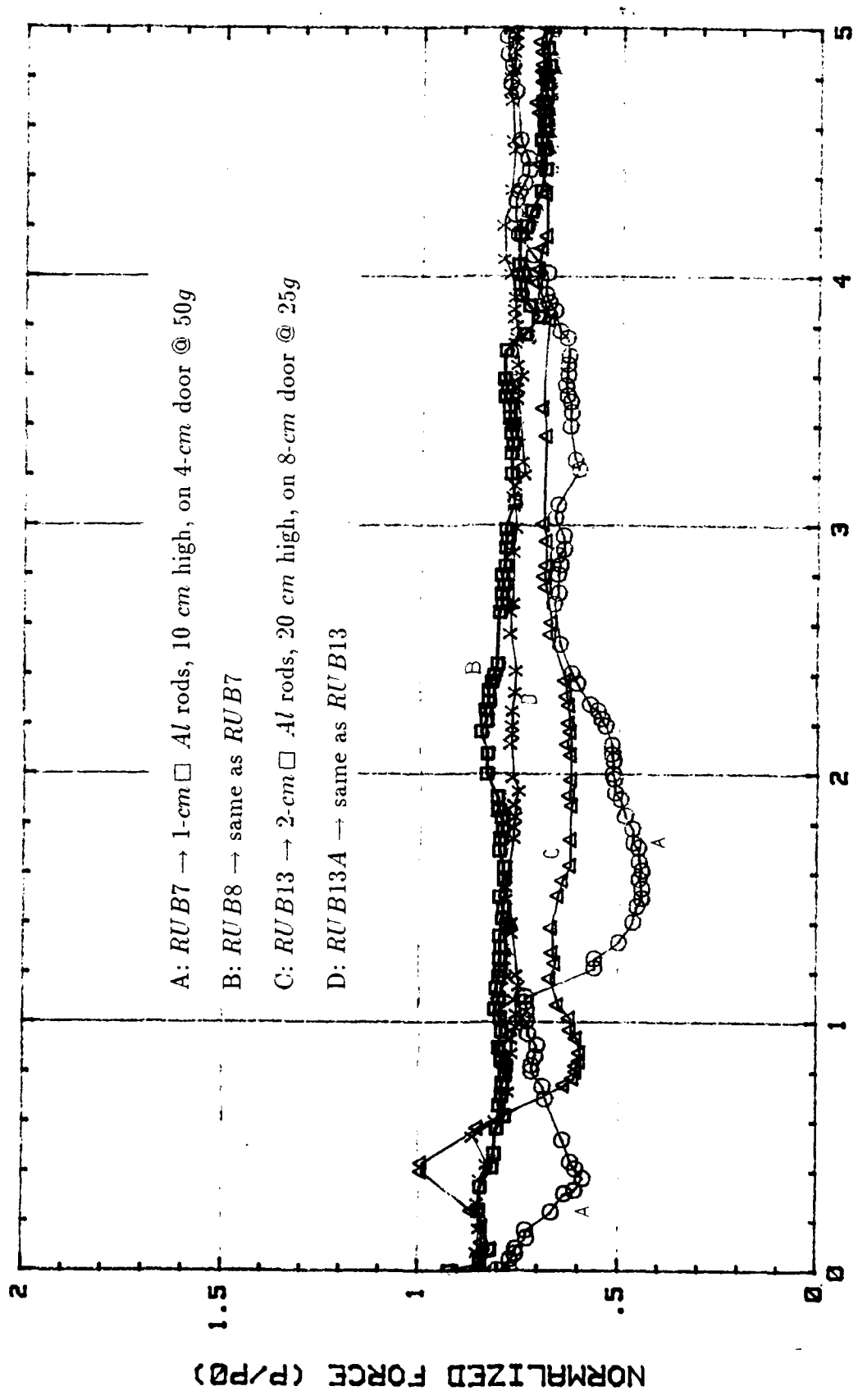

Figure 5-37: RUB "four-on-door" direct stack tests: Normalized force vs. displacement

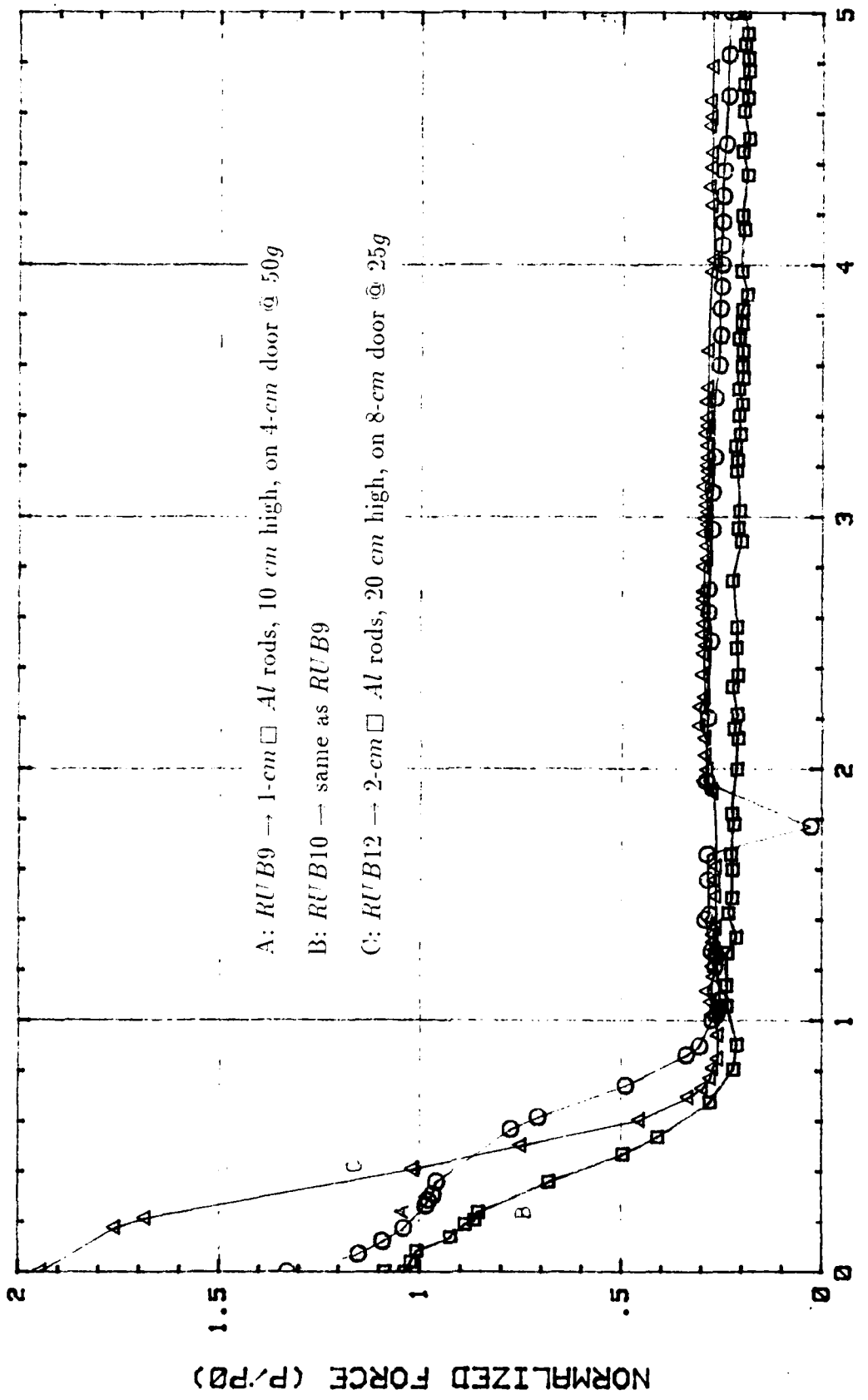

Figure 5.38: RUB "four-on-door" brick stack tests: Normalized force vs. displacement

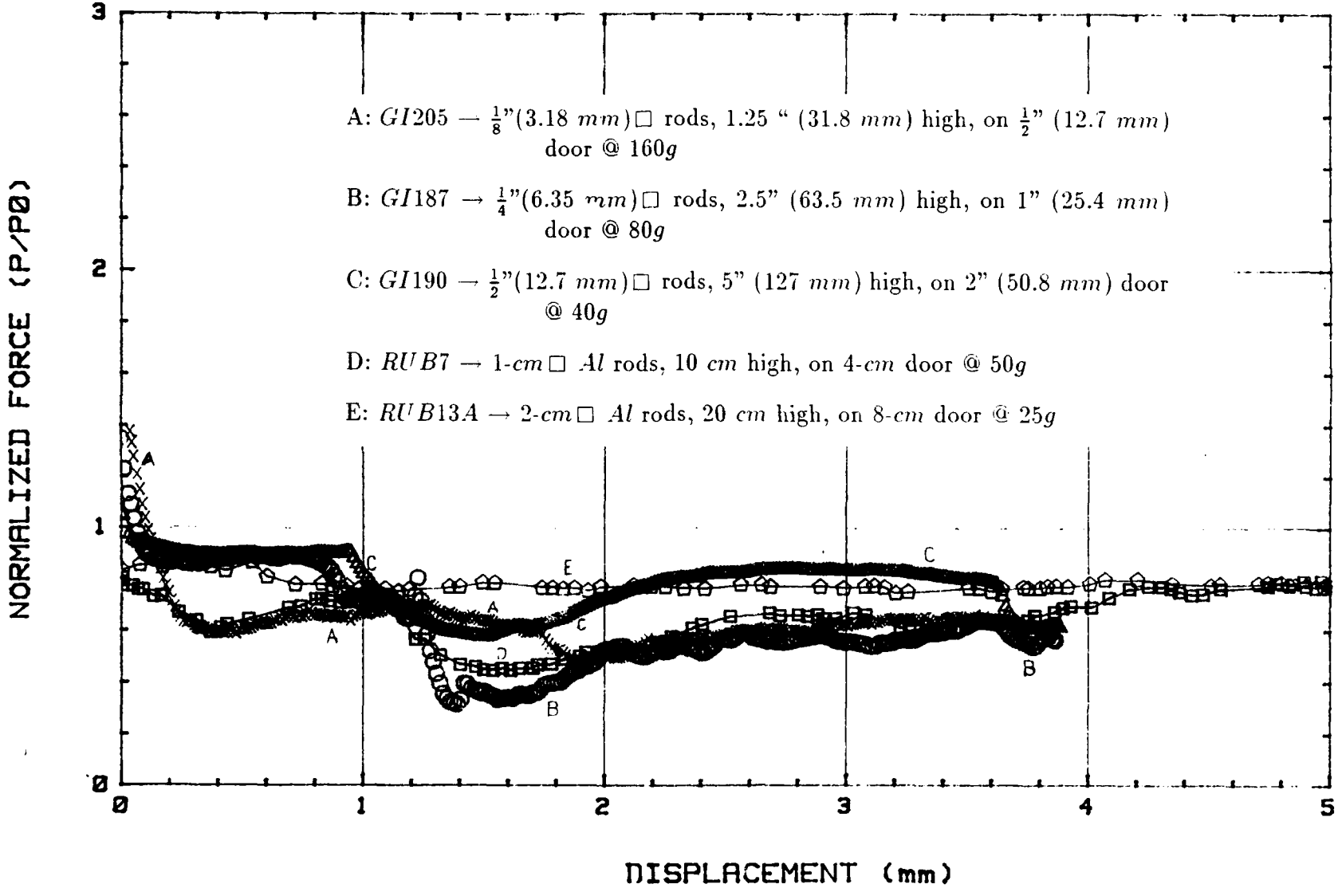

Figure 5-39: "Four-on-door" direct stack tests: Normalized force vs. displacement

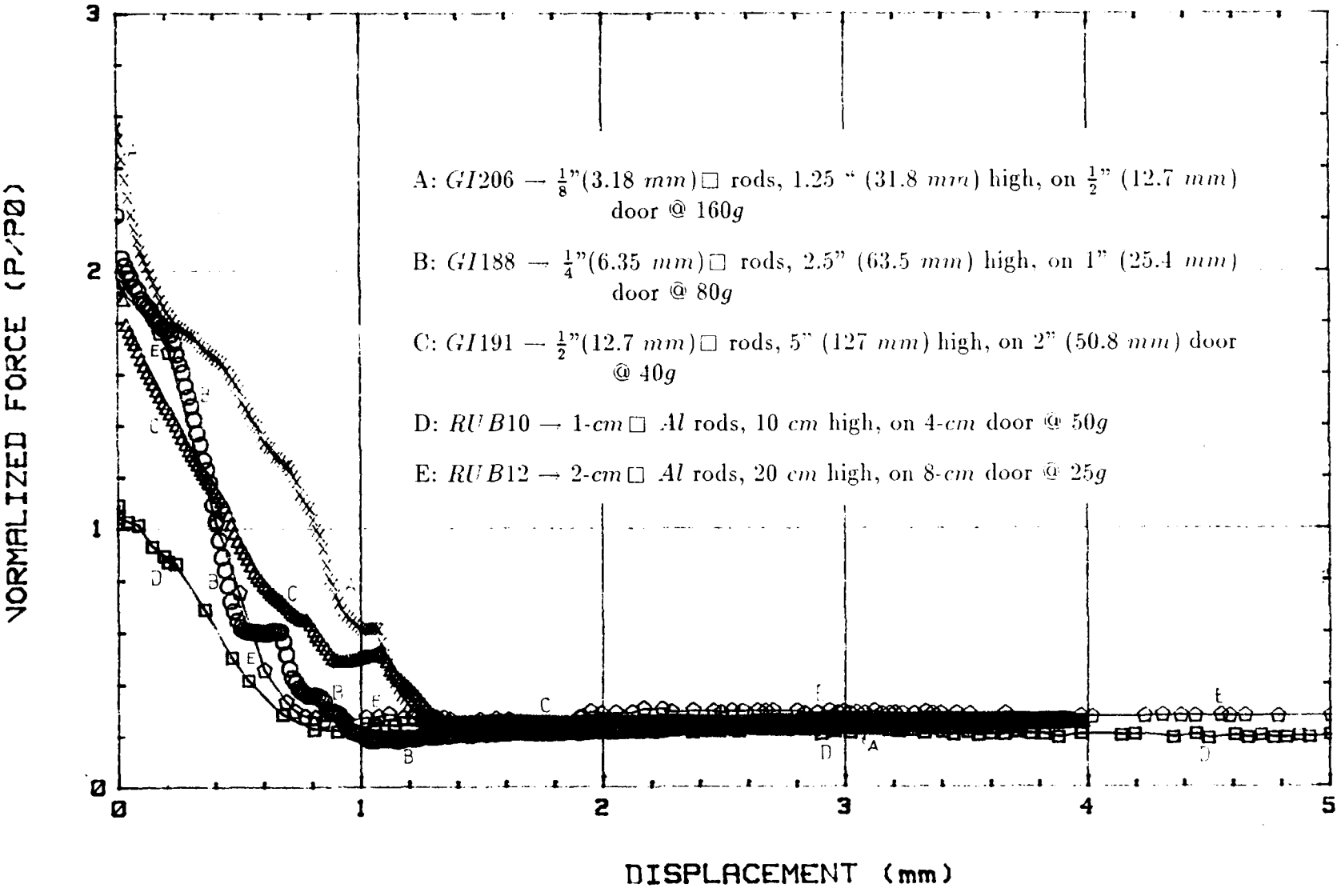

Figure 5-40: "Four-on-door" brick stack tests: Normalized force vs. displacement

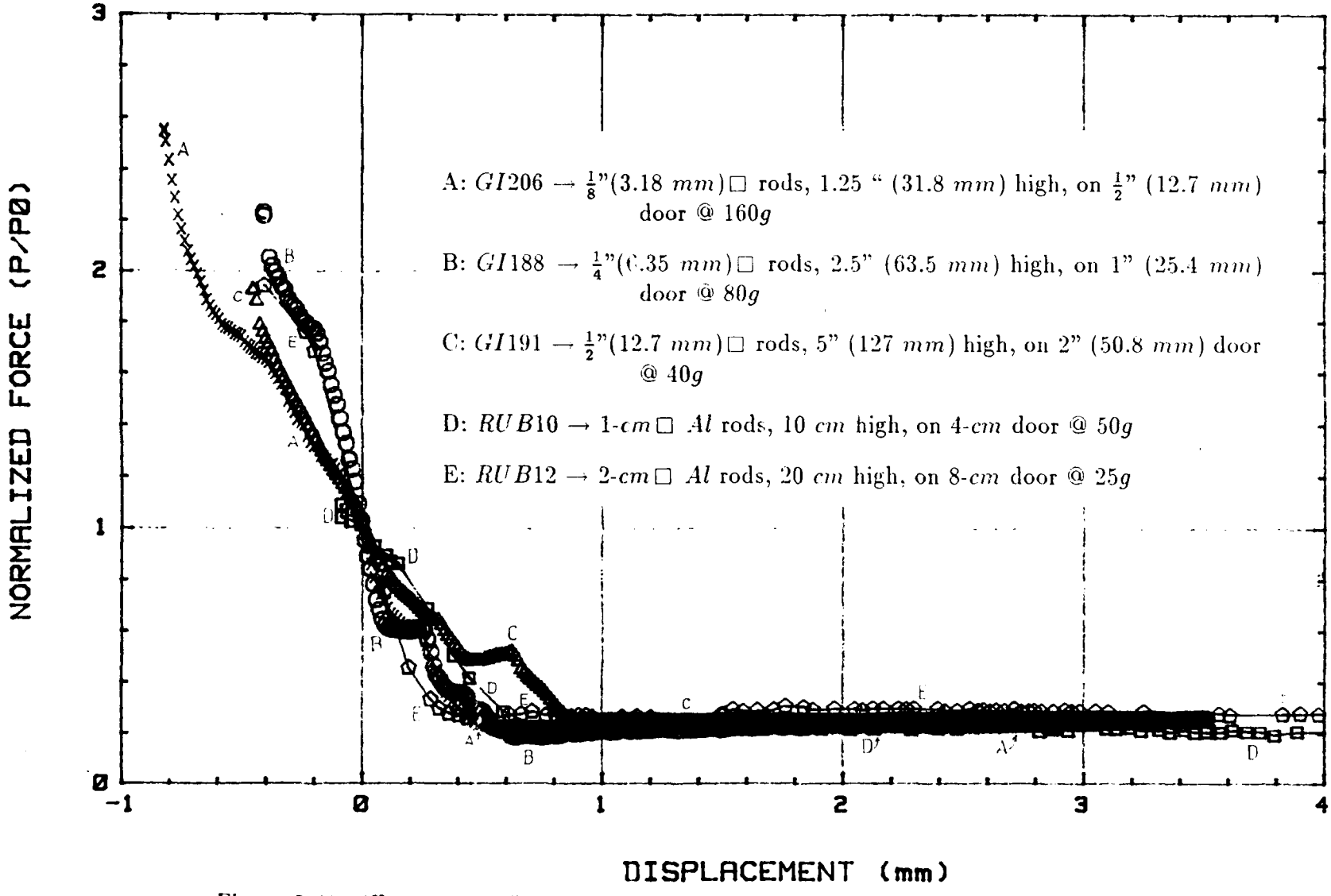

Figure 5-11: "Four-on-door" brick stack tests: Normalized force vs. adjusted displacement

remains constant for a while until the load drops again to a minimum value. Barring any "hang-ups," the columns of rods that fit above the door simply follow the settlement of the trapdoor.

For a brick stack assembly, the transition from the initial force to the minimum value as the door moves downward is relatively smoother. A triangular pattern of rods is formed above the door at the end of each test.

The stiffer trapdoor relative to its adjacent base gives rise to greater initial measured forces (i.e., before door lowering) in the brick stack than in the direct stack. This is due to the interlocking arrangement of the rods in the former, as opposed to vertical (potential) sliding planes all the way to the surface in the latter.

The *modelling of models* exercise has demonstrated that geometrically similar setups obtain appropriately scaled forces on the trapdoor. These scaled forces, however, occur at about the same displacement, regardless of the model size. Thus, the displacement values do not conform to the centrifuge scaling rules for length dimensions.

As one increases the number of rods that can fit across the trapdoor width in a brick stack, the resulting load vs. displacement curve tends to become smoother, resembling the data from a test with granular media.

The effect of different lateral confinements is more pronounced in the direct stack than in the brick stack.

Varying, by a factor of two, the gravity level at which the trapdoor experiment is performed on the same jointed medium apparently does not affect the resulting normalized load vs. displacement plot.

Chapter 6

Theoretical Considerations

In this chapter, theoretical analyses of the yielding trapdoor underneath a geomaterial mass are presented. Previously developed analyses to predict the load redistribution caused by trapdoor lowering are considered, and comparisons are made between predictions using these methods and experimental results. Conclusions are then drawn as to the methods which will provide the best estimate of the load acting on the trapdoor or a similar structure.

6.1 Soil Arching

6.1.1 Engesser's Theory

One of the earliest theories on soil arching has been presented by Engesser (1882). He discusses his scheme in the context of tunneling applications and postulates that the "arch" takes the shape of a parabola whose tangent through the edges of the tunnel (or trapdoor) makes an angle ϕ with the horizontal, where ϕ is the internal friction angle of the soil. As the tunnel roof (or trapdoor) displaces with respect to the adjacent substratum, the material below this arch tends to separate from the rest of the soil, and, consequently, the preexisting vertical load at the top of the arch gets transferred to the sides. This load redistribution also brings about an increase in the lateral stress across the

bottom portion of the arch. The effective vertical load P acting on the trapdoor consists, then, of the weight of soil W below the arch and the contribution of the vertical stress σ_{vr} induced by the increased lateral stress σ_{hr} just above the tunnel roof (or trapdoor) - which in turn is influenced by the material overlying the arch. (See Figure 6-1.)

By letting the horizontal axis be the x-axis, and the vertical axis the y-axis, with the origin at the left end of the arch (as in Figure 6-2, the equation of a parabola can be expressed in the form:

$$y = a_p x^2 + b_p x + c_p \tag{6.1}$$

The constants a_p, b_p, and c_p can be evaluated from the boundary conditions:

$$\begin{aligned}
&\text{At } x = 0,\ y = 0 && \Rightarrow c_p = 0 \\
&\text{At } x = 0,\ y' = 2a_p x + b_p = \tan\theta && \Rightarrow b_p = \tan\theta \\
&\text{At } x = B,\ y' = -\tan\theta && \Rightarrow a_p = -\tfrac{\tan\theta}{B}
\end{aligned}$$

The angle θ corresponds to the inclination from the horizontal of the tangent line through the ends of the parabola spanning the width B of the trapdoor. Hence, the parabolic equation is

$$y = -\frac{\tan\theta}{B}x^2 + \tan\theta \cdot x \tag{6.2}$$

The weight W per unit length of trapdoor can be computed from the area under the curve multiplied by the specific weight of the soil. Thus,

$$\begin{aligned}
W &= \gamma \int_0^B (-\frac{\tan\theta}{B}x^2 + \tan\theta \cdot x)dx \\
&= \gamma(-\frac{\tan\theta}{3B}x^3 + \frac{\tan\theta}{2}x^2)\,|_0^B \\
W &= \frac{\gamma B^2 \tan\theta}{6}
\end{aligned} \tag{6.3}$$

Engesser has quantified the effect of the additional vertical stress (σ_{vr}) brought about by the transfer of soil pressure to the sides by considering an imaginary structural arch, of thickness dh, whose shape is defined by the same parabola as above, and uniformly

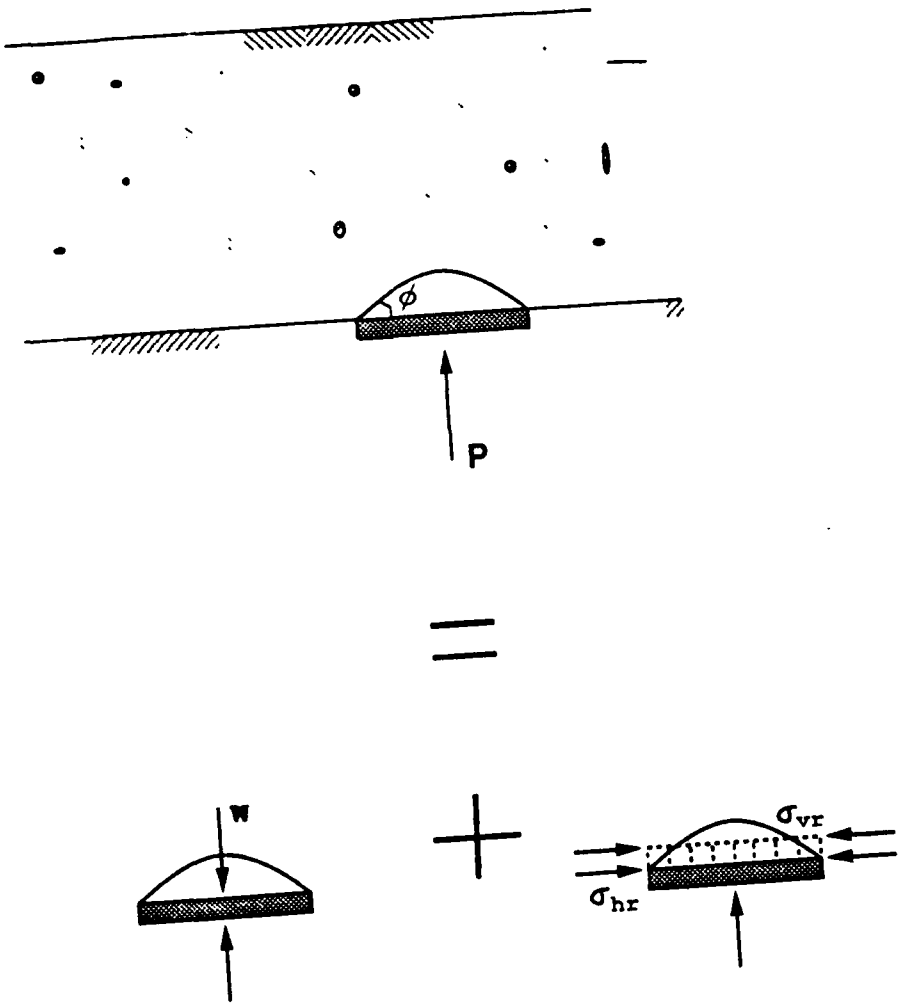

Figure 6-1: Engesser's (1882) approach

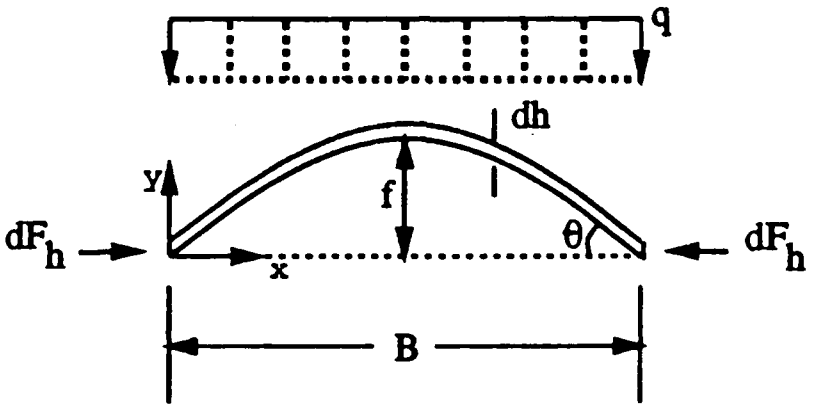

Figure 6-2: Free body diagram showing pertinent forces on imaginary structural arch in Engesser's (1882) analysis

loaded over its entire span (illustrated in Figure 6-2). The horizontal normal stress σ_{hr} at the bottom of the arch is then the lateral thrust reaction dF_h divided by dh. Assuming that σ_{hr} is constant across the bottom of the arch and that the soil is in a Rankine state, the vertical normal stress σ_{vr} is given by

$$\sigma_{vr} = K_a \sigma_{hr} \tag{6.4}$$

where $K_a = \frac{1-\sin\phi}{1+\sin\phi}$ is the conventional Rankine earth pressure coefficient for the active case[1].

The underlying assumption is that the lateral stresses at the ends of the arch are the same in the imaginary structure and in the actual case. The stress corresponding to the unit weight of the arch is $\gamma \cdot dh$. One would like to express σ_{vr} in terms of a compensatory unit weight γ^* such that the resulting uniform load on the arch is $q = dh \cdot (\gamma - \gamma^*)$. σ_{vr} is proportional to the overburden depth H and, thus, $\gamma^* H = \sigma_{vr}$. The net uniform loading q can then be expressed as

$$q = dh(\gamma - \frac{\sigma_{vr}}{H}) \tag{6.5}$$

For a parabolic arch of span B forming an angle θ with the horizontal at the ends, the lateral thrust dF_h due to the uniform load q can be shown to be (see, e.g., Leontovich, 1959)

$$dF_h = \frac{qB^2}{8f} = \frac{qB}{2\tan\theta} \tag{6.6}$$

where f is the rise of the arch. [From Equation (6.2), the height to the vertex of the parabola (i.e., at $x = \frac{B}{2}$) is $f = \frac{B\tan\theta}{4}$.]

The lateral stress σ_{hr} is, thus,

$$\sigma_{hr} = \frac{dF_h}{dh} = \frac{B}{2\tan\theta}(\gamma - \frac{\sigma_{vr}}{H}) \tag{6.7}$$

[1] In common terminology, this is actually a passive Rankine case, since $\sigma_h > \sigma_v$, and $\sigma_h = K_p \sigma_v$, where $K_p = 1/K_a$. The settling trapdoor situation, however, can be imagined to be a retaining wall moving away from the soil – the classic Rankine active condition – rotated by 90°.

Substituting Equation (6.7) in Equation (6.4) and simplifying, one arrives at

$$\sigma_{vr} = \frac{HB\gamma K_a}{2H\tan\theta + BK_a} \tag{6.8}$$

Engesser notes that for minimum σ_{vr}, $\theta = \phi$. The effective load P acting on the tunnel or trapdoor is the sum of the force from this vertical stress σ_{vr} and the weight W of the volume of soil underneath the assumed structural arch [Equation (6.3)]. Hence,

$$P = B^2\gamma[\frac{HK_a}{2H\tan\phi + BK_a} + \frac{\tan\phi}{6}] \tag{6.9}$$

This equation, as observed in Engesser's (1882) experiments (see Chapter 2), is valid for cases where $H/B > 1.5$.

Terzaghi(1943) makes little mention of Engesser's work and has apparently found this "structural arch" theory unattractive. Consequently, it has not been put into wide practice.

6.1.2 Silo Pressure Approach

Most theories on soil arching have stemmed from a consideration of the granular material inside a silo. The most commonly used formula for determining the force exerted at the base of a silo containing granular mass has been developed by Janssen (1895). Figure 6-3 displays the free body diagram on which this formula is based. It consists of a silo with diameter B and filled with granular material to a height H, and the objective is to derive an expression for the vertical force P at the base of the silo.

Consider the forces acting on a horizontal differential element of height dh, diameter B, and at depth h (Figure 6-2). Vertical forces on the element are the downward directed force at the top (F), the upward force at the bottom ($F + dF$), and the element's self-weight ($W = \gamma\pi B^2 dh/4$). The lateral stress [$\sigma = 4KF/(\pi B^2)$, where K is the coefficient of lateral earth pressure] is symmetric about the centerline, producing no net force on the element. In addition, if the element is assumed to move downward with respect to the

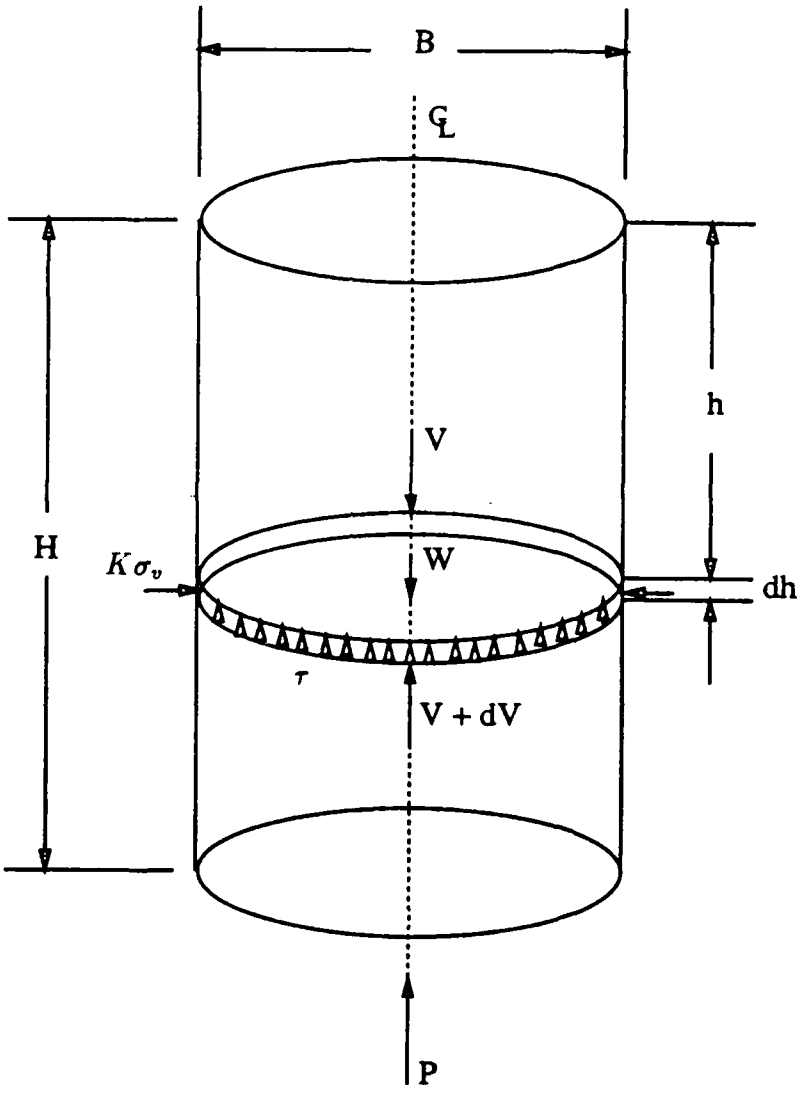

Figure 6-3: Free body diagram for silo theory

rigid walls of the silo, shear stresses [$\tau = 4KF\tan\phi/(\pi B^2)$, where $\tan\phi$ is the coefficient of friction between the granular material and the silo's walls) are mobilized. These shear stresses contribute an upward acting vertical force [$4KF\tan\phi dh/(\pi B^2)$] on the element. For vertical equilibrium, therefore:

$$F + dF + \frac{4KF\tan\phi dh}{\pi B^2} = F + \frac{\gamma\pi B^2 dh}{4} \tag{6.10}$$

This leads to a linear differential equation, the solution of which is:

$$F = \frac{\gamma\pi B^3}{16K\tan\phi}(1 - e^{-4K\tan\phi(h/B)}) \tag{6.11}$$

The value for the force P at the base is obtained by substituting H for h in this expression.

There are two assumptions inherent in this derivation. First, the coefficient of lateral stress (K) has the same value at all depths, and, second, the granular medium settles relative to the side walls sufficiently to develop shear stresses over the full depth of the silo.

For plane strain conditions, Marston and Anderson (1913) have followed an approach similar to Janssen's in determining the vertical loads on underground conduits. [See, e.g., Spangler and Handy (1982)]. The free body diagram considered is shown in Figure 6-4. In this figure, μ' is the coefficient of friction between the fill material and the sides of the ditch which may be equal to or less than $\tan\phi$. Equilibrium of vertical forces yields

$$V + dV + 2K\mu'\frac{V}{B_d}dh = V + \gamma B_d dh \tag{6.12}$$

The solution of the resulting linear differential equation is

$$V = \gamma B_d^2 \frac{1 - e^{-2K\mu'(h/B_d)}}{2K\mu'} \tag{6.13}$$

Note the close resemblance of Equation (6.13) to Equation (6.11). The vertical force P at the top of the conduit is obtained by substituting the overburden depth H for h. For

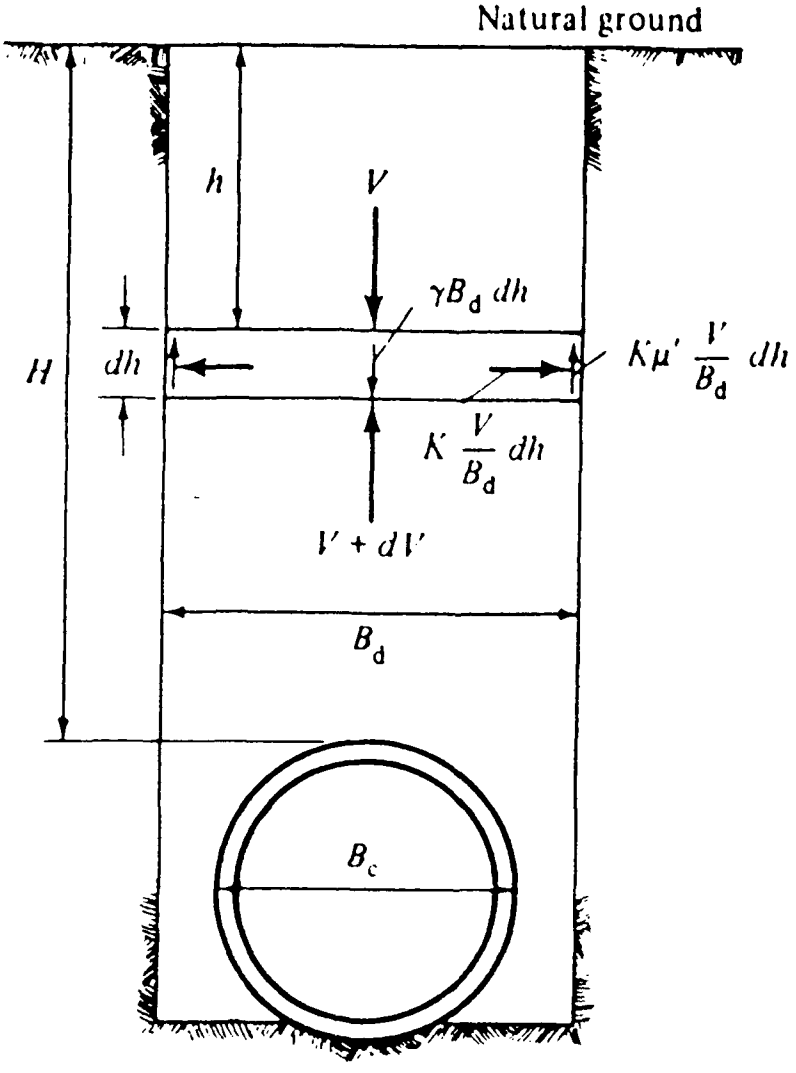

Figure 6-4: Marston's free body diagram for ditch conduit (from Spangler and Handy, 1982)

the trapdoor situation, the value of B_d is equal to B_t(the width of the trapdoor) and $\mu' = \tan\phi$.

In the original formulation, Marston prescribes K to be the Rankine ratio for the active case, i.e., $K = K_a = \frac{1-\sin\phi}{1+\sin\phi}$. Several others [Krynine (1945), Ladanyi and Hoyaux (1969), and Handy (1985)] have noted, however, that since K_a was derived from the assumption that the horizontal and vertical stresses are principal stresses, using K_a is valid only when there is no friction between the fill material and the sides of the ditch ($\mu' = 0$). If the vertical sides of the ditch are where the friction of the soil is mobilized, then an alternative value of K can be determined from the Mohr circle of Figure 6-5. In this diagram, the distance from the origin of the τ-σ space to the center of the Mohr circle is

$$OC = \frac{1}{2}(\sigma_h + \sigma_v)$$

If the stresses at the vertical sides of the ditch lie tangent to the Mohr-Coulomb envelope, the radius of the Mohr circle is

$$R = OC \sin\phi$$

Since the radius R is also equal to $\frac{(\sigma_v - \sigma_h)}{2\sin\phi}$, then

$$\frac{(\sigma_v - \sigma_h)}{2\sin\phi} = \frac{1}{2}(\sigma_h + \sigma_v)\sin\phi$$

which simplifies to

$$\sigma_h = K_K \sigma_v \tag{6.14}$$

where

$$K_K = \frac{1 - \sin^2\phi}{1 + \sin^2\phi} = \frac{\cos^2\phi}{1 + \sin^2\phi} \tag{6.15}$$

6.1.3 Bierbaumer's Scheme

The load on tunnel roofs (and, hence, on the trapdoor) can also be estimated from simplified derivations by Bierbaumer (1913). Expressions have been obtained for both

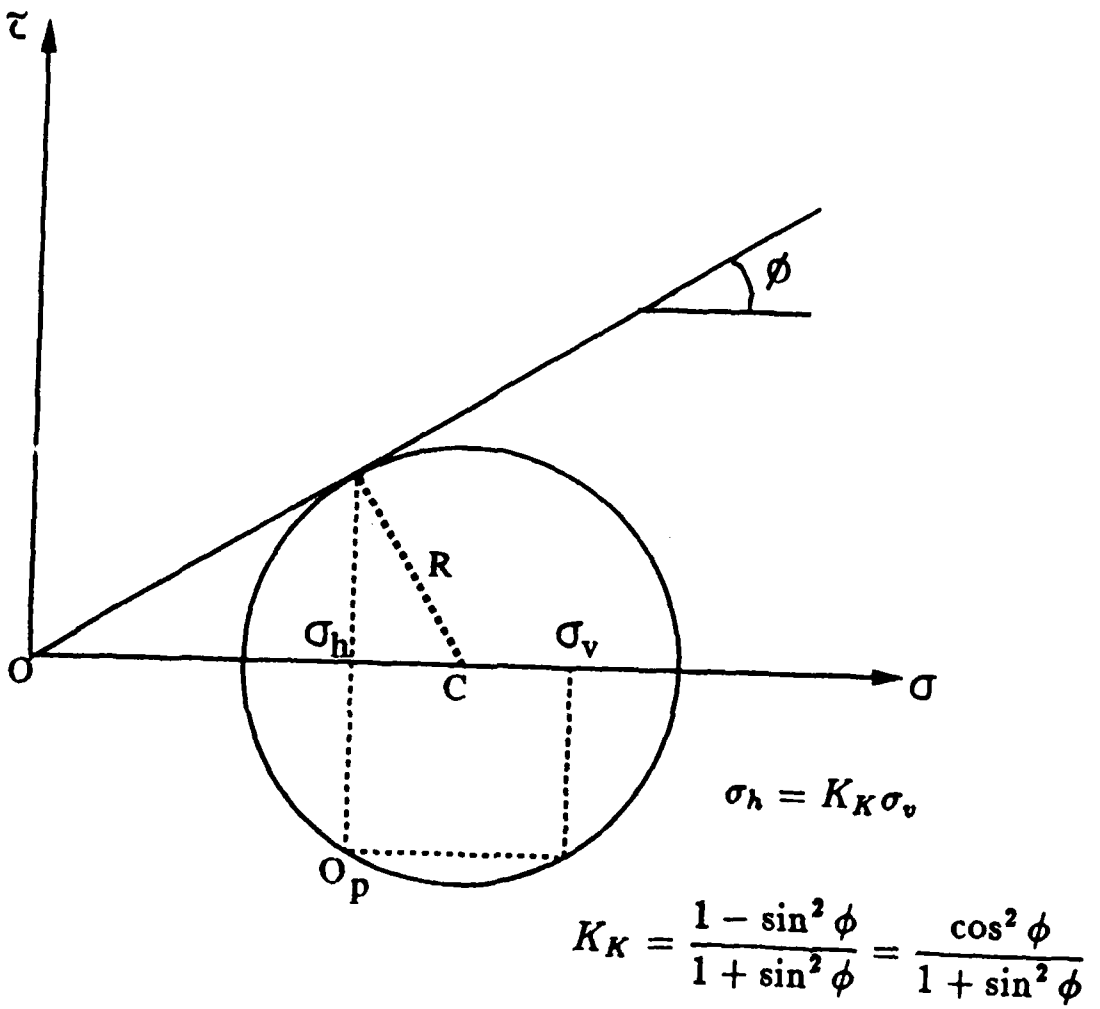

Figure 6-5: Mohr diagram for determining alternative value of K for use in Janssen-Marston formula

the minimum and maximum loads.

For the minimum load, Bierbaumer considers the equilibrium of a triangular prism whose sides make an angle ϕ with the vertical (Figure 6-6a). It can actually be shown that, if friction is fully mobilized along the sides, the forces on these sides have no vertical component. The load P_{min} on the tunnel roof, then, just balances the weight of the triangular prism:

$$P_{min} = \frac{\gamma B^2}{4 \tan \phi} \tag{6.16}$$

The expression for the maximum load is derived from the free body diagram of the mass bounded by two vertical failure surfaces, as depicted in Figure 6-6b. The vertical normal stress (σ_{nv}) is assumed to be linearly distributed. The horizontal normal stress (σ_{nh}) is related to σ_{nv} by:

$$\sigma_{nh} = K\sigma_{nv} = K\gamma H$$

and so σ_{nh} also varies linearly. If the material is in a Rankine active state,

$$K = K_a = \frac{1 - \sin \phi}{1 + \sin \phi}$$

The resultant horizontal force H_s acting on the sides is then

$$H_s = \frac{1}{2} K_a \gamma H^2$$

The weight of the failure mass is counteracted by the friction mobilized at the sides

$$f_s = H_s \tan \phi = \frac{1}{2} K \gamma H^2 \tan \phi$$

resulting in the net load on the trapdoor per unit length:

$$P_{max} = \gamma H (B - K_a H \tan \phi) \tag{6.17}$$

Note, again, the inconsistency of the assumption of a Rankine condition with a fully

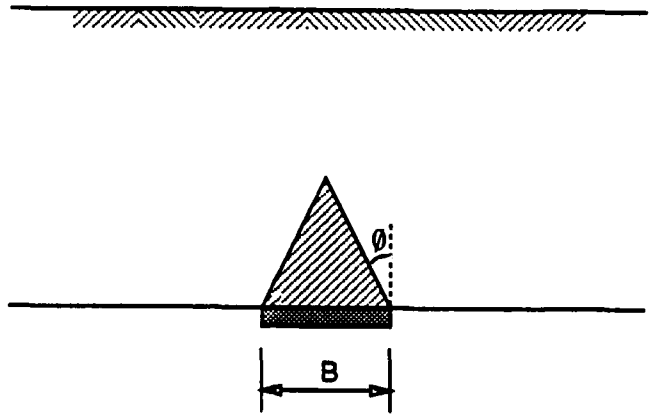

(a) Minimum load

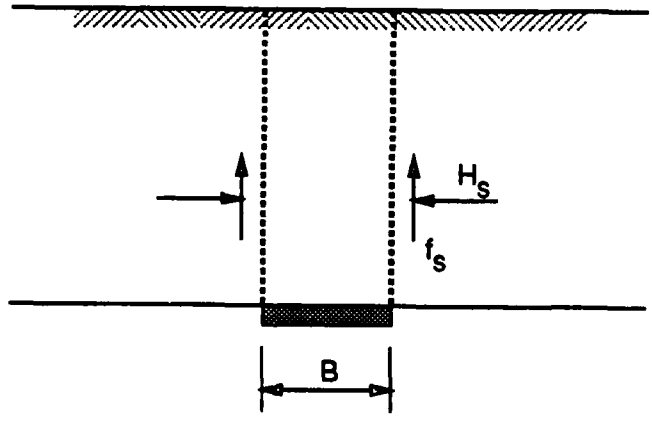

(b) Ultimate load

Figure 6-6: Free body diagrams used in Bierbaumer's (1913) scheme

mobilized friction at the sides. Alternatively, a value of K equal to K_K [Equation (6.15)] can be plugged in.

6.1.4 Terzaghi's Theory

A theoretical approach to the arching problem, following the same line of reasoning as in the silo pressure approach, has been put forward by Terzaghi (1943). This analysis is based on plane strain behavior within the soil. While actual sliding surfaces observed by Terzaghi in his experiments are believed to be slightly curved and extending a little bit beyond the width of the trapdoor (ac and bd in Figure 6-7), surfaces rising vertically from the trapdoor (ae and bf in Figure 6-7) are adopted in the analysis. As in the silo pressure approach, the vertical stress σ_V is assumed to be constant across the horizontal sections. The normal stress σ_h on the sliding planes equals $K\sigma_V$, where K is an empirical constant. In addition, the analysis considers a surcharge q to act at the surface of the soil, as well as cohesion c in the soil. Thus, the shearing stresses τ along the sliding surfaces satisfy the condition

$$\tau = c + \sigma \tan \phi \tag{6.18}$$

Referring to the free body diagram of Figure 6-7, the force equilibrium in the vertical direction for an infinitesimal slice of thickness dz is

$$\gamma B dz = B(\sigma_V + d\sigma_V) - B\sigma_V + 2c dz + 2K\sigma_V dz \tan \phi \tag{6.19}$$

or

$$\frac{d\sigma_V}{dz} = \gamma - \frac{2c}{B} - 2K\sigma_V \frac{\tan \phi}{B} \tag{6.20}$$

Solving this linear differential equation and imposing the boundary condition that

$$\sigma_V = q$$

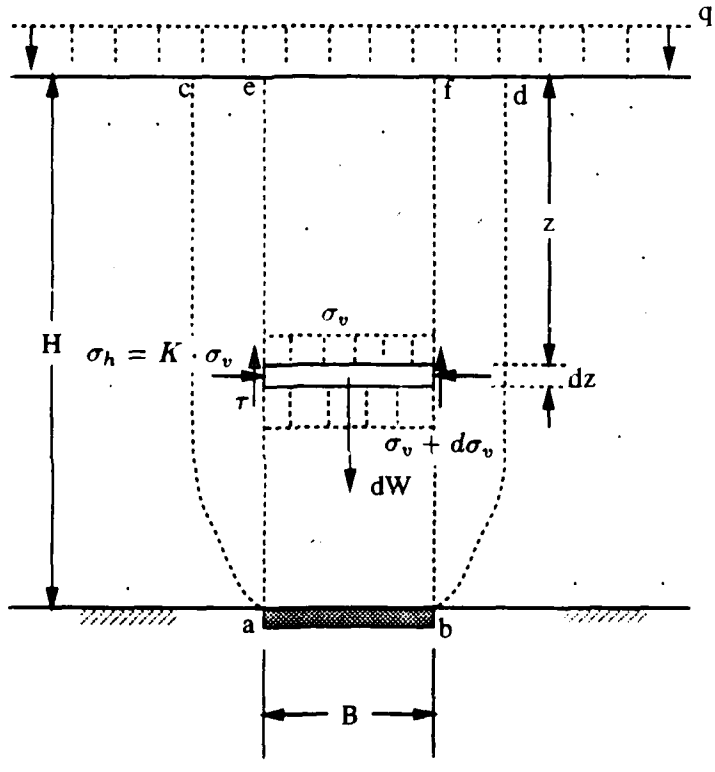

Figure 6-7: Actual and assumed sliding surfaces in Terzaghi's (1943) analysis

at $z = 0$, one obtains

$$\sigma_V = \frac{B(\gamma - 2c/B)}{2K \tan \phi}(1 - e^{-2K \tan \phi z/B}) + qe^{-2K \tan \phi z/B} \qquad (6.21)$$

The vertical force per unit length on the trapdoor is simply the product of the vertical stress σ_V at $z = H$ and the door width B. For the case of $c = 0$ and $q = 0$ simultaneously, the expression for the load P on the trapdoor becomes similar to Marston's formula [equation (6.13)], the only difference lying in the value of K assigned.

Since his experimental results indicate that soil stresses at a distance more than $2B$ above the trapdoor are unaffected by the door's displacement, Terzaghi assumes that shearing resistance is mobilized along the lower $2B$ of the sliding surface while the remaining overburden acts as a surcharge. This is equivalent to a situation of a soil of depth $2B$ above the trapdoor with a surcharge equal to $q + \gamma(H - 2B)$. The vertical load P per unit length of trapdoor is then

$$P = \frac{B^2(\gamma - 2c/B)}{2K \tan \phi}(1 - e^{-4K \tan \phi}) + B[q + \gamma(H - 2B)]e^{-4K \tan \phi} \qquad (6.22)$$

Obviously, when $H < 2B$, equation (6.21) applies.

6.1.5 Elastic Theory Schemes

Another popular approach to analyze the stress redistribution resulting from arching has been to invoke solutions from the theory of elasticity. While such methods do predict the redistribution of stresses as the ground structure system deforms, they also contain the underlying questionable assumption that the soil behavior is elastic.

Finn (1963) presents closed form solutions for the change in vertical stress resulting from translation or rotation of a trapdoor. He explicitly restricts his analysis to problems where displacements of the soil are very small and entirely elastic. A plane strain condition is assumed with the soil treated as a semi-infinite, linearly elastic medium overlying a trapdoor within a rigid horizontal boundary. For simplicity, the soil is considered to

have no self-weight. A typical distribution of the change in vertical stress across the base for a settling door is shown in Figure 6-8. The elasticity solution yields infinite tensile stresses near the edges of the trapdoor and infinite compressive stresses on the base next to the door.

Chelapati (1964) has extended Finn's work to account for material self-weight and a finite depth of cover. He superimposes stresses caused by the yielding trapdoor onto those due to material self-weight plus any surcharges. The problem of infinite stresses at the trapdoor edges still exists. Since granular soil cannot sustain tension, the stress on the door is assumed to be zero wherever tensile stresses tend to occur (see Figure 6-9). Compressive stresses on the base adjacent to the door are then reduced so as to produce no net change in the total vertical force on the lower horizontal boundary (i.e., door and base). The results are presented graphically, as in Figure 6-10, in terms of H, H/B, d (trapdoor deflection), p ($= q + \gamma H$, where q is surcharge pressure at the surface), E (modulus of elasticity of the soil), and μ (Poisson's ratio). The percent arching in Figure 6-10 refers to the percent reduction from the preexisting geostatic load p as a result of a trapdoor displacement d. One observes that as the ratio H/B increases, it takes less door movement (or greater $\frac{1}{d}$ value) to attain a certain percentage reduction from the same initial soil pressure. It has been suggested that plots similar to Figure 6-10 can be adopted for estimating the level of arching for specific values of displacement in a trapdoor-like setup if the pertinent soil properties are known. From his parametric studies, Chelapati concludes that for practical purposes the effect of the Poisson's ratio μ can be neglected over a wide range of parameters.

Bjerrum et al. (1972) believe that Chelapati's elastic solution could further be extended to give approximate values for the change in vertical stress ($\Delta\sigma_v$) at the center of a flexible section located within an otherwise rigid horizontal boundary (Figure 6-11). They propose the expression:

$$\Delta\sigma_v \approx 2\alpha\frac{\delta}{B}E \tag{6.23}$$

where α is a dimensionless coefficient whose value varies from about 0.3 to 1.0 depending

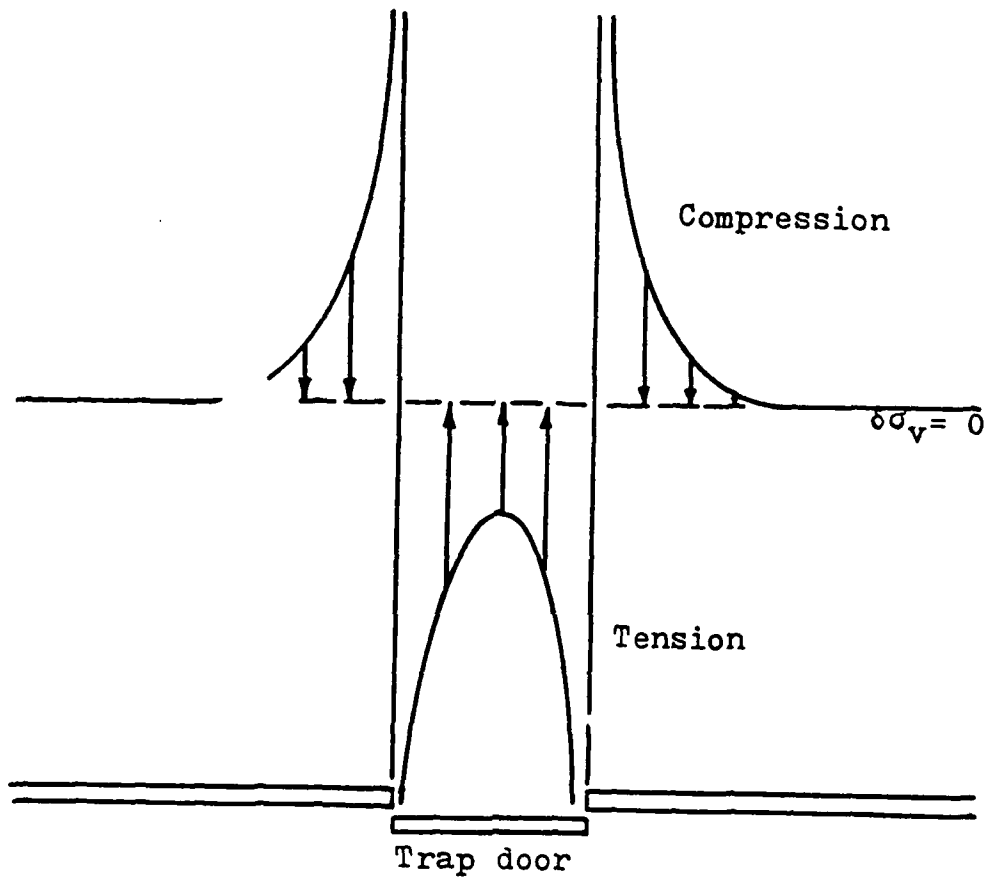

Figure 6-8: Typical distribution of change in vertical stress for active mode (from Finn, 1963)

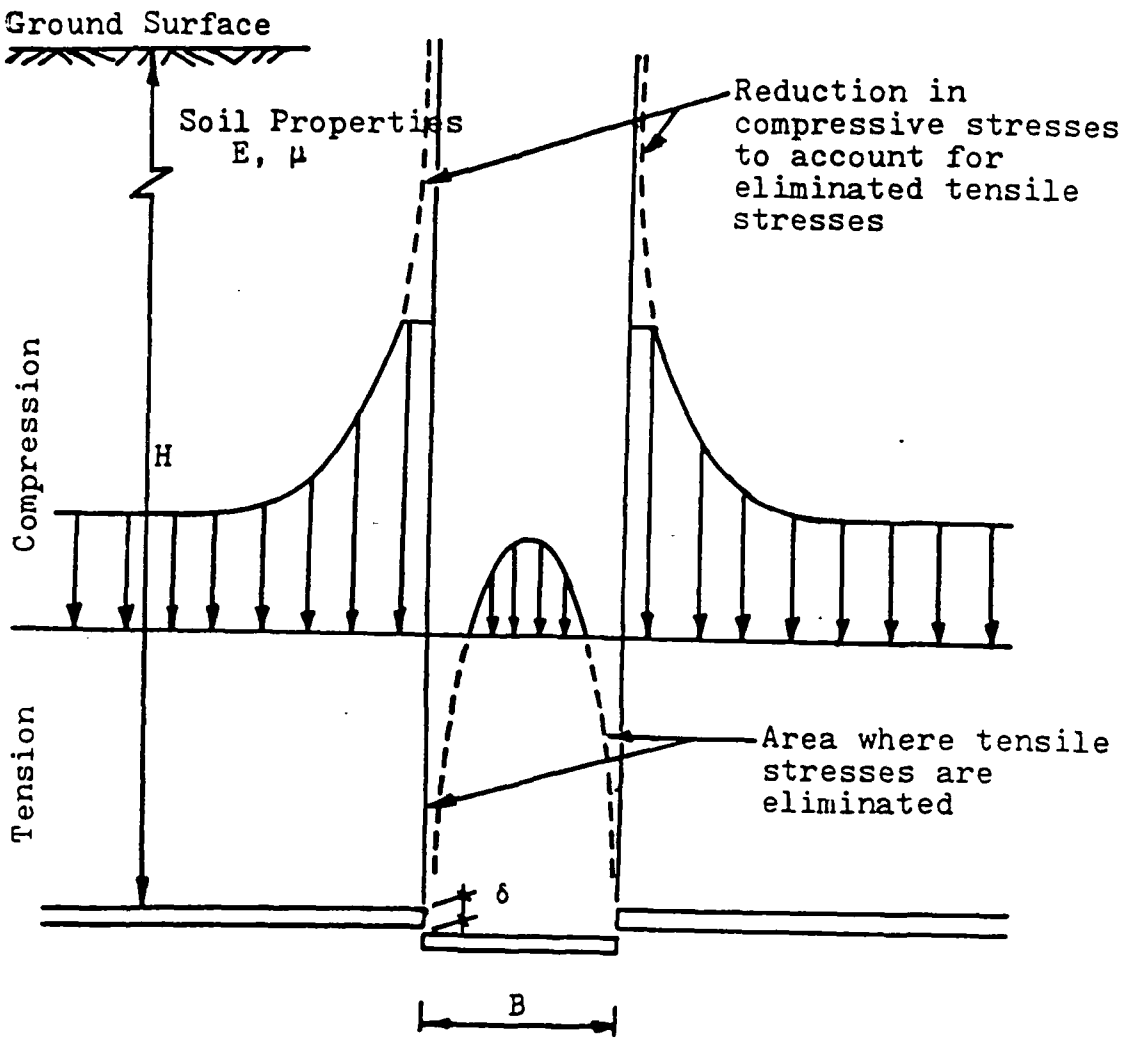

Figure 6-9: Chelapati's (1964) technique for eliminating tensile stresses in elastic solution for arching

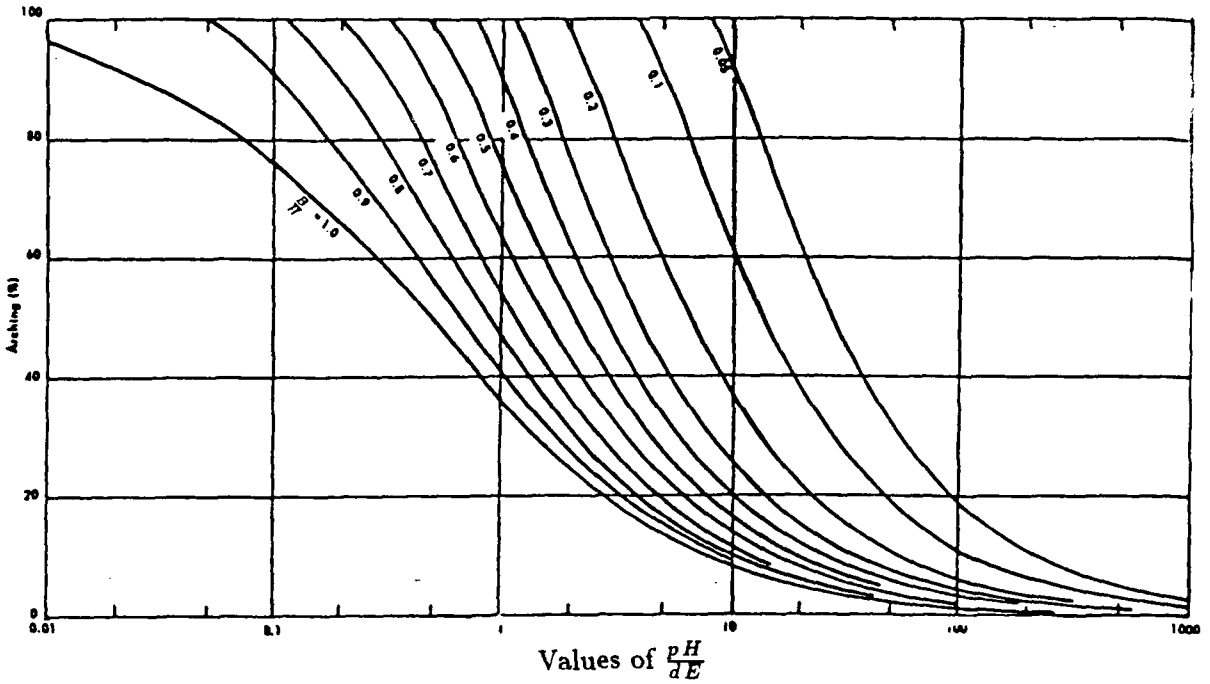

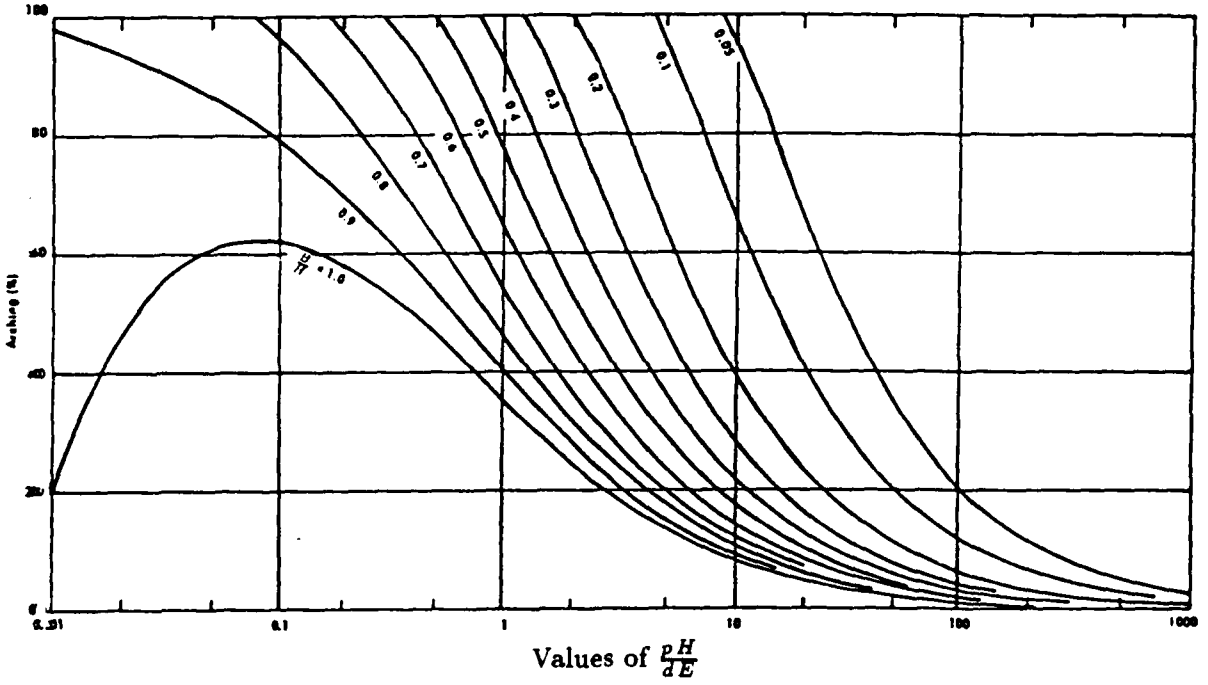

Figure 6-10: Typical results from Chelapati's (1964) technique

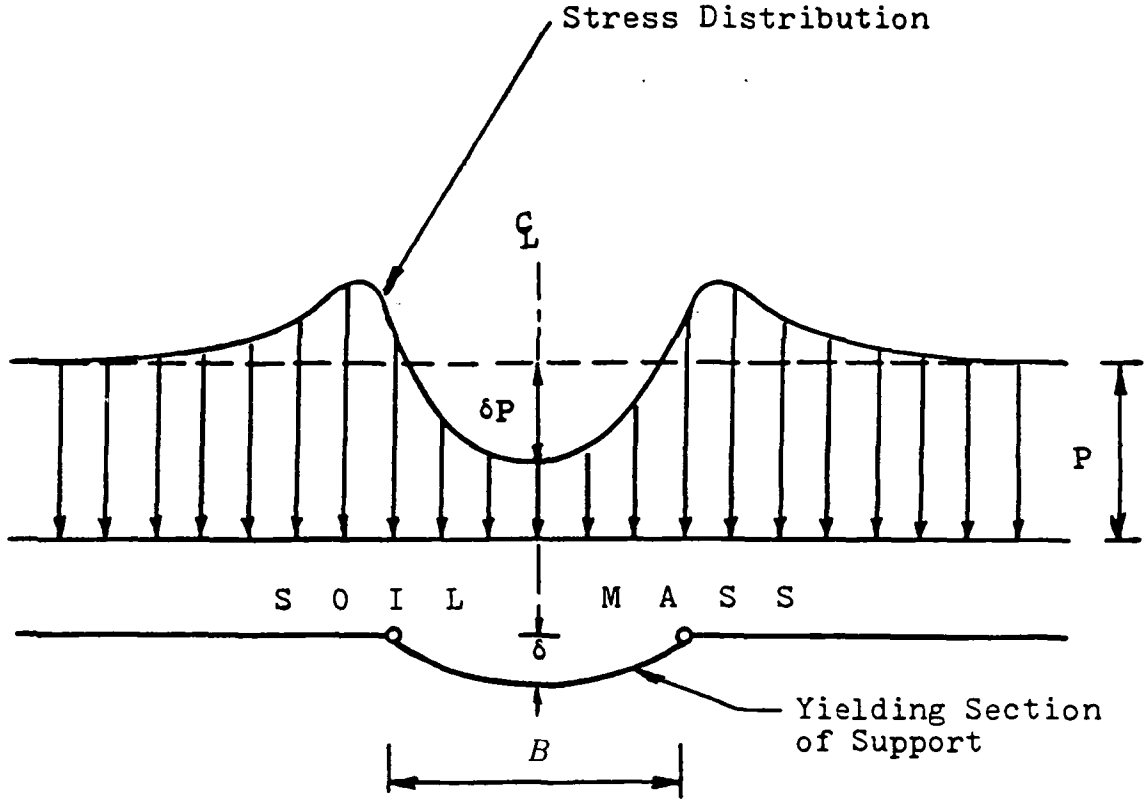

Figure 6-11: Stress change at center of yielding section (after Bjerrum et al., 1972)

upon the same parameters as in Chelapati's curves – H, H/B, d, p, E, and μ. Use of this expression is restricted to small values of $\Delta\sigma_v$, which makes the applicability of this elasticity approach questionable, in light of the sizable stress reduction observed in the laboratory and in the field.

The appropriateness of the elasticity-bases schemes for explaining the soil arching phenomenon has been challenged by Peck (1975), among others. Peck states, "The ground movements associated with construction, particularly in soft soils, are so large that the soil is likely to be stressed far beyond the limits of elasticity."

6.1.6 Evans's Plasticity-based Solution

To describe the non-recoverable deformations that occur in soils, Evans (1983) has adopted concepts from the theory of plasticity, based on earlier formulations [e.g., Davis (1968)]. A flow rule relates the incremental plastic shear strains ($\delta\epsilon_{shear}^{plastic}$) to the incremental plastic volumetric strains ($\delta\epsilon_{vol}^{plastic}$), as in Figure 6-12. The "plastic potential" is defined by the curve perpendicular to all plastic strain increment vectors. The angle of the plastic potential with respect to the horizontal is referred to as the "angle of dilation" (ν), so called because it represents the ability of the material to expand or contract. When $\nu > 0°$ the granular mass tends to expand (dilate), while for $\nu = 0°$ no volume change occurs. This angle also defines the direction of the plastic strain increment vector and is therefore a convenient variable in expressing the flow rule.

In order for the rate of plastic work to be non-negative, the dilation angle ν must be less than or equal to the friction angle ϕ [Atkinson and Potts (1975)]. For the case of $\nu = \phi$ the plastic potential (in the $\delta\epsilon_{shear}^{plastic}$-$\delta\epsilon_{vol}^{plastic}$ plane) will be shaped identically to the failure envelope (in τ-σ space). Thus, the plastic strain increments are related by the same ratio ($\tan\phi$) as the stresses along the failure surface. This "associated flow rule" is commonly adopted in geotechnical plasticity applications because it tremendously simplifies the mathematics of the problem.

The Coulomb criterion defines two directions, located at $\pm(45 - \frac{\phi}{2})$ to the major

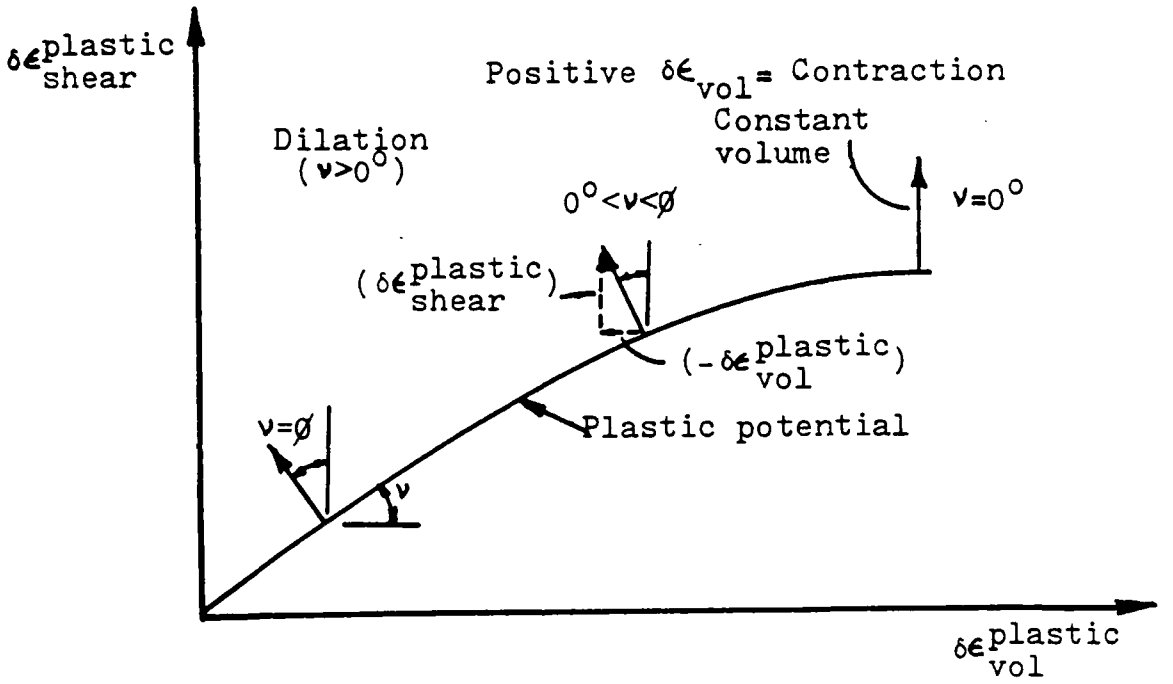

Figure 6-12: Plastic Flow Rule (from Evans, 1983)

principal stress at a point, along which

$$\tau = c + \sigma \tan \phi$$

is satisfied. These directions form within the stress field a loci of two families of curves, sometimes referred to as α and β lines and termed stress characteristics. The α and β lines always intersect at an angle of $90° \pm \phi$.

Analogously, one can determine velocity characteristics for a given problem from a consideration of the velocity (or strain rate) field. (The kinematic conditions of plastic failure in a material necessitate that a distribution of velocities be obtained.) Their orientations are defined by the plastic flow rule as they are directed at $\pm(45° - \frac{\nu}{2})$ to the major principal strain rate.

Incorporating the assumption that the major principal strain rate direction coincides with that of the major principal stress, one sees that for $\nu = \phi$ velocity and stress characteristics have identical orientations. At the other extreme, when $\nu = 0°$ velocity characteristics are orthogonal to each other and at 45° to the principal stress direction. Intermediate values of ν give intermediate locations for the characteristics.

The Coulomb failure criterion is satisfied along stress characteristics, but not necessarily along velocity characteristics. For a cohesionless medium, the normal stress (σ_{nc}) and shear stress (τ_c) along velocity characteristics can be shown with a Mohr diagram (Figure 6-13) to be related as:

$$\tau_c = \sigma_{nc} \frac{\cos \nu \sin \phi}{1 - \sin \nu \sin \phi} \tag{6.24}$$

For the associated flow rule ($\nu = \phi$) this reduces to the more common Mohr-Coulomb expression (with cohesion $c = 0$):

$$\tau_c = \sigma_{nc} \tan \phi \tag{6.25}$$

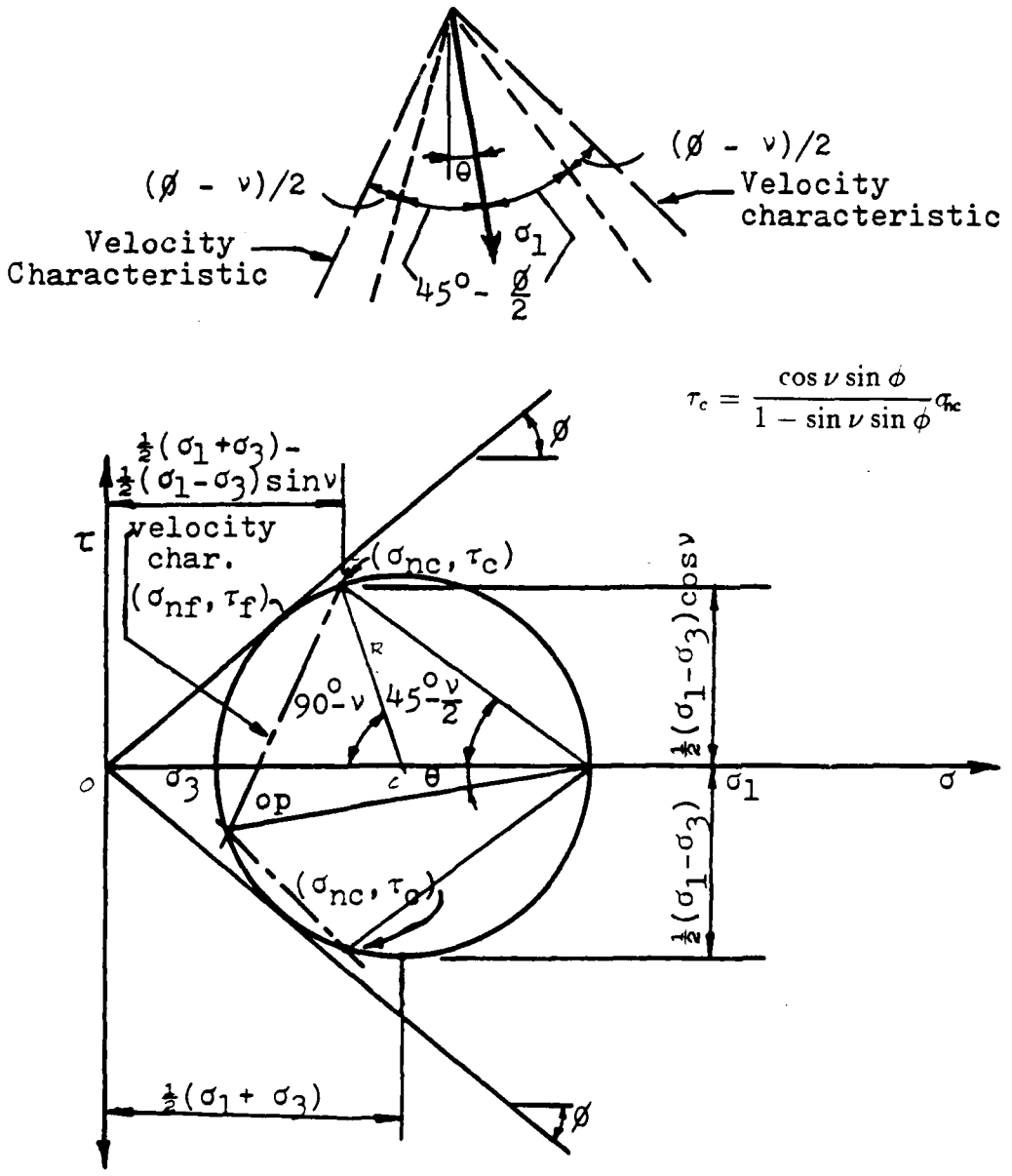

Figure 6-13: Mohr diagram for stresses along velocity characteristics (from Evans, 1983)

While a material is deforming it is common for discontinuities to develop within the velocity field, with an associated velocity jump across each discontinuity. Such a discontinuity, also called a "slip line," must be a velocity characteristic and the orientation of the change (jump) in velocity between the soil on either side of the discontinuity must be at the dilation angle (ν) to the plane of the discontinuity. [See, e.g., Davis (1968).] A settling trapdoor, for instance, creates a vertical jump in velocity at the trapdoor's edges, giving rise to the velocity discontinuity as shown in Figure 6-14. For compatibility with the derived characteristic field, this discontinuity should be a straight line. The symmetry of the problem dictates that a triangular prism develops above the door with the sides inclined at an angle ν with the vertical.

In his trapdoor experiments, Evans (1983) has observed that, in the active mode, a triangular shaped zone does form above the door. He then draws a free body diagram of a triangular section (Figure 6-15a) with the sloping sides forming an angle ν with the vertical. A state of "maximum arching" is said to occur, i.e., the load on the trapdoor is a minimum, when the dilation angle ν approaches the friction angle ϕ. [Note that this is exactly the same shape that Bierbaumer (1913) assumed.] For this configuration, the resultant of the forces due to the normal and shear stresses at each of the sides is directed along the horizontal and, thus, does not contribute to the vertical load. The minimum force P_{min} (per unit length) on the trapdoor is then due to the weight of the material comprising the prism:

$$F = \begin{cases} \gamma HB(1 - \frac{H}{B}\tan\phi) & \text{for } \frac{H}{B} < \frac{1}{2\tan\phi} \\ \frac{\gamma B^2}{4\tan\phi} & \text{for } \frac{H}{B} \geq \frac{1}{2\tan\phi} \end{cases} \tag{6.26}$$

The limiting values of the $\frac{H}{B}$ ratios above take into consideration the possibility that a trapezoidal prism is formed when the depth of the soil is not sufficient to contain a triangular one.

Eventually, with continued door displacement, the limiting case of vertical velocity discontinuities ($\nu = 0°$), originating from the trapdoor edges, is attained. The pertinent

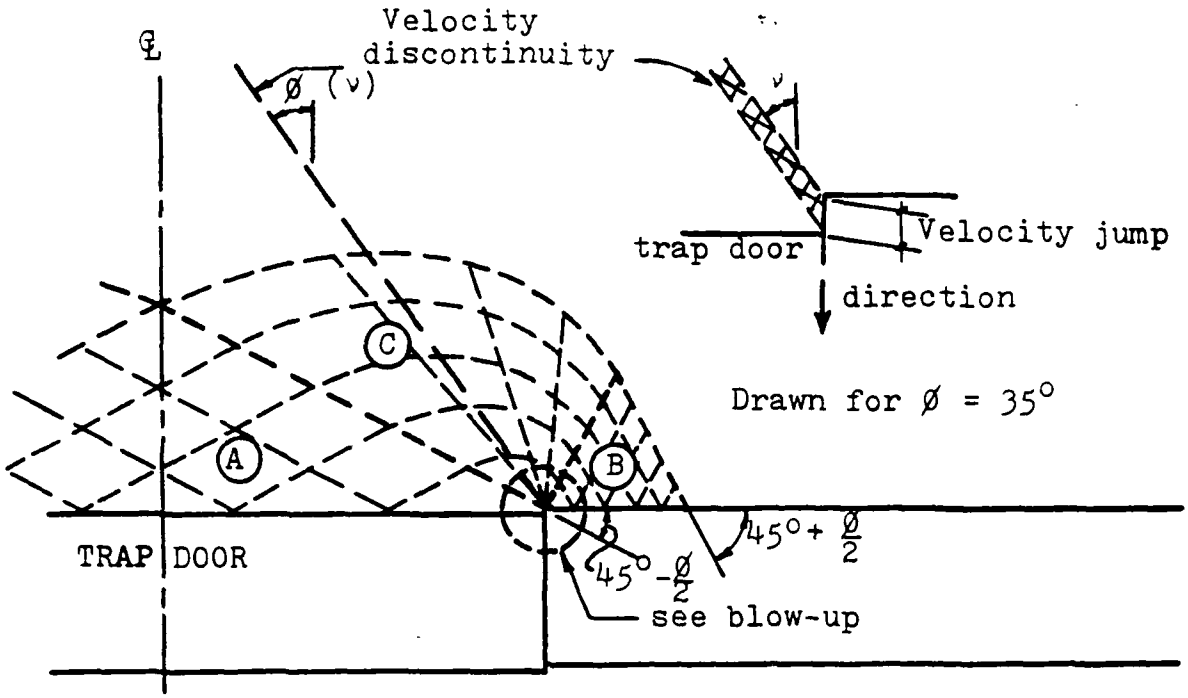

(a) Stress characteristics for active arching

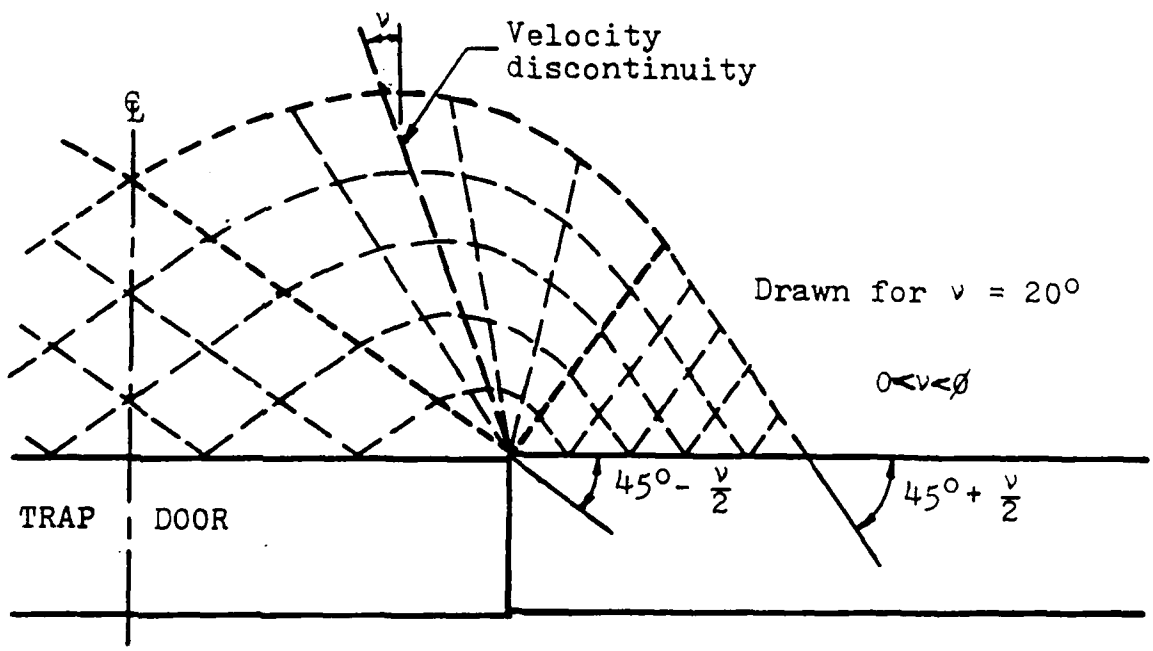

(b) Velocity characteristics for active arching

Figure 6-14: Characteristics for active arching (from Evans, 1983)

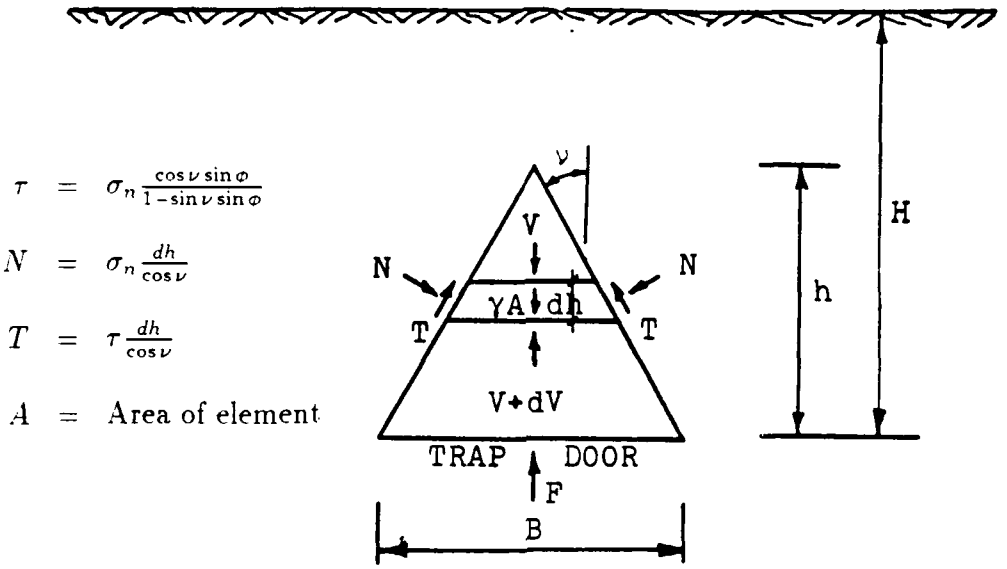

(a) Free body diagram for $\nu > 0°$

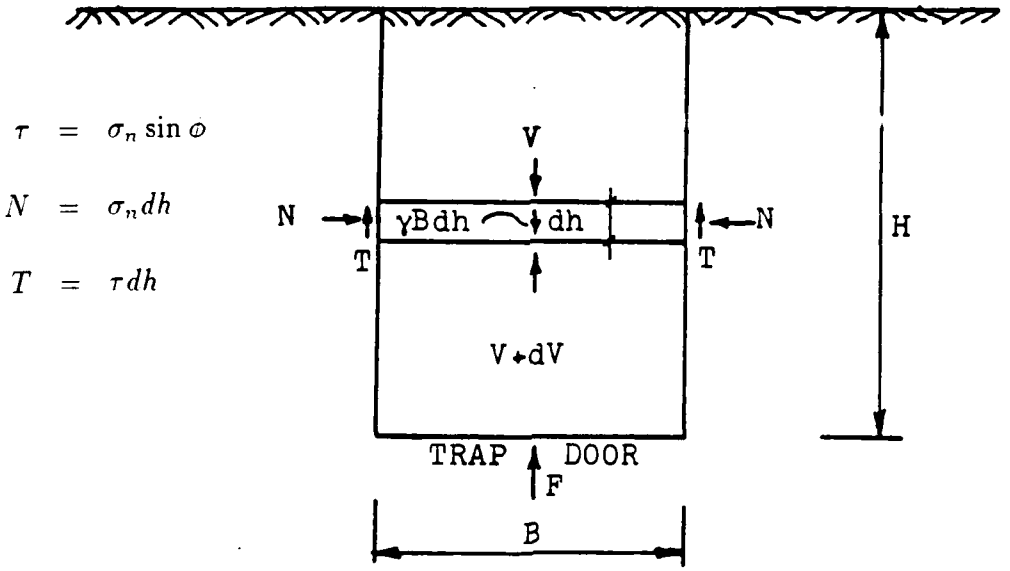

(b) Free body diagram for $\nu = 0°$

Figure 6-15: Free body diagrams for active arching (from Evans, 1983)

free body diagram, presented in Figure 6-15, is essentially the same as that in the silo theory, with the exception that shear and normal stresses on the boundary are related by:

$$\tau = \sigma_n \frac{\cos\nu \sin\phi}{1 - \sin\nu \sin\phi} = \sigma_n \sin\phi \tag{6.27}$$

Whether the shear resistance is mobilized over the entire height of the prism for large H is deemed questionable, so an approach similar to Terzaghi's is taken in that the soil at distances greater than $2B$ above the door is treated as surcharge. The resulting expressions are:

$$P_{ult} = \begin{cases} \frac{\gamma B^2(1-e^{-2K\frac{H}{B}\sin\phi})}{2K\sin\phi} & \text{for } \frac{H}{B} \leq 2 \\ \gamma B^2\left[\frac{(1-e^{-4K\sin\phi})}{2K\sin\phi} + (\frac{H}{B} - 2)e^{-4K\sin\phi}\right] & \text{for } \frac{H}{B} > 2 \end{cases} \tag{6.28}$$

For the transitional case of $0° < \nu < \phi$, a free body diagram with trapezoidally shaped differential elements can be constructed, but a solution is not readily apparent. Moreover, even if solution for the free body is possible, it is not clear what value for normal stress to use at the boundaries. It may, however, be concluded that values of the trapdoor force for $0° < \nu < \phi$ lie between the lower ($\nu = \phi$) and upper ($\nu = 0°$) limits.

A formulation corresponding to the passive mode has also been carried out. The free body diagrams considered are illustrated in Figure 6-16, and the subsequent derivation yields the following solutions:

- For "maximum arching" state (i.e., maximum load on door)

$$P_{max} = \gamma H B(1 + \frac{H}{B}\tan\phi) \tag{6.29}$$

- For ultimate state

$$P_{ult} = \begin{cases} \frac{\gamma B^2}{2K_a\sin\phi}(e^{2K_a\frac{H}{B}\sin\phi} - 1) & \text{for } \frac{H}{B} \leq 2 \\ \gamma B^2\left[\frac{1}{2K_a\sin\phi}(e^{4K_a\sin\phi} - 1) + (\frac{H}{B} - 2)e^{4K_a\sin\phi}\right] & \text{for } \frac{H}{B} > 2 \end{cases} \tag{6.30}$$

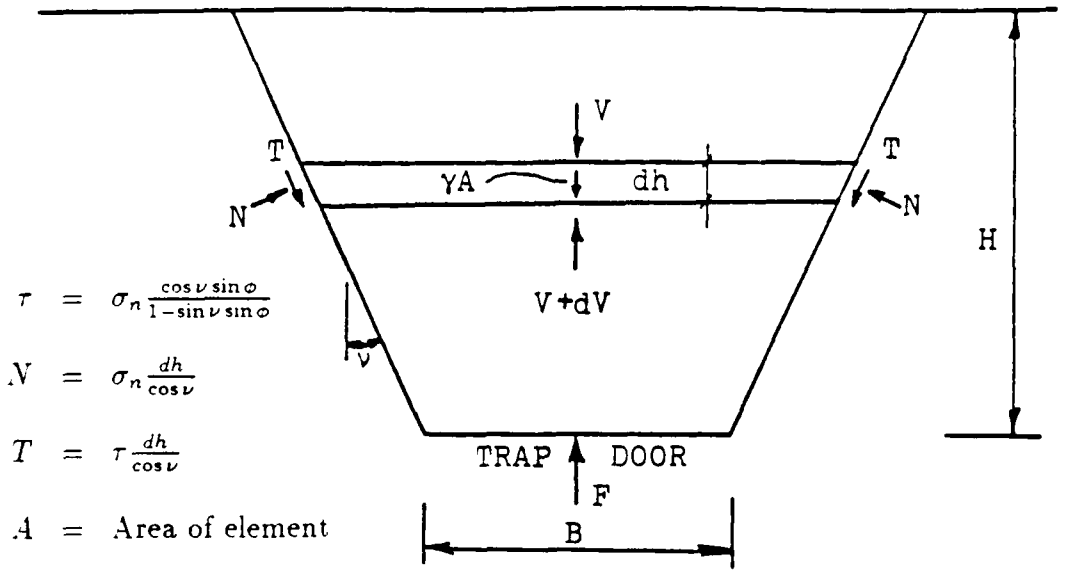

$\tau = \sigma_n \frac{\cos\nu \sin\phi}{1-\sin\nu \sin\phi}$

$N = \sigma_n \frac{dh}{\cos\nu}$

$T = \tau \frac{dh}{\cos\nu}$

A = Area of element

(a) Free body diagram for $\nu > 0°$

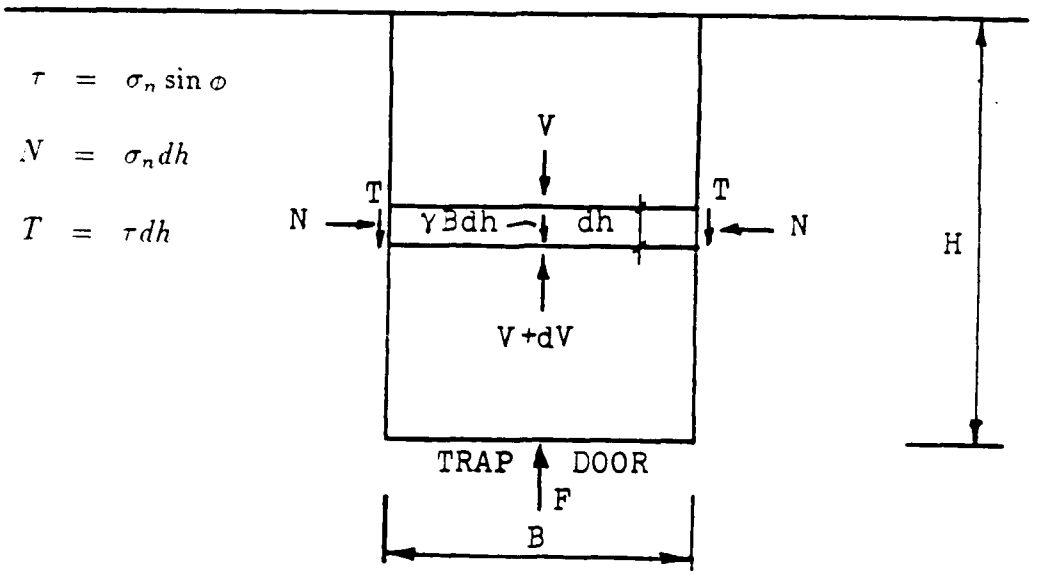

$\tau = \sigma_n \sin\phi$

$N = \sigma_n dh$

$T = \tau dh$

(b) Free body diagram for $\nu = 0°$

Figure 6-16: Free body diagrams for passive arching (from Evans, 1983)

where P is the force per unit length on the trapdoor and $K_a = \frac{1-\sin\phi}{1+\sin\phi}$ is the active earth pressure coefficient.

Evans (1983) has also tested his equations against his experimental results and has found reasonable agreement. He claims, therefore, that his theory adequately describes the arching phenomenon in granular soils.

6.1.7 Numerical Solutions

With the advent of sophisticated computing tools, numerical solutions undoubtedly surface as the most comprehensive methods available for the analysis of stress redistribution around buried structures. One distinct advantage of numerical techniques over analytical schemes lies in the analysis of situations involving complicated geometries and non-homogeneous material properites.

Getzler et al. (1970) have tried to solve the plane strain trapdoor problem with a finite difference method. Essentially, however, their formulation is the same elastic approach taken by Chelapati (1964). The soil is assumed to be linearly elastic and stresses associated with the settling of the trapdoor and the self-weight of the material are superimposed. From the numerical exercise, the principal compressive stress trajectories produced by the differential settling indicate clearly that an "arch" is formed in the overlying soil, abutting on both sides of the structure and transferring part of the load to those zones. These findings give credence to the theory which interprets the arching effect as a "structure-like" action of the overlying soil (see, e.g., Engesser, 1882, Whitman and Lusher, 1962), resulting in an arch in the planar case and in a dome in the spatial case.

To help explain the results obtained from his experiments, Stone (1988) has performed non-linear finite element analyses of the trapdoor tests. He reports that the choice of iteration scheme adopted to solve the non-linear stress-strain relations may considerably restrict the type of problem to which a particular finite element program can be applied. In general, though, the essential characteristics of the physical model tests have

been reproduced in the numerical analyses, which correctly predict an initial localization propagating from the edge of the trapdoor into the overlying soil. The strain distributions simulated numerically are seen to form an "arch" at small door displacements. What does not appear to be evident in the computer runs, however, is the discrete nature of the formation of the localizations which was observed in the physical model tests. Since the emphasis of Stone's experiments is on deformation patterns, no trapdoor load data have been presented.

Recently, Koutsabeloulis and Griffiths (1989) have carried out a finite element analysis of the trapdoor problem. They treat the soil as an elastic, perfectly plastic material. The Mohr-Coulomb failure criterion is used in conjuction with a non-associated flow rule. The domain is discretized with fifteen-node isoparametric triangular elements, as illustrated in Figure 6-17. They conduct a parametric study of both active and passive modes and propose expressions obtained from curve-fitting, to predict the load in situations similar to the trapdoor problem.

For the active mode, Koutsabeloulis and Griffiths (1989) present results as in Figure 6-18a for a soil with friction angle $\phi = 20°$, dilation angle $\psi = 0°$, and at-rest earth pressure coefficient $K_0 = 1$. The numerical analysis shows that the load tends to reach a finite value after it drops from the geostatic value. The minimum load ratio, i.e., the door load normalized with respect to the overburden stress, decreases as the depth of overburden H increases in proportion to the width D of the trapdoor – consistent with experimental observations. It has been suggested that the ultimate load ratio can be computed from the following expressions:

$$\frac{\sigma_v}{\gamma H} = \begin{cases} (R_{G_1})^{G_1 H/B \tan\phi} & \text{for } \frac{H}{B} \leq 2.5 \\ G_2 (R_{G_2})^{G_3 H/B \tan\phi} & \text{for } \frac{H}{B} > 2.5 \end{cases} \tag{6.31}$$

where R_{G_1}, R_{G_2}, G_1, G_2, and G_3 are dimensionless parameters that depend on the friction angle ϕ and are given in Figure 6-19.

A similar procedure has been implemented for the passive mode. Results for the soil

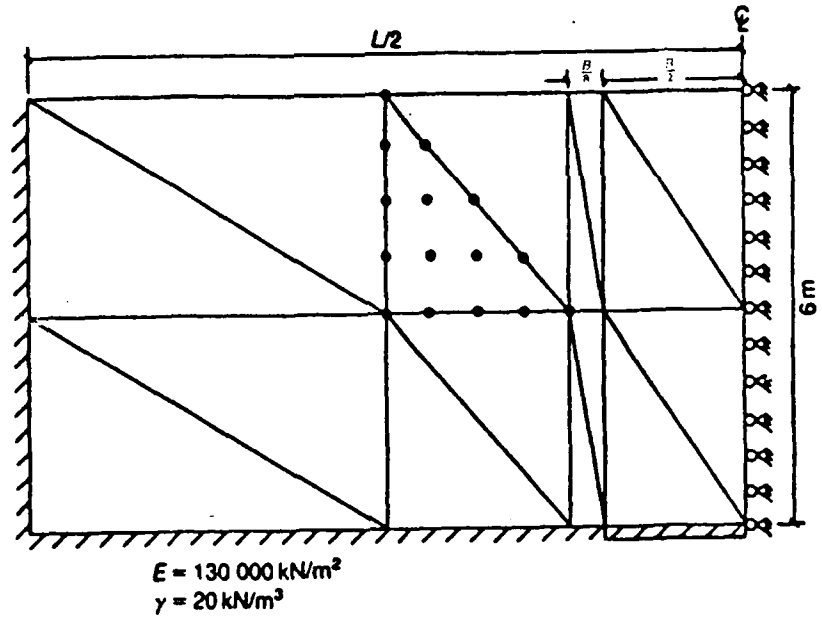

(a) $L/B = 5$

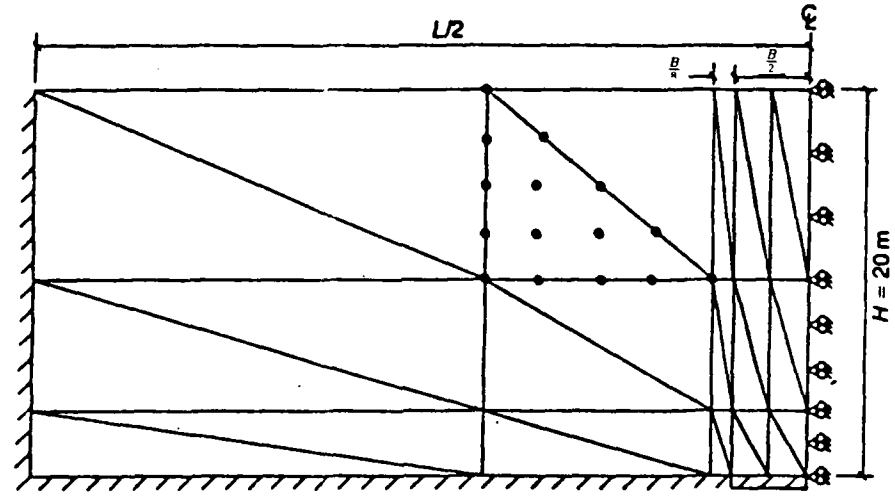

(b) $L/B = 10$

Figure 6-17: Finite element discretization of the trapdoor problem (from Koutsabeloulis and Griffiths, 1989)

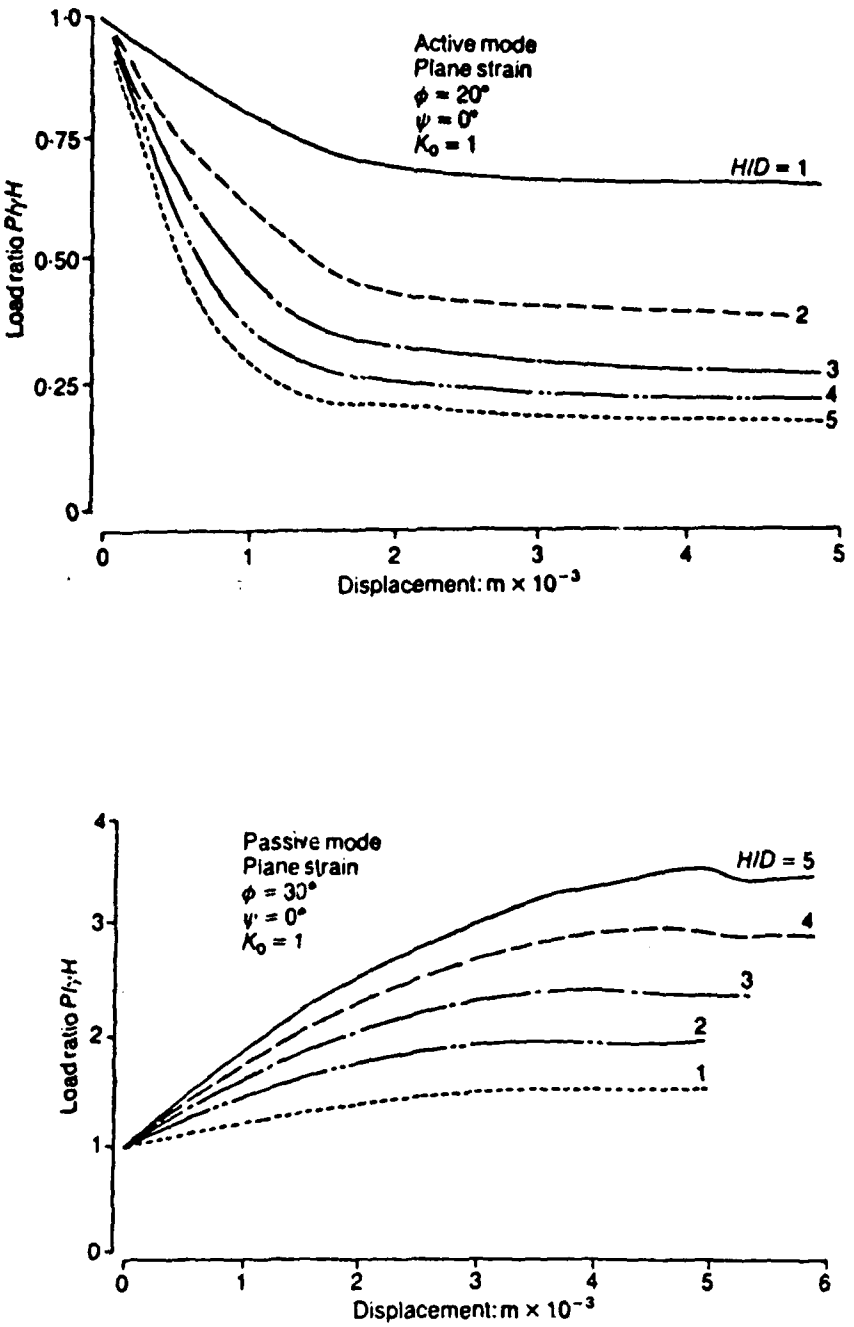

Figure 6-18: Results from numerical analyses: load ratio plotted against displacement (from Koutsabeloulis and Griffiths, 1989)

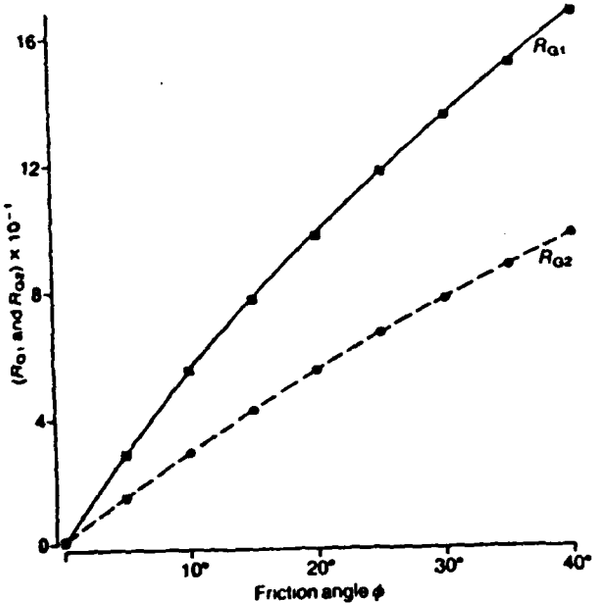

(a) Active mode, plane strain: Variation of R_{G_1} and R_{G_2} with friction angle ϕ

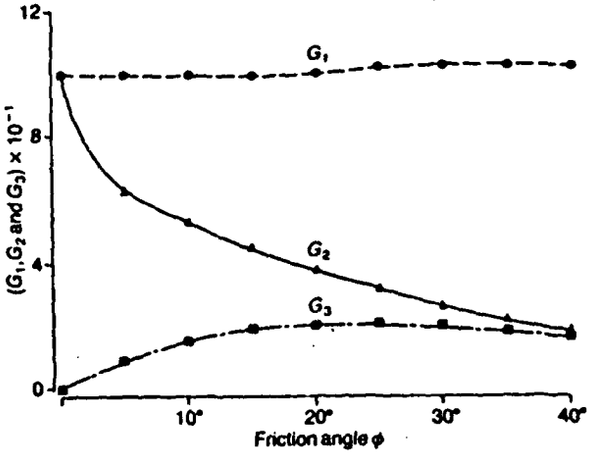

(b) Active mode, plane strain: Variation of G_1, G_2 and G_3 with friction angle ϕ

Figure 6-19: Parameters in Koutsabeloulis-Griffiths (1989) expressions for estimating loads due to arching

with $\phi = 30°$, $\psi = 0°$, and $K_0 = 1$ are provided in Figure 6-18b. The ultimate load ratio increases with increasing values of H/B, although the numerical analyses indicate that this ultimate load ratio is attained at much greater displacements compared to those observed in the various experiments. Koutsabeloulis and Griffiths (1989) has conducted a parametric study with numerical simulations of the passive mode. By fitting curves to their simulated data, they recommend the following equation for estimating the ultimate load ratio (passive case):

$$\frac{\sigma}{\gamma H} = H/B \sin(\phi + \psi) + 1 \tag{6.32}$$

where ψ is the dilation angle of the soil (Griffiths, 1986).

6.1.8 Comparative Analysis of the Various Theories

An effort to apply the different theories to the centrifuge experiments with sand and glass beads is carried out in this section. Apart from the solution methods themselves, a major difference in the various approaches lies in the value of K to use in the analysis. In Engesser's scheme, he has explicitly specified that $\sigma_v = K_a \sigma_h$, and so $K = \frac{\sigma_h}{\sigma_v} = 1/K_a = K_p$. The active lateral earth pressure coefficient K_a is commonly used in Janssen's formula, although several investigators [e.g., Ladanyi and Hoyaux (1969) and Handy (1985)] have suggested using $K = \frac{\cos^2 \phi}{1+\sin^2 \phi}$ based on the Mohr circle construction of Figure 6-5. Terzaghi treats K as an empirical constant and assigns a value of 1 to it for analysis purposes. Evans has actually measured the K value in some of his experiments; while he notes its variability depending on the vertical location as well as the level of trapdoor displacement, he picks out a value of 1.2 for K for application in his equations.

Using the respective values of K presented above, the resulting computations for the sand tests with varying H/B ratios are summarized in Table 6.1. The numbers in the table are the computed (P/P_0) values that the theories will predict. Recall that the sand friction angle is $\sim 39°$ and the results from the centrifuge trapdoor experiments for the minimum (which approximately is also the ultimate) (P/P_0) values are 0.36, 0.18, and 0.09 for $H/B = 1$, 2, and 4, respectively.

Table 6.1: Comparisons of different theories applied to the centrifuge tests with sand: Computed values of force on trapdoor normalized with respect to overburden (P/P_0)

H/B	Engesser	Jannsen		Terzaghi	Evans ($K = 1.2$)		K & G[a]
	$K = K_a$	$K = K_a$	$K = K_K$	$K = 1$	$(P/P_0)_{min}$[b]	$(P/P_0)_{ult}$	
1	0.258	0.836	0.719	0.495	0.309	0.516	1.463
2	0.133	0.708	0.538	0.297	0.154	0.315	2.163
4	0.068	0.523	0.335	0.168	0.077	0.182	0.217

[a] Koutsabeloulis and Griffiths
[b] These are the same as Bierbaumer's.

Since both Jannsen's and Terzaghi's theories are based on the ultimate state, they understably overpredict the measured loads in the centrifuge experiments, where vertical failure planes all the way to the top surface of the model have not been observed. The curve-fitted expressions by Koutsabeloulis and Griffiths are way off in estimating the minimum load, especially for depths which they consider shallow, i.e., $H/B \leq 2.5$. (It is disturbing that the load ratio computed from their equations for shallow depths actually increases with overburden depth [see Equation (6.31)]. Most of the experimental data to date indicate otherwise.) Those that assume a formation of an "arch" – Engesser and Evans – provide a better estimate of the minimum load. Engesser and Evans both tend to underpredict the minimum trapdoor load, although the latter apparently gives a better prediction.

The computed results for the glass bead tests ($\phi = 28.5°$, $H/B = 2$) are shown in Table 6.2. The results are presented for different values of K substituted in the equations. It can be seen that the calculated (P/P_0) values are highly sensitive to the assumed K. The centrifuge tests have yielded a minimum trapdoor load ratio of $(P/P_0)_{min} = 0.21 - 0.25$. The best estimate of the minimum door load comes, again, from Evans, whose expression for this minimum load is independent of the value of K. It is interesting, though, that the results predicted by Engesser are not too far from the experimental data, especially if $K = K_K = \frac{\cos^2\phi}{1+\sin^2\phi}$ is used.

Table 6.2: Comparisons of different theories applied to the centrifuge tests with glass beads ($H/B = 2$): Computed values of (P/P_0)

K	Engesser[a]	Silo/Terzaghi	Evans		K & G[b]
			$(P/P_0)_{min}$[c]	$(P/P_0)_{ult}$	
K_a	0.185	0.698	0.230	0.727	0.921
1	0.361	0.408	0.230	0.446	0.921
1.2	0.401	0.355	0.230	0.392	0.921
$\frac{\cos^2\phi}{1+\sin^2\phi}$	0.270	0.545	0.230	0.582	0.921

[a]The K values are treated in the context of $\sigma_v = K\sigma_h$, instead of the conventional definition.
[b]Koutsabeloulis and Griffiths
[c]These are the same as Bierbaumer's.

6.1.9 Proposed Theory

Since they both tend to predict the minimum door load quite well, the theories by Engesser, Bierbaumer and Evans merit closer examination. Possibly, this will lead to a better understanding of the arching mechanism, paving the way to an even better method of computing the minimum door load.

The slope (ϕ) assumed by Engesser that the tangent through the arch forms at the edges of the door with respect to the horizontal seems rather gentle. If one calculates the height of the parabolic arch corresponding to this angle, it is only about 15% of the door width for $\phi = 30°$. Based on visual observations from the centrifuge experiments, the arch definitely extends beyond that height, as also noted by Evans and others in their tests.

Evans does observe a triangle-like pattern above the trapdoor, extending to a considerable height at large door displacements. At smaller door displacements, however, this pattern is not readily apparent as an arch-shaped configuration. The minimum load on the trapdoor as measured in the experiments occurs at displacements in the order of $\sim$ 1-2% of the door width.

The observed minimum load at relatively small door displacements can probably be

explained by considering a parabolic arch oriented at an angle of $\theta = 90° - \phi$ at the edges (Figure 6-20), consistent with Evans's condition of the dilation angle $\nu = \phi$. This can now be analyzed in the same fashion as Engesser's derivation. In addition, the relation between the horizontal and vertical stresses at the level of the trapdoor can be obtained by hypothesizing that the surface defined by the arch represents a failure surface. In other words, the stresses acting on this surface, when plotted in the Mohr diagram, should correspond to the point on the circle tangent to the Mohr-Coulomb failure envelope (Figure 6-20).

It can be shown from Figure 6-20 that:

$$\sigma_v = \frac{\cos^2\phi}{1+\sin^2\phi}\sigma_h \tag{6.33}$$

By letting

$$K' = \frac{\sigma_v}{\sigma_h} = \frac{\cos^2\phi}{1+\sin^2\phi} \tag{6.34}$$

to stay in line with Engesser's formulation, an expression for the minimum load can be obtained by replacing K_a and ϕ in Equation 6.9 respectively with K' and $90° - \phi$. Since

$$\tan(90° - \phi) = \cot\phi$$

the resulting equation is

$$P_{min} = \gamma B^2\left(\frac{HK'}{2H\cot\phi + BK'} + \frac{\cot\phi}{6}\right) \tag{6.35}$$

Normalizing this with the geostatic force (per unit length) $P_0 = \gamma HB$, one obtains

$$\left(\frac{P}{P_0}\right)_{min} = \frac{B}{H}\left(\frac{K'}{2\cot\phi + \frac{B}{H}K'} + \frac{\cot\phi}{6}\right) \tag{6.36}$$

Applying this equation to the centrifuge experiments, it can be concluded from Table 6.3 that the proposed Engesser-Bierbaumer-Evans hybrid scheme provides a very

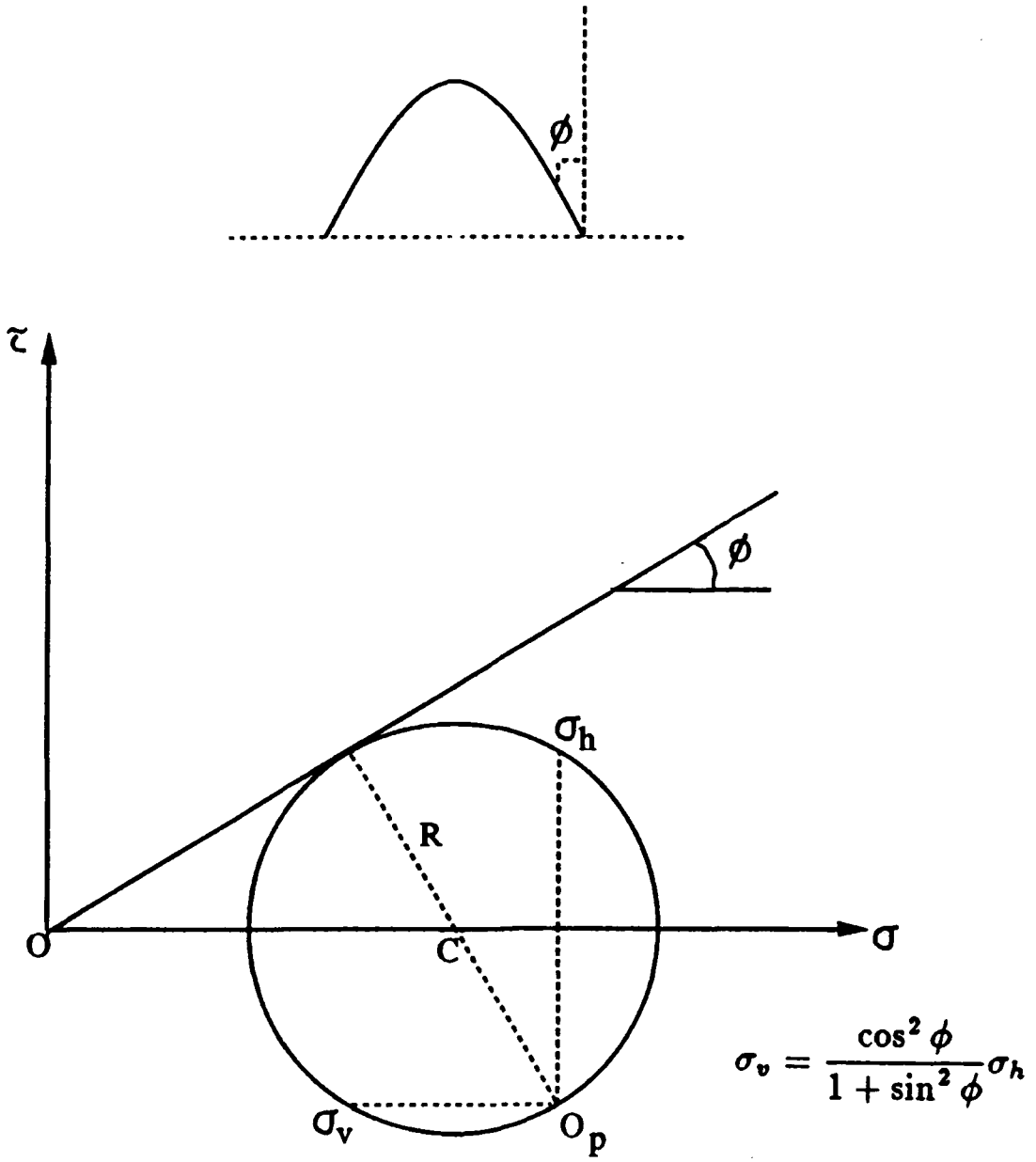

Figure 6-20: Proposed theory

Table 6.3: Predicted values of $(P/P_0)_{min}$ with proposed theory

H/B	$(P/P_0)_{min}$	
	Predicted	Measured
Tests with sand		
1	0.355	0.36
2	0.183	0.18
3	0.093	0.09
Tests with glass beads		
1	0.453	
2	0.232	0.21-0.25

good prediction of the minimum trapdoor load.

The computations result in about the same values when a triangular arch is assumed in the analysis (Evans's theory) as when a parabolic arch is assumed. This can possibly explain why the load tends to stay at a low level for quite a while as the "curved" arch slowly transforms into the triangular arch. Eventually, the soil structure will collapse, and the failure surfaces will become vertical [as observed by Stone (1988)], bringing about an increased load on the trapdoor with continued displacement. In this case, Jannsen's, Terzaghi's, or Evans's theory should provide a reasonable approximation of the ultimate door load. (Tables 6.1 and 6.2 show that all three tend to give similar predictions.)

6.2 Shearing along Joints

6.2.1 Simple FBD Approach

The load on the trapdoor in the experiments with jointed media can be estimated by analyzing a free body diagram, or FBD, (analogous to the silo problem) of the rods that tend to follow the trapdoor displacement. This FBD is presented in Figure 6-21, which considers the direct stack configuration.

The lateral stress on the sides of the sliding mass is assumed to vary linearly from a value of zero at the top surface to $\sigma_b = K\sigma_{v0} = K\gamma_s H$, where K is the lateral earth pressure coefficient, γ_s is the unit weight (at Ng) of the surrounding medium (e.g., glass beads), and H is the total model height. The shearing resistance on the sides is mobilized over the full height of the model; consequently, it also varies linearly with a magnitude equal to the the lateral stress multiplied by the coefficient of friction, $\mu_f = \tan\phi_{rod}$.

The weight per unit length of the rods mobilized during door lowering is $W = \gamma_{rod} B_m H$, where γ_{rod} is the unit weight (at Ng) of the model material, and B_m is the overall width of the mobilized body. The force P on the trapdoor per unit length can then be determined from the equilibrium of forces in the vertical direction:

$$\begin{aligned} P &= \gamma_{rod} B_m H - \tfrac{1}{2} K\gamma_s H^2 \tan\phi_{rod} \cdot 2 \\ &= \gamma_{rod} B_m H - K\gamma_s H^2 \tan\phi_{rod} \end{aligned} \tag{6.37}$$

Normalizing with respect to the weight P_0 of the material bounded by vertical planes through the edges of the trapdoor of width B, one obtains:

$$\frac{P}{P_0} = \frac{B_m}{B} - \frac{K\gamma_s H \tan\phi_{rod}}{\gamma_{rod} B} \tag{6.38}$$

If $B_m = B$, as in the case of the "four-on-door," "two-on-door," and "eight-on-door"

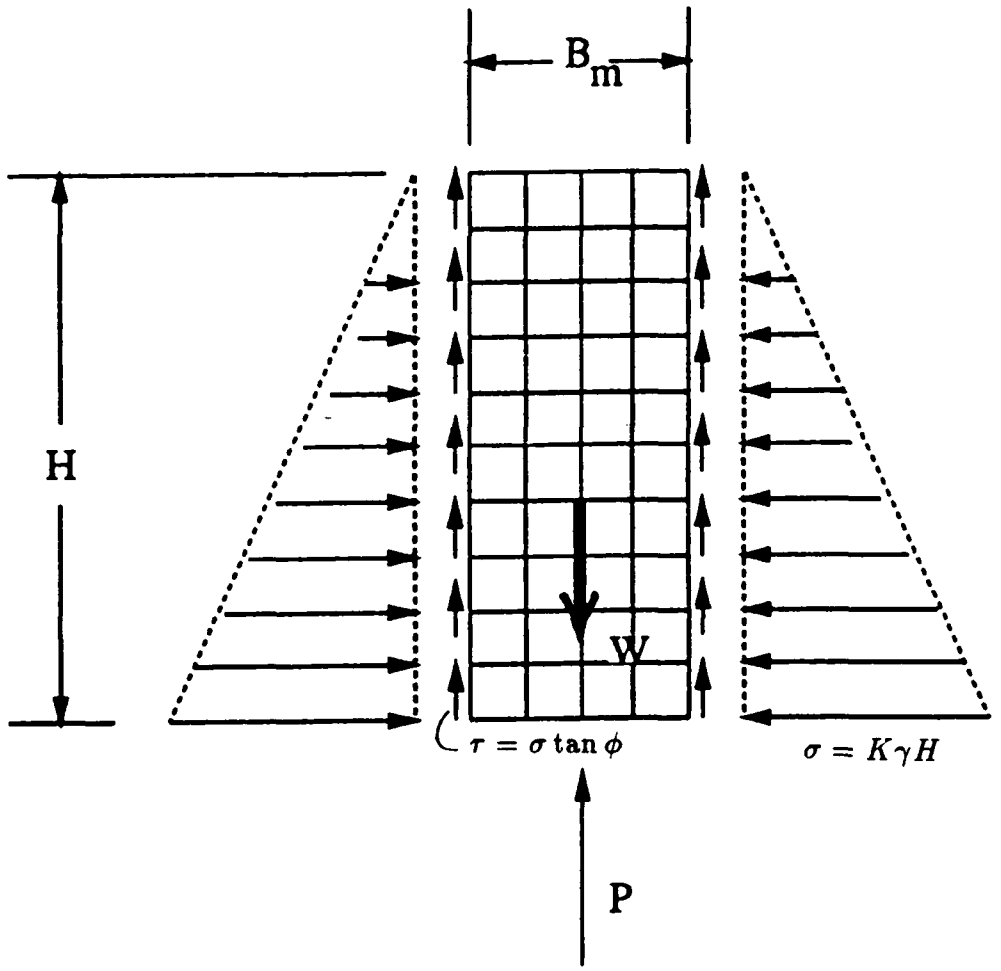

Figure 6-21: Free body diagram for determining the trapdoor force in the jointed media experiments

arrangements, this equation reduces to:

$$\frac{P}{P_0} = 1 - \frac{K\gamma_s H \tan\varphi_{rod}}{\gamma_{rod} B} \tag{6.39}$$

In the centrifuge tests, $\gamma_s \approx 100pcf$ $(15.7\ kN/m^3)$, $\gamma_{rod} = 0.098\ lb/in^3$ $(26.6\ kN/m^3)$, $H/B = 2.5$, and $\phi \approx 25°$. Assuming $K = K_0 = 1 - \sin\phi$ where $\varphi = 28.5°$, the computation yields $\frac{P}{P_0} = 0.64$, which lies within the range of the experimental data ($\sim$ 0.6-0.8). Again, this kind of an analysis is very sensitive to the value of K used. Furthermore, one should also bear in mind that in the centrifuge, the gravitational field acts radially, possibly decreasing the lateral stresses which are difficult to evaluate from any simple analysis. This undoubtedly requires a more detailed investigation which is beyond the scope of the present study.

A similar analysis can be performed for the brick stack. Owing to the smaller number of mobilized elements, the effect of friction on the trapdoor force is smaller than in the direct stack. Thus, the measured forces on the door are close to the weight (at Ng) of the rods that follow the door.

6.2.2 Suh and Sin's Friction Theory

As noted in Chapter 5, the force on the trapdoor in the direct stack tests tends to behave irregularly as the door displaces. One possible cause is the imperfect alignment of the rods due to inherent non-uniformities in the size of the rods. Errors in alignment are inevitably compounded with more rods arranged directly on top of each other.

A closer inspection of the results reveals that, in the context of the "simple FBD" approach described previously, the frictional resistance on the sides of the mobilized rods apparently increase as the door displacement ensues. This conforms with a relatively recent tribological theory advanced by Suh and Sin (1981). The frictional force (and, thus, the friction coefficient) is not a simple material property and is regarded as a function of the sliding distance (Figure 6-22) and the environment.

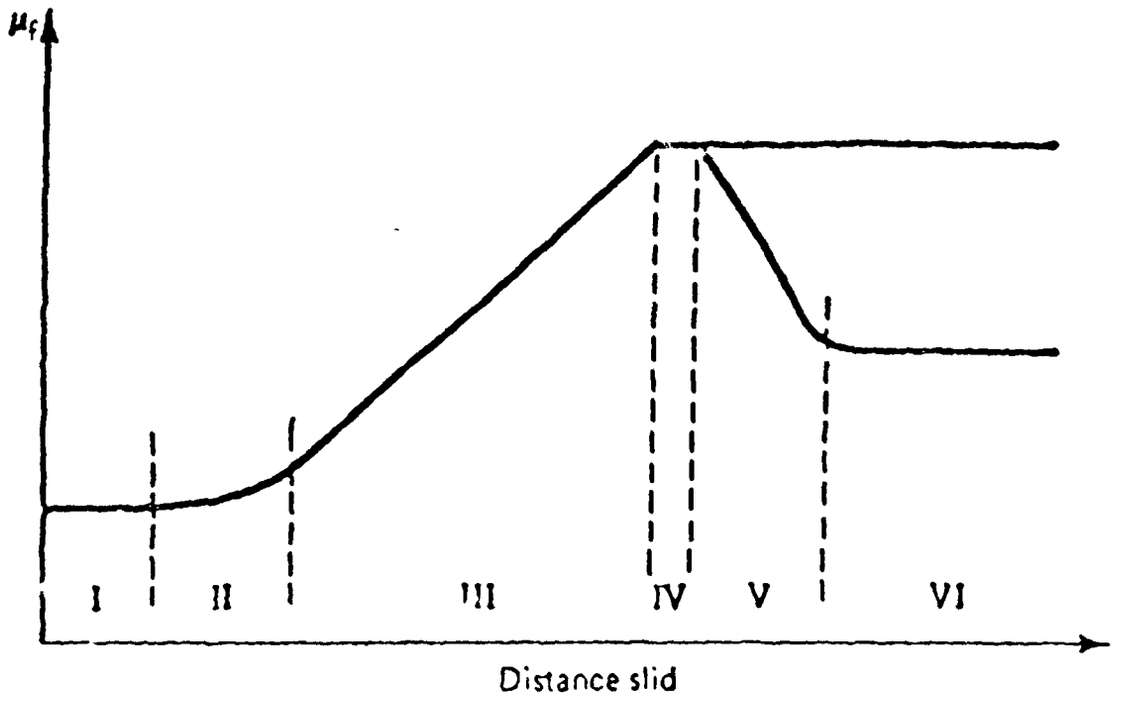

Figure 6-22: Variation of the friction coefficient with sliding distance (from Suh and Sin, 1981)

According to Suh and Sin, there are three components of friction: that due to the deformation of surface asperities (denoted μ_d), that due to plowing by wear particles and hard asperities (denoted μ_p), and that due to the adhesion of the flat portions of the sliding surface (denoted μ_a). These three basic mechanisms have been analyzed by means of the slip line field technique (as in the theory of plasticity). They state further:

> "Asperity deformation determines the static coefficient of friction and also affects the dynamic coefficient of friction, since asperities are continuously generated by the delamination of wear sheets. However, the contribution of asperity deformation to the dynamic coefficient of friction is not large relative to those of plowing and adhesion since the asperities deform readily (perhaps in one asperity contact) whereas the generation of asperities has to await the formation of delaminated wear particles which often requires a large amount of cyclic loading by the asperities of the opposing surface. Plowing takes place continuously whenever wear particles are entrapped between the sliding surfaces or when the asperities of the counterface plow, as when clean flat surfaces come into contact due to steady state sliding."

The time-dependent behavior of friction has also been considered qualitatively as consisting of different stages, as depicted in Figure 6-22. In the early stage (stage I), the value of the friction coefficient is controlled by plowing of the surface by asperities. In the second stage, the frictional force begins to rise slowly because of an increase in adhesion. Stage III is characterized by a steep increase in slope due to the rapid increase in the number of wear particles entrapped between the sliding surfaces as a consequence of higher wear rates. Stage IV is reached when the number of wear particles entrapped at the interface remains constant, and so the friction coefficient also tends to stay the same. In some cases, such as when a very hard stationary slider is slid against a soft specimen, the asperities of the hard surface are gradually removed (stage V), creating a mirror finish, causing a decrease in μ_f. Eventually, when the hard surface becomes mirror smooth to a maximum extent, the softer surface also acquires the same mirror

finish and the frictional force levels off (stage VI).

Suh and Sin's friction theory provides, then, a plausible explanation of the dependence of shearing behavior between surfaces on the absolute displacement. Even if the sizes of the sliding blocks are properly scaled, since they are made of the same material, the size of the (micro)asperities is unchanged, and the frictional properties are then affected by the same amount of sliding distance. In the case of granular media, expecially with the glass beads, the contact areas are essentially "points," as opposed to planar surfaces, and so their shearing characteristics are not grossly affected by moderate displacements. The greater probability of rolling between particles in granular media [see, e.g., Skinner (1963) and Paikowsky (1989)] over jointed media may negate the effects of friction due to interparticle sliding and, hence, allows proper scaling of mechanical behavior in models of granular masses.

Chapter 7

Conclusions

The trapdoor experiments in this study have led to new knowledge about arching in geomaterials and shearing along planar surfaces. The centrifuge tests with granular media conducted as part of this study are among the first experiments to satisfactorily measure the loads on the settling trapdoor underneath a soil mass in a high-gravity environment. Moreover, the trapdoor tests with simulated jointed rock carried out at MIT and at the Ruhr-Universität Bochum (RUB) in Germany are believed to be the first such tests. The results have shed some light onto the fulfillment of similitude requirements in geotechnical centrifuge models.

7.1 Similitude in Geotechnical Models

7.1.1 Results from Tests with Granular Media

Although one of the primary objectives of this research is to investigate the scaling relationships for centrifuge models of jointed media, an assessment of similitude in granular soil models is almost unavoidable. This actually serves as a benchmark upon which the examination of scaling in jointed models can be based.

A "modelling of models" exercise has been carried out with granular materials using various corresponding scales of particle size, door width, overburden depth, and gravity

level. The results show that these various scaled models of a granular medium overlying the trapdoor, when tested at similar stress levels, simulate the same prototype. In particular, the measured minimum loads on the trapdoor yield the same average stress in appropriately scaled setups. Moreover, the displacements at which these minimum loads occur are proportionately smaller in the smaller models, and are related by the same ratio as are the overall model dimensions. Thus, in the centrifuge trapdoor models with granular media, the criteria for similitude under plane strain conditions are satisfied. The same conclusion is also reached by considering dimensionless plots of force (normalized with respect to the theoretical overburden load) vs. displacement (normalized with respect to the trapdoor width).

Tests have also been conducted with different granular materials deposited to a particular height over the same trapdoor, lowered at identical centrifuge rotational speeds. The load vs. displacement curves obtained from these tests are fairly similar only at low values of displacement ($\sim$ 0.2% of the door width), and they tend to diverge at larger displacements. It is evident, therefore, that the particle size scaling is potentially an issue, at least when large particles are involved.

7.1.2 Results from Jointed Media Tests

The data obtained from the "modelling of models" series of experiments with jointed media both at MIT and at RUB have provided load-displacement plots which do not completely fulfill the similarity requirements for appropriately scaled arrangements. The force values, especially the minimum loads, approximately satisfy the similitude criteria in that the average stresses are about the same for all the scales considered. These forces, however, occur at about the same absolute door displacement, in violation of the centrifuge scaling laws (which stipulate that the normalized, not the absolute, displacements should be the same). Similitude requirements in connection with the scaling of length dimensions are, thus, not met by the observed displacements.

The dependence on absolute displacement of shearing between surfaces represents

a serious obstacle to centrifuge experimentation with models involving joints and other discontinuities. It may be extremely difficult, if at all possible, to extrapolate results from model tests to actual prototype conditions. This does not necessarily mean, however, that centrifuge modelling is totally useless for situations involving jointed media. The ability to generate body forces in the centrifuge – even after failure in the model occurs – makes it an invaluable tool in obtaining data against which analytical and numerical methods can be validated. Consideration of a centrifuge model test as an event by itself should prove extraordinarily useful in situations where actual field data are difficult to get, e.g., seismic behavior of structures and soils or rocks.

7.2 Arching in Geomaterials

The settling of a trapdoor underneath a soil gives rise to the development of an "arch" just above the door. This justifies the use of the term "arching" to describe the redistribution of stresses and reduction of loads on underground structures which tend to deform more relative to the surrounding soil. As the trapdoor displaces with respect to the adjacent base, the shape of the arch, initially curved, approaches a triangular configuration, as confirmed in the MIT centrifuge tests with granular media. Eventually, at very large trapdoor displacements, the arch collapses [as observed, not in the MIT experiments, but in the centrifuge experiments performed by Stone (1988)], and a prismatic body of the overlying material follows the movement of the trapdoor, increasing the load on the door.

The mechanism of arching discussed above is consistent with commonly understood relationships between (incremental) shearing strains and (incremental) volumetric strains in geomaterials. At small strains, a granular medium tends to dilate or increase in volume depending on the stress level and porosity. This ability of granular soils to carry shearing stresses brings about the formation of the arch above the trapdoor, and considerable dilation of the soil occurs soon after the door is displaced. At large strains,

the geomaterial tends to deform with hardly any change in volume. The eventual collapse of the arch leading to vertical failure surfaces is a manifestation of this stage of isochoric, or constant-volume, deformation.

Unlike some of the previous trapdoor experiments [e.g., Terzaghi (1936), Evans (1983)], the measured forces in the centrifuge tests of this research project remain at an approximately constant low level for a considerable amount of displacement. Since these centrifuge tests simulate the appropriate stress levels in the field, this observation of a "prolonged" minimum load on the trapdoor has significant implications in underground construction for granular soils. (The fact that the centrifuge scaling laws have been validated for granular media suggests that it is reasonable to extrapolate the centrifuge test results from the small-scale models to the prototype condition.) Many tunnel design and construction methods do consider load reduction relative to full overburden load. They are, however, rather conservative regarding the allowable displacements because of the eventual load increase with such displacement. The observations in this study indicate that relatively large displacements ($\sim$ 15% of the trapdoor width) do not lead to a substantial load increase.

The amount of load reduction is dependent on the depth of overburden and the width of the structure (trapdoor). The percentage decrease from the full overburden pressure increases with greater ratios of deposition depth H to trapdoor width B. For a particular door width, the shape and size of the arch appears to be the same regardless of the depth of cover, as long as the depth H is greater than about 1.5 times the door width B. Experiments performed with identical setups at different g's reveal that, for soils with $H/B \geq 2$ (deep enough such that a stable arch is likely to develop as the trapdoor is displaced), the load-displacement curves are about the same. On the other hand, when the geomaterial is relatively shallow ($H/B \leq\sim 1$), higher levels of stress tend to cause larger loads upon lowering of the trapdoor. The discrepancy in the latter is clearly related to the different amounts of dilation associated with dissimilar stress levels.

A hybrid scheme based on Engesser's (1882), Bierbaumer's (1913) and Evans's (1983)

formulations is proposed to predict the minimum loads on the structure due to active arching. The proposed expression for the minimum load is:

$$P_{min} = \gamma B^2 \left(\frac{K'}{2\cot\phi + \frac{B}{H}K'} + \frac{\cot\phi}{6}\right) \tag{7.1}$$

where B is the width of the trapdoor, H is the depth of overburden, γ is the unit weight of the soil, ϕ is the friction angle, and

$$K' = \frac{\cos^2\phi}{1+\sin^2\phi}.$$

The beauty of this "new" theory lies in the fact that one need not assume a value for the lateral coefficient of pressure K – the main source of controversy in other methods. It comes about automatically from a Mohr circle construction by hypothesizing that the arch itself is a failure surface (i.e., the stresses on this surface satisfy the Coulomb criterion for cohesionless materials: $\tau = \sigma\tan\phi$), with a slope from the vertical through the edges of the trapdoor equal to the friction angle of the soil. The shape of the arch is assumed to be a parabola, and the force on the trapdoor is the sum of the weight of material below this arch (which depends on B, γ, and ϕ) and the effect of the induced stresses from the sides due to the load redistribution (which is a function of H, γ, and ϕ).

Computations in this study have demonstrated that the predicted minimum load on the structure (trapdoor) is approximately the same whether the shape of the arch is curved, as in Engesser's theory, or triangular, as in Bierbaumer's or Evans's theory. Both shapes have indeed been observed experimentally, with the triangle-like pattern occuring at larger displacements. Thus, even if the arch configuration transforms from a curved to a triangular shape while the door is moved down, the load on the door is apparently unchanged. This explains why the measured forces, as soon as the minimum is attained, stay at more or less the same level for a considerable amount of displacement.

The trapdoor experiments both with granular and jointed media have shown some

interesting similarities. Specifically, the formation of a physical arch in the former is analogous to the brick stack case – where the elements are laid out in an alternating pattern as with a brick wall. As observed by Stone (1988) in his centrifuge tests, the rupture surfaces tend to become vertical as the trapdoor is continually lowered – just like in the direct stack arrangement. At very large displacements, therefore, the ultimate load on the structure can be estimated by methods similar to Jannsen's (1895), Terzaghi's (1943), or Evans's (1983) ultimate-state solution.

7.3 Recommendations for Future Work

Given the power of the centrifuge to apply continuous body force loading on a small-scale model, despite the violation of scaling rules in discontinua, emphasis should be directed towards investigation of basic mechanisms, including rock fracture, slope stability, soil-structure interaction, and fluid-saturated behavior of geologic materials. Although the scaling laws have been validated for granular media, it may not be a simple task to simulate a site-specific prototype in the centrifuge, considering that not all aspects of the field condition can readily be replicated in the model. Should such an opportunity arise, it is recommended that centrifuge tests be performed in conjunction with numerical models for the purpose of achieving the best possible design.

More detailed mathematical analyses should be performed in the future about the trapdoor scenario for comparison with the data obtained from the centrifuge experiments carried out in this study. In particular, a model which will adequately describe the entire load-displacement behavior needs to be developed. Such an exercise will help improve the predictive capabilities of constitutive models for granular soils, especially where arching is involved. In addition, knowledge of the displacement levels at which load magnitudes tend to change will prove invaluable in the design process. Mathematical models of discontinuum behavior can also be enhanced.

In view of the potential savings that can be derived from a consideration of the

reduced loads on underground structures, actual subterranean construction data have to be obtained. This will not only serve to check the existing theories, but will also aid in the establishment of guidelines for the design of future underground works.

Since most of the techniques which estimate the ultimate loads are highly sensitive to the value of K used, more research should be done on the effect of the lateral earth pressure coefficient in situations where large displacements are anticipated. Accurate determination of K is a complicated problem, because the measurements may be affected by the arching phenomenon itself, which is dependent on the stiffness characteristics of the load sensor and the surrounding soil. Nevertheless, the importance of determining the value of the lateral earth pressure coefficient for geotechnical applications cannot be overemphasized.

Future trapdoor experiments on the centrifuge can be performed to address more completely the issues pertaining to: (1) the displacement levels in the active mode at which the arch begins to collapse, increasing the trapdoor load; (2) passive arching, i.e., the resulting load-displacement curve as the door is pushed into the geomaterial; and (3) arching in saturated, as well as cohesive, geomaterials.

Bibliography

[1] Andersen, G. R. (1987), *Tilting Response of Centrifuge-Modeled Gravity Retaining Wall to Seismic Shaking*, S.M. Thesis, Department of Civil Engineering, MIT.

[2] Atkinson, J. H. and Potts, D. M. (1975), "A Note on Associated Field Solutions for Boundary Value Problems in a Variable ϕ - Variable ν Soil," *Geotechnique*, Vol. 25, pp. 379-384.

[3] Bierbaumer, A. (1913), *Die Dimensionerung des Tunnelmauerwerks*, Engelmann, Leipzig.

[4] Bjerrum, L., Frimann Clausen, C. J., and Duncan J. M. (1972), "Earth Pressures on Flexible Structures - A State-of-the-Art Report," *Proceedings, Fifth European Conference on Soil Mechanics and Foundation Engineering*, pp. 169-196.

[5] Bloomquist, D. G., Davidson, J. L., and Townsend, F. C. (1984), "Platform Orientation and Start-up Time During Centrifuge Testing," *Geotechnical Testing Journal*, Vol. 7, No. 4, pp. 195-199.

[6] Bolton, M. D., English, R. J., Hird, C. C., and Schofield, A. N. (1973), "Ground Displacements in Centrifugal Models," *Proceedings, Seventh International Conference on Soil Mechanics and Foundation Engineering*, Vol. 1, No. 1, pp. 65-70.

[7] Buckingham, E. (1914), "On Physically Similar Systems: Illustrations of the Use of Dimensional Equations," *The Physical Review*, Ser. 2, Vol. 4, No. 4, pp. 345-376.

[8] Bucky, P. B. (1931), *Use of Models for the Study of Mining Problems*, Technical Publication 425, American Institute of Mining and Metallurgical Engineers, pp. 3-28.

[9] Bulson, P. S. (1985), *Buried Structures: Static and Dynamic Strength*, Chapman and Hall.

[10] Chelapati, C. V. (1964), "Arching in Soil Due to the Deflection of a Rigid Horizontal Strip," *Proceedings, Symposium on Soil-Structure Interaction*, University of Arizona, pp. 356-377.

[11] Cheney, J. A. and Fragaszy, R. J. (1984), "The Centrifuge as a Research Tool," *Geotechnical Testing Journal*, Vol. 7, No. 4, pp. 182-187.

[12] Clark, G. B. (1960-1963), M.S. theses under his direction, School of Mines, Univesity of Missouri (Chan 1960, Esser 1962, Haycocks 1962, Oudenhoven 1962, Gomah 1963).

[13] Clark, G. B. (1981), "Geotechnical Centrifuges for Model Studies and Physical Property Testing of Rock and Rock Structures," *Colorado School of Mines Quarterly*, Vol. 76, No. 4.

[14] Davidenkov, N. N. (1936), "A New Method of Using Models for the Study of Equilibrium of Structures," *Technical Physics of the USSR*, Vol. III, No. 1, pp. 131-136 (in Russian).

[15] Davis, E. H. (1968), "Theories of Plasticity and the Failure of Soil Masses," *Soil Mechanics, Selected Topics*, edited by I. K. Lee, American Elsevier Publishing Company, Inc., pp. 341-380.

[16] Dobry, R. and Elgamal, A. W. (1989), Memorandum to U.S. institutions with centrifuge facilities, Department of Civil Engineering, Rensselaer Polytechnic Institute, April 27, 1989.

[17] Engesser, Fr. (1882), "Ueber den Erdduck gegen innere Stützwande (Tunnelwande)," *Deutsche Bauzeitung*, No. 16, pp. 91-93.

[18] Evans, C. H. (1983), *An Examination of Arching in Granular Soils*, S.M. Thesis, Department of Civil Engineering, MIT.

[19] Feld, J. (1948), "Early History and Bibliography of Soil Mechanics," *Proceedings, Second International Conference on Soil Mechanics and Foundation Engineering*, Vol. 1, pp. 1-7.

[20] Feynman, R. P., Leighton, R. B., and Sands, M. (1963), *The Feynman Lectures on Physics*, Addison-Wesley Publishing Co.

[21] Fuglsang, L. D. and Ovesen, N. K. (1988), "The Application of the Theory of Modelling to Centrifuge Studies," *Centrifuges in Soil Mechanics*, Craig, W. H., James, R. G., and Schofield, A. N. (eds.), pp. 119-138.

[22] Finn, W. D. L. (1963), "Boundary Value Problems of Soil Mechanics," *Journal of the Soil Mechanics and Foundations Division*, American Society of Civil Engineers, Vol. 89, No. SM5, pp. 39-72.

[23] Getzler, Z., Gellert, M., and Eitan, R. (1970), "Analysis of Arching Pressures in Ideal Elastic Soil," *Journal of the Soil Mechanics and Foundations Division*, American Society of Civil Engineers, Vol. 96, No. SM4, pp. 1357-1372.

[24] Griffiths, D. V. (1986), "Some Theoretical Observations on Conical Failure Criteria in Principal Stress Space," *International Journal of Solids and Structures*, Vol. 22, No. 5, pp. 553-565.

[25] Handy, R. L. (1985), "The Arch in Soil Arching," *Journal of Geotechnical Engineering*, American Society of Civil Engineers, vol. 111, no. 3, pp. 302-318.

[26] Hoek, E. (1965), "The Design of a Centrifuge for the Simulation of Gravitational Force Field in Mine Models," *Journal of South African Institute of Mining and Metallurgy*, Vol. 65, No. 9, pp. 455-487.

[27] Iglesia, G. R. (1991), *Trapdoor Experiments on the Centrifuge: A Study of Arching in Geomaterials and Similitude in Geotechnical Models*, Ph.D. Thesis, Department of Civil Engineering, MIT.

[28] Janssen, H. A. (1895), "Versuche über Getreidedruck in Silozellen," *Z. d. Vereins deutscher Ingenieure*, Vol. 39, p. 1045 (partial English translation in *Proceedings of the Institute of Civil Engineers*, London, 1896, p. 553).

[29] Jessberger, H. L. and Scherbeck, R. (1990), *Bericht über die Zentrifugenmodellversuche zur Thematik der Gewölbewirkung in geklüftetem Material im zuge der Kooperation RUB-MIT*, Ruhr-Universität Bochum.

[30] Joseph, P. G., Einstein, H. H., and Whitman, R. V. (1987), *A Literature Review of Geotechnical Centrifuge Modeling with Particular Emphasis on Rock Mechanics*, MIT Report to the Air Force Engineers and Service Center, Tyndall Air Force Base, Florida.

[31] Ko, H. Y., Azevedo, R., and Sture, S. (1982), "Numerical and Centrifugal Modeling of Excavations in Sand," *Deformation and Failure of Granular Materials*, P. A. Vermeer and H. J. Luger (eds.), A. A. Balkema.

[32] Koutsabeloulis, N. C. and Griffiths, D. V. (1989), "Numerical Modelling of the Trapdoor Problem," *Geotechnique*, Vol. 39, No. 1, pp. 77-89.

[33] Krsmanović, D., Tufo, M., and Langof, Z. (1966), "Shear Strength of Rock Masses and Possibilities of Its Reproduction on Models," *Proceedings of the First International Society for Rock Mechanics*, pp. 537-542.

[34] Ladanyi, B. and Hoyaux, B. (1969), "A Study of the Trap-Door Problem in a Granular Mass," *Canadian Geotechnical Journal*, vol. 6, no. 1, pp. 1-15.

[35] Leontovich, V. (1959), *Frames and Arches: Condensed Solutions for Structural Analysis*, McGraw-Hill Book Company, Inc.

[36] Luscher, U. and Höeg (1965), "The Beneficial Action of the Surrounding Soil on the Load-Carrying Capacity of Buried Tubes," *Proceedings, Symposium on Soil-Structure Interaction*, University of Arizona, pp. 393-402.

[37] Marston, A. and Anderson, A. O. (1913), "The Theory of Loads on Pipes in Ditches and Tests of Cement and Clay Drain Tile and Sewer Pipe," *Bulletin 31*, Iowa Engineering Experiment Station.

[38] McNulty, J. W. (1965), *An Experimental Study of Arching in Sand*, Ph.D. Thesis, Department of Civil Engineering, Univesity of Illinois.

[39] McWilliams, P. C. (1989) *Bureau of Mines Geotechnical Centrifuge Research – A Review*, U.S. Bureau of Mines Information Circular.

[40] Paikowsky, S. G. (1989), *A Static Evaluation of Soil Plug Behavior with Application to the Pile Plugging Problem*, Ph.D. Thesis, Department of Civil Engineering, MIT.

[41] Panek, L. A. (1952), *Centrifugal Testing Apparatus for Mine-Structure Stress Analysis*, U.S. Bureau of Mines Report of Investigations 4883.

[42] Phillips, E. (1869), "D'equilibre des Solides Elastiques Semblables," *Computes Rendus de l'Academie des Sciences*, Vol. 68., pp. 75-79.

[43] Pokrovsky, G. I. (1933), *Zeitschrift fur Technische Physik*, Vol. 14, No. 4 (in German with earlier references in Russian).

[44] Pokrovsky, G. I. and Fyodorov, I. S. (1975), *Centrifugal Model Testing in the Mining Industry* (vol. 1) *and Construction Industry* (vol. 2), Building Research Establishment, England.

[45] Ramberg, H. (1967), *Gravity, Deformation and the Earth's Crust*, Academic Press.

[46] Rowe, P. W. (1975), "Displacement and Failure Modes of Model Offshore Gravity Platforms Founded on Clay," *Offshore Europe 1975*, Spearhead Publications, Ltd., pp. 218.1-218.17.

[47] Schmidt, R. M. and Holsapple, K. A. (1980), "Theory and Experiments on Centrifuge Cratering," *Journal of Geophysical Research*, Vol. 85, No. B1, pp. 235-252.

[48] Schofield, A. N. (1980), "Cambridge Geotechnical Centrifuge Operations," *Geotechnique*, Vol. 20, pp. 227-268.

[49] Scott, R. F. and Morgan, N. R. (1977), *Feasibility and Desirability of Constructing a Very Large Centrifuge for Geotechnical Studies*, Report 760-170, National Science Foundation.

[50] Skinner, A. E. (1969), "A Note on the Influence of Interparticle Friction on the Shearing Strength of a Random Assembly of Spherical Particles," *Geotechnique*, Vol. 19, pp. 150-157.

[51] Spangler, M. G. and Handy, R. L. (1982), *Soil Engineering*, Harper and Row Publishers.

[52] Stone, K. J. L. (1988), *Modelling of Rupture Development in Soils*, Ph.D. Dissertation, Wolfson College, Cambridge University.

[53] Stone, K. J. L. and Güttler, U. (1989), *Bochum-MIT Collaboration on active arching experiments: Report from preliminary centrifuge tests*, Ruhr-Universität Bochum.

[54] Suh, N. P. and Sin, H.-C. (1981), "The Genesis of Friction," *Wear*, Vol. 69, pp. 91-114.

[55] Szechy, K. (1973), *The Art of Tunnelling*, Akademiai Kiado, Budapest.

[56] Tan, T. S. and Scott, R. F. (1985), "Centrifuge Scaling Considerations for Fluid-Particle Systems," *Geotechnique*, Vol. 35, pp. 461-470.

[57] Terzaghi, K. (1936), "Stress Distribution in Dry and in Saturated Sand Above a Yielding Trap-Door," *Proceedings, First International Conference on Soil Mechanics and Foundation Engineering*, pp. 307-311.

[58] Terzaghi, K. (1943), *Theoretical Soil Mechanics*, John Wiley and Sons, Inc.

[59] Terzaghi, K. and Peck, R. B. (1968), *Soil Mechanics in Engineering Practice*, John Wiley and Sons, Inc.

[60] Vardoulakis, I., Graf, B., and Gudehus, G. (1981), "Trap-Door Problem with Dry Sand: A Statical Approach Based Upon Model Test Kinematics," *International Journal for Numerical and Analytical Methods in Geomechanics*, vol. 5, pp. 57-78.

[61] Whitman, R. V. and Luscher, U. (1962), "Basic Experiment into Soil-Structure Interaction," *Journal of the Soil Mechanics and Foundations Division*, American Society of Civil Engineers, Vol. 88, No. SM6, pp. 135-167.

Appendix A

Summary Table of MIT Centrifuge Tests Performed

The following table provides a summary of the various experiments (as well as trials) performed in the MIT centrifuge.

Centrifuge Tests Performed (March '88 - September '90)

Date	*Test*	*Description*	*Remarks*
03/14/88	*GI*1	No soil; investigate performance of transducers and data acquisition system	Wires shorted out
03/18/88	GI2	No soil; broken wires fixed; determine workability of design	Motor barely works @ 40g
03/21/88	*GI*3	No soil; determine if motor by itself works at high g	Motor by itself works
03/28/88	*GI*4	No soil; collar connecting motor shaft to worm shaft modified	Setup works only up to 40g
03/29/88	*GI*5	No soil; collar redesigned	Setup again works only up to 40g
04/6/88	*GI*6	No soil; wedge disconnected for the time being	Motor-worm-gear system works up to 80g
04/13/88	*GI*7	No soil; no wedge; collar modified (again); shaft-bearing connections changed	Without wedge, setup works up to 120g
04/14/88	*GI*8	No soil; wedge (re)connected to shaft	Works up to 80g, then wires turn loose, test stopped
04/20/88	*GI*9	Empty; broken wires fixed	Motor works (up to 80g); notice slight drop in load cell readings upon start of motor
04/21/88	*GI*10	Steel weights placed on trapdoor segments	Motor "locked up" @ 40g, restarts @ ~20-25g

Centrifuge Tests Performed (March '88 - September '90)

Date	*Test*	*Description*	*Remarks*
04/29/88	*GI*11	Steel weights on door segments; gear box remodeled	System works fine up to 120g, has trouble starting @ 140g
05/5/88	*GI*12/A	Wider door (1.1") placed (for narrower grap between sides and doors); steel weights on door segments; *GI*12A has weights but no doors atop the load cells	Motor works up to < 120g; LC3 wire broken
05/6/88	*GI*13/A	LC3 wire fixed; basically a repeat of *GI*12; *GI*13A has weights but no doors atop the load cells	Notice slight drop in load as soon as motor starts for *GI*13; virtually no load drop in *GI*13A
05/11/88	*GI*14	Taper placed on door edges; repeat of *GI*13 for further calibration	Motor stopped at 80g
05/18/88	*GI*15/ABC	Graphite powder applied at rubbing junctions; same as previous three (3) tests; *GI*15 -- doors + weights; *GI*15A -- doors only; *GI*15B -- doors above weights atop load cells; *GI*15C -- doors (w/o pins) + weights	Motor works up to 140g; *GI*15 and *GI*15A *GI*ve erratic readings; *GI*15B and *GI*15C have much better load cell performance
05/19/88	*GI*16	Alignment pins/buttons modified; same as before	Modest improvement in load cell performance observed
07/8/88	*GI*17	Run to check workability of setup after long 'layoff'; steel weights placed on top of doors	Motor works up to 120g
07/26/88	*GI*18	First test with soil: brown (relatively fine) sand 3.5" deep, 1.1"-wide door to be lowered @ 80g	Motor locked up; sand grains got through trench
07/28/88	*GI*19	Re-run of *GI*18	Motor locked up
	*GI*20	Coarse (NJ 4/14) sand used, 1.5" deep	Motor locked up.
07/29/88	*GI*21	Back to steel weights	Motor locked up, works only @ 75 rpm (~10g)

Centrifuge Tests Performed (March '88 - September '90)

Date	*Test*	*Description*	*Remarks*
08/2/88	*GI*22	Gearbox re-adjusted; same as *GI*21	Setup works up to 40g
08/3/88	*GI*23	Rubbing junctions lubricated with teflon spray; otherwise, same as before	System works up to 120g
08/5/88	*GI*24	Test with 4" coarse sand; 1.1" door lowered @ 80g	No mechanical problems
08/8/88	*GI*25	Repeat of *GI*24	
08/9/88	*GI*26	6" coarse sand on 1.1" door, lowered @ 80g	
08/11/88	*GI*27	Same as *GI*26	
08/12/88	*GI*28	Same as *GI*26 and *GI*27	
	*GI*29	4" coarse sand on 1.1" door, lowered @ 80g	
08/16/89	*GI*30	Empty (for calibration)	
08/22/89	*GI*31	6" coarse sand on 1.1" door, lowered @ 80g	Based on data from *GI*24-*GI*31, repeatability of test results not readily apparent
	*GI*31A	Empty (for calibration)	
08/23/88	*GI*32	Empty (for calibration); buttons put back on door segments	
	*GI*33	6" coarse sand; buttons on trapdoor segments	
08/24/88	*GI*34	6" coarse sand; same as *GI*33	Results now seem to be repeatable
08/26/88	*GI*35	Empty (for recalibration)	
08/30/88	*GI*36	6" coarse sand	
08/31/88	*GI*37	2" coarse sand	In practically all tests run so far, load cell measurements of geostatic force seem to be rather low
09/2/88	*GI*38	Empty	

Centrifuge Tests Performed (March '88 - September '90)

Date	*Test*	*Description*	*Remarks*
09/9/88	*GI*39	Empty; load cells moved from trench to side to check their response behavior with minimal wire slack	
09/16/88	*GI*40	Same as *GI*39 but with steel weights this time	
09/27/88	*GI*41	Teflon-coated aluminum placed at the base; empty (for calibration)	
09/27/88	*GI*41A	Steel weights (for calibration)	
09/27/88	*GI*41B	Trapdoor segments (and weights) on outer load cells placed on top of middle ones for calibration	
09/27/88	*GI*41C	Doors + weights + motor running	Motor works only up to 90 rpm
09/28/88	*GI*42	Rubbing junctions lubricated with teflon spray; otherwise same as *GI*41C	Motor works only up to 90 rpm
09/29/89	*GI*43	Teflon plate put back; test with steel weights	Motor works up to 120g
10/3/88	*GI*44	Test with 6" coarse sand	
10/4/88	*GI*45	6" coarse sand	
	*GI*46	Empty (for calibration)	
10/7/88	*GI*47	Teflon-coated aluminum base; 6" coarse sand	Motor works this time
10/12/88	*GI*48	2" coarse sand	LC4 not working
10/14/88	*GI*49	2" coarse sand; LC4 fixed	
10/18/88	*GI*50	Package empty	
	*GI*51	4" coarse sand	
	*GI*52	6" coarse sand	
10/20/88	*GI*53	Empty, with motor runing at 80g to investigate friction effects	

Centrifuge Tests Performed (March '88 - September '90)

Date	*Test*	*Description*	*Remarks*
	*GI*54	1" coarse sand	
	*GI*55	1" coarse sand; no tape on middle segment of trapdoor	
10/25/88	*GI*56	6" coarse sand; no tape on middle segment of trapdoor	
10/26/88	*GI*57	Empty, with motor running @ 80g	
11/9/88	*GI*58	"4-on-door" direct stack of 1/4"[] balsa wood rods to 3" height; confining stress provided by means of 1/4" hexagonal aluminum rods on the sides; 1.1" door lowered @ 80g	Rods above trapdoor held in place by the shearing resistance of the "joints"
11/10/88	*GI*59	"4-on-door" direct stack of 1/4"[] balsa wood rods to 3" height; 1.1" door to be lowered at 80g	Motor locked up
11/23/88	*GI*60	Rubbing junctions re-lubricated; test *GI*59 redone	Motor works
11/28/88	*GI*61	"4-on-door" direct stack of 1/4"[] balsa wood rods to 3" height; 1.1" door lowered at 80g; no confining stress imposed	
11/29/88	*GI*62	"4-on-door" brick stack of 1/4"[] balsa wood rods stacked to 3" height; 1.1" door lowered at 80g; no confining stress	Data lost; erroneous key pressed while storing in disc
12/1/88	*GI*63	Repeat of *GI*62	
12/2/88	*GI*64	Empty (for recalibration)	
01/26/89	*GI*65	Empty; wider (2") door used	
01/27/89	*GI*66	4" coarse sand; 2" door lowered at 40g	

Centrifuge Tests Performed (March '88 - September '90)

Date	*Test*	*Description*	*Remarks*
02/10/89	*GI*67	Package empty; first run with new load cell setup	LCI not working; motor locked up at 80g
02/14/89	*GI*68	Package empty	Motor working but struggling at 80g
02/15/89	*GI*69	Package empty	Motor locked up at 80g
02/16/89	*GI*70	2" coarse sand	Motor locked up at 80g
	*GI*71	Package empty	Motor locked up at 80g
02/28/89	*GI*72	Package empty	Motor locked up at 80g
	*GI*73	Package empty; wedge disconnected	Motor works up to 160g
	*GI*74	Package empty; rubbing junctions lubricated with teflon spray	Motor works this time
03/1/89	*GI*75	6" coarse sand	
	*GI*76	4" coarse sand	
	*GI*77	Package empty	
03/2/89	*GI*78	2" coarse sand	
	*GI*79	1" coarse sand	
	*GI*80	6" coarse sand	
03/3/89	*GI*81	Package empty	
03/6/89	*GI*82	Package empty but door loaded with steel weights	
	*GI*83	6" coarse sand	
03/8/89	*GI*84	Package empty but door loaded with steel weights	
03/14/89	*GI*85	Package empty; setup remodified to have each force transducer in between two balls for fully concentric loading;1.1" door lowered @ 80g	No significant change in load measurements observed
03/15/89	*GI*86	1.1" door loaded with steel weights; g-level increased to 120g in 20g increments	For calibration purposes

Centrifuge Tests Performed (March '88 - September '90)

Date	*Test*	*Description*	*Remarks*
	*GI*87	6" coarse sand; 1.1" door lowered @ 80g	
03/16/89	*GI*88	4" coarse sand; 1.1" door lowered @ 80g	
	*GI*89	2" coarse sand; 1.1" door lowered @ 80g	
	*GI*90	1" coarse sand; 1.1" door lowered @ 80g	
03/17/89	*GI*91	Repeat of *GI*85	
03/27/89	*GI*92	"4-on-door" direct stack of 1/4"[] *Al* rods, 3" high (with no confining stress; 1.1" door lowered @ 80g	Pile of rods collapsed (due to absence of confining stress) during spin-up
	*GI*93	"4-on-door" direct stack of 1/4"[] *Al* rods, 2.5" high (this time with some confining stress ~ $K_0\sigma_v$); 1.1" door lowered @ 80g	
03/28/89	*GI*94	"4-on-door" brick stack of 1/4"[] *Al* rods, 2.5"; 1.1" door lowered @ 80g	
03/29/89	*GI*95	"4-on-door" brick stack of 1/4"[] rods, 2.5" high; 1.1" door lowered @ 40g	
03/30/89	*GI*96	1.1" door loaded with steel weights, lowered @ 80g	No significant change in load readings as motor is started
04/6/89	*GI*97	"4-on-door" direct stack of 1/2"[] *Al* rods, 5" high, on 2" door, lowered @ 40g	Door a bit narrower than total width of 4 rods; hence, some hanging on the side occured
04/7/89	*GI*98	"3-on-door" direct stack of 1/2"[] *Al* rods, 5" high, on 2" door, lowered @ 40g	
04/10/89	*GI*99	Repeat of *GI*98	
04/11/89	*GI*100	Package empty; 2" door lowered @ 40g	No significant change in load readings as motor is started

Centrifuge Tests Performed (March '88 - September '90)

Date	*Test*	*Description*	*Remarks*
04/12/89	*GI*101/A	Brick stack of 1/2"[] *Al* rods, 5" high; 2" door lowered @ 40g	
04/13/89	*GI*102	4" coarse sand; 2" door lowered @ 40g	
04/14/89	*GI*103	5"coarse sand; 2" door lowered @ 40g	
04/17/89	*GI*104	2" coarse sand; 2" door lowered @ 40g	
04/18/89	*GI*105	2" door loaded with steel weights	
04/20/89	*GI*106	4" coarse sand; 2" door lowered @ 80g	
04/27/89	*GI*107	"3-on-door" direct stack of 1/4"[] *Al* rods, 2.5" high; 1" door lowered @ 80g	Hang-up observed
05/2/89	*GI*108	Repeat of *GI*107	
05/3/89	*GI*109	"3-on-door" direct stack of 1/4"[] *Al* rods, 2.5" high; 1" door lowered @ 40g	
05/4/89	*GI*110	"3-on-door" brick stack of 1/4"[] *Al* rods, 2.5" high; 1" door lowered @ 80g	
	*GI*111	"3-on-door" brick stack of 1/4"[] *Al* rods, 2.5" high; 1" door lowered @ 40g	
	*GI*112	"3-on-door" direct stack of 1/4"[] balsa wood rods, 2.5" high; 1" door lowered @ 80g	
	*GI*113	"3-on-door" direct stack of 1/4"[] balsa wood rods, 2.5" high; 1" door lowered @ 40g	

Centrifuge Tests Performed (March '88 - September '90)

Date	*Test*	*Description*	*Remarks*
05/8/89	*GI*114	"3-on-door" brick stack of 1/4"[] balsa wood rods, 2.5" high; 1" door lowered @ 80g	
	*GI*115	"3-on-door" brick stack of 1/4"[] balsa wood rods, 2.5" high; 1" door lowered @ 40g	
05/10/89	*GI*116	1" coarse sand on 1" door, lowered @ 80g	
	*GI*117	4" coarse sand on 1" door, lowered @ 80g	
05/11/89	*GI*118	2.5"coarse sand on 1" door, lowered @ 80g	
	*GI*119	2" coarse sand on 1" door, lowered @ 80g	
05/12/89	*GI*120	"3-on-door" direct stack of 1/2"[] balsa wood rods, 5" high; 2" door lowered @ 40g	
05/15/89	*GI*121	"3-on-door" brick stack of 1/2"[] balsa wood rods, 5" high; 2" door lowered @ 40g	
05/16/89	*GI*122	Same as *GI*121	
05/17/89	*GI*123	"3-on-door" direct stack of 1/2"[] balsa wood rods, 5" high; 2" door lowered @ 40g	
	*GI*124/A	Same as *GI*123	*GI*124: Stack of rods collapsed shortly after door was lowered; *GI*124A: re-run of *GI*124
05/18/89	*GI*125	"3-on-door" direct stack of 1/2"[] balsa wood rods, 5" high; 2" door lowered @ 80g	
05/25/89	*GI*126	"3-on-door" brick stack of 1/2"[] *Al* rods, 5" high; 2" door lowered @ 80g	

Centrifuge Tests Performed (March '88 - September '90)

Date	*Test*	*Description*	*Remarks*
06/08/89	*GI*127	Empty package (for recalibration); first run to 160g with 0.5" door	LC1 wire broken @ <160g
06/09/89	*GI*128	LC1 wire fixed; 1" coarse sand on 0.5" door, lowered @ 160g	Door "hung up" due to tight placement
07/27/89	*GI*129	No soil; door width trimmed a bit; another trial run	Door "hung up" again when it was supposed to drop
07/28/89	*GI*130	Empty; door opening widened a bit	No hang-up this time
08/01/89	*GI*131	1" coarse sand on 0.5" door, lowered @ 160g	Data erroneous (although discovered much later)
08/02/89	*GI*132	2" coarse sand on 0.5" door, lowered @ 160g	LC1, LC2 wires disconnected while in flight
08/03/89	*GI*133	LC1, LC2 wires re-soldered; repeat of *GI*132	Data erroneous
08/04/89	*GI*134	0.5" coarse sand on 0.5" door, lowered @ 160g	Data erroneous
08/24/89	*GI*135	4" coarse sand on 0.5" door, lowered @ 160g	Data erroneous
09/06/89	*GI*136	Proximity sensor (PS) probe @ middle segment of 1" door; plan on testing up to 160g	PS blackbox-driver, loosely mounted on the arm, flew off @~100g and blew into pieces
09/07/89	*GI*137	"3-on-door" direct stack of 1/2"[] *Al* rods, 2.5" high, on 2" door, lowered @ 40g; lateral confinement: 1/4"ϕ circular Al rods with a few 1/8"ϕ rods	
09/08/89	*GI*138	"3-on-door" direct stack of 1/2"[] *Al* rods, 2.5" high, on 2" door, lowered @ 40g; lateral confinement: coarse sand (+ cellophane sheet)	

Centrifuge Tests Performed (March '88 - September '90)

Date	*Test*	*Description*	*Remarks*
09/11/89	*GI*139	"3-on-door" direct stack of 1/4"[] *Al* rods, 1.25" high, on 1" door, lowered @ 80g; lateral confinement: 1/4"ϕ circular Al rods with a few 1/8"ϕ rods	
09/12/89	*GI*140	"3-on-door" direct stack of 1/4"[] *Al* rods, 1.25" high, on 1" door, lowered @ 80g; lateral confinement: coarse sand (+ cellophane sheet)	
10/06/89	*GI*141	Proximity sensor (PS) probe @ middle segment of 1" door; test up to 80g	First test with new proximity sensor; deflection readings "bottomed out" @ ~40g; probe face apparently placed too close to trapdoor that probe "kissed" door @ high g
	*GI141*A	PS probe @ adjacent base just beside the middle door segment	Same initial probe-surface gap as *GI141*, hence, readings also "bottomed out" @ ~40g
10/10/89	*GI*142	PS probe @ middle segment of 1" trapdoor	Larger initial probe-surface gap
	*GI*142A	PS probe @ adjacent base just beside the middle door segment	Same initial probe-surface gap as *GI*142
10/12/89	*GI*143	PS probe @ LC4 segment of 1" trapdoor	
	*GI*143A	PS probe @ LC1 segment of 1" trapdoor	
10/17/89	*GI*144	PS probe @ middle segment of 1" trapdoor	Although similar to *GI*142, may have slightly different initial probe-surface gap and positioning
10/31/89	*GI*145	PS probe @ middle door segment of 1" door	Re-run of previous tests but with the old (larger diameter) probe

Centrifuge Tests Performed (March '88 - September '90)

Date	*Test*	*Description*	*Remarks*
	*GI*145A	PS probe @ LC1 segment of 1" door	
	*GI*145B	PS probe @ LC4 segment of 1" door	
11/01/89	*GI*146	PS probe @ adjacent base, right next to the middle door segment	Old probe used
	*GI*146A	PS probe @ adjacent base, right next to the LC1 segment	
	*GI*146B	PS probe @ adjacent base, right next to the LC4 segment	
11/03/89	*GI*147	"4-on-door" direct stack of 1/4"[] *Al* rods, 2.5" high, on 1" door, lowered @ 80g; lateral confinement: 3-mmϕ glass beads	
11/06/89	*GI*148	"4-on-door" brick stack of 1/4"[] *Al* rods, 2.5" high, on 1" door, lowered @ 80g; lateral confinement: 3-mmϕ glass beads	
11/08/89	*GI*149	"8-on-door" direct stack of 1/8"[] *Al* rods, 2.5" high, on 1" door, lowered @ 80g; lateral confinement: 3-mmϕ glass beads	First try with "eight-on-door" arrangement
11/09/89	*GI*150	"8-on-door" "Semi-brick" stack of 1/8"[] *Al* rods, 2.5" high, on 1" door, lowered @ 80g; lateral confinement: 3-mmϕ glass beads	
11/15/89	*GI*151	PS probe @ middle segment of 2" door; test up to 40g	
	*GI*151A	PS probe @ LC1 segment of 2" door	

Centrifuge Tests Performed (March '88 - September '90)

Date	*Test*	*Description*	*Remarks*
	*GI*151B	PS probe @ LC4 segment of 2" door	
	*GI*151C	PS probe @ adjacent base right next to middle segment	
11/20/89	*GI*152	"4-on-door" direct stack of 1/2"[] *Al* rods, 5" high, on 2" door, lowered @ 40g; lateral confinement: 6-mmϕ glass beads	
11/22/89	*GI*153	"4-on-door" brick stack of 1/2"[] *Al* rods, 5" high, on 2" door, lowered @ 40g; lateral confinement: 6-mmϕ glass beads	Some hang-up problems occurred: only three of four rod columns centered over door came down
11/27/89	*GI*154	Repeat of *GI*153	No hang-up problems this time
11/28/89	*GI*155	"8-on-door" direct stack of 1/4"[] *Al* rods, 5" high, on 2" door, lowered @ 40g; lateral confinement: 6-mmϕ glass beads	
11/30/89	*GI*156	"8-on-door" "semi-brick" stack of 1/4"[] *Al* rods, 5' high, on 2" door, lowered @ 40g; lateral confinement: 6-mmϕ glass beads	
12/14/89	*GI*157	Repeat of *GI*156	
01/09/90	*GI*158	5" coarse sand on 2" door @ 40g, with pre-lowering	
01/12/90	*GI*159	"4-on-door" direct stack of 1/8"[] *Al* rods, 1.25" high, on 0.5" door @ 160g; lateral confinement: 1.5-mmϕ glass beads	

Centrifuge Tests Performed (March '88 - September '90)

Date	*Test*	*Description*	*Remarks*
01/17/90	*GI*160	Same as *GI*159	Motor locked up @ 160g, works on spin-down @ 80g; LC1 broken
	*GI*160A	Repeat of *GI*160	Motor works this time; LC1 still broken, and other data appear to be erroneous
01/29/90	*GI*161	"4-on-door" brick stack of 1/8"[] *Al* rods, 1.25" high, on 0.5" door @ 160g; lateral confinement: 1.5-mmϕ glass beads	LC1 was fixed, but got disconnected again in flight
01/30/90	*GI*162	Proximity sensor (PS) probe over middle segment of 0.5" door, up to 160g	
01/31/90	*GI*163	PS probe @ middle segment of 0.5" door, up to 160g	
	*GI*163A	PS probe @ LC1 segment of 0.5" door, up to 160g	
	*GI*163B	PS probe @ LC4 segment of 0.5" door, up to 160g	
	*GI*163C	PS probe @ "transition face" on the bracket/spacer adjacent to the door	
	*GI*163D	PS probe @ adjacent base	
02/01/90	*GI*164	1.5-mmϕ glass beads, 1" deep, on 0.5" door @ 160g	Door has tape on the edges (to prevent grains from falling through the trench) -- may have affected load measurements
	*GI*165	1.5-mmϕ glass beads, 1.5" deep, on 0.5" door @ 160g	Door has tape on the edges
02/03/90	*GI*166	1.5-mmϕ glass beads, 2" deep, on 0.5" door @ 160g	Door has tape on the edges

Centrifuge Tests Performed (March '88 - September '90)

Date	*Test*	*Description*	*Remarks*
02/08/90	*GI*167/AB	Door segments removed; package tested up to 160g; *GI*167A -- w/o bracket/spacer on side of motor; *GI*167B -- w/o brackets/spacers on both sides	For calibration of load cells
02/08/90	*GI*168/A	Door segments removed; package tested up to 40g	For calibration
02/10/90	*GI*169	"4-on-door" direct stack of 1/8"[] *Al* rods, 1.25" high, on 0.5" door @ 160g; lateral confinement: 1.5-mmϕ glass beads	
02/13/90	*GI*170	1.5-mmϕ glass beads, 1" deep, on 0.5" door @ 160g	No tape on door edges ; plates beside door squeezed in
	*GI*171	1.5-mmϕ glass beads, 1.5" deep, on 0.5" door @ 160g	No tape on door edges
02/14/90	*GI*172	"2-on-door" direct stack of 1/4"[] *Al* rods, 1.25" high, on 0.5" door @ 160g; lateral confinement: 3-mmϕ glass beads	
02/21/90	*GI*173	"4-on-door" brick stack of 1/4"[] *Al* rods, 2.5" high, on 1" door @ 80g; lateral confinement: 3-mmϕ glass beads	Length of ten "key rods" above door = 1/2 length of door
02/23/90	*GI*174	3-mmϕ glass beads, 2" deep, on 1" door @ 80g	LC4 disconnected in flight
02/24/90	*GI*175	Repeat of *GI*174	
02/25/90	*GI*176	Empty package, with 1" door, tested up to 80g	For calibration
02/26/90	*GI*177	"2-on-door" direct stack of 1/2"[] *Al* rods, 2.5" high, on 1" door @ 80g; lateral confinement: 6-mmϕ glass beads	

Centrifuge Tests Performed (March '88 - September '90)

Date	*Test*	*Description*	*Remarks*
02/26/90	*GI*178	6-mmϕ glass beads, 3.5" deep, on 2" door @ 40g	
02/27/90	*GI*179	3-mmϕ glass beads, 3.5" deep, on 2" door @ 40g	
02/28/90	*GI*180	"4-on-door" direct stack of 1/8"[] *Al* rods, 1.25" high, on 0.5" door @ 160g; lateral confinement: 1.5-mmϕ glass beads	Only middle segment used; length of rods = 1"; edge effects highly probable
03/07/90	*GI*181	"4-on-door" brick stack of 1/8"[] *Al* rods, 1.25" high, on 0.5" door @ 160g; lateral confinement: 1.5-mmϕ glass beads	Only middle segment used; length of rods = 1"; edge effects highly probable
03/20/90	*GI*182	"4-on-door" direct stack of 1/4"[] *Al* rods, 1.5" high, on 2" door (but not lowered) @ 80g; no lateral confinement	For calibration
03/21/90	*GI*183/AB	Glass beads, 2" deep, on 2" door @ 80g: *GI*183 --> ϕ = 6 mm: *GI*183A --> ϕ = 3 mm; *GI*183B --> ϕ = 1.5 mm	
03/23/90	*GI*184	Same as *GI*183	
	*GI*184A	Coarse sand, 2" deep, on 2" door @ 80g	
03/27/90	*GI*185	"4-on-door" direct stack of 1/4"[] *Al* rods, 2.5" high, on 1" door @ 80g; lateral confinement: 3-mmϕ glass beads	Hang-ups observed in LC1 and LC4 segments
	*GI*186	"4-on-door" brick stack of 1/4"[] *Al* rods, 2.5" high, on 1" door @ 80g; lateral confinement: 3-mmϕ glass beads	Hang-up observed in LC2 and LC4 segments
03/28/90	*GI*187	Repeat of *GI*185	
	*GI*188	Repeat of *GI*186	

Centrifuge Tests Performed (March '88 - September '90)

Date	*Test*	*Description*	*Remarks*
03/30/90	*GI*189	6-mmϕ glass beads, 4" deep, on 2" door @ 40g	First run with "glass window" on one side (LC1)
04/04/90	*GI*190	"4-on-door" direct stack of 1/2"[] *Al* rods, 5" high, on 2" door @ 40g; lateral confinement: 6-mmϕ glass beads; "Glass windows" mounted on both sides	
	*GI*191	"4-on-door" brick stack of 1/2"[] *Al* rods, 5" high, on 2" door @ 40g; lateral confinement: 6-mmϕ glass beads	
04/05/90	*GI*192	"4-on-door" brick stack of 1/2"[] *Al* rods, 5" high, on 2" door @ 80g; lateral confinement: 6-mmϕ glass beads	
04/06/90	*GI*193	"4-on-door" direct stack of 1/8"[] *Al* rods, 1.25" high, on 0.5" door @ 160g; lateral confinement: 1.5-mmϕ glass beads	LC1 disconnected during door lowering
04/09/90	*GI*194	"4-on-door" brick stack of 1/8"[] *Al* rods, 1.25" high, on 0.5" door @ 160g; lateral confinement: 1.5-mmϕ glass beads	
04/19/90	*GI*195	3-mmϕ glass beads, 2" deep, on 1" door @ 80g	"Glass windows" broke @ ~80g
04/20/90	*GI*196	1.5-mmϕ glass beads, 1" deep, on 0.5" door @ 160g	LC1 disconnected during door lowering
05/15/90	*GI*197	NJ coarse sand, 1" deep, on 1" door @ 80g	LC1 disconnected in flight
05/16/90	*GI*198	NJ coarse sand, 2" deep, on 1" door @ 80g	

Centrifuge Tests Performed (March '88 - September '90)

Date	*Test*	*Description*	*Remarks*
05/17/90	*GI*199	NJ coarse sand, 2.5" deep, on 1" door @ 80g	
	*GI*200	NJ coarse sand, 4" deep, on 1" door @ 80g	
05/18/90	*GI*201	2-mmϕ glass beads, 2" deep, on 1" door @ 80g	
05/19/90	*GI*202	3-mmϕ glass beads, 2" deep, on 1" door @ 80g with pre-lowering	
05/21/90	*GI*203	"2-on-door" direct stack of 1/2"[] *Al* rods, 2.5" high, on 1" door @ 80g; lateral confinement: 3-mmϕ glass beads	
05/23/90	*GI*204	"3-on-door" semi-brick stack of 1/4"[] *Al* rods, 2.5" high, on 1" door @ 80g; lateral confinement: 3-mmϕ glass beads	
05/24/90	*GI*205	"4-on-door" direct stack of 1/8"[] *Al* rods, 1.25" high, on 0.5" door @ 160g; lateral confinement: 1.5-mmϕ glass beads	LC1 disconnected in flight
05/30/90	*GI*206	"4-on-door" brick stack of 1/8"[] *Al* rods, 1.25" high, on 0.5" door @ 160g; lateral confinement: 1.5-mmϕ glass beads	LC1 disconnected again
05/31/90	*GI*207	Proximity sensor (PS) probe over middle segment of 0.5" door, tested up to 160g	PS wiring got pulled off in flight
	*GI*207A	Repeat of *GI*207	
	*GI*207B	PS probe over "intermediate" surface of bracket/spacer next to 0.5" door	

Centrifuge Tests Performed (March '88 - September '90)

Date	*Test*	*Description*	*Remarks*
	*GI*207C	PS probe over adjacent base	
06/03/90	*GI*208	1.5-mmϕ glass beads, 1" deep, on 0.5" door @ 160g	
06/11/90	*GI*209	"4-on-door" brick stack of 1/8"[] *Al* rods, 1.25" high, on 0.5" door @ 160g; lateral confinement: 1.5-mmϕ glass beads	
06/26/90	*GI*210	1.5-mmϕ glass beads, 1" deep, on 0.5" door @ 160g with pre-lowering	
08/14/90	*GI*211	6-mmϕ glass beads, 2" deep, on 0.5" door @ 80g	
	*GI*212	0.5-mmϕ glass beads, 2" deep, on 2" door @ 80g	
09/01/90	*GI*213	0.5-mmϕ glass beads, 2" deep, on 0.5" door @ 80g	